Dietary titanium dioxide particles and intestinal health

A thesis presented in partial fulfilment of the requirements for the degree of

Doctor of Philosophy

in

Nutritional Science

at Massey University, Manawatū,

New Zealand.

Sebastian Riedle

2014

Abstract

The purpose of this dissertation was to investigate the relationship between food-grade titanium dioxide particles and intestinal health, in particular the development of Crohn's disease after uptake of titanium dioxide particles in intestinal lymphoid tissues.

Crohn's disease is a common form of inflammatory bowel disease. It is characterised by chronic inflammation of the gastrointestinal tract and affects approximately 1 in 1,000 people. The aetiology of Crohn's disease is unclear, but both genetic and environmental factors are involved in the development of the disease.

The gene that is most commonly associated with Crohn's disease is the nucleotide-binding oligomerisation domain (*NOD*) 2 gene. The diet is one of the most likely environmental factors that have been proposed to play a role in Crohn's disease. It has been hypothesised that uptake of titanium dioxide particles, which are used as a whitening agent in processed foods, toothpaste, and pharmaceuticals, by macrophages in intestinal lymphoid tissues negatively affects intestinal health and contributes to the development of Crohn's disease.

To investigate this hypothesis, immune cell-stimulating properties of titanium dioxide were first assessed *in vitro* with macrophages derived from wild-type mice and mice with a Crohn's disease-like *Nod2* gene variant. These mouse models were also used to determine particle uptake in intestinal lymphoid tissues *in vivo* after exposure to titanium dioxide with the diet and effects of this dietary exposure on intestinal health and urine metabolites.

The results from the *in vitro* studies showed that titanium dioxide induced the release of the pro-inflammatory cytokine interleukin-1β. For the first time, it has been shown that accumulation of particles in intestinal lymphoid tissues was a consequence of titanium dioxide intake with the diet. However, this had no negative effects on growth performance and intestinal health of both wild-type mice and mice with a Crohn's disease-like *Nod2* gene variant. Nevertheless, differences in urine metabolite profiles between wild-type mice exposed to titanium dioxide and unexposed wild-type mice indicated that consumption of a titanium dioxide-containing diet affected the metabolism.

This dissertation forms the foundation for future studies with animal models about the relationship between titanium dioxide and intestinal health.

Acknowledgements

Firstly, I owe my deepest gratitude to my supervisor Dist. Prof. Harjinder Singh (Riddet Institute, Massey University, Palmerston North, NZ) for taking on the responsibilities that come with supervising a PhD project and for his guidance and advice throughout the years.

Furthermore, I am most grateful for the support, guidance, and advice that I received from my co-supervisors Dr Nicole Roy and Dr Don Otter (both AgResearch, Palmerston North, NZ). Their support throughout the years was invaluable. Without their constant encouragement, openness to pursue new ideas, and valuable feedback this dissertation would not have been what it is now.

In addition, I am very thankful for the support offered by my co-supervisors Dr Laetitia Pele and Dr Jonathan Powell (both Medical Research Council Human Nutrition Research, Cambridge, UK) who laid the foundations for this PhD project through their extensive previous research in the field of dietary particles. Their knowledge, enthusiasm for the project, and advice through many e-mails and telephone conference calls was much appreciated. It was a great pleasure to meet Dr Pele and Dr Powell in person several times throughout this project to discuss the progress face-to-face and to carry out laboratory work at their institute.

Moreover, I would like to thank the people who kindly assisted me during this PhD project including Ms Kelly Armstrong, Dr Matthew Barnett, Dr Mark McCann, Mr Jason Peters, and Ms Leigh Ryan (all AgResearch, Palmerston North, NZ) for training in laboratory work, discussions, and/or help with sample collection during the animal studies; Ms Genevieve Baildon and Mr Ric Broadhurst (both AgResearch, Hamilton, NZ) for providing the animals for the studies and training in sample collection; Dr Jianyu Chen, Mr Douglas Hopcroft, and Ms Jordan Taylor (all Manawatū Microscopy and Imaging Centre, Massey University, Palmerston North, NZ) for help with and training in various microscopy techniques; Dr Nuno Faria and Ms Carolin Haas (both Medical Research Council Human Nutrition Research, Cambridge, UK) for assistance with laboratory work; Dr John Koolaard and Ms Catherine Lloyd-West (both AgResearch, Palmerston North, NZ) for advice on statistical analyses and R; Ms Denise Martin (AgResearch, Palmerston North, NZ) for administrative support; Ms Heike Schwendel (AgResearch, Palmerston North, NZ) for help during sample analysis with mass spectrometry; Mr Paul Smale (AgResearch, Mosgiel, NZ) for providing a

custom-made image analysis program; and Dr Wayne Young (AgResearch, Palmerston North, NZ) for advice on R and providing the R code for metabolomics data analysis.

Many thanks go to my colleagues and other students from the Food Nutrition & Health and the Rumen Microbiology teams at AgResearch (Palmerston North, NZ) for their friendship, help, and support throughout the years.

I would also like to thank the staff and students from the Biomineral Research team at the Medical Research Council Human Nutrition Research institute (Cambridge, UK) who always made me feel very welcome during my visits.

Last but not least, I thank my wife Sabine for her love, support, understanding and encouragement when I most needed it.

Finally, I would like to acknowledge the financial support for this project granted by the Riddet Institute, AgResearch, Nutrigenomics New Zealand, and the Medical Research Council, UK. Personally I was supported with a doctoral scholarship from Massey University and a stipend from AgResearch, for which I am very grateful.

All animal experiments that were carried out during the course of this project were in compliance with the New Zealand Animal Welfare Act 1999 and were approved by the Grasslands Ethics Committee (Palmerston North, NZ).

Table of contents

List of figures

List of tables

List of appendices

List of abbreviations

$[M+H]^+$	Positive molecular ion
$[M-H]^-$	Negative molecular ion
1,007fs	Frameshift mutation at amino acid position 1,007
A5	Annexin-V
AIN	American Institute of Nutrition
ANOVA	Analysis of variance
APC	Antigen presenting cell
ASC	Apoptosis-associated speck-like protein containing a CARD
ATG16L1	Autophagy-related 16-like 1 gene
B cell	Bursa-derived cell
BMDC	Bone marrow-derived DC
BMDM	Bone marrow-derived macrophage
CARD	Caspase recruitment domain
CCL	CC chemokine ligand
CD	Crohn's disease
CD[number]	Cluster of differentiation [number]
CX_3CR	CX_3C chemokine receptor
DAPI	4',6-Diamidino-2-phenylindole
DC	Dendritic cell
DNA	Deoxyribonucleic acid
DSS	Dextran sodium sulphate
EDS	Energy-dispersive X-ray spectroscopy
ELISA	Enzyme-linked immunosorbent assay
FACS	Fluorescence-activated cell sorting
FAE	Follicle-associated epithelium
FBS	Foetal bovine serum
FDR	False discovery rate
FSC	Forward scatter
GALT	Gut-associated lymphoid tissue
GC-MS	Gas chromatography mass spectrometry
H&E	Haematoxylin and eosin
HSD	Honest significant difference

IBD	Inflammatory bowel disease
IFN	Interferon
IFR	Interfollicular region
Ig	Immunoglobulin
IL	Interleukin
Il10$^{-/-}$	*Il10* gene-deficient
IL12B	IL-12 p40 subunit-encoding gene
IL-1Ra	IL-1 receptor antagonist
ILF	Isolated lymphoid follicle
IκB	Inhibitor of NF-κB
LC-MS	Liquid chromatography mass spectrometry
LP	Lamina propria
LPMC	LP mononuclear cell
LPS	Lipopolysaccharide
M cell	Microfold cell
m/z	Mass-to-charge
MANOVA	Multivariate ANOVA
MCP	Monocyte chemotactic protein
MDP	Muramyl dipeptide
MFI	Median fluorescence intensity
MIP	Macrophage inflammatory protein
MLN	Mesenteric lymph node
mRNA	Messenger ribonucleic acid
NF	Nuclear factor
NLR	NOD-like receptor
NLRP	NOD, leucine-rich repeats domain, and pyrin domain
NMR	Nuclear magnetic resonance spectroscopy
NOD	Nucleotide-binding oligomerisation domain
NOD2	*NOD2* gene (human)
NOD2	NOD2 protein (human)
Nod2	*Nod2* gene (mouse)
Nod2	Nod2 protein (mouse)
Nod2$^{-/-}$	*Nod2* gene-deficient
Nod2$^{m/m}$	*Nod2* gene mutation

NTA	Nanoparticle tracking analysis
p	Probability
PBMC	Peripheral blood mononuclear cell
PBS	Phosphate-buffered saline
PGN	Peptidoglycan
PI	Propidium iodide
PLS-DA	Partial least squares discriminant analysis
PMT	Photomultiplier tube
PP	Peyer's patch
PRR	Pattern recognition receptor
RIP	Receptor-interacting protein
ROS	Reactive oxygen species
RPMI	Roswell Park Memorial Institute
SD	Standard deviation
SED	Subepithelial dome
SEM	Scanning electron microscopy
SNP	Single nucleotide polymorphism
SSC	Side scatter
T cell	Thymus-derived cell
TCM	Tissue culture medium
TEM	Transmission electron microscopy
TGF	Transforming growth factor
Th	T helper
TiO_2	Titanium dioxide
TLR	Toll-like receptor
TNBS	2,4,6-Trinitrobenzenesulfonic acid
TNF	Tumour necrosis factor
UC	Ulcerative colitis
WST	Water-soluble tetrazolium salt
WT	Wild-type

Introduction

Nowadays, the majority of foodstuffs available in supermarkets can be classified as processed foods. These products are often modified with additives, e.g. to enhance flavour, increase shelf life, and/or make the product more appealing to the consumer. The latter is often achieved through the addition of food colourants. The colours that are approved for use in foodstuffs cover the whole standard palette from yellow, red, and blue, to white, silver, and gold.

Titanium dioxide (TiO_2) is the only available white food colourant. It is commonly used to enhance the appearance of confectionary, salad dressings, and chewing gums. Most toothpastes also contain TiO_2 as well as many pharmaceuticals and dietary supplements. In its original form, titanium dioxide is a naturally occurring mineral. As a whitening agent it is used in particulate form, with the particle size ranging from less than 100 nm to several 100 nm.

These TiO_2 particles have been referred to as exogenous dietary particles, to distinguish them from endogenous dietary particles that naturally occur in the gastrointestinal tract. Endogenous dietary particles consist of calcium phosphate, and they are formed spontaneously in the small intestine following the secretion of calcium and phosphate ions into the intestinal lumen. Both exogenous and endogenous dietary particles are taken up by phagocytic cells in Peyer's patches (PPs) which are defined aggregates of immune cells in the mucosa of the small intestine. PPs provide the main route of entry for antigens from the lumen. Thus, they have an important role in maintaining the balance between tolerance to harmless antigens, e.g. from food or commensal bacteria, and initiation of an immune response against pathogens. This balance is known as intestinal homeostasis.

The uptake of exogenous dietary TiO_2 particles, which can adsorb luminal antigens, in PPs might disrupt this homeostasis and lead to a pro-inflammatory immune response. If this inflammation persists for a long period of time it could contribute to the development of inflammatory bowel disease (IBD), specifically Crohn's disease (CD).

Despite decades of research, the aetiology of CD is still incompletely resolved. It is known that that both genetic and environmental factors contribute to the development of CD. Diet might be one of the environmental factors as the incidence of CD is higher in developed countries which are characterised by an increased consumption of processed foods.

Furthermore, several genetic risk factors have been linked to the development of CD. Through genome-wise association studies it has been shown that mutations in the nucleotide-binding oligomerisation domain (*NOD*) 2 gene are the highest genetic risk factors that are associated with an increased likelihood to develop CD. The most common *NOD2* variant is a frameshift mutation at amino acid position 1,007 (1,007fs) that results in the expression of a truncated protein. The NOD2 protein is an intracellular receptor for bacterial cell wall fragments, and its activation leads to the production of pro-inflammatory cytokines.

It has been hypothesised that people with mutations in the *NOD2* gene will be at a greater risk from TiO_2 particle-induced disruption of intestinal homeostasis. Delivery of NOD2-activating ligands into the cell by TiO_2 particles will cause an increased production of pro-inflammatory cytokines in this group. A mouse model with a mutation in the *Nod2* gene that matches the human 1,007fs variant has been created. This model is ideally suited to examine this hypothesis in more detail.

The main purpose of this dissertation was to carry out *in vitro* and *in vivo* experiments with this specific mouse model to investigate the potential of dietary TiO_2 particles to cause a disruption of intestinal homeostasis in the presence of this particular CD-associated genetic variant. The results will be helpful to evaluate potential risks associated with the increased use of TiO_2 as a whitening agent in processed foods and other products intended for oral intake.

Chapter 1 **Literature review**

1.1 The gastrointestinal tract and Crohn's disease

The gastrointestinal tract has a larger surface area than any other organ of the human body (approximately 200 m^2 to 400 m^2) [1-3]. The main function of the gastrointestinal tract is the digestion of food and absorption of nutrients, water, and other compounds. Commensal microorganisms play an important role in this process, and it is crucial that a homeostasis is maintained between the tolerance of beneficial microbes and effective eradication of invasive pathogens [1]. Furthermore, tolerance must also be maintained towards food antigens. When the proper responses to the intestinal microbiota are disturbed, or food antigens elicit immune reactions, pathological consequences can arise resulting in gastrointestinal inflammation or food allergies. This literature review will focus on a particular type of dietary antigens, namely dietary particles, and their role in intestinal homeostasis. The first section will give a brief overview of the gastrointestinal tract and its associated immune system.

1.1.1 Structure and function of the mammalian gastrointestinal tract

The gastrointestinal tract can be divided in an upper part, which comprises the oesophagus and the stomach, and in a lower part, which consists of the small and large intestine. The small intestine has three sections, namely the duodenum, jejunum, and ileum. The colon can be further divided into the caecum, colon, rectum, and anal canal. In general, the gastrointestinal tract can be considered as a tube that extends from the mouth to the anus, and its overall structure is similar throughout the whole length (Figure 1.1). The space enclosed by the gastrointestinal tract is referred to as the lumen. This central part contains the ingested substances, especially food, commensal organisms, and potentially also parasites. Technically, it constitutes an external environment of the body. The innermost layer of the gastrointestinal tract that separates the lumen from the rest of the body is the mucosa which is made up by three different tissue types. A simple columnar epithelium forms the outside border of the mucosa and faces the lumen. The connective tissue below the epithelium is referred to as lamina propria (LP), and the muscular tissue of the muscularis mucosae separates the mucosa from the submucosa. The submucosa is a connective tissue that contains blood vessels, lymphatics, nerves, and glands. The muscularis externa is a smooth muscle tissue and forms the next section of the gastrointestinal tract. It consists of an inner circular layer and an outer longitudinal layer, and these muscles work together to move the

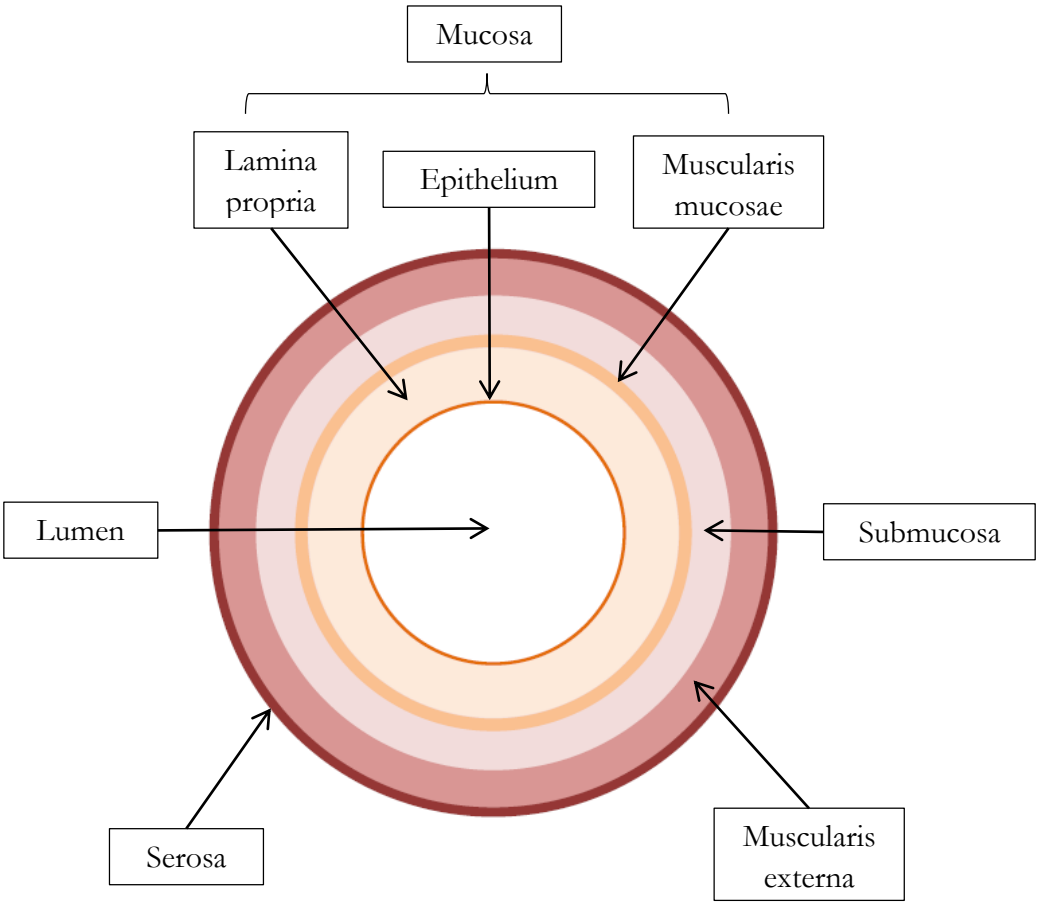

Figure 1.1 *Schematic overview of the structure of the gastrointestinal tract.*

This diagram depicts the distinctive layers of the gastrointestinal tract as seen in a generalised cross-section.

intestinal content forward. The outermost structure of the gastrointestinal tract is the serosa, which comprises a simple squamous epithelium, and a thin layer of connective tissue and separates the gastrointestinal tract from the abdominal cavity [4].

The small intestine is the principal site for food digestion and nutrient absorption. A feature of the small intestine is the presence of villi, which are projections of the mucosa into the lumen. This increases the surface area of the small intestine and thus enables more efficient absorption. Another characteristic of the small intestine is the presence of special glands, the 'crypts of Lieberkühn' or crypts. They are located in the LP from which they are separated by epithelial cells that form a continuum with the epithelial cells of the villi. The main function of the colon is water and electrolyte resorption. After the passage through the gastrointestinal tract, all undigested food components are excreted. There are also crypts present in the colon, but no villi [4].

Different cell types are present in the small and large intestinal epithelium. The most prevalent cells are enterocytes, which are specialised in nutrient absorption. Their surface area is increased at the luminal side by of the presence of microvilli. This gives the surface of the small and large intestinal wall the appearance of a 'brush border' [5]. In addition to their nutrient absorption function, enterocytes of the small intestine also secrete digestive enzymes. Furthermore, all enterocytes release several kinds of antimicrobial peptides, which inhibit the colonisation of the epithelial surface by intestinal microbes [3]. Paneth cells, which are located at the base of crypts in the small intestine, also produce antimicrobial peptides, namely α-defensins. Another common epithelial cell type is the goblet cell. Their main function is the secretion of mucins, which are highly glycosylated proteins that make up the mucous layer. The mucous layer is composed of an outer and an inner part, and together they form a physical barrier that protects the epithelium from intestinal bacteria. Enteroendocrine cells are also present in the intestinal epithelium. They produce hormones that affect the gastrointestinal physiology. All epithelial cells are derived from pluripotent stem cells that are located at the base of crypts, and they are constantly renewed as they undergo apoptosis once they reach the tips of the villi [3].

As mentioned earlier, the gastrointestinal tract also has an important role in maintaining immune homeostasis. The gastrointestinal tract is constantly exposed to antigens derived from food and the intestinal microbiota. In healthy individuals, this exposure does not elicit an immune response, yet the gastrointestinal immune system remains able to react to invading pathogens. Many different types of immune cells are involved in maintaining this homeostasis. Some of these immune cells occur in organised gut-associated lymphoid

tissue (GALT), whereas others are distributed throughout the LP and epithelium [5]. The GALT consists of mesenteric lymph nodes (MLNs), isolated lymphoid follicles (ILFs), and PPs. The latter are organised lymphoid structures that occur in the mucosa of the small intestine in close contact with the epithelium (Figure 1.2). They were originally described in 1677 by the Swiss pathologist Johann Conrad Peyer [6]. The number and distribution of PPs along the small intestine varies between species. For example, in humans hundreds of PPs occur mainly in the terminal ileum, whereas in mice up to ten PPs can be found which are distributed the small intestine [6, 7]. PPs and MLNs are only present in mammals, but ILFs are also found in other vertebrates which indicates that they are the evolutionary oldest GALT [2, 8]. Unlike PPs the occurrence of ILFs is not restricted to the ileum and they are also present in the colon.

The structure of PPs has similarities with MLNs, but PPs also have some unique features. Both types of GALT contain large bursa-derived (B) cell-dense follicles with germinal centres and thymus-derived (T) cell-dense areas. B cells and T cells are lymphocytes, and they are the main cell types of the adaptive immune system, which provides an antigen-specific response to invasive pathogens. Through the establishment of memory cells, the adaptive immune system is able to respond quickly to reinfection with the same pathogens. The main function of B cells is the production of antibodies, which is facilitated by a certain type of T cells, namely T helper (Th) cells. In PPs Th cells occur mainly in the interfollicular regions (IFRs) that are located between the follicles. In contrast to lymph nodes, PPs lack afferent lymphatics. Instead, antigen can enter PPs *via* specialised cells in the follicle-associated epithelium (FAE). These cells are called microfold (M) cells, and they differ from enterocytes by the presence of shorter microvilli, a thinner mucous layer, and invaginations on their basolateral side. The latter feature allows close contact between M cells and phagocytic antigen presenting cells (APCs), e.g. macrophages and dendritic cells (DCs).

These APCs are part of the innate immune system, which provides a first line of defence against pathogens. In contrast to the adaptive immune system, the innate immune response is unspecific and no immune memory is established. However, APCs also act as important mediators between the innate and adaptive immune systems. Antigens that have been taken up by APCs through phagocytosis are subsequently presented to lymphocytes and this activates the adaptive immune response. In the gastrointestinal tract antigens are initially taken up from the lumen by M cells, which pass them to underlying APCs by transcytosis. The area below the FAE is referred to as subepithelial dome (SED), and it is characterised by the presence of many APCs, in particular DCs. Below the SED area are the B cell-dense

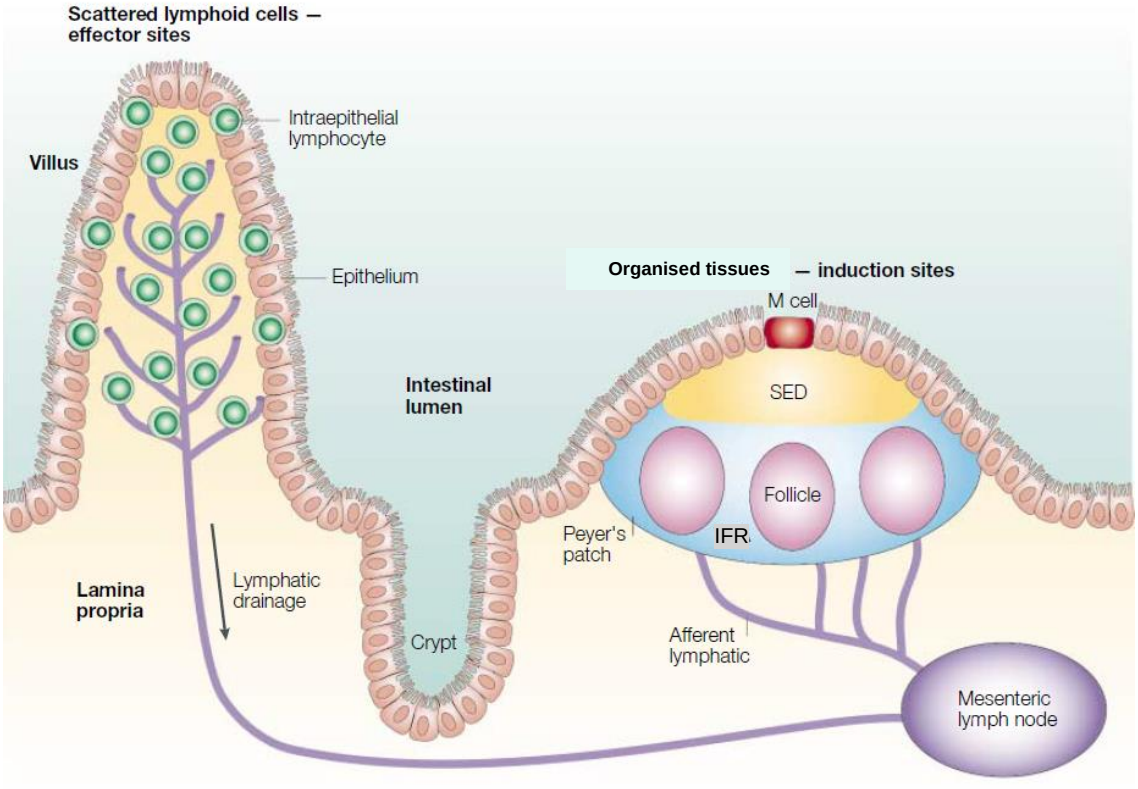

Figure 1.2 *Schematic overview of the small intestine including lymphoid tissues.*

Characteristic for the small intestine is the presence of villi, which protrude into the intestinal lumen (light green), and crypts, which are invaginations of the mucosa. The epithelium (brown) and the LP (beige) are part of the mucosa. The mucosa also contains lymphoid cells. The lymphoid tissues in the small intestine can be separated in induction and effector sites. Induction sites are formed by immune cells that occur together in organised tissues, also called GALT. The two types of GALT that are shown in this overview are PPs and MLNs. ILFs, a third form of GALT, are not shown in this figure. The epithelium that covers PPs is referred to as FAE. Characteristic for the FAE is the presence of M cells (red) which transport antigens from the intestinal lumen to the mucosa. Three different regions can be distinguished in PPs: the SED is the area just below the FAE (yellow), follicles make up the main part of the PPs (pink), and between the follicles lie the IFRs (blue). PPs do not have afferent lymphatics, but they possess efferent lymphatics which are the afferent lymphatics for the MLNs (purple). These lymphatics allow immune cells to travel from PPs to MLNs (purple). Immune cells from the LP and intraepithelial lymphocytes (green) can also reach MLNs *via* the lymphatic drainage system (purple). Figure adapted from reference [5]. Permission to use this figure in this dissertation has been obtained online from Nature Publishing Group.

follicles, which comprise most of the immune cells in PPs. In addition to Th cells, the IFRs also harbour DCs. The most important function of PPs is the induction of immunoglobulin (Ig) A-producing B cells in the germinal centres of the follicles, which is mediated by Th cells that have been activated by APCs.

ILFs are structurally similar to PPs, but they are smaller. ILFs are also covered with an M cell-containing FAE, and they contain mainly B cells and DCs. Like PPs, ILFs are also a site for DC-mediated IgA class-switching of B cells, but in ILFs this occurs independently of activated Th cells [2, 9]. In PPs, Th cells become activated by interacting with antigen-loaded APCs in the IFRs [5, 6, 10]. Furthermore, DCs promote the expression of specific cell surface molecules on Th cells and B cells that enable the lymphocytes to return to the intestinal mucosa after circulation in the blood [5, 11]. Imprinting of lymphocytes with intestinal homing receptors also takes place in the MLNs from where the Th cells and B cells leave the mucosa *via* efferent lymphatics. After their return to the intestinal mucosa the lymphocytes will reside in the LP. There, Th cells exert either effector or regulatory functions through the production of pro- and anti-inflammatory cytokines, respectively [2]. B cells differentiate into plasma cells, and they produce large amounts of IgA which is secreted into the lumen by epithelial cells through transcytosis [1]. Interactions of secreted IgA with intestinal microbes limit their ability to gain access to the intestinal mucosa, and it also neutralises toxins that are produced by intestinal pathogens [9].

Maintaining intestinal homeostasis is a complex process as it involves many different immune cell types, especially subsets of APCs and Th cells. The immune cells interact with the intestinal microbiota and with each other either through direct cell-cell interactions or the production of cytokines and anti-microbial peptides [1, 2, 11, 12]. Disturbances of the intestinal homeostasis may result in inflammation. If this becomes a chronic condition it may eventually lead to the establishment of IBD.

1.1.2 Crohn's disease as a form of inflammatory bowel disease

CD is a chronic inflammatory disorder of the gastrointestinal tract. The prevalence of CD, i.e. the number of people affected by this disease, is highest in Europe and North America with approximately 100 cases per 100,000 people [13], and some studies reporting up to 300 cases per 100,000 people [14]. New Zealand also has a high prevalence with 145 cases per 100,000 persons reported for Canterbury [15]. The incidence, i.e. frequency of new cases per year, of CD has increased considerably over the last decades, even in Asian and Latin American countries that used to have a low incidence of CD [13]. CD is only one of two

distinct forms of IBD, the other one being ulcerative colitis (UC) [16]. Inflammation in CD can occur at any location of the gastrointestinal tract, but the areas which are most often affected are the terminal ileum and the colon [17]. The pathological features of CD are that the intestinal inflammation is transmural, i.e. affecting all layers of the gastrointestinal tract, and discontinuous with alternating inflamed regions and unaffected sections [18, 19]. In contrast, UC exclusively affects the colon and rectum and the inflammation is continuous [16, 18].

Inflammatory diseases can generally be classified as either Th1 or Th2 cytokine-mediated according to the presence of pro-inflammatory cytokines produced by different subsets of cluster of differentiation (CD) 4^+ Th cells. While Th1 cells differentiate in the presence of interleukin (IL)-12 and produce interferon (IFN)-γ, Th2 cells develop under the influence of IL-4, in the absence of IL-12, and produce IL-4, IL-5, and IL-13 [20, 21]. Further subsets of Th cells have been identified since the initial description of Th1 and Th2 cells, and another important pro-inflammatory subset are Th17 cells [22]. The development of this Th cell subset is promoted by transforming growth factor (TGF)-β, IL-1β and IL-6, and the cells require IL-23, which is produced by APCs [23-25]. Th17 cells are characterised by the expression of the pro-inflammatory cytokine IL-17 as well as IL-22 which enhances epithelial barrier function [26, 27].

Initially, the assumption that CD was a Th1 cytokine-mediated disease was supported by several studies [28]. For instance, it was shown that macrophages from the LP of CD patients produced increased amounts of IL-12 [29, 30], and T cells isolated from inflamed areas of CD patients expressed elevated amounts of IFN-γ and decreased levels of IL-4 compared to T cells from healthy control tissues [30, 31]. However, IL-12 consists of two subunits, p35 and p40, and the p40 subunit is also part of IL-23 which is a heterodimer comprising the subunits p19 and p40 [32]. Thus, effects that were ascribed to IL-12 in earlier studies of intestinal inflammation might also have been caused by IL-23 [28]. This hypothesis has been strengthened by observations that IL-23 and Th17 cells play an important role in animal models of intestinal inflammation [33-36]. In humans, increased expression of both IL-12 and IL-23 during active CD has been observed [37], and Th17 cells were isolated from areas with active CD [38]. In general, Th17 cells are present in the blood and intestinal mucosa of both healthy individuals and CD patients [39, 40], but in CD patients the number of Th17 cells was increased [41]. These studies show that Th17 cells play a role in CD, but it is still unclear to which extent IL-17 and other Th17 cytokines contribute to the intestinal inflammation in CD [26, 28]. The current understanding is that CD is mediated by both Th1

and Th17 cytokines, but that their relative contribution to inflammation changes, e.g. depending on the stage of the disease [42].

Other pro-inflammatory cytokines like tumour necrosis factor (TNF)-α, IL-1β, and IL-6, which are primarily produced by innate immune cells, also play a role in CD [16, 43]. Increased amounts of these cytokines were detected in affected tissues from CD patients [44], and LP mononuclear cells (LPMCs) from CD patients produced more of these cytokines compared to LPMCs from control tissues [45]. Moreover, one commonly used drug for the treatment of CD is infliximab which targets TNF-α [16].

The Th1, Th2, and Th17 subsets are also referred to as effector $CD4^+$ T cells because they promote immune system activation in response to external stimuli [46]. A further subset of $CD4^+$ T cells are regulatory T cells. These lymphocytes play an important role in the maintenance of intestinal homeostasis through the production of the anti-inflammatory cytokine IL-10, which inhibits effector T cell responses to innocuous antigens, e.g. from the commensal microbiota [47]. The essential role of regulatory T cells for intestinal homeostasis is reflected by observations that mutations in genes from the IL-10 pathway increase susceptibility to develop CD or UC [48, 49]. Furthermore, *Il10* gene-deficient ($Il10^{-/-}$) mice, which do not produce any IL-10, develop spontaneous chronic enterocolitis [50].

The aetiology for CD is still unresolved, but both genetic and environmental factors appear to play a role in the development of the disease [51]. A genetic involvement for CD has been implicated by twin studies which showed that incidence was higher in monozygotic twins than in dizygotic twins [52, 53]. However, the concordance rate for monozygotic twins to develop CD ranged only from 25 % to 58 %, and the involvement of genetic factors alone could not explain the increased incidence of CD observed over the last half century [54]. Therefore, an environmental component seems to contribute to CD pathogenesis. Several environmental risk factors have been proposed over the years including diet, domestic hygiene in childhood, mycobacterial infection, oral contraceptives, smoking, and vaccination [13, 51]. Exogenous dietary particles have also been implicated in the development of CD (Section 1.5.1) [55, 56]. The gastrointestinal tract is constantly exposed to dietary antigens, so it seems likely that the diet is playing a role in CD development. However, studies that investigated the relationship between dietary factors, e.g. high intake of sugar, and CD risk have often yielded conflicting results [13, 57]. This could in turn be due to genetic factors that influence individual disease susceptibility.

1.2 The role of the microbial pattern recognition receptor NOD2 in Crohn's disease

Much progress has been made over the last two decades in the characterisation of genetic susceptibility to CD, and it has emerged that particularly mutations in the *NOD2* gene are associated with CD [58-60]. The NOD2 protein is an intracellular pattern recognition receptor (PRR) that specifically recognises a bacterial cell-wall component [61]. Since the discovery of the association between mutations in the *NOD2* gene and increased CD-susceptibility much research has been carried out to characterise the function of NOD2, which has been the subject of many reviews [62-65]. Of particular interest are its contribution to the maintenance of intestinal homeostasis and why mutations in this gene are associated with an increased risk to develop CD [66, 67]. Mouse models with defects in the *Nod2* gene have been created to investigate these questions.

1.2.1 Genetic susceptibility to Crohn's disease

Even though twin studies have shown that there is clearly a genetic component involved in CD they also indicated that CD must be a complex genetic disease. The concordance between monozygotic twins was approximately 60 % which indicated that CD associated genes are not inherited according to a Mendelian fashion [18, 53]. It is now known that more than 70 loci are associated with CD [68]. The region with the highest association was identified in 1996 on chromosome 16 [69]. At that time it was unknown which gene from that region was implicated in disease susceptibility, so the locus was referred to as IBD1. Some years later, the *NOD2* gene was identified on chromosome 16q12 [70]. Subsequently, it was shown that variants of *NOD2* were more prevalent in CD patients thus confirming *NOD2* as the IBD1 locus and as the first gene associated with CD [59, 60]. The most commonly observed single nucleotide polymorphism (SNP) in *NOD2* was a cytosine insertion at the nucleotide position 3,020. This SNP resulted in a frameshift mutation at amino acid position 1,007, and it caused the formation of a stop codon which led to the transcription of a NOD2 protein that lacked its last 33 amino acids. This *NOD2* allele was more common in CD patients compared to healthy controls and patients with UC, and the risk to develop CD was increased by 1.5-fold and 17.6-fold for hetero- and homozygous carriers, respectively [60].

Apart from the 1,007fs allele, many other SNPs have been identified in *NOD2*, but only some of them were associated with CD. In particular, there were two other common mutations that occurred with increased frequency in CD patients. Both of them are missense mutations and result in an amino acid change from either arginine to tryptophan at amino acid position 702, or glycine to arginine at amino acid position 908 [59, 60]. It has been calculated that the three most common *NOD2* variants together represented 81 % of the total CD-associated mutations [71]. Hugot and colleagues reported that there was a 3-fold increased risk to develop CD for heterozygous carriers of one of the three most common *NOD2* variant alleles. This risk was increased approximately 40 times for people with homozygous *NOD2* mutations [59].

Since the initial description of *NOD2* as the IBD1 locus, many other studies have replicated this finding, and variations in *NOD2* were consistently associated with CD in patients of Caucasian descent in Europe and North America [58, 71-75]. This has also been confirmed for CD patients from New Zealand [76]. It has been estimated that approximately 50 % of Caucasian CD patients carry at least one *NOD2* allele variant and that 17 % have homozygous *NOD2* mutations [59, 71]. Of note, in African American and Japanese CD patients the association between *NOD2* mutations and CD was much lower or not observed at all [77-79]. In addition, mutations in several other genes have been associated with CD, e.g. autophagy-related 16-like 1 (*ATG16L1*) and immunity-related GTPase family M, which are both involved in autophagy [72, 73], and IL-23 receptor, Janus kinase 2, signal transducer and activator of transcription 3, and IL-12 p40 subunit-encoding gene (*IL12B*), which are all part of the IL-23 signalling pathway [80, 81]. Variants of *ATG16L1* and IL-23 pathway genes, except *IL12B*, were also observed in CD patients in New Zealand [82-84].

Mutations in genes from the IL-23 pathway were shown to be also associated with UC [85], but overall the contribution of genetic factors to disease occurrence was lower in UC in comparison to CD [18]. However, the total number of genetic loci that were associated with IBD has recently been increased to 163, and most of these loci were associated with both CD and UC [86]. Nevertheless, mutations in *NOD2* were specifically associated with CD and never with UC [58-60, 71, 76, 85, 86]. Moreover, CD patients with *NOD2* mutations usually have an earlier age of onset for the disease, a more severe disease progression, and the ileum is more often affected compared to CD patients without variations in *NOD2* [71, 87]. To understand why the *NOD2* variant alleles are so strongly associated with CD

development, it is important to understand more about the function of the NOD2 protein in intestinal homeostasis.

1.2.2 Structure and function of NOD2

The NOD2 protein was discovered in 2001 by Ogura and co-workers [70]. It is structurally related to the NOD1 protein [88], and both belong to a bigger family of microbial PRRs called NOD-like receptors (NLRs). The NLR proteins all have similar tripartite structures with an amino-terminal effector domain, a central NOD, and a carboxy-terminal leucine-rich repeats domain for ligand recognition [89]. The effector domain in NOD2 consists of two caspase recruitment domains (CARDs), and the leucine-rich repeats domain is composed of ten repeats with 27 amino acids each [59, 60]. The NLR family currently comprises 22 proteins in humans and 33 proteins in mice including the frequently studied group of inflammasome proteins, e.g. NOD, leucine-rich repeats domain, and pyrin domain (NLRP) 1 and NLRP3 [90]. Another group of PRRs are the Toll-like receptors (TLRs), which were previously considered to be the main immune receptors of the innate immune system [91]. However, the importance of NLRs as innate immune receptors has now been recognised [92]. Similar to TLRs, NLRs recognise microbial-associated molecular patterns, e.g. bacterial cell wall fragments. Unlike TLRs, which are membrane-associated proteins and occur on the plasma membrane and on endo- or lysosomal vesicles [93], NLRs are localised in the cytoplasm [94].

Both NOD1 and NOD2 detect fragments of the bacterial cell wall molecule peptidoglycan (PGN). It has been shown that NOD1 recognises γ-D-glutamyl-meso-diaminopimelic acid, which is present almost exclusively in Gram-negative bacteria [88]. The ligand for NOD2 is *N*-acetyl muramic acid linked to L-alanine and D-glutamate, also known as muramyl dipeptide (MDP), which is part of the PGN from all bacteria [61, 95]. Recently it has been shown that MDP binds directly to NOD2 [96, 97]. Whereas NOD1 is expressed by many cell types, the expression of NOD2 is more limited. However, NOD2 is present in many cell types of the gastrointestinal tract especially in monocytes including macrophages and DCs [70, 95], but also in lymphocytes [98], epithelial cells [99], and Paneth cells [100].

There are several possibilities how PGN and its fragments can get access into these cells. First, invasive bacteria can enter cells directly. When the bacteria replicate within the cells, PGN fragments are released into the cytoplasm [101]. Furthermore, APCs can take up bacteria by phagocytosis and digest them in phagolysosomes, which then release MDP into the cytoplasm [102]. Pathogenic bacteria are also able to deliver PGN directly to the

cytoplasm through bacterial secretion systems [103] or with outer membrane vesicles in the case of Gram-negative bacteria [104, 105]. Finally, intracellular uptake of extracellular PGN fragments is possible through oligopeptide transporters that are located in the plasma membrane or in the endosome [106, 107], in which case the PGN fragments have to be taken up by endocytosis first [108, 109].

Regardless of the route of uptake, intracellular MDP can be recognised by NOD2 and activates the NOD2 signalling cascades. The best characterised NOD2 signalling pathway to date is the activation of nuclear factor (NF)-κB. Here, recognition of MDP by NOD2 leads to a conformational change and subsequent auto-oligomerisation of two NOD2 proteins [70, 110]. This results in the recruitment of the serine-threonine kinase receptor-interacting protein (RIP) 2 which also contains a CARD, and it binds to NOD2 through a CARD-CARD interaction [70, 111]. Subsequently, RIP2 promotes the polyubiquitylation of inhibitor of NF-κB (IκB) kinase γ which leads to the phosphorylation of IκB kinase β by the TGF-β-activated kinase 1 complex [112-115]. Following this, the IκB becomes phosphorylated and dissociates from NF-κB which allows NF-κB to translocate to the nucleus and initiate the transcription of pro-inflammatory cytokines and chemokines, as well as defensins [116, 117].

An alternative, but less well-characterised, NOD2 signalling pathway results in the activation of mitogen-activated protein kinases which are involved in the initiation of several cellular processes, including inflammation [114, 118]. Several studies have also investigated the regulation of the NOD2 signalling pathways, but so far results have been inconclusive and further research will be necessary to establish which factors influence NOD2 signalling [62].

1.2.3 Mouse models with *Nod2* gene modifications

After the identification of *NOD2* as the most important CD susceptibility gene, there has been much interest in the question of how mutations in *NOD2* can ultimately lead to the establishment of CD. To further investigate this question, three mouse models with a disrupted *Nod2* gene were created.

In the first model that was created the first exon in the *Nod2* gene, which encodes the start codon, the first CARD, and part of the second CARD, was deleted. This generated a complete gene knock-out, and mice that were *Nod2* gene-deficient ($Nod2^{-/-}$) consequently did not express the Nod2 protein [98]. It was observed that these $Nod2^{-/-}$ mice responded with an increased production of the Th1 cytokines IL-12 and IFN-γ to stimulation with PGN

or other TLR2 ligands [119]. Therefore, Watanabe and colleagues suggested that Nod2 functions as a negative regulator of the TLR2 signalling pathway, and the absence of Nod2 results in increased pro-inflammatory cytokine production mediated by unregulated NF-κB activation after TLR2 signalling. This finding was corroborated by two other studies from the same group. The authors demonstrated that *Nod2*$^{-/-}$ mice developed TLR2-mediated colitis after challenge with bacterial antigen [120], and MDP administration protected wild-type (WT) mice, but not *Nod2*$^{-/-}$ mice, from chemically-induced colitis by down-regulating TLR responses [121]. In contrast to these findings, other groups reported reduced production of cytokines, including IL-12, after co-stimulation of cells with homozygous *NOD2* mutations from CD patients with TLR ligands and MDP [122-124].

Macrophages from a second *Nod2*$^{-/-}$ mouse model also responded normally to TLR2 stimulation [125]. This *Nod2*$^{-/-}$ model was created by deleting the third exon of the *Nod2* gene which contains the second CARD and NOD. These *Nod2*$^{-/-}$ mice showed increased susceptibility to oral bacterial infection which was due to reduced expression of antimicrobial defensins by Paneth cells. This led to the speculation that intact NOD2 signalling is important for proper intestinal epithelial barrier function, and that mutations in *NOD2* could contribute to intestinal inflammation because of an increased bacterial burden. Support for this hypothesis came from observations that CD patients with homozygous *NOD2* mutations expressed reduced levels of α-defensin messenger ribonucleic acid (mRNA) in the ileal mucosa [126, 127]. However, this finding has been disputed by Simms and colleagues who found no decreased α-defensin expression in ileal tissue from CD patients with *NOD2* mutations [128]. Another study showed that *Nod2*$^{-/-}$ mice on a C57BL/6 background also had no increased antimicrobial defensin expression compared to C57BL/6 WT mice [129]. The loss of epithelial barrier function in CD might also be the result of impaired autophagy with a concomitant increase in intestinal bacterial burden. For example, it has been shown that CD-associated mutations in the autophagy gene *ATG16L1* led to a reduced bacterial clearance in human epithelial cells [130]. Discussions around the underlying mechanism aside, it is still unknown if a reduced epithelial barrier function is a cause or an effect of intestinal inflammation [64].

The third mouse model that has been used to investigate the role of Nod2 in intestinal inflammation differs from the other two models described above because it is not a complete gene knock-out model. Instead, this model has a mutation in the *Nod2* gene that is similar to the most common human CD-associated *NOD2* variant, the 1,007fs mutation [131]. Mice that were homozygous for this *Nod2* gene mutation (*Nod2*$^{m/m}$) expressed a Nod2 protein that

lacked the last 33 amino acids. These mice showed an increased production of IL-1β in response to MDP stimulation as a result of elevated NF-κB activity. Furthermore, the *Nod2*$^{m/m}$ mice were also more susceptible to dextran sodium sulphate (DSS)-induced colitis compared to WT mice, but co-administration of IL-1 receptor antagonist (IL-1Ra) with DSS led to amelioration of intestinal inflammation. Increased levels of IL-1β were also observed in the inflamed mucosa from patients with IBD [44, 132]. In contrast, *ex vivo* studies have shown that MDP-stimulated immune cells from CD patients with homozygous 1,007fs mutations did not secrete more IL-1β [133-136]. The truncated form of the human NOD2 protein was also unable to activate NF-κB *in vitro* and *ex vivo* which indicates a loss-of-function phenotype for this *NOD2* mutation [61, 95]. However, these results are in contrast to the observation that NF-κB activity is increased in CD patients [16]. Moreover, drugs that inhibited NF-κB activity showed promising results in initial clinical studies [137].

In summary, the mouse models with manipulated *Nod2* genes provided valuable, but somewhat conflicting, insights into the biological function of Nod2. They are important *in vivo* models to study the role of Nod2 both during intestinal homeostasis and inflammation. The *Nod2*$^{m/m}$ mouse model, in particular, provides an ideal tool to examine the role of dietary particles in a genetic background that is associated with the development of CD in humans.

1.3 Dietary particles in the gastrointestinal tract

There are two types of dietary particles that can be encountered in the gastrointestinal tract. They are referred to as endogenous and exogenous particles, respectively, based on their original source. As the name implies, endogenous particles are formed *de novo* in the small intestine. In contrast, exogenous particles are taken up orally, mainly with the diet. In the following three sections, these two types of dietary particles will be discussed in more detail, and potential mechanisms regarding their uptake in the gastrointestinal tract will be considered.

1.3.1 Endogenous dietary particles

Calcium and phosphate ions are important for physiological functions, especially for bone health. The absorption of these ions in the small intestine has been well documented, but it is not yet widely known that re-secretion of both ions also occurs in the jejunum and ileum [138]. This re-secretion leads to the formation of particulate calcium phosphate in the intestinal lumen. It has been shown that calcium phosphate particles made up more than

85 % of the total detectable inorganic particles in the small intestine of rats [139]. Endogenous calcium phosphate particles have also been identified in the intestinal lumen of dogs, mice and humans [140-142]. In mice and humans, the luminal particles varied in size from 50 nm to 500 nm [142]. In both mice and humans, calcium phosphate particles were also identified in the GALT of the small intestine, namely PPs [140, 142, 143]. However, the observed sizes of the particles in PPs differed between mice and humans. In mice, the calcium phosphate particle sizes ranged from 50 nm to 400 nm, but in humans the particles had diameters between 500 nm and 1,000 nm [142]. This discrepancy could be explained by the differences in detection methods. The particles in human PP tissues were identified by scanning electron microscopy (SEM) whereas those in PPs from mice were characterised by transmission electron microscopy (TEM). The latter method resulted in a higher resolution of the individual particles, and the larger size range obtained for the particles in human GALT was probably due to agglomeration which could not be resolved with SEM [142].

The term 'endogenous particles' was coined by Urbanski and colleagues who were the first to observe calcium phosphate in human PPs, but they did not describe their appearance and location within the GALT further [144]. This has been the subject of research by Powell and co-workers who showed that the calcium phosphate particles accumulated in phagocytic cells throughout the PPs, particularly in the SED area [142, 143]. It has also been shown that calcium phosphate particles can adsorb antigens from the intestinal lumen [145]. The co-localisation of calcium phosphate particles and adsorbed antigens has been confirmed in PPs from mice [142].

Whether this process of calcium phosphate particle formation in the lumen of the distal small intestinal tract, adsorption of luminal antigens, and uptake of this particle-antigen complex by phagocytic cells in PPs has any biological relevance is currently unknown [55]. This observation has nevertheless led to the generation of several hypotheses (Section 1.5.1). However, it is important to note that calcium phosphate particles are not the only particulate substances that occur in the small intestine. The gastrointestinal tract, at least of people from industrialised countries, is constantly exposed to two other types of inorganic nanometre- and/or micrometre-sized particles, namely TiO_2 and particulate silicates [55, 146]. Unlike calcium phosphate, these latter particles are not of endogenous origin and are consequently referred to as 'exogenous particles'. This term was also originally introduced by Urbanski and colleagues [144].

1.3.2 Exogenous dietary particles

Exogenous dietary particles were first detected in human PPs cells after histological sections of the ileum, which were removed from patients with various gastrointestinal diseases or *post mortem*, were examined by light microscopy [56]. The cells that contained the particles were described by Shepherd and co-workers as macrophages, but the authors did not perform any immunohistochemical analysis to confirm this statement. The particles, which were referred to as 'pigment' in this report because of their dark brown or black appearance under light microscopy, were granular and located in the cell cytoplasm. Particles were detected in PPs from adults and children from the age of six, but not in younger children. Pigmented cells were observed in 34 cases out of 42 cases examined (81 %), and particles were present irrespective of disease. The particles were further analysed with energy-dispersive X-ray spectroscopy (EDS) in a scanning electron microscope. The main elements detected were aluminium, silicon, and titanium. Furthermore, pigment-containing cells were also observed in several instances in MLNs. In two cases cells that contained particles were also found in submucosal lymphatics of the ileum. Shepherd and colleagues speculated that the pigment probably accumulated in PPs as a result of dietary intake because the same types of particles that were detected in the PPs were known to be frequently used as food additives. In addition, they were also a common component in pharmaceuticals and toothpaste.

Two years later, another paper also described the occurrence of 'pigment' in the LP of ileal biopsies [144]. Urbanski and colleagues detected pigment in PPs of all 14 examined cases. Some pigment was also observed in the submucosa, but in those cases it was closely associated with PPs. The pigment consisted of several types of particles as determined by EDS. Approximately one third were endogenous calcium phosphate particles (see Section 1.3.1). The other particles were characterised as silica and aluminium- or magnesium-rich silicates. Some pigment also contained titanium. The authors concluded that the non-calcium phosphate particles must be derived from the environment, and, as previously mentioned, therefore they referred to them as 'exogenous particles'. A small amount of particles also contained iron, but the authors could not identify their origin with certainty. Particles that resembled the exogenous pigment from the intestine were also detected in the lung in four cases in which additional autopsy specimen from the lung were available. These findings led the authors to speculate that the exogenous particles in PPs might be derived from atmospheric dust. Their hypothesis stated that the exogenous particles first accumulate in the lung through inhalation of particle-containing dust. In the lung, they

would be taken up by macrophages, and the particle-containing phagocytes would then be expectorated and swallowed. However, Urbanski and co-workers could not rule out the hypothesis put forward by Shepherd and co-workers that the particles were primarily derived from the diet [56]. Moreover, the authors agreed with Shepherd and co-workers that the accumulation of pigment in PPs indicated that it had to be taken up from the intestinal lumen, regardless of the original source. It should be noted that, as in the earlier study by Shepherd and colleagues the particle-containing cells were classified as macrophages, but no further explanation regarding the characterisation of these cells was given.

Several years later, Powell and colleagues characterised the exogenous particles in more detail [147]. The presence of exogenous particles in ileal PPs reported by Shepherd and colleagues and Urbanski and colleagues was confirmed with light microscopy. In addition, Powell and co-workers also observed particles in colonic lymphoid follicles. Detailed analysis with confocal microscopy and TEM showed that pigmented cells contained abundant amounts of particles in phagosomes within the cell cytoplasm. Three types of exogenous particles were detected by EDS. The first type was identified as TiO_2 particles with the anatase crystal shape and a diameter between 100 nm to 200 nm. This type of particles represented 29 % of the analysed exogenous material that was found in pigmented cells. The second type, which comprised 58 % of the analysed particles, was identified as aluminium-containing silicates with a flaky, crystalline shape and sizes from less than 100 nm up to 400 nm in length. Their morphology and chemical composition, especially of the larger particles, resembled the clay mineral kaolinite. Iron was often detected together with these particles, as well as group IA elements (sodium and potassium), and group IIA elements (magnesium and calcium). The third type was identified as mixed silicates to which 13 % of the total detected particles belonged. These particles consisted of silicon together with sodium, potassium, magnesium, and iron, but they did not contain aluminium. The particles had variable shapes and ranged in length from 100 nm to 700 nm. Powell and co-workers emphasised that oral intake was the most likely explanation for the observed accumulation in intestinal lymphoid tissues because, as already mentioned by Shepherd and colleagues, both TiO_2 particles and silicates were used as food additives or in pharmaceuticals. However, it was pointed out that silicates could also be taken up accidentally with food contaminated with soil or dust because silicates are the most common minerals of the earth's crust.

In processed foods synthetic silicates are used especially in powdered products as binders, desiccants, and anti-caking agents to prevent agglomeration and poor flow during processing [146, 147]. For example, they can be found in icing sugar, milk powder, chewing

gum, sliced or grated cheese, beverage whiteners, dry cereals, instant soup mixes, salt and seasonings [148, 149]. Silicate particles are also used in pharmaceuticals and toothpastes [150]. Silicates can usually be added at maximum levels of up to 1,000 mg/L or mg/kg, but in some instances also at *quantum satis* [148, 149]. On the other hand, they may also be present naturally in some cheeses as a result of the fermentation process [149]. On product labels particulate silicates are usually listed under their food additive numbers according to the International Numbering System for Food Additives [148]. This numbering system has been adopted by many countries worldwide, including New Zealand and Australia [151]. In Europe an 'E' for Europe precedes the otherwise identical international numbers [149]. The food additives that correspond to the exogenous silicate particles detected in PPs are sodium aluminosilicate with the food additive number 554, calcium aluminium silicate with the number 556, and aluminium silicate/kaolinite with the number 559 [146, 148, 149, 151].

Similar to particulate silicates, the other frequently detected type of exogenous material in PPs, TiO_2, is also frequently used as a food additive. The particulate form of TiO_2 has a high refractive index and this makes it an ideal whitening agent. Naturally, the use of TiO_2 as a food colourant for low fat milk and mozzarella cheese has been investigated [152, 153]. Although TiO_2 was not detected in milk-based products like mozzarella and cottage cheese in the UK [154], it has been reported that white dairy products in the USA routinely contained low amounts of TiO_2 [155].

Products that contain TiO_2 are required to indicate this on the product label either directly or using its assigned food additive number (171) [148, 151, 156]. It has, however, been shown that not all manufacturers comply with this requirement, and sometimes the presence of TiO_2 is not indicated on the ingredients lists [154, 155]. Foods which contain TiO_2 as a whitening agent include confectionery, salad dressings, and chewing gums [150, 154, 155]. The titanium levels in products investigated by Lomer and colleagues ranged from 0.001 % to 0.782 % [154]. Weir and co-workers showed that the titanium concentrations in the products that contained TiO_2 were between 1 ng/mg and 1,000 ng/mg which corresponded to the amounts detected by Lomer and colleagues [155].

In general, TiO_2 can be used as a food additive according to 'good manufacturing practice' or *quantum satis* [148, 149]. Examples for TiO_2-containing foodstuffs that are available in New Zealand supermarkets are given in Tables 1.1 and 1.2. Apart from processed foods, TiO_2 is also used as a whitening agent in pharmaceuticals and food supplements [150, 157]. Toothpastes have also been shown to contain TiO_2 particles [150, 155], and most toothpastes

Table 1.1 *Confectionery and other foodstuffs with TiO_2 available in New Zealand supermarkets.*

Brand	***Product***	***Brand***	***Product***
Allen's	Funfair thrills jelly beans	*Pascall*	Jaybees
	Kool mints		Party pack
Awesome Value	Jelly beans	*Queen - Quality*	Glitter writing gels
Cadbury	Pebbles	*Decorations*	Jungle icing decorations
	Mini drops	*Rainbow*	Frighteners mix
Chupa Chups	Chuck lollipops		Kiwi summer mix
	Cremosa	*Regina*	Kiwi party mix
	Twice	*Skittles*	Fruity
Dollar Sweets	Choc minis		Sours
	Mini baking beans		Wild berry
Jelly Belly	20 assorted flavours	*Starburst*	Party mix
	Assorted flavours	*Tasti*	Milkies choc strawberry
	Citrus mix		Milkies choc vanilla
	Fruit bowl		Muffin bakes double white choc
	Ice cream parlour mix	*WeightWatchers*	Custard & apple
	Sours		Coconut delight indulgent bar
M&M's	Crispy	*Woolworths home brand*	Jelly beans
	Milk chocolate	*Woolworths select*	Fruit bars custard & apple
	Minis		Fruit bars custard & blueberry
	Mix ups	*Wrigley's*	Eclipse chewy mints fruit trio
	Peanuts		Eclipse chewy mints peppermint
	Raspberry flavour		Eclipse chewy mints spearmint
Mentos	Aqua kiss 3D strawberry-green apple-raspberry		Eclipse chewy mints strawberry & watermelon
	Pure fresh fresh mint		Eclipse ice peppermint
	Pure fresh spearmint		Eclipse ice spearmint
Nestlé	Smarties		Extra active citrus
Oki-Doki	Discobits bars		Extra active peppermint
Pam's	Party mix		Extra active spearmint
Old El Paso	Jumbo tortillas		Extra professional spearmint
	Light tortillas		Extra professional strongmint
	Tortillas		Extra professional white lemon lime
	Wholegrain tortillas		Extra professional white peppermint

As of May 2014 at Pak'n save, 327 Ferguson St, Palmerston North, and Countdown, Corner Ferguson St and Ashley St, Palmerston North.

Table 1.2 *Mayonnaises and white dressings with (highlighted in red) or without TiO_2 available in New Zealand supermarkets.*

Brand	***Product***	***TiO_2***	***Brand***	***Product***	***TiO_2***
Alfa One	Creamy mayo	no	*Eta (continued)*	Sour cream & chives dressing	no
	Lite mayonnaise	no		Traditional salad dressing	no
	Real mayonnaise	no		Yoghurt & garlic dressing	no
Best Foods	Light mayonnaise	no	*Heinz*	Mayonnaise	yes
	Real mayonnaise	no		Original sandwich spread	no
Budget	Salad dressing	no		Salad cream	yes
Dukes	Real mayonnaise	no		Salad cream original	no
Edmonds	Coleslaw	no		S. g.[2] dijonnaise	no
	Light mayonnaise	no		S. g. dressing NZ honey & 3 mustards	no
	Mayonnaise	no		S. g. dressing parmesan Caesar	no
	Ranch	no		S. g. dressing ranch	no
Eta	Caesar dressing	no		S. g. mayonnaise	no
	Coleslaw dressing	no		S. g. mayonnaise lite	no
	Condensed milk-style dressing	no		S. g. tartare	no
	Garlic mayonnaise	no	*Hellman's*	Real mayonnaise	no
	Greek-style feta dressing	no	*Pam's*	Classic mayonnaise American style	no
	Greek-style yoghurt dressing	no		Coleslaw dressing	no
	Honey mustard mayonnaise	no		Honey mustard	no
	Kiwi-style onion mayonnaise	no		Hollandaise	no
	Lite & free feta & garlic dressing	yes		Mayonnaise	no
	Lite & free honey mustard dressing	no		Potato salad	no
	Lite & free mayonnaise	yes		Salad dressing	no
	Lite & free potato salad dressing	yes		Tartare sauce	no
	Lite & free ranch dressing	yes	*Paul Newman's Own*	Creamy Caesar	no
	Lite & free salad dressing	yes		Light honey & mustard	no
	Lite & free tartare sauce	yes		Ranch	no
	Mayonnaise	no	*WeightWatchers*	Honey & mustard dressing	yes
	Potato salad dressing	no	*Woolworths homebrand*	Mayonnaise	yes
	Ranch dressing	no		Potato salad dressing	no

As of May 2014 at Pak'n save, 327 Ferguson St, Palmerston North, and Countdown, Corner Ferguson St and Ashley St, Palmerston North. [2]Abbreviations specific for this table: S. g. = "Seriously good".

available in supermarkets in New Zealand contain TiO_2 (Table 1.3). The European Food Safety Authority estimated that the daily TiO_2 intake with medicinal products, food supplement tablets, and confectionary could be as high as 1.3 mg/kg body weight, but it was pointed out that this was probably an over-estimation [157].

Assessing the intake of exogenous particles was also the subject of another study by Lomer and colleagues. It was estimated that the individual median daily intakes were 2.5 mg/d for TiO_2 and 35 mg/d for aluminium-containing silicates [150]. This confirmed the results from a previous report in which the average daily intakes per person had been estimated to be 5.4 mg for TiO_2 and 32.3 mg for particulate silicates [158]. These estimated intakes for exogenous dietary particles were similar for patients with CD and healthy controls [150]. Weir and colleagues modelled the average daily TiO_2 intake for the USA based on their results on TiO_2-containing products [155]. They concluded that children under the age of ten would ingest 1 mg/kg to 2 mg/kg body weight, and that the TiO_2 intake would be lower for teenagers and adults with approximately 0.2 mg/kg to 0.7 mg/kg body weight.

It should be noted that the regulation concerning the use of aluminium-containing food additives for the European Union has recently been modified, and from 1 February 2014 the use of the aluminium-containing silicates E 554, E 556 and E 559 as food additives is not allowed anymore in the European Union [159]. There is an exception for E 554 which can still be used in concentrations of up to 20 mg/kg for the surface treatment of ripened cheese [159]. The reason for this new regulation on aluminium-containing silicates was a recommendation by the European Food Safety Authority to reduce the weekly intake for aluminium to 1 mg/kg body weight. Silicates that do not contain aluminium (E 551 to E 553) are considered to be suitable anti-caking agent replacements for the aluminium-containing silicates. This food regulation has not yet been officially adopted by New Zealand and Australia, but it seems that most manufactures are not using aluminium-containing silicates as food additives in products that require anti-caking agents. In fact, during the investigations for products that contain exogenous dietary particles it was discovered that none of the products that listed anti-caking agents on their product labels contained the food additives 554, 556, or 559. Instead, the most frequently used anti-caking agent was silicon dioxide with the food additive number 551. Therefore, it seems that New Zealanders are not exposed to aluminium-containing silicates with the diet through the consumption of processed foods.

Table 1.3 *Toothpastes with (highlighted in red) or without TiO_2 available in New Zealand supermarkets.*

Brand	***Product***	***TiO_2***	***Brand***	***Product***	***TiO_2***
AIM	Freshmint	yes	*Macleans*	Extreme clean	yes
Colgate	Advanced whitening	yes	*(continued)*	High definition white illuminating mint	yes
	Advanced whitening tartar control	yes		High definition white tingling mint	yes
	Cavity protection	no		Big teeth[5]	yes
	Cavity protection cool mint	no		Little teeth[6]	yes
	Cavity protection sparkling mint gel[2]	yes		Milk teeth[7]	yes
	Dora the explorer[3]	yes		Protect freshmint	yes
	Maximum cavity protection clean mint	yes		Protect mildmint	yes
	Maximum cavity protection fresh mint	yes		Sensitive fresh mint	yes
	MaxFresh	yes	*Mouthfresh*	Cool mint	yes
	MaxWhite crystal mint	yes		Extra mint	yes
	MaxWhite one ice	yes		Fresh mint gel	yes
	My first mild mint gel[4]	no		Ice mint gel	yes
	Optic white	no	*Parodontax*	Daily fluoride toothpaste	no
	Optic white enamel white	no	*Pearl Drops*	Extra white	yes
	Total advanced clean	yes	*Pronamel*	Gentle whitening	yes
	Total advanced fresh	no	*Red Seal*	Herbal	no
	Total advanced whitening	yes		Kids[3]	no
	Total mint stripe	yes		Natural	no
	Total original	yes		Smokers	no
	Triple action original mint	yes	*Sensodyne*	Daily care	yes
	Sensitive enamel protect	yes		Daily care gel	no
	Sensitive multi protection	yes		Daily care and whitening	yes
	Sensitive pro-relief	yes		Fresh impact	no
	Sensitive pro-relief and whitening	yes		Gentle whitening	yes
	Sensitive whitening	yes		Rapid relief	yes
	Whitening	yes	*White Glo*	Express whitening system	yes
Macleans	Advance freshmint	yes		Extra strength whitening toothpaste	yes
	Advance mildmint	yes			

As of May 2014 at Pak'n save, 327 Ferguson St, Palmerston North and Countdown, Corner Ferguson St and Ashley St, Palmerston North. [2]For children from 6 years. [3]Age not specified. [4]For children up to 6 years. [5]For children from 7 years. [6]For children from 4 years to 6 years. [7]For children up to 3 years.

As mentioned earlier, the initial studies in which particle-containing cells were identified in PPs mentioned that the cell type that contained the particles were macrophages [56, 144, 160]. According to these studies this was indicated by the morphology of the cells which was investigated microscopically. The first study that investigated the cell phenotype with immunohistochemistry was carried out by Powell and co-workers [161]. In this report it was shown that particle-containing cells stained positive for CD68, which is a marker for mature macrophages. This was later confirmed in another study that investigated the phenotype and activation state of pigmented PP cells in more detail with immunohistochemistry and immunofluorescence [162]. Tissue was obtained from patients with CD, UC, non-IBD colitis and adenocarcinoma, and pigment-containing cells were present in 45 % of the investigated specimen. The presence of exogenous particles was not correlated with any disease type. Around 80 % of the pigmented cells expressed CD68, a marker for mature macrophages. Most of the remaining cells with exogenous particles stained positively for MAC387, a marker for less mature macrophages. Although approximately half of the cells from all investigated specimens were positive for the activation marker human leukocyte antigen-DR, no expression of the co-stimulatory molecule CD86 was observed. This indicated that the cells had low immunological activity. The cell phenotype of particle-containing cells was not influenced by disease type or the degree of inflammation, i.e. even in tissues that showed signs of inflammation the particle-containing cells appeared inactive. Within the cells, the protease cathepsin D was not detected in most of the lysosomes that contained particles. The absence of this enzyme in the majority of the lysosomes indicated that the cells were metabolically inactive.

Taken together, the studies discussed in this section showed that exogenous particles were present in GALT, and the most likely source of these particles were food additives. The exogenous particle-containing cells have been identified as phagocytes, in particular macrophages, and they were observed predominantly at the base of PPs.

1.3.3 Particle uptake across the intestinal epithelium

Several pathways exist for dietary particles to gain access to the intestinal mucosa. Four main mechanisms have been reviewed by Powell and co-workers [163].

One mechanism is particle uptake by enterocytes *via* endocytosis. This pathway is probably only relevant for particles in the lower nanometre range like ferritin [164]. Ferritin is a 12 nm small structure which contains an iron oxide core and occurs naturally in meat and plants. It has been shown that ferritin is taken up *via* endocytosis by intestinal epithelial cells, and

utilised as a dietary iron source by these cells. However, enterocytes can also take up particles with sizes of around 2 μm *in vitro* [165].

Another process has been called paracellular transcytosis because here particles are not taken up by enterocytes but instead cross the intestinal epithelium between adjacent cells. Until recently, this has only been a theoretical route because under normal conditions tight junctions between enterocytes ensure the intestinal epithelial barrier is impermeable to insoluble luminal antigens [166, 167]. However, as will be discussed below, Awaad and co-workers observed paracellular transport of particles between enterocytes of the FAE [168].

A third possible mechanism for particles to cross the intestinal epithelium is persorption through which particles gain access to the intestinal mucosa through gaps in the epithelium. These gaps form at the tips of villi after enterocytes have been shed into the intestinal lumen during the normal regeneration process of the intestinal epithelium. The concept of persorption has been established nearly 40 years ago for the uptake of organic material in the micrometre size range, like starch and pollen [169]. Since then, only one further study has confirmed uptake of particles in the intestine *via* this process [170]. Therefore, its physiological relevance remains unknown and disputable.

Finally, particles can be transported across the intestinal epithelium *via* M cells in the FAE. Transcytosis of luminal antigens through M cells and the subsequent uptake of these antigens by PP immune cells is an important process for the maintenance of intestinal homeostasis [171]. It seems that this transport is non-specific and a common route for particulate substances, including TiO_2 [172], to gain access to the intestinal mucosa. This process has been well documented in several studies for different types and sizes of particles [165, 173-178].

In a recent report, Awaad and colleagues described two additional pathways for particle uptake across intestinal epithelium of mice [168]. Using fluorescent thiol-organosilica particles with different sizes from 95 nm to 1,050 nm the authors observed that, apart from the classical uptake route *via* M cells, some particles were also taken up by enterocytes in the FAE. Other particles were shown to pass between adjacent enterocytes of the FAE similar to the paracellular uptake route reported above. These results still need to be confirmed with other types of particles and with PPs from different animal models. However, these new findings indicate that there might be more uptake routes for particulate luminal antigens into PPs apart from the commonly recognised M cell transport.

Another potential mechanism for particle uptake across intestinal epithelium is the direct sampling of luminal antigens by mucosal phagocytes. These cells, which are now generally considered as macrophages after they were initially classified as DCs [11, 179], reside in the LP in close proximity to enterocytes. They are able to form dendrites which can extend across the epithelium and sample bacteria from the intestinal lumen [180]. These macrophages express tight junction proteins to preserve the integrity of the epithelial barrier during the process. Typical for these phagocytes is a high expression of the cell surface CX_3C chemokine receptor (CX_3CR) 1 [181]. Interestingly, Lelouard and co-workers also identified lysozyme-expressing CX_3CR1^+ phagocytes in the SED of PPs [182, 183]. These cells, which had the highest phagocytic activity of all PP phagocytes, were efficient in taking up fluorescent particles with a diameter of 400 nm *in vitro* [182]. Similarly to CX_3CR1^+ macrophages in the LP, the PP CX_3CR1^+ cells were located directly beneath the epithelial layer. It was observed that they extended dendrites across the FAE through specific pores in M cells. This allowed these phagocytes to take up antigens, including fluorescent particles with a size of 500 nm, from the intestinal lumen *in vivo* [183]. The authors speculated that an advantage of this direct sampling mechanism lies in the protection of M cells from potentially harmful luminal antigens, or it could also provide a quicker way to initiate mucosal immune responses [183]. However, the physiological importance of non-specific antigen sampling by phagocytes that extend dendrites across the intestinal epithelium *in vivo* has been disputed [11, 179]. It has been shown that the absence of transepithelial dendrites did not impair pathogen uptake across the intestinal epithelium [184]. Therefore, M cell-mediated uptake is still considered to be the most important route for luminal antigens to gain access to the intestinal mucosa.

A number of possibilities have been discussed in this section that allow the uptake of luminal antigens by intestinal cells. The focus of the following sections will be to review the currently known biological consequences when intestinal cells or animals, including humans, are exposed to exogenous dietary particles.

1.4 Effects of titanium dioxide on cultured cells, animal models, and humans

With the advances in nanoscience and nanotechnology in recent years, there has also been an increased interest to investigate effects of nanoparticles and microparticles *in vitro* and *in vivo*. The term 'nanoparticle' usually refers to particles with a size below 100 nm whereas

'microparticles' have a diameter between 100 nm and 1,000 nm [163]. According to these rather arbitrary definitions, dietary particles would mostly be classified as microparticles. However, some of the particles observed in human PPs had diameters below 100 nm [147]. Therefore, in this dissertation the general term 'particles' will be used to avoid confusion. As previously mentioned (Section 1.3.2), dietary exposure to exogenous particles in New Zealand occurs mostly in the form of TiO_2. Thus, the following sections will specifically focus on studies that investigated the effects of TiO_2 particles.

1.4.1 Effects of titanium dioxide on intestinal and macrophage-like cell lines

Although many published reports investigated the effects of TiO_2 particles on mammalian cultured cells, only a few studies have reported this in intestinal cell lines [185]. An overview of these studies is presented in Table 1.4.

The study by de Berardis and colleagues showed that TiO_2 particles with a size and crystal structure that are similar to dietary TiO_2 did not inhibit cell growth and were not cytotoxic after incubation for 24 h even in high concentrations. No increased secretion of the pro-inflammatory cytokines IL-6 and TNF-α was detected, but there was an increased release of the pro-inflammatory chemokine IL-8 after incubation with 5 $\mu g/cm^2$ TiO_2 for 24 h [186].

Another study showed that TiO_2 particles with an average primary particle size below 100 nm were cytotoxic at low concentrations of 20 $\mu g/cm^2$ to Caco-2 cells, another colon carcinoma cell line [187]. However, TiO_2 particles with diameters up to 300 nm were only cytotoxic at high concentrations of 80 $\mu g/cm^2$ after stimulation with the particles for 4 h. These types of particles did not induce damage to the deoxyribonucleic acid (DNA) when genotoxicity was investigated in the dark because of the photocatalytic activities of TiO_2. The TiO_2 nanoparticles also did not induce oxidative stress. These results showed that not only exposure time and concentration but also particle size affected TiO_2 cytotoxicity to Caco-2 cells. To investigate this observation further, the same group compared the cytotoxic and genotoxic effects of several different types of TiO_2 particles in a separate study [188]. All particle types, except anatase TiO_2 with an average crystal size of 215 nm, were cytotoxic to Caco-2 cells, at least after exposure to 80 μg/mL particles for 24 h. As demonstrated in the previous study, cytotoxicity increased with increasing particle concentration for all investigated types of TiO_2 particles, but none of the particle types induced DNA damage or oxidative stress.

Table 1.4 *Summary of studies that investigated effects of TiO_2 particles on cultured human cell lines.*

Cell type	***Cell line***	***Particle type***	***Particle size (nm)[1]***	***TiO_2 concentration***	***Time (h)***	***Investigated effects***	***Cytokines analysed***	***Reference***
Colon carcinoma	Caco-2	Anatase Anatase/rutile	40-300[2] 20-80[2]	5-80 μg/cm^2	4, 24	Cytotoxicity, genotoxicity, oxidative stress	n/a[8]	[187]
	Caco-2	Anatase Anatase Anatase Anatase/rutile Anatase/rutile	215[3] 7[3] 4[4] 25[4] 22[4]	10-160 μg/cm^2	4, 24	Cytotoxicity, genotoxicity, gene expression, oxidative stress	n/a	[188]
	Caco-2	Anatase/rutile	< 40[2], 220[5], > 500[6]	1-1000 μg/mL	24, time course	Cytotoxicity, particle uptake, TEER[7]	n/a	[189]
	LoVo	n/a	319[4]	1-40 μg/cm^2	24, 48, 72	Cell growth, cytokine release, cytotoxicity, oxidative stress[7]	IL-6, IL-8, TNF-α	[186]
	LS174T	n/a	21[5]	200-1000 μg/cm^2	24	Cytotoxicity[7]	n/a	[190]

(Continued on next page)

Table 1.4 *Summary of studies that investigated effects of TiO_2 particles on cultured human cell lines (continued).*

Cell type	***Cell line***	***Particle type***	***Particle size (nm)[1]***	***TiO_2 concentration***	***Time (h)***	***Investigated effects***	***Cytokines analysed***	***Reference***
Macrophage-like	THP-1	Anatase Anatase Anatase Rutile Rutile Rutile	< 50,000[2] < 25[2] 10[2] < 5,000[2] 30-40[2] 10 × 40[2]	20-500 μg/mL	24	Cytokine release, particle uptake[7]	IL-1β, TNF-α	[191]
	THP-1	Anatase Anatase/rutile	28[4], 292[5] 24[4], 209[5]	20-120 μg/mL	24	Cytokine release, cytotoxicity	IL-1β	[192]
	U937	n/a	70[2]	80 μg/mL	24	Cytokine release, cytotoxicity, gene expression	IL-1β, IL-1Ra, TNF-α	[193]

[1]Average size or size range. [2]Particle size according to manufacturer. [3]Particle size determined by X-ray diffraction. [4]Particle size determined by TEM. [5]Particle size determined by dynamic light scattering with particles suspended in water. [6]Particle size determined by dynamic light scattering with particles suspended in culture medium. [7]Amongst other investigated effects. [8]Abbreviations specific for this table: n/a = not applicable or data not available.

In another study with Caco-2 cells, Koeneman and colleagues investigated whether exposure to TiO_2 particles could affect intestinal barrier function [189]. Confluent Caco-2 cells are a model cell line for the human intestinal barrier because they express tight and adherence junction proteins, like enterocytes *in vivo*. A common *in vitro* assessment of epithelial integrity is the transepithelial electrical resistance assay. Koeneman and colleagues reported that incubation of Caco-2 cells with TiO_2 particles did not affect epithelial integrity and occurrence of adherence junctions between the cells even at high concentrations of 1,000 μg/mL. Some TiO_2 particles were, however, taken up by a small number of cells through transcytosis after 24 h exposure to TiO_2. This did not affect cell viability.

The cytotoxic effects of TiO_2 nanoparticles with an average size of 20 nm were also investigated in a third human colon carcinoma cell line, namely LS174T [190]. In accordance to the previously mentioned studies, the particles were not cytotoxic even after exposure to high concentrations of 1,000 μg/mL. Unfortunately, the particle characterisation was relatively poor, especially considering that the TiO_2 particles were specifically manufactured and not purchased from a commercial supplier.

Although a number of, mostly toxicological, studies have been conducted with TiO_2 particles and different cell lines, the results from these studies most likely cannot be applied to intestinal epithelial cells. It has been pointed out that enterocytes are generally less responsive to exogenous stimuli [163]. More research with intestinal-derived cell lines is required to examine the responses of enterocytes to TiO_2 particles in more detail. It is also important to note that intestinal uptake of exogenous dietary particles is not limited to intestinal epithelial cells. As mentioned earlier (Section 1.3.2), exogenous particles were in fact almost exclusively observed in macrophages in human GALT [147, 162]. Thus, the effects of TiO_2 particles on these cells need to be considered [163].

The effects of TiO_2 particles on macrophage-like cell lines have been more extensively studied than interactions between TiO_2 particles and intestinal cell lines (see Table 1.5.). This is mainly due to the interest in particle uptake by alveolar macrophages after lung exposure to TiO_2, and TiO_2 particle effects on lung cells have received the most attention of all cell types used for *in vitro* studies [185]. In the following paragraphs these studies with alveolar macrophages have not been included, and only studies with other types of macrophage-like cell lines, which can be considered as models for intestinal macrophages, will be discussed.

One study that looked at the effects of TiO_2 on phagocytic cells was conducted with a cell line derived from human monocytes, namely THP-1 [191]. These cells can be differentiated

Table 1.5 *Summary of studies that investigated effects of TiO_2 particles on cultured murine cell lines.*

Cell type	*Cell line*	*Particle type*	*Particle size (nm)*[1]	*TiO_2 concentration*	*Time (h)*	*Investigated effects*	*Cytokines analysed*	*Reference*
Macrophage-like	Ana-1	Anatase Anatase Anatase Rutile	100[2], 98[3] 25[2], 21[3] 5[2], 12[3] 100[2], 148[3]	12.5-600 μg/mL	24	Cytotoxicity, oxidative stress	n/a[8]	[194]
	J774A.1	n/a n/a	220[2] 20[2]	100 μg/mL	24	Cytotoxicity, phagocytosis[7]	n/a	[195]
	RAW264.7	Anatase/rutile	40[2]	50 μg/mL	3	Cytokine release[7]	TNF-α	[196]
	RAW264.7	Rutile/anatase	30-40[2]	30-300 μg/mL	24	Cytokine release, cytotoxicity, gene expression[7]	IL-1β, MIP-1α, TNF-α	[197]
	RAW264.7	Anatase	5-10[2], 350-500[4], 200-400[5]	10-1000 μg/mL	3, 4, 20, 24	Cytotoxicity, oxidative stress, particle uptake[7]	n/a	[198]
	RAW264.7	Anatase Anatase/rutile	40-300[2] 20-80[2]	1-80 μg/cm^2	4, 24	Cytotoxicity[7]	n/a	[199]

(Continued on next page)

Table 1.5 *Summary of studies that investigated effects of TiO_2 particles on cultured murine cell lines (continued).*

Cell type	***Cell line***	***Particle type***	***Particle size (nm)[1]***	***TiO_2 concentration***	***Time (h)***	***Investigated effects***	***Cytokines analysed***	***Reference***
Macrophage-like	RAW264.7	Anatase/rutile	20-30[2], 175[4], 364[6]	10 μg/mL	6, 16	Cytokine release, cytotoxicity, oxidative stress, particle uptake[7]	TNF-α	[200]
	RAW264.7	Anatase Anatase Anatase/rutile	100[2], 444[4], 349[6] 10[2], 262[4], 669[6] 20[2], 338[4], 307[6]	10-300 μg/mL	24	Cytokine release, cytotoxicity, oxidative stress	TNF-α	[201]

[1]Average size or size range. [2]Particle size according to manufacturer. [3]Particle size determined by TEM. [4]Particle size determined by dynamic light scattering with particles suspended in culture medium. [5]Particle size determined by dynamic light scattering with particles suspended in saline. [6]Particle size determined by dynamic light scattering with particles suspended in water. [7]Amongst other investigated effects. [8]Abbreviations specific for this table: n/a = not applicable or data not available.

into macrophage-like cells with phorbol myristate acetate. The secretion of IL-1β by the differentiated macrophages was compared after treatment with several forms of TiO_2 particles. Analysis with microscopy showed that all TiO_2 particle types were taken up by the macrophages to a similar extent. Interestingly, the TiO_2 particles with anatase crystal structure induced less IL-1β release at lower concentration compared to rutile forms. Anatase TiO_2 particles only induced IL-1β secretion at higher concentrations. Other effects of TiO_2 particles on the differentiated THP-1 cells, e.g. cytotoxicity, were not investigated.

A problem with *in vitro* studies that investigate effects of TiO_2 is the lack of standardised testing procedures. This means that different laboratories often use different protocols to assess common effects that are investigated in toxicological studies, e.g. cytotoxicity. This lack of standardisation makes it difficult to compare reported results. A recent study addressed this problem by investigating the cytotoxicity of several nanomaterials, including two crystalline forms of TiO_2, according to a standardised protocol [192]. The release of IL-1β after particle stimulation was also assessed. Eight different laboratories across the USA took part in this project, and they used differentiated THP-1 cells as a model for human phagocytic cells. The results showed that both forms of TiO_2 neither caused cytotoxicity nor led to an increase in IL-1β secretion by the cultured macrophages. The inflammatory response of differentiated U-937 cells, another human macrophage-like cell line, to TiO_2 particles with sizes from 20 nm to 160 nm has also been investigated [193]. Initial tests for metabolic activity and cell membrane integrity showed that TiO_2 particles were not cytotoxic to U-937 cells, even at relatively high concentrations. Exposure to TiO_2 particles for 24 h induced up-regulation of the PRR genes *TLR7* and *TLR10*. However, the secretion of pro-inflammatory cytokines, including IL-1β, was not increased after TiO_2 stimulation.

At present, only a few studies have investigated the effects of TiO_2 stimulation of human macrophages *in vitro*. There are, however, several studies that investigated responses of murine macrophages after TiO_2 exposure. For example, a recent study investigated cytotoxicity and oxidative stress induced by four different types of TiO_2 particles on Ana-1 cells, an immortalised murine macrophage cell line from C57BL/6 WT bone marrow cells [194]. The three anatase TiO_2 types with different crystal sizes and the one type of rutile particles investigated all showed increasingly cytotoxic effects with increasing concentrations from concentrations as low as 25 μg/mL. However, cell membrane damage only occurred at concentrations of 200 μg/mL and above. The amount of intracellular reactive oxygen species (ROS), a measure for oxidative stress, also increased with increasing particle

concentrations for all types of TiO_2 crystals. These results suggested that TiO_2 particles have the capacity to cause cell damage regardless of particle type.

Cytotoxicity after TiO_2 exposure was also studied in J774A.1 cells, another murine macrophage cell line [195]. Incubation with TiO_2 particles with a mean diameter of 220 nm (according to the manufacturer) decreased cell viability by approximately 5 % compared to untreated control cells. When the macrophages were incubated with TiO_2 particles with a mean size of 20 nm, the cell viability dropped by nearly 20 %. Both types of particles decreased the phagocytic yield which was measured by studying the uptake of fluorescently labelled 1 μm latex beads with flow cytometry. The phagocytic uptake of the TiO_2 was not investigated.

However, another group has shown that another murine macrophage cell line, namely RAW264.7 cells, avidly took up TiO_2 particles after only 3 h incubation [198]. Anatase TiO_2 particles with a size range from 350 nm to 500 nm in tissue culture medium (TCM) were used to investigate cytotoxic effects amongst other cellular effects. Cell viability was negatively affected by either increased TiO_2 concentration at the same exposure time or increased exposure time at the same TiO_2 concentration. Incubation with a TiO_2 suspension of 100 μg/mL also induced apoptosis.

Several other researchers have also used RAW264.7 cells for studying the impact of TiO_2 particles on phagocytic cells. For example, Wilhelmi and co-workers investigated the cytotoxicity of two types of TiO_2 particles with this cell line [199]. Using several carefully conducted cytotoxicity assays, they found that both types of TiO_2 particles did not affect cell viability. This was also the case even at relatively high TiO_2 concentrations. These observations have been confirmed in another recent study. Xiong and colleagues reported that the cytotoxicity of TiO_2 particles was low for RAW264.7 macrophages, but TiO_2 particles with an average size of 260 nm in TCM were more cytotoxic than TiO_2 particles with a diameter of around 450 nm in TCM at a concentration of 300 μg TiO_2/mL [201]. However, all forms of TiO_2 particles induced TNF-α secretion by the macrophages. This increased cytokine secretion was positively correlated with increased particle concentration for all three types of TiO_2 particles. The highest concentration of TNF-α could be detected in supernatants from cells incubated with TiO_2 particles that had an average size of 260 nm in TCM at concentrations of 100 μg/mL and above.

TNF-α secretion after TiO_2 stimulation of RAW264.7 macrophages was also determined in two other studies. Incubation with 40 nm TiO_2 particles at a dose of 50 μg/mL for 3 h

increased TNF-α secretion by approximately 70 % compared to untreated control cells [196]. In contrast, no TNF-α release was detected in another study after 6 h exposure to 10 μg/mL TiO_2 particles with an average size of 175 nm in TCM [200]. Cell viability after 16 h stimulation with the particles was also not affected. Interestingly, the study by Xia and colleagues also showed that although TiO_2 particles induced ROS under abiotic conditions they did not lead to oxidative stress in cells. The authors pointed out that TiO_2 had a high photocatalytic activity under illumination, but TiO_2 particles did not show this activity in the dark.

The effects of TiO_2 stimulation on cytokine secretion are frequently investigated *in vitro*, but so far there has been only one study that also investigated cytokine gene expression changes in response to TiO_2 [197]. Most cytokine genes investigated by Palomäki and colleagues, including IL-1β and IL-12p40, were not affected by TiO_2 exposure. However, mRNA levels of the pro-inflammatory cytokines IL-6 and TNF-α, as well as the pro-inflammatory chemokine macrophage inflammatory protein (MIP)-1α, which is also known as CC chemokine ligand (CCL) 3, were increased after TiO_2 stimulation of RAW264.7 macrophages. In addition, the concentrations of TNF-α and MIP-1α in the supernatants were also elevated after TiO_2 exposure. The secretion of IL-1β was also determined, but no increased amounts of IL-1β were detected in the supernatants of TiO_2 stimulated RAW264.7 macrophages. As far as the literature search for this dissertation has shown, the study by Palomäki and co-workers is the first one that links TiO_2 exposure of phagocytic cells to both elevated gene expression and increased secretion of pro-inflammatory cytokines. Furthermore, of the several different kinds of nanomaterials investigated, only TiO_2 or TiO_2-silica particles induced secretion of TNF-α.

In summary, it can be stated that understanding responses to TiO_2 *in vitro* is currently an active field of research, but that it is difficult to draw conclusions because of contradictory results (Table 1.6). What has emerged from these studies is, however, that observed effects of TiO_2 strongly depend on particle type, particle size, cell type used, concentration of the particle suspensions, and exposure time of the cells to the particles. Although the results from the studies discussed in this part are difficult to compare, these reports are nevertheless useful for designing future *in vitro* TiO_2 exposure studies.

First, it is important to characterise the particles both in their original form and after suspension in TCM. Some studies only reported the primary particle sizes provided by the manufacturer [187]. Studies that additionally analysed the particle sizes after suspension in water and/or TCM showed that particle sizes in suspensions can be different from primary

Table 1.6 *Studies that investigated TiO_2 particle exposure on intestinal and phagocytic cell lines and their reported effects.*

Investigated effect on cells	***Reference that reported an increase in the studied effect after TiO_2 stimulation***	***References that reported no change in the studied effect after TiO_2 stimulation***
Cytokine release		
- IL-1β	[191]	[192] [193]
- TNF-a	[196] [197] [201]	[186] [193] [200]
Cytotoxicity	[186] [187] [188][1] [194] [195] [197] [198]	[188][2] [189] [190] [192] [193] [199] [200] [201]
Oxidative stress	[194] [198]	[186] [187] [188] [200]

[1]For anatase or mixed anatase/rutile TiO_2 particles with average sizes between 4 nm to 25 nm. [2]For anatase TiO_2 particles with an average size of 215 nm.

particle sizes because of agglomeration [189, 198, 200, 201]. Many studies used TiO_2 powders with primary particle sizes below 100 nm even though food-grade TiO_2 mostly consists of TiO_2 particles with diameters larger than 100 nm [155].

Another important factor that is not adequately discussed in these studies concerns the use of high particle concentrations for *in vitro* studies. If the particle concentrations are high, e.g. 100 μg/mL and above [189, 191, 197], observed results should be interpreted with caution. In these instances, effects might simply be explained by the inhibition of normal cellular functions and not because of particle-specific effects [163].

Finally, the exposure time of the cells to the particle suspensions should also be considered carefully when interpreting results of *in vitro* studies. Several reports have shown that cytotoxicity increases with prolonged exposure, and it is possible that effects at late time points are not primarily caused by the particles but instead are the results of increased cell death [198]. The shortcomings of *in vitro* studies to assess toxicity of nanoparticles and microparticles have been discussed in more detail by Powell and co-workers [163]. A useful, and potentially more relevant, approach to examine biological effects caused by exposure to dietary particles is to conduct studies with animal models.

1.4.2 Effects of titanium dioxide on animal models after gastrointestinal exposure

Many reports have been published about the effects of TiO_2 on animals. However, in many of these *in vivo* studies the route of exposure to the TiO_2 particles was through injection, either subcutaneously or directly into the bloodstream. In several other studies, the animals were exposed to the TiO_2 particles by air or intranasally, and the effects on the lungs and alveolar macrophages were determined. Only a few studies have investigated the effects of oral TiO_2 exposure on animals (Table 1.7).

In one study, rats were orally given 500 nm TiO_2 particles at a daily dose of 12.5 mg/kg body weight for 10 days [172]. Subsequently, the distribution of the particles was assessed in several organs. Most TiO_2 particles were detected in the PPs, MLNs, colon, peritoneal tissue, and liver. Some particles were also visible in the small intestine, spleen, and lung. No particles were observed in the heart and kidneys. The relative concentration of TiO_2 particles was highest for PPs. These results showed that a relatively short oral exposure to a moderate dose of TiO_2 resulted in a substantial uptake of particles, and PPs were the main access route

Table 1.7 *Summary of studies that investigated effects of TiO_2 particles on animals.*

Route of administration	***Exposure frequency***	***Duration of study (d)***	***Animals (Strain)***	***Particle type***	***Particle size (nm)[1]***	***TiO_2 concentration***	***Investigated effects***	***TiO_2 occurrence in tissue***	***Reference***
Diet	Continuous	721	Mice (B6C3F1), Rats (Fisher 344)	Anatase	n/a	25,000 ppm, 50,000 ppm	Body weight, carcinogenicity	Not investigated	[202]
Drinking water	Continuous	5	Mice (C57BL/6)	Anatase/ rutile	21[2], 160[3]	50-500 mg/kg	Genotoxicity, cytokine gene expression[7]	Not investigated	[203]
Oral gavage	Once at beginning	7	Mice (Kunming)	n/a	120[2]	5,000 mg/kg	Histopathology[7]	ICP-MS[8]	[204]
	Once at beginning	14	Mice (ICR/CD-1)	n/a n/a n/a	155[4] 80[2] 25[2]	5,000 mg/kg	Body weight, histopathology[7]	ICP-MS	[205]
	Once at beginning	14	Rats (n/a[8])	Rutile/ anatase	140[3]	175-5,000 mg/kg	Body weight, mortality	Not investigated	[206]

(Continued on next page)

Table 1.7 *Summary of studies that investigated effects of TiO_2 particles on animals (continued).*

Route of administration	***Exposure frequency***	***Duration of study (d)***	***Animals (Strain)***	***Particle type***	***Particle size (nm)[1]***	***TiO_2 concentration***	***Investigated effects***	***TiO_2 occurrence in tissue***	***Reference***
Oral gavage	Daily	5	Rats (Sprague Dawley)	Anatase	< 25[2], 284[4]	1-2 mg/kg	Body weight, histopathology[7]	SEM, ICP-MS	[207]
	Daily	10	Mice (C57BL/6)	Anatase Anatase	260[2] 66[3]	100 mg/kg	Cytokines (intestine), histopathology[7]	ICP-AES[8]	[208]
	Daily	10	Rats (Sprague Dawley)	Rutile	500[2], 475[5]	12.5 mg/kg	TiO_2 tissue distribution	LM, SEM, ICP-AES	[172]
	Daily	14	Rats (Wistar)	Rutile/ anatase	< 50[6]	160-1,000 mg/kg	Body weight, histopathology[7]	Not investigated	[209]
	Daily	30	Mice (ICR/CD-1)	Anatase	7.5[2]	5-150 mg/kg	Histopathology[7]	Not investigated	[210]
	Every 2nd day	30	Mice (ICR/CD-1)	Anatase	5[6]	62.5-250 mg/kg	Body weight, histopathology[7]	Not investigated	[211]

[1]Average size or size range. [2]Particle size according to manufacturer. [3]Particle size determined by dynamic light scattering with particles suspended in water. [4]Particle size determined by SEM/TEM. [5]Particle size determined by photon correlation spectroscopy. [6]Particle size determined by X-ray diffraction. [7]Amongst other investigated effects. [8]Abbreviations specific for this table: ICP-AES = inductively coupled plasma atomic emission spectrometry, ICP-MS = inductively coupled plasma mass spectrometry, n/a = data not available.

for the particles into the body. However, potential effects induced by the TiO_2 particles were not investigated.

The purpose of a similar 10-day study conducted with mice that received daily doses of 100 mg/kg body weight TiO_2 particles with average sizes smaller than 100 nm or 250 nm was to investigate potential modulatory effects of the TiO_2 particles on small intestinal immune function [208]. An increase in mucosal $CD4^+$ T cells was detected after TiO_2 exposure, and this observation was independent of the particle type used. The concentrations of cytokines associated with a Th1 immune response, e.g. IFN-γ and TNF-α, were also increased in the ileum after TiO_2 treatment. Both types of particles caused similar effects. It was shown that TiO_2 accumulated in the small intestine of treated animals, but the histological distribution of the particles was not further determined. Importantly, when the quantitative uptake of TiO_2 in the small intestine was investigated the PPs were not removed for the analysis. Therefore, it remained unclear if the observed TiO_2 content was mainly the result of PPs containing TiO_2, or if TiO_2 particles did also accumulate in the small intestinal LP.

Nevertheless, the literature review has revealed that these two studies were the only ones that investigated consequences of oral TiO_2 particle exposure on the gastrointestinal tract of mammalian animal models. In other *in vivo* studies in which TiO_2 particles were administered orally the effects on the gastrointestinal tract have not been the focus of the research.

For example, Warheit and colleagues have examined the effects of a single treatment with three types of TiO_2 particles at various concentrations on rats [212]. After two weeks, no increased mortality and weight loss was observed. Moreover, no gross organ or tissue damage was visible at necropsy. The authors concluded that a single exposure to TiO_2 of up to 5,000 mg/kg body weight did not induce general toxicity symptoms in rats.

In two similar studies, mice were exposed to a single TiO_2 particle dose of 5,000 mg/kg body weight *via* oral gavage. Wang and colleagues showed that such a high acute exposure with either 25 nm, 80 nm, or 155 nm TiO_2 particles led to accumulation in liver, spleen, kidney, lung, and brain [205]. This provided indirect evidence that TiO_2 particles have been taken up in the gastrointestinal tract and then were systemically dispersed throughout the body. However, according to the organ coefficients, which were calculated by dividing the respective tissue weight by the body weight, only the coefficients of liver from female mice exposed to TiO_2 were different from control animals. The coefficients of liver from male mice, as well as of spleen and kidneys from both female and male mice, were similar between

TiO_2-treated and control animals. Histological comparison of stained tissue sections by microscopy showed pathological changes in liver, kidneys, stomach, and brain after exposure to 80 nm TiO_2 particles. Other examined tissues, including spleen and lung, from TiO_2-treated animals appeared normal, and no tissues showed histopathological changes after exposure to 155 nm or 25 nm particles. Several serum biomarkers, including levels of alanine aminotransferase, blood urea nitrogen, and lactate dehydrogenase, were also affected by treatment with TiO_2 particles in the nanometre range. However, no acute toxic effects were observed.

In the second study in which a dose of 5,000 mg/kg body weight TiO_2 particles was administered to mice *via* oral gavage, the coefficients of liver, kidney and brain were also investigated, and no differences were observed between TiO_2-treated mice and control animals [204]. Increased amounts of TiO_2 were detected in liver and kidneys, and this corresponded with histopathological changes in both organs. Slight changes were also observed in cortex and hippocampus tissues. There was an increase in ROS and changes in the activities of biomarkers for oxidative stress, namely glutathione peroxidase and superoxide dismutase, in these four tissues. However, liver function was not affected negatively by TiO_2 treatment and no nephrotoxicity was detected.

In two other oral exposure studies, rats were administered daily doses of TiO_2 *via* oral gavage. In the first study, Tassinari and co-workers have examined the effects of a 5 d exposure to two low TiO_2 doses, namely 1 mg/kg and 2 mg/kg body weight [207]. The authors found that this had no effect on body weight gain and organ coefficients of spleen, uterus, ovaries, testes, thyroid and adrenal glands. Furthermore, no effect on the food intake was detected for female and male rats on the 1 mg/kg dose, but males that received 2 mg/kg had a reduced food intake compared to controls. Male rats that were exposed to the higher dose also had increased testosterone levels in the serum whereas TiO_2 treatment reduced testosterone levels for females. For both female and male rats the titanium content of the spleen was elevated at a dose of 2 mg/kg body weight, but not at 1 mg/kg. All investigated organs showed histopathological changes after exposure to the higher dose. In contrast to these results, in the second study in which female and male rats were continuously exposed to relatively high TiO_2 particle doses of up to 1,000 mg/kg body weight for 14 d no effects on bodyweight, organ coefficients, and histopathological changes were observed [209].

Two studies investigated the effects of daily intragastric administration of TiO_2 on mice for 30 d. In the first study, mice were exposed to anatase TiO_2 nanoparticles at concentrations of 5 mg/kg, 50 mg/kg, or 150 mg/kg body weight, and the histopathological changes and

oxidative stress in the spleen were investigated [210]. Mice that received a daily dose of 5 mg/kg showed no signs of abnormal pathology, but the animals that were exposed to the two higher doses showed histopathological changes in the spleens. These changes were potentially due to oxidative damage because markers for oxidative stress were increased in the spleen tissues from these animals. However, it was not investigated whether this increased oxidative stress was the direct result of TiO_2 accumulation in the spleen or an indirect effect. Effects on other organs were not investigated. In a second study, mice were administered daily doses of 125 mg/kg or 250 mg/kg body weight anatase TiO_2 nanoparticles [211]. Both treatments led to reduced weight gain and lower organ-to-body weight coefficients of liver, kidney, spleen, and thymus although food intake was unaffected. Increased activity of serum biomarkers for liver function, namely alanine aminotransferase, alkaline phosphatase, aspartate aminotransferase, lactate dehydrogenase, and cholinesterase, as well as changes in haematological parameters were also observed with both doses. Furthermore, analysis with flow cytometry showed a decrease of lymphocytes in the peripheral blood of animals treated daily with 250 mg/kg TiO_2 particles.

The literature search has revealed only one publication in which TiO_2 particles were administered together with the diet. In a study that was conducted more than three decades ago by the US National Cancer Center to investigate potential carcinogenic properties of TiO_2, rats and mice were fed two diets that contained TiO_2 particles at two different concentrations [202]. The animals were exposed to the TiO_2 particles for 103 weeks and sacrificed one week later. There was no difference in body weight between the treated groups and the control groups. The survival was also not affected for rats and male mice, but female mice had a decreased survival rate that was dependent on particle dose. There was no relationship between TiO_2 exposure and tumour development for both rats and mice. These results suggested that TiO_2 particles were not carcinogenic. Unfortunately, those particles were not well characterised and it was only mentioned that anatase TiO_2 was used.

Since then, only one other study has investigated genotoxic effects of TiO_2 particles after oral administration [203]. Trouiller and co-workers exposed mice to up to 500 mg/kg body weight in drinking water for 5 d. Several assays to examine DNA damage were conducted with the conclusion that the highest TiO_2 particle dose was genotoxic in mice. There was an increased mRNA expression of the pro-inflammatory cytokines IFN-γ and TNF-α, but not of the anti-inflammatory cytokines IL-10 and TGF-β, in the peripheral blood from TiO_2-treated animals compared to control mice.

Similar to the situation with the *in vitro* studies, it is difficult to draw general conclusions from the studies on the effects of TiO_2 *in vivo* so far. However, detrimental effects as a result of TiO_2 exposure were often only detected with relatively high exposure concentrations in animal studies. Such high doses usually do not apply to humans who ingest less than 1 mg/kg body weight TiO_2 on average [155]. To be able to draw meaningful conclusions from *in vivo* exposure studies, it would be important to adjust the administered TiO_2 doses to levels that are comparable to the average human TiO_2 intake [213]. However, the individual human TiO_2 intake can be quite variable, and some people can have a much higher intake than the average TiO_2 intake [150, 214].

Apart from the doses used for *in vivo* studies, the exposure time must also be considered. Most studies were only carried out over a short period of time. In contrast, humans are exposed to TiO_2 over a long time. In fact, this exposure starts in early childhood and continues throughout life [56, 155]. Thus, more chronic exposure studies, as opposed to short term acute exposure studies, would be needed to further investigate possible long term adverse health effects of TiO_2 particles in animal models. Similar to the shortcomings of *in vitro* studies (see Section 1.4.1), most *in vivo* studies that investigated consequences of oral TiO_2 exposure have not used food-grade TiO_2. In fact, most studies do not mention the types of application for which the investigated TiO_2 particle type is used for. Often, TiO_2 particles that have only industrial applications, e.g. as photocatalyst, have been used instead of food-grade TiO_2 which mainly consists of anatase particles with sizes between 100 nm to 200 nm [147, 155]. Considering the ubiquitous exposure to dietary TiO_2, it is also important to study the consequences of this exposure directly in humans. As such studies are difficult to carry out, a more practical alternative would be to investigate effects of food-grade TiO_2 particles on primary human cells *ex vivo* and *in vitro*.

1.4.3 Effects of titanium dioxide and bacterial lipopolysaccharide co-stimulation on cultured human cells

The effects of food-grade TiO_2 particles were also tested in several studies with primary human cells or macrophages derived from peripheral blood mononuclear cells (PBMCs) by Powell and co-workers (Table 1.8). Their research has focused on testing the hypothesis that exogenous particles (in particular TiO_2) cause intestinal pathology in conjunction with co-stimulatory molecules. In this scenario, the exogenous particles will adsorb luminal antigens, e.g. from commensal microorganisms, and this particle-antigen-complex is taken up by phagocytes in the mucosa. This co-stimulation of phagocytic immune cells then causes

Table 1.8 *Summary of studies that investigated effects of TiO_2 particles with LPS co-stimulation on cultured human cells.*

Cell type	***Control cells***	***CD***	***UC***	***Particle type***	***Particle size (nm)***	***TiO_2 concentration***	***LPS (ng/mL)***	***Time (h)***	***Investigated effects***	***Cyto-/chemokines analysed***	***Reference***
PBMCs	healthy	no	no	Anatase	200[1]	5 μg/mL[2]	1	24	Cell viability, SN[5] cytokines[4]	MIP-1α, MCP-1, IL-1β, TNF-α, IL-6, TGF-β, and IL-1Ra	[215]
	Non-IBD	yes	no	Anatase	200[1]	5 μg/mL[2]	1	24	SN cytokines	IL-1β	[216]
Colon explants	Non-IBD	yes	yes	Anatase	200[1]	5 μg/mL[2]	2000[3]	24	SN and tissue cytokines	IL-1β	[216]
Colon LPMCs	Non-IBD	yes	yes	Anatase	200[1]	5 μg/mL[2]	1	1-72	SN cytokines	IL-1β	[217]
	Non-IBD	yes	yes	Anatase	200[1]	5 μg/mL[2]	1	24	Cell viability, SN cytokines	IL-1β, IL-1Ra	[217]
Monocyte-derived MΦ[5]	healthy	yes	no	Anatase	200[1]	0.5-50 μg/mL	n/a[5]	24	Cell viability, SN cytokines, TiO_2 uptake	TNF-α and IL-8	[218]
	healthy	yes	no	Anatase	200[1]	5	10	24	SN cytokines	IL-8, TNF-α, IL-10, and TGF-β	[218]
	healthy	yes	no	Anatase	200[1]	0.5-50 μg/mL	n/a or 10	24	Phagocytosis	n/a	[218]

[1]Average particle size according to manufacturer [2]Additional 4 mmol/L calcium ions added to culture medium to facilitate adsorption of LPS to TiO_2. [3]Lower LPS doses (1-100 ng/mL) investigated initially but did not induce a response in intestinal tissue explants. [4]Amongst other investigated effects. [5]Abbreviations specific for this table: MΦ = macrophages, n/a = not applicable, SN = supernatant.

inflammatory responses mediated by intracellular PRR signalling as a response to the luminal antigens [219].

A common bacterial antigen in the intestinal lumen is lipopolysaccharide (LPS), which is part of the outer cell membrane of all Gram-negative bacteria, e.g. *Escherichia coli*. When PBMCs from healthy volunteers were incubated with a TiO_2-LPS conjugate consisting of 5 μg/mL TiO_2 and 1 ng/mL LPS the responses were different to stimulation with the same concentrations of TiO_2 or LPS alone [215]. For example, there was no difference in cell viability between untreated control cells and TiO_2-stimulated cells. In contrast, the number of dead cells increased from less than 10 % in unstimulated control cells to 30 % in PBMCs that were co-stimulated with TiO_2 + LPS. Furthermore, the secretion of the pro-inflammatory cytokines IL-1β, TNF-α, and IL-6 was not affected by incubation with TiO_2 alone, but it was increased after treatment with TiO_2 + LPS. Stimulation with LPS alone also led to an increased secretion of pro-inflammatory cytokines, but the concentrations were lower compared to stimulation with TiO_2 + LPS. The secretion of the MIP-1α, which promotes pro-inflammatory immune responses, was also increased in cells stimulated with TiO_2 + LPS. In contrast, TiO_2 + LPS stimulation led to reduced or unchanged secretion of the anti-inflammatory cytokines TGF-β and IL-1Ra, respectively. The chemokine responsible for recruiting monocytes to sites of inflammation, monocyte chemotactic protein (MCP)-1, which is also known as CCL2, was also reduced following stimulation with TiO_2 + LPS. To investigate if uptake of the TiO_2-LPS conjugate by phagocytosis caused the responses, cells were incubated with TiO_2 + LPS in the presence of cytochalasin D, which inhibits phagocytosis, or poly I, which blocks the scavenger receptor and therefore inhibits scavenger receptor-mediated uptake. As expected, phagocytosis of the particle-antigen conjugate was decreased in both cases compared to untreated cells in a concentration dependent manner. At the same time, the number of dead cells and the amount of secreted IL-1β decreased with increasing concentrations of the phagocytosis inhibitors. Taken together, these results suggest that a conjugate between exogenous dietary particles and an abundant luminal bacterial antigen could trigger pro-inflammatory responses, and that phagocytic immune cells were the cells that were mainly responsible for this response.

Powell and colleagues also investigated the responses of cells obtained from IBD patients after stimulation with exogenous particles and luminal antigens. In one study, PBMCs from non-IBD control patients and patients with CD were isolated and stimulated with TiO_2 and LPS either alone or in combination [216]. There was no increase in IL-1β secretion when the cells were incubated with TiO_2 alone compared to untreated controls. Stimulation with LPS

led to a moderately increased release of IL-1β. However, the production of IL-1β by TiO_2 + LPS stimulated PBMCs was even further elevated. This increased IL-1β secretion was observed equally in cells from controls and CD patients. In addition to PBMCs, colon mucosal tissue samples were collected from the same patients and additional patients with UC. The intestinal explants were stimulated in a similar way as the PBMCs and both the supernatants and homogenised tissues were analysed for IL-1β content. Again, no increased amounts of IL-1β were detected in both sample types when the tissues were stimulated with TiO_2 or LPS alone. Treatment with the TiO_2-LPS conjugate resulted in increased amounts of IL-1β in the supernatants and tissue homogenates from non-IBD controls. However, no increased IL-1β production was detected in tissue samples from IBD patients. This was probably due to high IL-1β baseline levels in those samples, which might have masked the detection of further increases. The conclusion was that co-stimulation with a particle-antigen conjugate increased secretion of the pro-inflammatory cytokine IL-1β from PBMCs, but the effect on intestinal cells from IBD patients requires further research.

This was addressed in another study in which colon LPMCs from IBD patients and non-IBD controls were incubated with the TiO_2-LPS conjugate [217]. First, the secretion of IL-1β over time was investigated when the cells were incubated with the particle-antigen conjugate or TiO_2 and LPS alone for 1 h to 72 h. No IL-1β was detected at any time point in the supernatants from control cells stimulated with the single components alone. In contrast, co-stimulation with TiO_2 + LPS induced the secretion of IL-1β in both IBD and control LPMCs. The maximum amount of IL-1β released by cells from IBD patients and controls was observed after 24 h and 15 h, respectively. Cells from IBD patients secreted more IL-1β compared to control cells. This result was in contrast to the observation by Powell and colleagues. As previously mentioned, no difference in IL-1β secretion between PBMCs from CD patients and controls was observed in that study either at baseline or after TiO_2 + LPS treatment [216]. In addition, colon mucosal tissue explants did not show increased IL-1β release after TiO_2 + LPS stimulation, probably because of high baseline levels. In contrast, LPMCs from IBD patients had higher baseline levels of IL-1β and still showed an increased cytokine release after stimulation with the particle-antigen conjugate [217]. The amount of IL-1β that was detected after stimulation with the TiO_2-LPS conjugate was positively correlated with the degree of baseline inflammation, i.e. cells from IBD patients with higher IL-1β baseline levels secreted even higher amounts of IL-1β after TiO_2 + LPS stimulation compared to control cells. It should be noted that the LPMCs from IBD patients were isolated from colon regions that showed signs of inflammation because a higher number of

cells could be isolated from those regions compared to uninflamed areas. However, the IL-1β response per cell was the same regardless of whether the cells were isolated from inflamed or uninflamed regions. There was also no difference in the response between LPMCs that were obtained from CD and UC patients. The use of primary intestinal cells allowed a more targeted examination of the pro-inflammatory effects of TiO_2 + LPS co-stimulation. However, the effects of TiO_2 on the cytokine response could only be related to the whole cell population.

Therefore, in an *in vitro* study the responses of macrophages derived from PBMCs were investigated in more detail [218]. The baseline levels of the inflammation-associated chemokine IL-8 and cytokine TNF-α were elevated in cells from CD patients compared to healthy controls. The baseline levels of the anti-inflammatory cytokine IL-10 were also increased, but the baseline amount of TGF-β was reduced in the supernatant of cells from CD patients. Similar to the studies mentioned previously, incubation with TiO_2 alone had no effect on cytokine release. However, co-stimulation with TiO_2 + LPS induced secretion of TNF-α and IL-8, and decreased the amount of secreted TGF-β. These results were more pronounced in macrophages from CD patients. Unfortunately, the secretion of IL-1β was not investigated. In addition, the effects of TiO_2 incubation on phagocytosis were also studied. The uptake of TiO_2 particles was similar between controls and CD patients. There was a positive correlation between increasing TiO_2 concentration and increase in granularity, which was used to assess particle uptake. The phagocytic activity was not affected by the presence of TiO_2 particles in the TCM, but the capacity to take up fluorescent beads decreased with increasing particle concentration. However, this was not observed with macrophages derived from CD patients. When the cells were incubated additionally with LPS the reduction in phagocytic capacity at high TiO_2 concentrations was also unchanged for cells from healthy controls.

In summary, the *ex vivo* and *in vitro* studies with human cells showed that exposure to TiO_2 particles alone did not affect the production of cytokines. However, relatively small amounts of TiO_2 could induce the production of pro-inflammatory cytokines when additional luminal bacterial antigen in the form of LPS was present. The secretion of IL-1β involves several steps in which pro-IL-1β is processed to mature IL-1β by inflammasomes [220]. In this context, stimulation with LPS induced the production of pro-IL-1β [221], and particulate substances were able to activate the NLRP3 inflammasome [222, 223]. However, the studies described in this section have shown that the secretion of other pro-inflammatory cytokines and chemokines was also influenced by stimulation with the TiO_2-LPS conjugate. Although

increased apoptosis might have affected changes in cytokine production in some studies [215, 217], in the study by Butler and colleagues the cell viability of macrophages was not much affected by increasing particle concentration [218]. Therefore, the observed changes in cytokine production were probably due to co-stimulation with TiO_2 + LPS.

Even though valuable results were obtained by studying the effects of TiO_2 particles on human cells *ex vivo* and *in vitro* it is important to also consider potential effects caused by TiO_2, or exogenous particles in general, on humans directly.

1.4.4 Effects of titanium dioxide on humans

Although TiO_2 has been used as a pigment extensively for several decades, not only as a food colourant but also in sunscreens, paint, paper, and plastics, there are surprisingly few studies that examined the direct effects of TiO_2 on humans. One reason for this might be that studies to examine such effects would be relatively difficult to conduct. There was also no immediate demand for these kinds of studies given that it has been shown that TiO_2 has a low toxicity *per se* [224]. Thus, it is generally assumed that TiO_2 does not pose a health risk for humans and, as discussed above (Section 1.3.2), it can actually be used under very low restrictions as a food and pharmaceutical additive [149, 156]. However, recently TiO_2 has been re-classified as possibly carcinogenic to humans by the International Agency for Research on Cancer from the World Health Organisation [225, 226]. This decision was based on studies that report an increased incidence of lung tumours after airway exposure to TiO_2 particles in mice and rats [227-229]. There is, however, no evidence for this in humans although exposure levels are high during the manufacturing of TiO_2 particles [230]. After long term dietary exposure, no correlation between cancer formation and TiO_2 exposure was detected in rats and mice [202].

Only one publication has been found that described direct effects of oral TiO_2 exposure on humans [231]. Healthy male volunteers ingested a single dose of 22.9 mg anatase TiO_2 either in gelatine capsules with a TiO_2 content of 2 % weight per volume or in powdered form. An increase in TiO_2 levels in the blood was detected as soon as 15 min after uptake with maximum levels detected after 4 h to 12 h regardless of the form of administration. These results indirectly proved that TiO_2 particles were taken up in the gastrointestinal tract after oral administration. Unfortunately, no other parameters apart from TiO_2 levels in the blood were investigated.

Another study investigated the effect of titanium and TiO_2 on the so-called yellow nail syndrome [214]. This disease is characterised by the development of thickened yellow nails, respiratory problems and lymphedema. Nail clippings from patients with yellow nail syndrome regularly contained high levels of titanium ions in contrast to nail clippings from healthy controls. Most of the patients had some form of titanium implant, but for eight out of 34 patients investigated the high levels of titanium ions detected in nail clippings were caused by ingestion of high amounts of TiO_2 either with drugs, confectionary, and/or chewing gum. The authors reported that they observed an improvement of disease symptoms for patients on TiO_2-containing drugs after they switched to replacement drugs without TiO_2. However, for some drugs it was difficult to find alternatives that did not contain TiO_2.

As mentioned earlier, a link between TiO_2 exposure and CD has also been suggested [56, 147]. Lomer and colleagues investigated the effects of reducing exogenous particle intake on disease activity and remission in two studies [232, 233]. In the first study 20 CD patients were blindly assigned to either a control diet or a diet low in exogenous dietary particles [232]. The control diet was similar to the diet low in particles except that foods and pharmaceuticals which contained exogenous particles were not specifically discouraged. After four months, patients on the low particle diet had a lower disease activity and seven patients were in remission. However, none of the patients on the control diet were in remission and there was no change in disease activity index. The disease activity index was higher for patients in the control group compared to patients on the low particle diet.

These results prompted a follow up study with an increased number of CD patients in which the effects of a low particle diet in conjunction with a normal or reduced calcium intake were compared [233]. The patients and examining physicians were again blinded in respect to the assigned diets. Patients on control diets were supplemented with 5 mg TiO_2 per day to ensure intake of at least the average amount of TiO_2 for people in developed countries diet [150]. In this second study no positive effects of a low particle diet on disease activity and remission were observed.

One reason for the discrepancy between the two studies could have been that the baseline disease activity index was lower in the second study. For ethical reasons, treatment with immunosuppressant drugs was continued throughout both studies if necessary. Therefore, reducing exogenous dietary particle intake might only lead to detectable positive effects in patients on medication with a high disease activity index. Another reason could have been that in the initial study processed foods had been generally excluded from the diet of the low

particle group because the exact sources of exogenous particles were not yet fully known. When the second study was conducted the foods that contained particles had been largely identified [150], so the control and low particle diets were more similar to each other than in the first study. Thus, the observed effects in the first study could have been the result of the comparison of an unprocessed diet with a 'normal' Western diet which is usually rich in processed foods [233]. The additional TiO_2 supplementation of the control diet groups in the second study did not affect disease activity.

A drawback of both studies was that the exact amount of exogenous particles that were taken up by both control and particle-restricted groups was unknown. The intake of exogenous particles by patients on a low particle diet still could have been considerable because of the unregulated use of additional pharmaceuticals and supplements [233]. Despite these limitations, the results of the carefully designed second study indicated that reducing exogenous dietary particle alone intake did not improve CD symptoms. The authors speculated that exogenous particles could nevertheless be involved in the aetiology of CD, which would not have been possible to detect in these two studies because only patients with established disease were recruited [55, 233].

The effects of dermal exposure to TiO_2 have also been studied in CD patients [234]. A TiO_2 particle suspension in water was injected intradermally in the abdominal wall. Skin biopsies were taken six weeks later and histologically examined for signs of inflammation. No response was observed, and TiO_2 was not detected anymore at the site of injection in the skin biopsies.

Taken together, the results of the above studies that examined effects of TiO_2 particles directly in humans are inconclusive. The current data does not appear to support a role of exogenous dietary particles in ongoing CD pathogenesis.

1.5 Concluding remarks

1.5.1 Hypotheses concerning dietary particles

Exogenous dietary particles and their role in intestinal function have been explored extensively by Dr Jonathan Powell and his team since their exact identities have been elucidated by Powell and colleagues in 1996 [147]. Over the years a number of excellent reviews have been published by Powell and co-workers, which discussed the possible biological functions of endo- and exogenous dietary particles in intestinal homeostasis with

a special emphasis on the relationship between exogenous particles and development of CD [55, 143, 146, 161, 163, 219].

The possible biological functions for the re-secretion of calcium and phosphate ions in the distal small intestine and the resulting formation of particulate calcium phosphate have been the subject of some discussion. It has been observed that these endogenous dietary particles can adsorb luminal antigens [145]. Some studies suggested that this process might assist with the clearance of toxic antigens from the intestinal lumen [145, 235, 236]. However, in regard to the large amount of potential cytotoxic antigens in the intestinal lumen, it seems unlikely that this process would be of biological relevance. Importantly, it has been shown that calcium phosphate particles are also taken up by immune cells in PPs [142, 143]. This observation led to alternative hypotheses regarding the function of dietary calcium phosphate particles. It could be possible that these endogenous particles play an important role in establishing tolerance to dietary antigens.

Induction of tolerance could be achieved through several mechanisms. First, it has been shown that calcium phosphate particles induced apoptosis in intestinal cells *in vitro* [217], and increased dietary calcium supplementation led to increased apoptosis in the distal colon in mice [237]. The uptake of apoptotic cells by antigen presenting cells results in the induction of tolerance [238, 239]. This could be of relevance for the gastrointestinal tract where endogenous dietary particles cause apoptosis, and these apoptotic cells are subsequently taken up by intestinal phagocytes which then release tolerogenic signals [55, 143, 146]. Another possible mechanism of tolerance induction by endogenous dietary particles could be the result of uptake of these particles by hyporesponsive intestinal phagocytes [55]. It has been shown that intestinal phagocytes do not activate the immune system, but they still retain their phagocytic activity and promote tolerance [240]. It could also be possible that uptake of calcium phosphate particles would directly lead to immune tolerance, but such a mechanism remains elusive [55].

Exogenous dietary particles, on the other hand, could disrupt this natural process of endogenous particle-mediated immune tolerance, regardless of its mechanism. This could result in the development of intestinal inflammation. Similar to endogenous dietary particles, TiO_2 and other exogenous dietary particles can adsorb antigen onto their surfaces [198, 241, 242]. It has been suggested that if this exogenous particle-antigen complex is taken up by intestinal phagocytic cells this would not lead to the induction of tolerance, but it would instead induce an inflammatory response. Prolonged exposure could then lead to the development of CD [55, 143].

Several observations have contributed to the development of this hypothesis. First, it has been noted that exogenous particles accumulate in the region of the gastrointestinal tract that is most commonly affected by CD, namely the PPs [56, 243]. Earlier studies have also shown that when silica dust or sand particles were introduced in the gastrointestinal tract of dogs they developed symptoms with a similarity to CD [244, 245]. Furthermore, it has been shown that soil particles, including silicates and TiO_2, are the cause of podoconiosis [246]. This is a disease which resembles elephantiasis and is characterised by swelling of the legs as a result of the occlusion of the draining lymphatics. The disease is only found in certain regions in Africa with volcanic soils. The soil particles are taken up in the feet by walking barefoot, and the disease progression can be stopped by wearing shoes [143, 217]. Interestingly, only a small number of people in the respective areas are affected by podoconiosis despite the fact that the whole population is exposed to these particles. This suggests that there is a genetic component which makes some people more susceptible to develop this disease [146, 147]. Taken together, these observations indicate that exogenous dietary particles might indeed be involved in the aetiology of CD, as proposed already in the first study that documented their occurrence in PPs [56].

As mentioned in the beginning of this literature review (Section 1.1.2), the causes for CD are still unknown, but it is likely that both environmental and genetic components contribute to the disease [247]. It has been noted that the rising incidence in CD corresponds to increased usage of exogenous dietary particles in processed foods [146, 219]. As reported in the previous section, the first study that investigated a direct link between exogenous dietary particles and CD showed that a reduced particle intake ameliorated disease symptoms [232]. However, a follow up study could not reproduce the results from the initial study [233]. This observation suggested that exogenous dietary particles did not play a role in maintaining the disease once it has been established. However, exposure to exogenous particles could still be a crucial factor for the initial establishment of CD [233]. Furthermore, it is possible that only people with a genetic susceptibility to CD would be affected by exogenous particles [55]. It has been suggested that it would be of particular interest to study the consequences of exogenous dietary particle exposure in a mouse model with a defective *Nod2* gene to investigate effects of exogenous dietary particles under these circumstances [163].

1.5.2 Hypothesis, aims, and structure of this dissertation

The overall goal of this dissertation is to investigate the hypothesis that exogenous dietary particles are involved in the establishment of intestinal inflammation, especially if there is a

genetic predisposition for the development of CD. Mutations in the *NOD2* gene are the most frequently associated genetic aberrations in patients with CD. Thus, a mouse model with a homologous mutation to the most frequent *NOD2* mutation found in CD patients was selected as a model for this dissertation.

Only one type of exogenous particles, namely TiO_2, was selected for this study. This decision was based on the observation that processed foods available in supermarkets in New Zealand do not contain aluminium-containing silicates as anticaking agents. Moreover, recent law changes in the European Union have banned the use of aluminium-containing silicates as food additives. There has also been on-going interest, especially over the last decade, to investigate the toxicity of TiO_2 particles both *in vitro* and *in vivo* in a variety of models. However, most of the *in vitro* studies did not investigate effects of TiO_2 particles on intestinal epithelial or immune cells, and the majority of the *in vivo* studies did not examine effects on the gastrointestinal tract or GALT. Therefore, the purpose of this study was to investigate effects of food-grade TiO_2 particles both *in vitro* and *in vivo*.

The focus of Chapter 2 was to investigate effects of TiO_2 particles on immune cells obtained from mice and humans. Dietary TiO_2 particles can adsorb luminal antigens, including bacterial products like PGN and its fragment MDP. The NOD2 protein is an intracellular PRR that is activated by MDP. It was suggested that TiO_2 particles adsorb MDP and PGN, and this particle-antigen conjugate is taken up by phagocytic cells. It was expected that exposure of immune cells to the particle-antigen conjugate will lead to increased responses compared to stimulation with either TiO_2 particles or bacterial antigens alone. Furthermore, it was speculated that macrophages from *Nod2*$^{m/m}$ mice will be more responsive to TiO_2-antingen stimulation than cells obtained from WT mice.

To examine potential effects of dietary TiO_2 particles on intestinal function, the research focus was shifted from *in vitro* studies to *in vivo* studies in Chapter 3. First, it was important to determine how TiO_2 can be best administered to mice with the diet. It was expected that TiO_2 particles will accumulate in PPs in the distal small intestine, and that this will happen after a relatively short-term exposure over several weeks. The uptake of TiO_2 particles *via* the diet by WT mice was assessed for several particle doses and sampling time points to determine the most suitable concentration and exposure time for the second *in vivo* study.

The effects of dietary TiO_2 exposure on *Nod2*$^{m/m}$ mice were studied in comparison to WT mice in Chapter 4. It was expected that if TiO_2 particles indeed play a role in the aetiology of CD *Nod2*$^{m/m}$ mice will develop spontaneous intestinal inflammation.

Urine samples were collected in both *in vivo* studies to investigate metabolite profiles in Chapter 5. Changes in urine metabolites were previously described for patients with CD compared to healthy individuals. Therefore, if TiO_2 particles contributed to a CD-like disease in the *in vivo* studies it was expected to detect differences in urine metabolites of the respective groups compared to unexposed WT mice.

Finally, the findings from the investigations of this dissertation were summarised and discussed in a broader context in Chapter 6. To conclude, future perspectives and implications of this project were highlighted.

A diagram outlining the structure of this dissertation is presented in Figure 1.3.

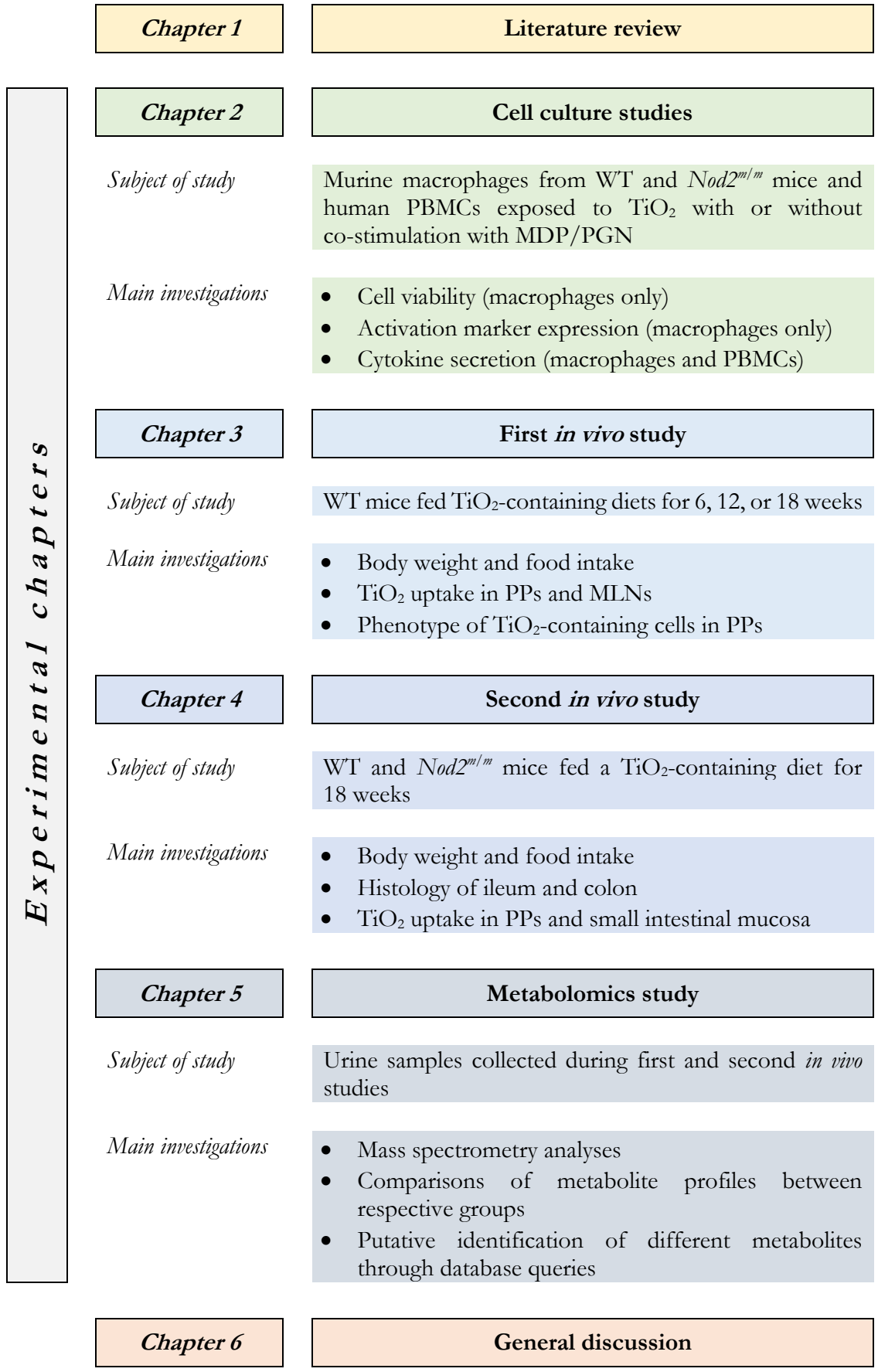

Figure 1.3 *Overview of the structure of this dissertation.*

This diagram shows the structure of this dissertation including the main contents of the experimental chapters.

Chapter 2 Exposure of cultured immune cells to titanium dioxide with or without co-stimulation with bacterial antigens

2.1 Introduction

When TiO_2 particles were detected for the first time in human PPs, it was mentioned that they accumulated specifically in macrophages, which were identified based on morphology in SEM [56] and TEM images [144]. Later studies confirmed these observations with TEM and confocal microscopy, and showed that the TiO_2 particles were located in phagolysosomes of mature macrophages [147, 161, 162]. It has been speculated that this uptake of TiO_2 particles can contribute to the development of IBD, namely CD [56, 146, 147].

Support for this hypothesis came from observations that TiO_2 particles activated cultured macrophages and induced the production of pro-inflammatory cytokines, particularly IL-1β, after TiO_2 stimulation *in vitro* [191, 197] or human PBMCs *ex vivo* [216]. Furthermore, increased levels of IL-1β correlated positively with the presence of inflammation in the colon [132]. It has been shown that only naïve intestinal macrophages from IBD patients, but not those from healthy controls, had the capacity to secrete IL-1β [248]. Moreover, non-affected intestinal tissues from CD patients expressed increased levels of pro-inflammatory cytokines compared to tissues from healthy controls [44]. Cultured macrophages from CD patients also secreted more pro-inflammatory cytokines after TiO_2 stimulation compared to cells from healthy controls [217, 218]. However, a decreased exposure to exogenous dietary particles, including TiO_2, did not improve disease progression for CD patients [233].

Because CD is a complex disease with contributions of both genetic and environmental factors [16], it has been speculated that only some people with a genetic predisposition to develop CD would be affected by exogenous particles [55]. Mutations in the *NOD2* gene are most commonly associated with CD development [59, 60]. Therefore, it might be possible that CD patients with *NOD2* variations respond differently to TiO_2 particles compared to healthy controls or CD patients with WT *NOD2* alleles [163].

A mouse model with a mutation in *Nod2* has been created that is homologous to the most common human *NOD2* variant allele, the 1,007fs mutation [131]. NOD2 is an intracellular receptor for the universal bacterial cell wall molecule MDP, and its activation triggers the transcription of pro-inflammatory cytokines *via* the NF-κB and mitogen-activated protein kinases signalling pathways [70]. Intact NOD2 signalling is required for the maintenance of intestinal homeostasis [62]. Bone marrow-derived macrophages (BMDMs) from *Nod2*$^{m/m}$ mice produced increased levels of IL-1β after stimulation with MDP [131]. Therefore, it has

been proposed that the human *NOD2* allele 1,007fs is a gain-of-function mutation, and CD patients with this mutation might develop intestinal inflammation as a result of increased production of pro-inflammatory cytokines in response to stimuli from the intestinal microbiota [131].

It has been shown that NOD2 signalling is also crucial for the induction of Th17 responses [249, 250], so improper NOD2 activation could result in an increased Th17 response by intestinal Th cells, which is characteristic for CD [41, 251]. Th17 cells that produce IL-17 can induce the secretion of IL-1β and TNF-α by macrophages, and together these cytokines promote increased recruitment of additional pro-inflammatory Th17 cells to the site of inflammation [252]. It has also been shown that IL-17 is a crucial cytokine for the development of intestinal colitis in mice [35].

2.2 Hypothesis and aims

The hypothesis to be tested in this chapter was that exposure to dietary TiO_2 particles leads to activation of macrophages and the production of pro-inflammatory cytokines, in particular IL-1β. This is further augmented by co-stimulation with MDP or PGN, of which MDP is a subunit, because of activated Nod2 signalling. Particulate TiO_2 adsorbs smaller molecules like MDP and PGN [198]. Therefore, these molecules are taken up by phagocytic cells more efficiently when they are co-incubated with TiO_2 particles compared to stimulation with MDP or PGN alone [253].

The aims of this study were to examine the responses of BMDMs from WT and *Nod2*$^{m/m}$ mice to dietary TiO_2 particles without or with MDP/PGN co-stimulation by measuring cell viability, cell activation, and pro-inflammatory cytokine expression (TNF-α and IL-1β). Furthermore, the secretion of the pro-inflammatory cytokines IL-1β and IL-17 by human PBMCs was assessed after incubation with TiO_2 alone or with additional MDP/PGN co-stimulation to investigate a possible connection between NOD2 activation and a pro-inflammatory Th17 response.

2.3 Materials and methods

2.3.1 Titanium dioxide particles

Food-grade anatase TiO_2 was obtained from Sensient Colors (St. Louis, MO, USA). The particle size details given by the manufacturer stated that 50 % of the particles were smaller than 700 nm, and 90 % were smaller than 1.7 μm. It was noted that this size range was determined by laser diffraction with a Malvern Mastersizer Diffractometer by Huntsman Tioxide (Houston, TX, USA). A 1 mg/mL suspension of the TiO_2 powder in distilled water (Life Technologies, Auckland, NZ) with 0.5 % bovine serum albumin (Life Technologies) was prepared to determine the particle size more accurately. This suspension was then observed by TEM to determine the size and morphology of the primary particles, which is a commonly used method to characterise TiO_2 particles [186, 194, 254]. With TEM, electrons are transmitted through the sample, and the morphology can be visualised due to absorption of the electrons by the material. The advantage of TEM compared to other microscopy methods is its high resolution, which can be below 100 nm. To detect the TiO_2 particles with TEM, a drop of the particle suspension was placed on a 200-mesh carbon coated copper grid. Excessive liquid was absorbed with filter paper, and the particles were observed with a Philips CM10 TEM at 80 kV. Images were digitally recorded with iTEM software (Olympus Soft Imaging Solutions, Münster, Germany). This software was also used for subsequent image analysis to measure the diameter of the particles.

Additionally, the sizes of TiO_2 particles in TCM were determined by nanoparticle tracking analysis (NTA) with a NanoSight NS500 machine (NanoSight, Amesbury, UK). This method is based on determining the sizes of particles with the Stokes-Einstein equation based on their Brownian motion similarly to classical particle characterisation by dynamic light scattering. With NTA, however, individual particles are recorded on video and their hydrodynamic diameter is determined based on their diffusion. Results obtained by NTA are comparable to those obtained by dynamic light scattering, and NTA is the preferred method to analyse polydispersed nanoparticles [255].

For the NTA the TiO_2 powder was suspended at different concentrations in Roswell Park Memorial Institute (RPMI) 1640 medium (Sigma-Aldrich, Gillingham, UK) supplemented with 10 % foetal bovine serum (FBS; PAA Laboratories, Yeovil, UK) and 1 % penicillin-streptomycin antibiotics (Sigma-Aldrich). Several concentrations from 5 μg/mL to 100 μg/mL TiO_2 were analysed, which corresponded to the TiO_2 concentration used in the

cell culture experiments. The particle-TCM suspensions were sonicated in a water bath for 10 min and vortexed immediately prior to analysis. Videos of the particle suspensions were recorded for 1 min, and particle sizes were determined with NTA analytical software version 2.3 (NanoSight). Three samples of each TiO_2 suspension were analysed.

2.3.2 Animals

The use of mice for bone marrow cell collection for *in vitro* experiments was approved by the Grasslands Animal Ethics Committee (Palmerston North, NZ) in compliance with the New Zealand Animal Welfare Act 1999.

All mice used for tissue collection were provided by the AgResearch Ruakura Small Animal Colony (Hamilton, NZ) and transported by plane to the AgResearch Grasslands Small Animal Unit (Palmerston North, NZ). The mice were acclimatised to the new environment for at least one week prior to sampling. The animals were housed in groups of up to five in 29 cm × 16 cm × 12 cm plastic cages containing pressed aspen wood chips as bedding (Fort Richard Laboratories, Auckland, NZ) and shredded high purity paper (The Andersons, Maumee, OH, USA) as nest building material. A plastic tube and stainless steel ring were provided for environmental enrichment. The environmental conditions of the room in which the mice were housed were controlled automatically. The room temperature was kept constant at approximately 22 °C, the humidity was around 60 %, the light-dark cycle was 12 h, and the air was exchanged 12 times per h. The mice received the standard rodent diet 'Mouse Diet' (LabDiet, St. Louis, MO, USA) in pellet form, and the animals had unrestricted access to food and drinking water. The bedding, nesting material and water was changed at least once per week, and the health of the mice was checked daily.

Female mice with an age from 10 weeks to 18 weeks were used for the experiments. The WT mice were from the C57BL/6 strain. The original C57BL/6 breeding pairs were purchased from The Jackson Laboratory (Bar Harbor, ME, USA). The breeding pairs for the *Nod2*$^{m/m}$ mice on a C57BL/6 background, as originally described by Maeda and co-workers [131], were kindly provided by Lars Eckmann (University of California, San Diego, La Jolla, CA, USA).

After the original homozygous *Nod2*$^{m/m}$ mice breeding pairs were obtained, they were back-crossed for at least 10 generations with C57BL/6 mice at the AgResearch Ruakura Small Animal Colony. Homozygous offspring *Nod2*$^{m/m}$ mice from homozygous *Nod2*$^{m/m}$ females and males that carried a heterozygous *Nod2* mutation were used for the experiments.

2.3.3 Culture of murine bone marrow-derived macrophages

Bone marrow cells from femurs and tibias were collected from the mice for the culture of BMDMs [256]. The animals were euthanised with CO_2 asphyxiation followed by cervical dislocation and the bones collected in cold RPMI 1640 medium (Life Technologies). Next, the bones were briefly sterilised in 70 % ethanol, and the epiphyses were cut with sterile scissors. The bone marrow cells were flushed out of the diaphysis with cold RPMI 1640 medium.

A single cell suspension was prepared by passing the cells first through a 19-gauge needle (BD, Singapore) and then through a 70 μm cell strainer (BD Labware, Franklin Lakes, NJ, USA). The collected cells were resuspended in TCM consisting of RPMI 1640 medium with additional 10 % FBS (Life Technologies) and 1 % penicillin-streptomycin antibiotics (Life Technologies). In addition, 10 μg/mL macrophage colony-stimulating factor (eBioscience, San Diego, CA, USA) was added to the TCM to induce differentiation of macrophages [256].

The concentration of live cells in the resuspended cell suspension was assessed by staining with 0.2 % trypan blue (Life Technologies, Eugene, OR, USA). Live cells, which have an intact cell membrane, will not be stained with trypan blue [257]. The proportion of live cells in the total cell suspension was determined with a Countess automated cell counter (Invitrogen, Carlsbad, CA, USA). It was necessary to assess the number of viable cells, so that the cell concentration for the subsequent culture of BMDMs could be adjusted to approximately 1×10^6 live cells/mL by adding a respective amount of additional TCM containing 10 μg/mL macrophage colony-stimulating factor.

Next, 1 mL or 10 mL of this cell suspension was plated in non-tissue culture-treated 24-well plates or 100 mm × 20 mm cell culture dishes (both from BD Labware), respectively. The cells were cultured at 37 °C in 7 % CO_2/93 % air. Half of the media was replaced on d 3 and d 6 with fresh TCM containing 10 μg/mL macrophage colony-stimulating factor. The BMDMs were fully differentiated on d 7, and were ready to be used in TiO_2 stimulation assays as described in the following paragraphs.

The cells were kept in culture until d 10 if the cells were not used for experiments immediately on d 7. In that case, half of the TCM was replaced with fresh TCM containing 10 μg/mL macrophage colony-stimulating factor on d 7 and again on d 9 if the cells had not been used for TiO_2 stimulation assays until then.

2.3.4 Exposure of bone marrow-derived macrophages to titanium dioxide with or without bacterial antigens

Prior to incubation with TiO_2 particles, the BMDMs were pre-stimulated with 10 ng/mL LPS from *E. coli* O111:B4 (Sigma-Aldrich, Auckland, NZ) for 3 h in TCM. Only activated BMDMs are able to express co-stimulatory molecules and produce cytokines [191, 197, 258-260]. LPS is commonly used in concentrations between 1 ng/mL and 100 ng/mL to activated cultured cells, and a concentrations of 10 ng/mL LPS was selected based on a previous publication that investigated the response of cultured human macrophages to TiO_2 stimulation [218].

After pre-stimulation, the cells were washed with TCM before the addition of the TiO_2 suspensions or just TCM for cells used as controls. A 1 mg/mL stock suspension of TiO_2 particles was prepared in distilled water. This was used for the preparation of five TiO_2 working suspensions (5/10/25/50/100 μg/mL TiO_2) by adding the respective volume of the TiO_2 stock suspension to TCM. Before the TiO_2 working suspensions were added to the BMDMs, the suspensions were sonicated in a water bath for 10 min to ensure a homogenous distribution of the TiO_2 particles in the TCM.

For co-stimulation experiments with bacterial antigens either PGN from *Bacillus subtilis*, an intestinal commensal species [261], or synthetic MDP (both from Sigma-Aldrich) were added to the TiO_2 working suspensions at a final concentration of 10 μg/mL. These concentrations are routinely used in cell culture experiments with MDP and PGN [131, 253, 262, 263].

The BMDMs were incubated at 37 °C in 7 % CO_2/93 % air in all experiments. For the stimulation experiments, the BMDMs were exposed to TiO_2 particles for 3 h. It has been shown that after incubation for 3 h the TiO_2 particles are taken up by cultured cells [196, 198, 264]. Because previous studies reported the effects of TiO_2 after incubation for 24 h [191, 197, 216, 218], it was decided to also perform experiments in which the cells were kept in culture for this time period in total. In these experiments, the BMDMs were initially stimulated with TiO_2 for 3 h, and then the particles were removed by washing with TCM and the cells incubated for another 21 h in TCM (3 h + 21 h stimulation).

2.3.5 Metabolic activity analysis

The metabolic activity of BMDMs exposed to TiO_2 was assessed with the water-soluble tetrazolium salt (WST)-1 cell proliferation assay. The WST-1 assay is commonly used to

measure the metabolic activity of cultured cells exposed to TiO_2 particles [187]. In this assay, the tetrazolium salt WST-1 is reduced by mitochondrial succinate-tetrazolium reductase to its corresponding formazan dye. As the enzyme is only produced by live cells, the amount of dye generated is an indirect measurement for cell viability. Thus, this assay can be used to determine the cytotoxicity of TiO_2 particles without or with MDP/PGN co-stimulation to BMDMs. Differentiated BMDMs that had been cultured in Petri dishes were harvested by incubation with the non-enzymatic cell dissociation solution Cellstripper (Mediatech, Manassas, VA, USA) for 30 min at 37 °C in 7 % CO_2/93 % air followed by vigorous pipetting. Then, the BMDMs were resuspended in TCM with 10 μg/mL macrophage colony-stimulating factor at a concentration of approximately 1×10^5 cells/mL. Next, 100 μL of the cell suspension was plated in tissue culture-treated 96-well plates (Corning, Corning, NY, USA). The cells were left to adhere to the plates overnight at 37 °C in 7 % CO_2/93 % air.

On the next day, the media was removed, and the cells were washed in 100 μL TCM. Then, TiO_2 working suspensions without or with MDP/PGN were added and the BMDMs incubated for 3 h (3 h time point). The cells were washed in TCM before 150 μL TCM containing 10 % WST-1 cell proliferation reagent (Clontech, Mountain View, CA, USA) was added to the wells. Alternatively, TCM alone was added after 3 h, and the cells were incubated for further 21 h. After this additional incubation period, the BMDMs were incubated with TCM containing the WST-1 reagent as described above. In both cases, after the cells were exposed to the WST-1 reagent they were incubated for 2 h at 37 °C in 7 % CO_2/93 % air. After this incubation time, the absorbance of the samples was measured with a FlexStation 3 microplate reader (Molecular Devices, Sunnyvale, CA, USA) at 450 nm with the reference wavelength at 650 nm according to the protocol for the WST-1 cell proliferation assay provided by the manufacturer. The data were analysed with Soft Max Pro software version 5.4.1 (Molecular Devices). All stimulations were performed in triplicate and the experiment repeated once.

2.3.6 Flow cytometry analysis

The viability, cell morphology, and expression of cell surface activation markers after TiO_2 stimulation was determined with flow cytometry. Flow cytometry is a technique that allows to detect size, granularity, and fluorescent signals of cells that have been tagged with fluorescently labelled antibodies against specific molecules, often cell-surface antigens. In the flow cytometer the stained cells pass through a laser beam in the flow cell, and the scattered light as well as any fluorescent signal emitted by the cells are digitally recorded by

photomultiplier tubes (PMTs). The detection of a signal by the detectors is called an event. Scattered light is recorded by the forward scatter (FSC) and side scatter (SSC) detectors. The FSC signal is dependent on the size of the cell, and the SSC signal corresponds to the granularity of the cell. Larger cells have higher FSC values compared to smaller cells, and cells with a high level of internal complexity, e.g. through the presence of granules, have a high SSC profile. In addition, each fluorescent detector records emitted light of a specific wavelength. Cells that highly express a specific antigen which has been fluorescently labelled by incubation with an antigen-specific antibody will show high fluorescence values in the respective detection channel. The advantage of flow cytometry is that it is a high throughput method because several thousand events can be detected per second. Furthermore, several characteristics can be measured at the same time.

For the flow cytometry experiments BMDMs were first stimulated with TiO_2 suspension without or with MDP or PGN for 3 h or 3 h + 21 h. Then, the stimulated BMDMs were incubated in cold phosphate-buffered saline (PBS; Life Technologies) for 30 min on ice and collected by vigorous pipetting. The cells were resuspended in 150 µL cold fluorescence-activated cell sorting (FACS) buffer, which consisted of PBS containing 2 % FBS, 1 mM ethylenediamine tetra-acetic acid (Life Technologies), and 0.01 % sodium azide (BDH Laboratory Supplies, Poole, UK). Next, the BMDMs were incubated with 1 µg/mL anti-mouse CD16/32 fragment crystallisable region receptor blocking antibody (clone 93; BioLegend, San Diego, CA, USA) for 15 min on ice to prevent unspecific binding of the fluorescently labelled antibodies. Then, the cells were incubated with fluorescently labelled antibodies (all from Biolegend) for 15 min on ice in the dark. The anti-mouse antibodies used for the staining included a marker for murine macrophages, namely phycoerythrin-labelled F4/80 (clone BM8), and Alexa Fluor 488/647-labelled antibodies for the detection of the cell surface activation molecules CD86 (clone GL-1) and CD80 (clone 16-10A1), respectively. The antibodies were used at a concentration of 1 µg/mL for F4/80, or 2.5 µg/mL for both CD80 and CD86.

Titration of the antibodies had shown that at these concentrations the fluorescent signal in relation to the amount of antibody used was adequate. Briefly, for the titration 1×10^6 splenocytes from WT mice were incubated with the respective antibodies in concentrations representing 6-fold serial dilutions from 1:50 to 1:1600 relative to the original antibody concentration. Then, the percentage of cells that stained positive with the respective antibody were compared between the dilution steps. The initial concentrations, which represented a dilution of 1:50 relative to the original antibody concentration, were 4 µg/mL for F4/80 and

10 μg/mL for CD80 and CD86. It was observed that the fluorescent signal at a dilution of 1:200 was similar to the signal obtained at a dilution of 1:50 for all antibodies (data not shown). Therefore, all antibodies were used at a dilution of 1:200 in the subsequent flow cytometry experiments, which corresponded to the antibody concentrations mentioned in the previous paragraph.

Immediately prior to analysis, 0.8 μg/mL propidium iodide (PI; Life Technologies) was added to each sample to be able to assess cell viability through PI exclusion. The stained cell suspensions were analysed with a FACS Calibur flow cytometer (BD Biosciences, San Jose, CA, USA) with a 488 nm argon-ion laser and a 635 nm red-diode laser. With this type of flow cytometer four different fluorescent signals can be detected at the same time in addition to FSC and SSC signals. At least 12,000 total events per sample were acquired with the CellQuest Pro software version 6.0 (BD Biosciences), and the data were analysed with FlowJo version 9.4.3 (Tree Star, Ashland, OR, USA). The gating strategy for the analysis of the flow cytometry data is shown in Figure 2.1. The first step of the analysis was to exclude cell fragments by selecting only events with a FSC intensity greater than 200. Then, the cell viability was determined by separating events based on their PI fluorescence. PI is a red fluorescent dye that binds to nucleic acids and can only penetrate cells with damaged plasma membranes. Therefore, PI staining can be used to assess cell viability because only dead cells will incorporate PI and show positive staining. PI that is bound to nucleic acids can be excited by the 488 nm laser and will emit detectable light in the red spectrum. Thus, live cells can be distinguished from dead or apoptotic cells by flow cytometry. All events with a PI fluorescence less than 10^1 on a logarithmic scale were considered PI negative (PI^-) and therefore viable. Next, the PI^- events that were also F4/80 positive ($F4/80^+$) were selected for further analysis. Events with a F4/80 fluorescence greater than 10^1 on a logarithmic scale were considered $F4/80^+$. Fully differentiated BMDMs were expected to express F4/80, a general marker for murine macrophages [265].

The parameters that were subsequently investigated from this PI^- $F4/80^+$ cell population were the median intensities of the FSC, SSC, CD80, and CD86 signals. The measurements of FSC and SSC signals have been used previously to assess TiO_2 uptake of cultured cells [264, 266]. In addition, the SSC ratio was determined by dividing the median SSC intensity of TiO_2-treated BMDMs by the median SSC intensity of the control cells of the respective genotype [266]. The median fluorescence intensity (MFI) signals of the co-stimulatory molecules CD80 and CD86 were also evaluated. These cell-surface molecules bind to the receptors CD28 or cytotoxic T-lymphocyte antigen 4 (also known as CD152) on

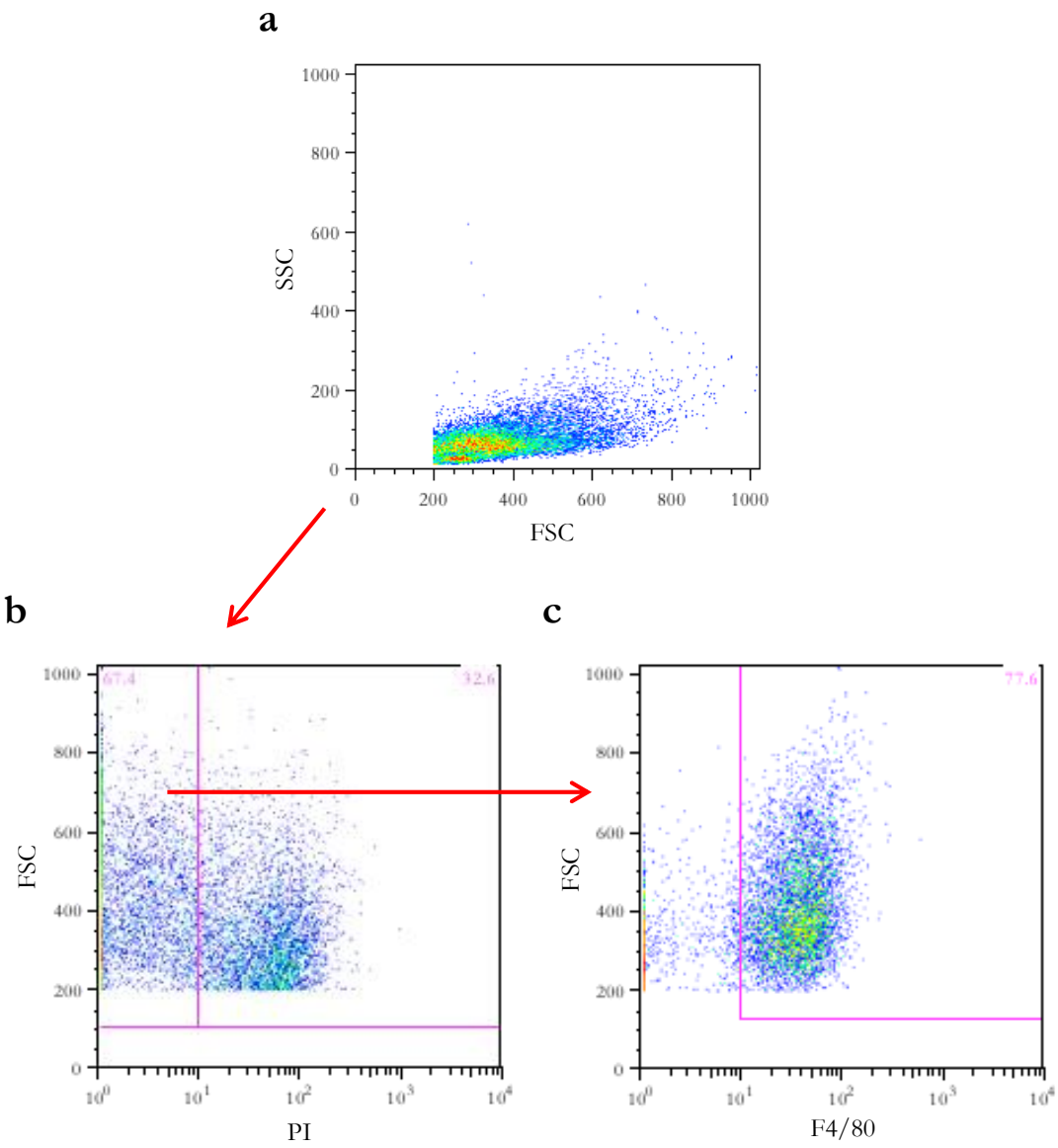

Figure 2.1 *Gating strategy for flow cytometry analysis of TiO_2-exposed BMDMs.*

TiO_2-exposed BMDMs were analysed by flow cytometry. At least 12,000 events were acquired per sample. (**a**) All acquired events with a FSC intensity greater than 200 were selected for further analysis. (**b**) Fluorescence of PI against FSC intensity was analysed. Events were considered PI^- when the PI fluorescence was less than 10^1. (**c**) F4/80 expression against FSC was assessed for all PI^- events. Events were considered $F4/80^+$ when the F4/80 fluorescence was greater than 10^1. Shown are representative frequency dot plots of BMDMs incubated for 3 h in TCM. A colour range from blue to red is used to indicate the frequency of dots on the same spot; blue represents a single event, red represents most events. The pink lines indicate the gates with the percentage of events in the respective gate shown in the top corners.

T cells [267-269]. Interaction of the co-stimulatory molecules with CD28 is required for T cell activation by APCs [270]. Thus, assessing the expression of CD80 and CD86 on BMDMs after treatment with TiO_2 particles may inform on the ability of these cells to stimulate immune responses by effector immune cells. All treatments for the flow cytometry analysis were performed in triplicate and the experiment repeated once.

2.3.7 Exposure of human peripheral blood mononuclear cells to titanium dioxide with or without bacterial antigens

This work was carried out at the Medical Research Council Human Nutrition Research institute in Cambridge, UK. Cryopreserved PBMCs were used in all experiments. Collection of blood from volunteers for isolation of PBMCs was approved by the research ethics committee of Cambridge (reference number 03/296). The cell isolation and cryopreservation was carried out by Ms Carolin Haas and Dr Rachel Hewitt (both Medical Research Council Human Nutrition Research, Cambridge, UK) according to established protocols. Briefly, the PBMCs were isolated from whole blood of healthy volunteers by gradient centrifugation using Lymphoprep (Axis-Shield, Oslo, Norway). Then, the isolated PBMCs were resuspended in TCM containing 10 % dimethyl sulfoxide (Sigma-Aldrich, Gillingham, UK) at a concentration of approximately 100×10^6 cells/mL. The isolated PBMCs were frozen in 1 mL aliquots at −80 °C.

For the TiO_2 stimulation experiments, one aliquot per donor was thawed in a water bath at 37 °C, and the cells were washed once in 50 mL TCM to remove the dimethyl sulfoxide. The PBMCs were resuspended in 50 mL TCM and acclimatised to cell culture conditions overnight at 37 °C in 5 % CO_2/95 % air. On the next day, the PBMCs were resuspended in fresh TCM with 10 ng/mL LPS at a concentration of 1×10^6 cells/mL, plated in 24-well plates at 1 mL/well, and incubated for 3 h at 37 °C in 5 % CO_2/95 % air. Then, the cells were treated with TiO_2 suspensions from 25 μg/mL to 100 μg/mL in TCM without or with MDP or PGN similar to the co-stimulation experiments of murine BMDMs (Section 2.3.4). The PBMCs were incubated with the treatments for 3 h and the first set of supernatants was collected (3 h time point). Fresh TCM without TiO_2 particles and MDP/PGN was added to the cells, and they were incubated for another 21 h before the second set of supernatants was collected (3 h + 21 h time point). Again, fresh TCM containing 10 μg/mL phytohaemagglutinin, a mitogen that specifically stimulates T cells [45], was added to the cells. The PBMCs were incubated for further 48 h (3 h + 69 h time point), and the supernatants were collected before the cells were discarded. All supernatants were stored

at −20 °C until required for cytokine analysis (Section 2.3.8). The experiment was performed three times with PBMCs from three different donors.

2.3.8 Cytokine detection in cell culture supernatants

For the detection of IL-1β and TNF-α in the supernatants of TiO_2-stimulated BMDMs the cells were first exposed to TiO_2 for 3 h, and the first set of supernatants was collected (3 h time point). Then fresh TCM without TiO_2 and bacterial antigens was added to the cells. The BMDMs were incubated for further 21 h when the second set of supernatants was collected (3 h + 21 h time point). The supernatants were kept at −20 °C until the cytokines were measured by enzyme-linked immunosorbent assay (ELISA). Three samples per treatment condition were collected and analysed independently, and the experiment was repeated once.

The IL-1β concentration was also determined in supernatants from TiO_2-stimulated PBMCs that were collected after 3 h and 3 h + 21 h. In addition, the amount of secreted IL-17 was assessed in the supernatants collected at the 3 h + 69 h time point (Section 2.3.7).

All cytokines were detected with DuoSet ELISA Development kits (R&D Systems, Minneapolis, MN, USA) following the instructions provided by the manufacturer. Briefly, 96-well high bind stripwell microplates (Corning) were coated with specific capture antibodies against the respective cytokines overnight. The next day, the capture antibodies were removed, any non-specific binding sites were blocked by incubation with 1 % bovine serum albumin in PBS, and 100 µL sample or standard added to each well. Each sample and standard was analysed in duplicate. After 2 h the samples were aspirated and the plates incubated with antigen-specific biotinylated detection antibodies for 2 h. Streptavidin conjugated to horseradish-peroxidase was added to each well after the detection antibodies were removed, and the plates were incubated for 20 min. Then, the amount of antigen in each well was visualised by adding 100 µL substrate solution consisting of equal amounts of hydrogen peroxide and tetramethylbenzidine. The colour reaction was stopped after 20 min by adding 50 µL 1 M sulphuric acid. The absorbance of the wells was measured with a FlexStation 3 microplate scanner at 450 nm with the wavelength correction set to 570 nm according to the recommendations from the manufacturer. The data was analysed with Soft Max Pro software version 5.4.1 by generating a standard curve from the absorbance values of the standards and calculating the cytokine concentrations of the samples based on this standard curve.

2.3.9 Statistical analysis

All statistical comparisons were performed with R version 3.0.0 [271] after consultation with statisticians Dr John Koolaard and Ms Catherine Lloyd-West (both AgResearch, Palmerston North, NZ). Results of the statistical analyses were considered significant for *p* (probability)-values less-than 0.05. Normal distribution of the data was checked with the Shapiro-Wilk test, and equality of variances between groups was assessed using Bartlett's test before group comparisons were conducted to decide which statistical test should be used (see Appendix A).

For the figures, the data were depicted with means ± standard deviations (SD) in all plots. All graphs were created with SigmaPlot version 12.5 (Systat Software, San Jose, CA, USA).

The results from the TiO_2 stimulation experiments of BMDMs were analysed with two-way analysis of variance (ANOVA) with 'genotype' (WT/*Nod2*$^{m/m}$) and 'TiO_2 concentration' (0/5/10/25/50/100 μg/mL TiO_2) as factors. The output of the two-way ANOVA provided three *p*-values. One *p*-value described the interaction effect between the two factors, and two additional *p*-values were calculated for the effect of each individual factor on the observed results. A potential alternative non-parametric test for a two-way ANOVA would be the Friedman test [272]. However, the Friedman test only provides one *p*-value which is equivalent to the *p*-value for 'Interaction'. No statement about the influence on the observed results of either the genotype or TiO_2 concentration would be possible with this non-parametric test. Therefore, a two-way ANOVA was carried out in all cases, even though in some instances the ANOVA assumptions were not met (see Appendix A). This is a statistically valid method, but the results of the two-way ANOVA will have to be interpreted with caution if the ANOVA assumptions were not met [273]. In cases with a significant interaction between the two factors, a pairwise comparison between all group means was performed with Tukey's honest significant difference (HSD) *post-hoc* test. In these cases, the comparisons of interest were between WT and *Nod2*$^{m/m}$ BMDMs exposed to the same TiO_2 concentration and between TiO_2-treated and untreated cells.

The ELISA results of TiO_2-stimulated PBMCs were analysed with either one-way ANOVA, if the normal distribution and equality of variances assumptions were met, or the non-parametric Kruskal-Wallis test if the assumptions were not met. In both cases, the TiO_2 concentration represented the grouping factor. If the result of the ANOVA or Kruskal-Wallis test were statistically significant, the group means were pairwise compared with Tukey's HSD test or Wilcoxon rank sum test with Bonferroni correction, respectively.

2.4 Results

2.4.1 Characterisation of food-grade titanium dioxide particles

The TiO_2 particles were obtained from a commercial supplier of food grade TiO_2. According to the manufacturer, the particles had anatase crystal structure. This was confirmed with TEM (Figure 2.2a). The average particle size was determined from the TEM images by measuring 133 TiO_2 particles with image analysis software. The mean primary particle size was 118.8 ± 45.0 nm. The size distribution of the TiO_2 particles is shown as a relative frequency histogram in Figure 2.2b. More than two thirds (77.5 %) of the particles had a diameter between 100 nm and 200 nm, and 13.5 % were smaller than 100 nm.

Sizes of particles can vary depending on the medium used for preparing the particle suspension and final particle concentration [274]. The NTA results showed that the size distributions of the TiO_2 particles in TCM were indeed different from the results obtained for TiO_2 particles suspended in water with TEM (Figure 2.2c). The average sizes of TiO_2 particles suspended in TCM in different concentrations were all larger than the average size of TiO_2 particles suspended in water. Moreover, the recorded size distributions of TiO_2 particles in TCM varied depending on the concentrations. The average sizes were 212.9 nm (for a concentrations of 5 μg/mL), 251.8 (10 μg/mL), 233.8 nm (25 μg/mL), 202.4 nm (50 μg/mL), and 160.3 nm (100 μg/mL).

2.4.2 Cytotoxicity of titanium dioxide

Statistical analysis of the results from the WST-1 assay showed that the BMDMs from *Nod2*$^{m/m}$ mice exposed to TiO_2 alone or in addition with MDP or PGN for 3 h + 21 h had a lower metabolic activity compared to WT cells (Figure 2.3). However, there was no significant difference between *Nod2*$^{m/m}$ and WT mice if they were exposed for 3 h (Table 2.1). The TiO_2 concentration only had a significant impact on the metabolic activity of BMDMs when they were co-stimulated with PGN for 3 h. In this case, the metabolic activity was increased for TiO_2 concentrations from 10 μg/mL to 50 μg/mL. For all other treatments, the metabolic activity was not influenced by TiO_2 particle concentration. Neither was there an interaction effect between genotype and TiO_2 concentration for any of the investigated treatments and time points.

Another method to determine particle toxicity was the assessment of cell viability with flow cytometry and PI staining. For all treatments, the viability of both WT and *Nod2*$^{m/m}$ BMDMs

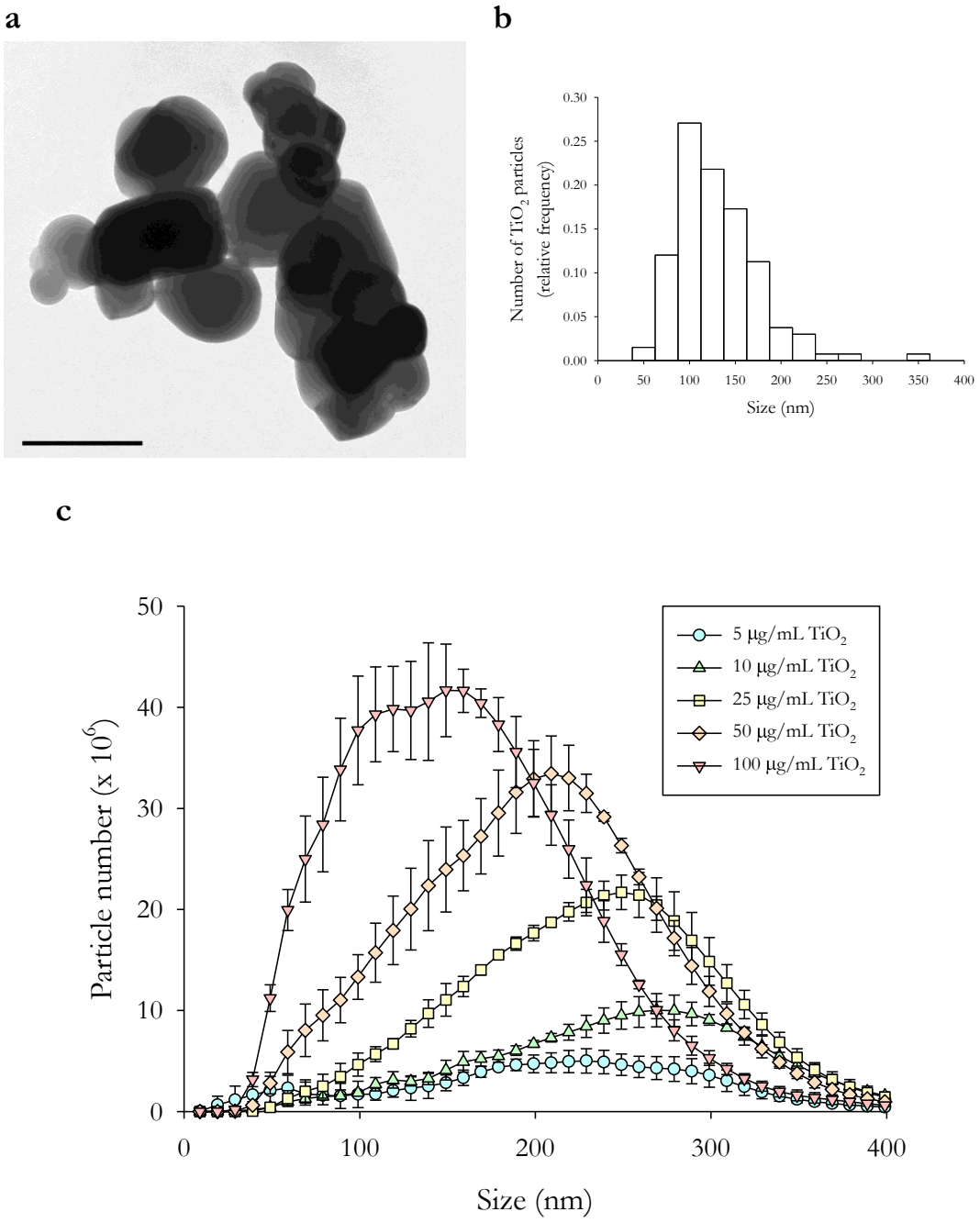

Figure 2.2 *TiO_2 particle characterisation.*

Food-grade anatase TiO_2 particles were characterised with TEM and NTA. (**a**) A TiO_2 particle suspension with a concentration of 1 mg/mL was prepared in distilled water and the particles were observed with TEM; a representative image is shown; scale bar = 200 nm. (**b**) The size distribution of TiO_2 particles in distilled water according to measurements from the TEM images is shown as a histogram; n = 133. (**c**) Five TiO_2 suspensions were prepared in TCM and analysed by NTA; n = 3.

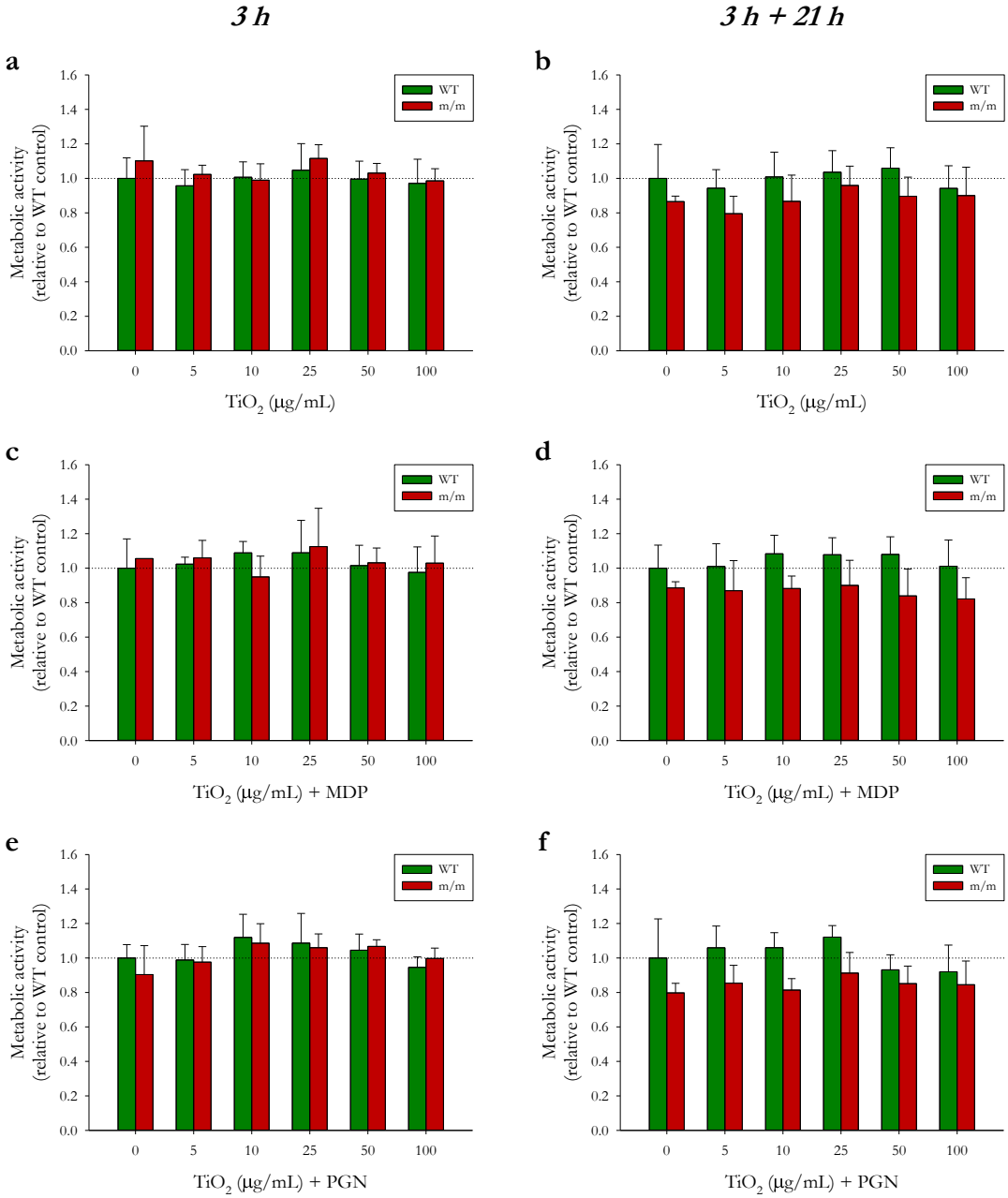

Figure 2.3 *Metabolic activity of BMDMs after TiO_2 exposure with or without MDP/PGN co-stimulation.*
Murine WT or *Nod2*$^{m/m}$ (m/m) BMDMs were pre-stimulated for 3 h with LPS (10 ng/mL). Then BMDMs were incubated with TiO_2 particle suspensions at the indicated concentrations without or with MDP or PGN (10 µg/mL respectively) in TCM for 3 h (**a, c, e**) or 3 h followed by further incubation in TCM for 21 h (**b, d, f**). BMDMs were stimulated with TiO_2 only (**a, b**), TiO_2 + MDP (**c, d**), or TiO_2 + PGN (**e, f**). Metabolic activity was determined by WST-1 assay after 3 h (**a, c, e**) or 3 h + 21 h incubation (**b, d, f**). Plots depict relative changes compared to respective WT control without TiO_2 (dashed line). Shown are results from two independent experiments with three replicates per exposure condition; means ± SD; n = 6, except for *Nod2*$^{m/m}$ control cells with all co-stimulation conditions after 3 h and 3 h +21 h, and *Nod2*$^{m/m}$ cells exposed to 5 µg TiO_2/mL with MDP and PGN co-stimulation after 3 h +21 h with 5 µg/mL where n = 1-5. Results were compared with two-way ANOVA (Table 2.1).

Table 2.1 *Two-way ANOVA results for metabolic activity comparison of murine BMDMs exposed to TiO_2 with or without MDP/PGN co-stimulation.*

Incubation time (h)	***Co-stimulation***	**p-*value*[1]**		
		Genotype	***TiO_2***	***Interaction***
3	-	0.12	0.20	0.82
	MDP	0.83	0.50	0.55
	PGN	0.94	< 0.01	0.73
3 + 21[2]	-	< 0.001	0.26	0.86
	MDP	< 0.001	0.69	0.90
	PGN	< 0.001	0.10	0.41

[1]Statistical comparison with two-way ANOVA with *Nod2* genotype (WT/*Nod2*$^{m/m}$) and TiO_2 concentration (0/5/10/25/50/100 µg/mL TiO_2) as factors. [2]Incubation for 3 h with TiO_2 and respective co-stimulant followed by 21 h incubation in TCM alone.

decreased significantly ($p < 0.001$) with increasing TiO_2 particle concentrations (Table 2.2 & Figure 2.4). The decrease in viability was similar for all co-stimulation conditions, i.e. without or with MDP or PGN. There was also a significant ($p < 0.05$) genotype specific effect for most of the treatments, except with MDP and PGN co-stimulation for the 3 h + 21 h time point. BMDMs from *Nod2*$^{m/m}$ mice showed a lower viability under all treatments at 3 h and for exposure to TiO_2 alone at 3 h + 21 h. This was independent of TiO_2 exposure, however, as there was no significant statistical interaction effect, except for the 3 h + 21 h time point for TiO_2 alone. Under these conditions exposure to 5 μg/mL TiO_2 led to a significantly decreased ($p < 0.01$) cell viability in *Nod2*$^{m/m}$ cells compared to those from WT mice. Furthermore, *Nod2*$^{m/m}$ BMDMs exposed to 5 μg/mL TiO_2, and cells from both WT and *Nod2*$^{m/m}$ mice exposed to 10 μg/mL TiO_2 and more were significantly less viable ($p < 0.001$) than unexposed WT cells.

2.4.3 Phenotype and morphology of bone marrow-derived macrophages after exposure to titanium dioxide

All treatment conditions lead to a significant reduction ($p < 0.05$) in F4/80 expression after TiO_2 exposure (Table 2.2). The decrease was highest for TiO_2 + PGN co-stimulation for 3 h (Figure 2.5). The F4/80 expression was significantly lower ($p < 0.05$) in *Nod2*$^{m/m}$ cells in all treatments, except TiO_2 + MDP/PGN co-stimulation for 3 h + 21 h. There was no significant interaction effect between *Nod2* genotype and TiO_2 concentration. Only cells that were positive for F4/80 were further analysed for FSC/SSC intensities and activation marker expression (see Figure 2.1).

Representative dot plots depicting the FSC *versus* SSC profiles of BMDMs incubated with or without TiO_2 particles in TCM alone are shown in Figure 2.6. The median FSC was significantly affected ($p < 0.001$) by the TiO_2 concentration for all treatments and time points (Table 2.3). It was negatively correlated with particle concentration in the media, i.e. it decreased with increasing particle concentration (Figure 2.7). The genotype also had an effect on the median FSC in all groups, except with TiO_2 alone or MDP co-stimulation after 3 h. For all other treatment groups, the median FSC was significantly higher ($p < 0.05$) for *Nod2*$^{m/m}$ BMDMs compared to WT cells. There were no significant interaction effects for all conditions and time points.

Incubation of BMDMs with TiO_2 had a significant effect ($p < 0.001$) on the median SSC intensities under all treatment conditions (Table 2.3). The increase in SSC was positively

Table 2.2 *Two-way ANOVA results for viability and F4/80 expression comparison of murine BMDMs exposed to TiO_2 with or without MDP/PGN co-stimulation.*

Parameter	***Incubation time (h)***	***Co-stimulation***	**p-*value*[1]**		
			Genotype	***TiO_2***	***Interaction***
Viability	*3*	-	< 0.001	< 0.001	1.00
		MDP	< 0.01	< 0.001	0.85
		PGN	< 0.05	< 0.001	1.00
	3 + 21[2]	-	< 0.001	< 0.001	< 0.01
		MDP	0.36	< 0.001	0.22
		PGN	0.97	< 0.001	0.54
F4/80	*3*	-	< 0.001	< 0.05	0.46
		MDP	< 0.001	< 0.001	0.65
		PGN	< 0.001	< 0.001	0.29
	3 + 21[2]	-	< 0.05	< 0.001	0.95
		MDP	0.27	< 0.001	0.11
		PGN	0.05	< 0.001	0.88

[1]Statistical comparison with two-way ANOVA with *Nod2* genotype (WT/*Nod2*$^{m/m}$) and TiO_2 concentration (0/5/10/25/50/100 μg/mL TiO_2) as factors. [2]Incubation for 3 h with TiO_2 and respective co-stimulant followed by 21 h incubation in TCM alone.

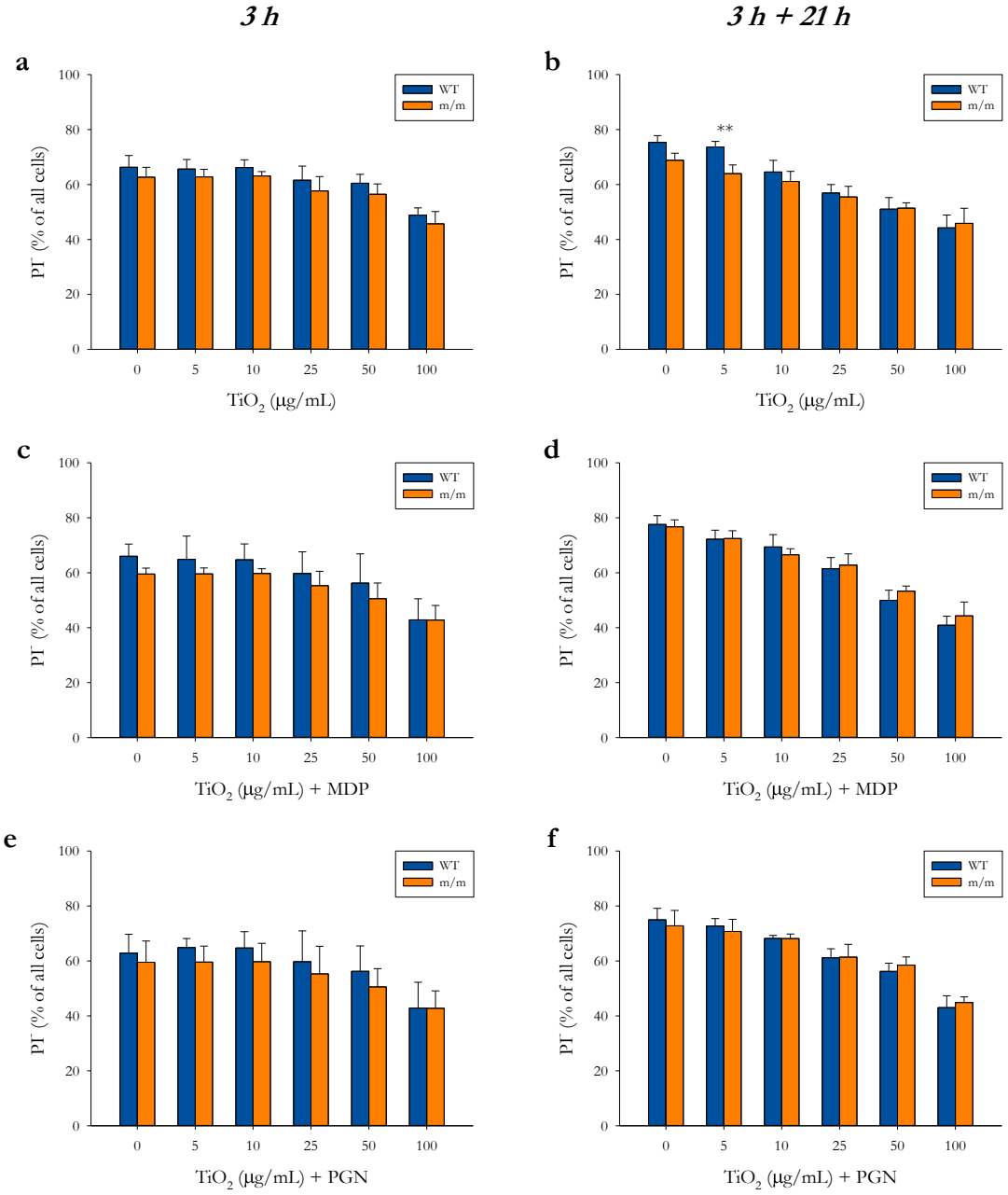

Figure 2.4 *Viability of BMDMs after TiO_2 exposure with or without MDP/PGN co-stimulation.*

Murine WT or *Nod2$^{m/m}$* (m/m) BMDMs were pre-stimulated for 3 h with LPS (10 ng/mL). Then BMDMs were incubated with TiO_2 particle suspensions at the indicated concentrations without or with MDP or PGN (10 µg/mL respectively) in TCM for 3 h (**a, c, e**) or 3 h followed by further incubation in TCM for 21 h (**b, d, f**). BMDMs were stimulated with TiO_2 alone (**a, b**), TiO_2 + MDP (**c, d**), or TiO_2 + PGN (**e, f**). BMDMs were collected for analysis by flow cytometry after 3 h (**a, c, e**) or 3 h + 21 h incubation (**b, d, f**), and the viability was assessed with PI staining. Shown are results from two independent experiments with three replicates per exposure condition respectively; means ± SD; $n = 6$. Results were compared with two-way ANOVA (Table 2.2). (**b**) Pairwise group comparisons with Tukey's HSD test; $^{**}p < 0.001$ = significant differences between WT and *Nod2$^{m/m}$* BMDMs exposed to the same TiO_2 concentration.

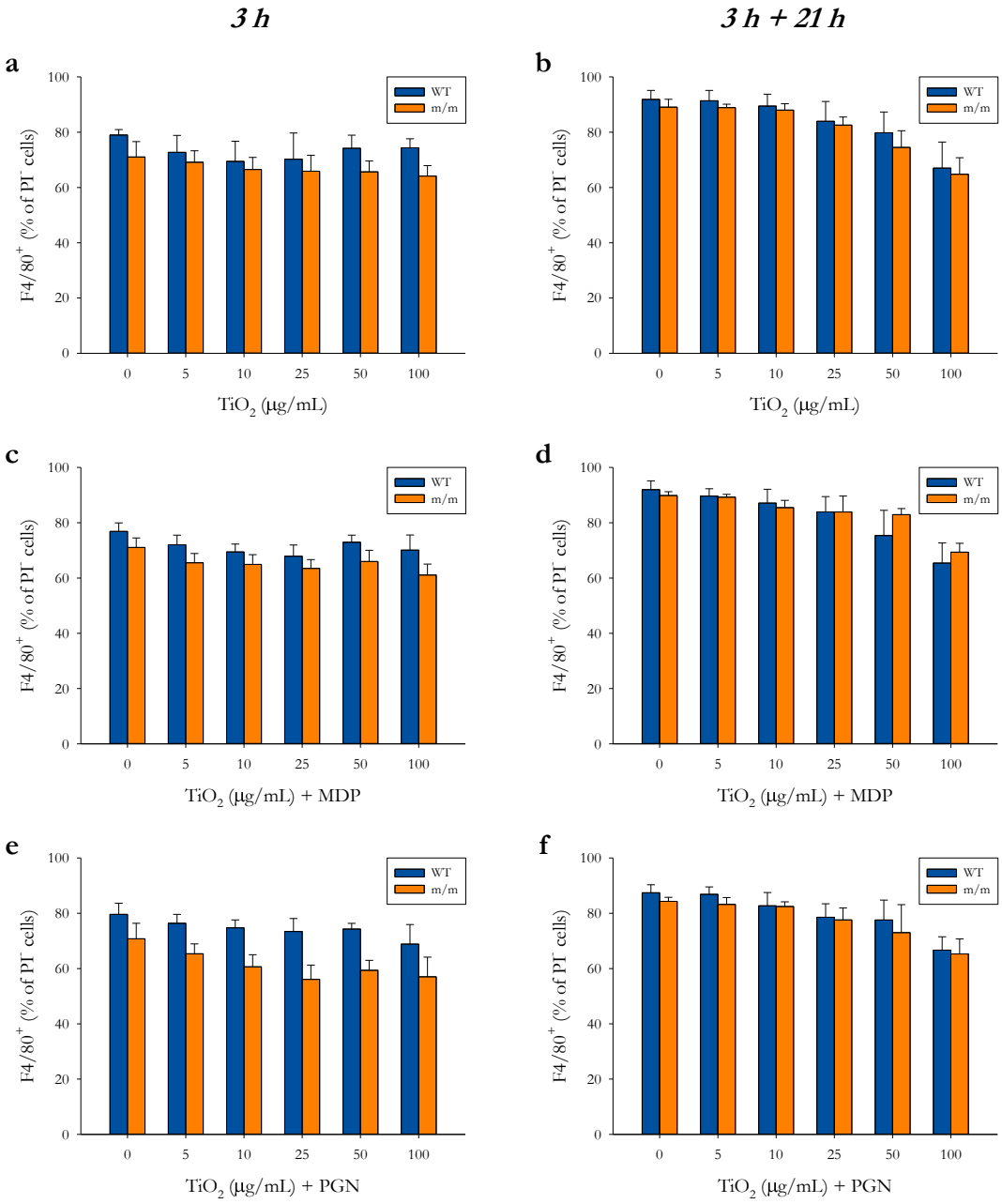

Figure 2.5 *F4/80 expression of BMDMs after TiO_2 exposure with or without MDP/PGN co-stimulation.*

Murine WT or *Nod2$^{m/m}$* (m/m) BMDMs were pre-stimulated for 3 h with LPS (10 ng/mL). Then BMDMs were incubated with TiO_2 particle suspensions at the indicated concentrations without or with MDP or PGN (10 µg/mL respectively) in TCM for 3 h (**a, c, e**) or 3 h followed by further incubation in TCM for 21 h (**b, d, f**). BMDMs were stimulated with TiO_2 alone (**a, b**), TiO_2 + MDP (**c, d**), or TiO_2 + PGN (**e, f**). BMDMs were collected for analysis by flow cytometry after 3 h (**a, c, e**) or 3 h + 21 h incubation (**b, d, f**), and F4/80 expression of PI^- events was determined. Shown are results from two independent experiments with three replicates per exposure condition respectively; means ± SD; $n = 6$. Results were compared with two-way ANOVA (Table 2.2).

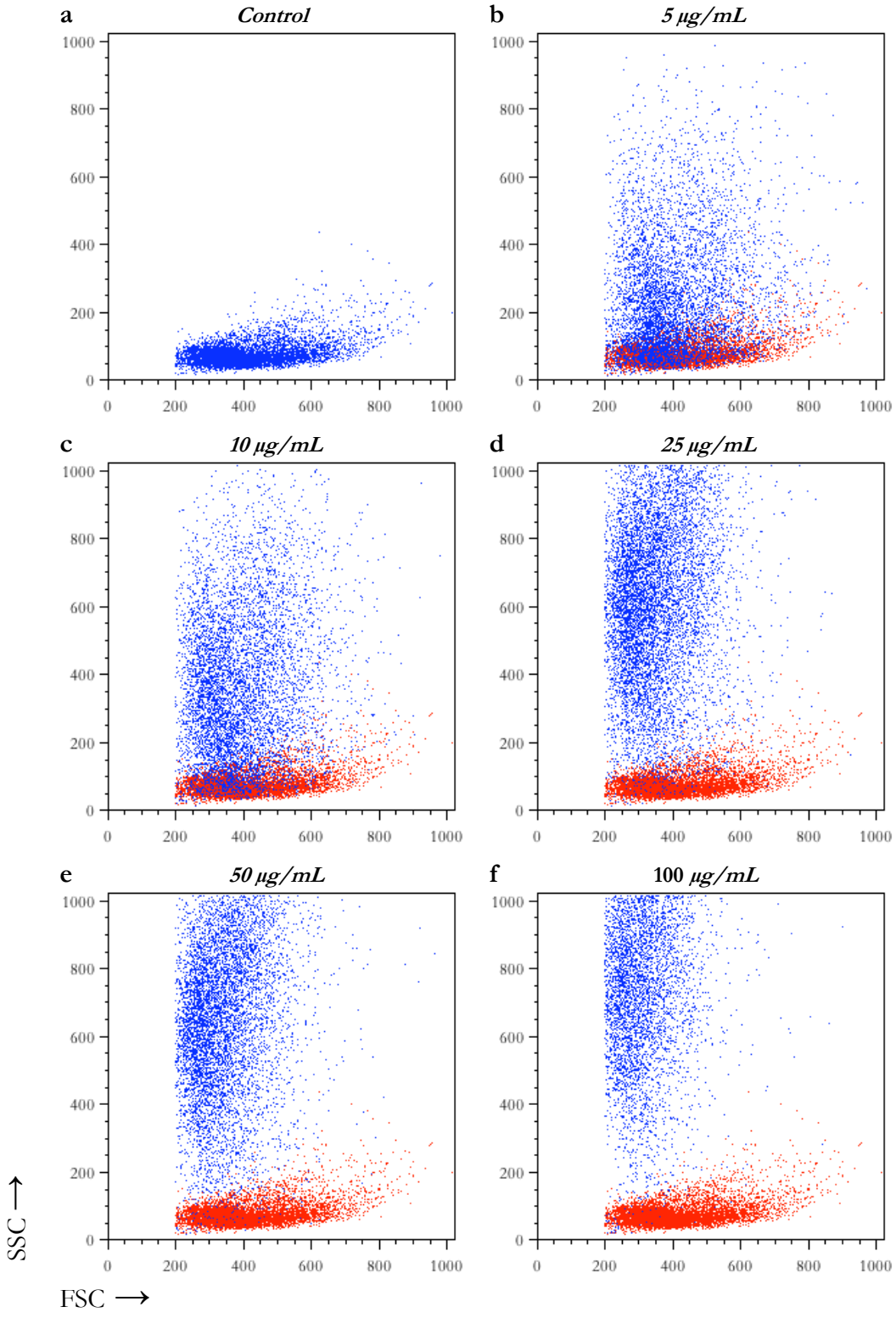

Figure 2.6 *FSC versus SSC dot plots of TiO_2-exposed BMDMs.*

FSC and SSC intensities of TiO_2 exposed murine WT BMDMs were determined with flow cytometry. BMDMs were incubated in TCM without (**a**), or with 5 µg/mL (**b**), 10 µg/mL (**c**), 25 µg/mL (**d**), 50 µg/mL (**e**), or 100 µg/mL (**f**) TiO_2 particles. The cells were collected for analysis with flow cytometry after 3 h. Blue dot plots represent events of PI^- $F4/80^+$ BMDMs incubated with respective TiO_2 concentrations in TCM alone. (**b-f**) For comparison events of BMDMs incubated without TiO_2 (**a**) are shown (red dots).

Table 2.3 *Two-way ANOVA results for FSC and SSC intensities and relative SSC increase comparison of murine BMDMs exposed to TiO_2 with or without MDP/PGN co-stimulation.*

Parameter	Incubation time (h)	Co-stimulation	p-value[1]		
			Genotype	TiO_2	Interaction
FSC intensity	*3*	-	0.39	< 0.001	1.00
		MDP	0.15	< 0.001	1.00
		PGN	< 0.01	< 0.001	0.76
	3 + 21[2]	-	< 0.05	< 0.001	0.07
		MDP	< 0.001	< 0.001	0.11
		PGN	< 0.001	< 0.001	0.30
SSC intensity	*3*	-	0.21	< 0.001	0.99
		MDP	0.24	< 0.001	0.99
		PGN	0.10	< 0.001	0.81
	3 + 21[2]	-	0.34	< 0.001	0.98
		MDP	0.89	< 0.001	0.74
		PGN	< 0.01	< 0.001	0.34
SSC ratio	*3*	-	< 0.001	< 0.001	0.42
		MDP	< 0.01	< 0.001	0.72
		PGN	< 0.01	< 0.001	0.49
	3 + 21[2]	-	0.72	< 0.001	0.99
		MDP	< 0.01	< 0.001	0.42
		PGN	0.59	< 0.001	0.64

[1]Statistical comparison with two-way ANOVA with *Nod2* genotype (WT/*Nod2*$^{m/m}$) and TiO_2 concentration (0/5/10/25/50/100 µg/mL TiO_2) as factors. [2]Incubation for 3 h with TiO_2 and respective co-stimulant followed by 21 h incubation in TCM alone.

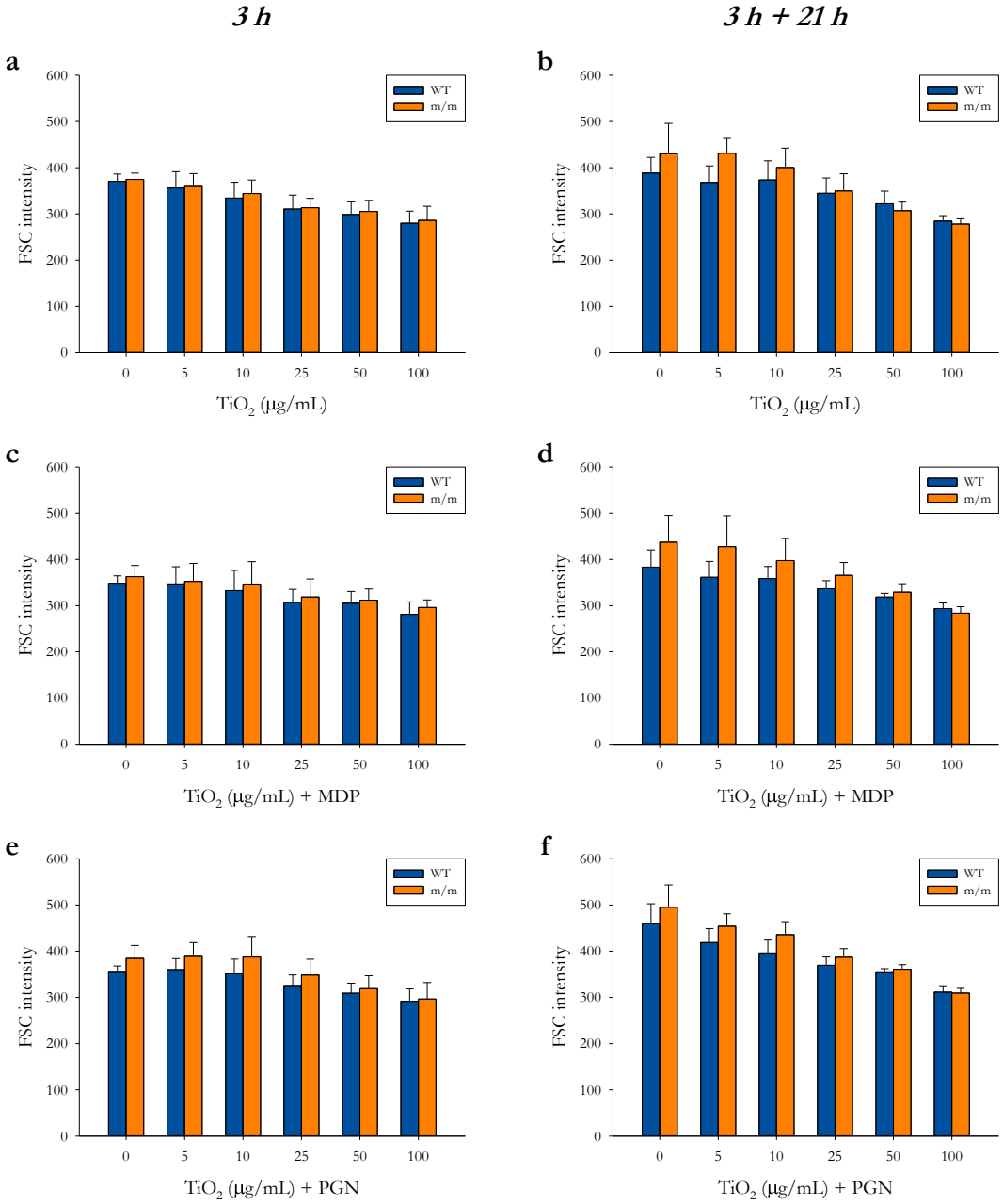

Figure 2.7 *FSC intensity of BMDMs after TiO_2 exposure with or without MDP/PGN co-stimulation.*

Murine WT or *Nod2*$^{m/m}$ (m/m) BMDMs were pre-stimulated for 3 h with LPS (10 ng/mL). Then BMDMs were incubated with TiO_2 particle suspensions at the indicated concentrations without or with MDP or PGN (10 µg/mL respectively) in TCM for 3 h (**a, c, e**) or 3 h followed by further incubation in TCM for 21 h (**b, d, f**). BMDMs were stimulated with TiO_2 alone (**a, b**), TiO_2 + MDP (**c, d**), or TiO_2 + PGN (**e, f**). BMDMs were collected for analysis by flow cytometry after 3 h (**a, c, e**) or 3 h + 21 h incubation (**b, d, f**), and the median FSC intensity of PI^- $F4/80^+$ BMDMs was determined. Shown are results from two independent experiments with three replicates per exposure condition respectively; means ± SD; n = 6. Results were compared with two-way ANOVA (Table 2.3).

correlated with increasing TiO_2 concentrations for all groups (Figure 2.8). A significant genotype effect was only detected for TiO_2 + PGN co-stimulation for the 3 h + 21 h time point ($p < 0.01$). No interaction effects between genotype and TiO_2 concentration were observed.

As expected from the above results, the average SSC ratio increased with increasing particle concentration for all treatments and both *Nod2* genotypes (Figure 2.9). The SSC ratio for the 100 μg/mL TiO_2 dose was at least 10-fold higher for all co-stimulation conditions and time points compared to unexposed cells. The effect of TiO_2 treatment was significant ($p < 0.001$) for all conditions (Table 2.3). In contrast to results for average absolute SSC increases, there was a significant genotype effect ($p < 0.01$) on the average SSC ratio for all groups, except the 3 h+ 21 h time points for TiO_2 alone and TiO_2 + PGN. In agreement with the results for average absolute SSC increase, there were also no interaction effects for the average SSC ratios.

2.4.4 Activation of bone marrow-derived macrophages after exposure to titanium dioxide

The expressions of the activation markers CD80 and CD86 were also determined with flow cytometry. Results were reported as ratios of TiO_2-treated to untreated WT cells because of some variability in the absolute values between the independent experiments. The overall expression of CD80 was significantly greater ($p < 0.001$) in BMDMs from *Nod2*$^{m/m}$ mice, except for the treatments with TiO_2 in TCM alone or together with PGN for the 3 h + 21 h time points (Table 2.4 & Figure 2.10). The CD86 MFI were also significantly higher ($p < 0.001$) in cells from *Nod2*$^{m/m}$ mice, except for the treatments with TiO_2 in TCM alone or with MDP co-stimulation for the 3 h + 21 h time point (Table 2.4 & Figure 2.11). TiO_2 exposure significantly decreased CD80 MFI ($p < 0.05$), except with MDP co-stimulation after 3 h. In contrast, CD86 expression was significantly increased ($p < 0.01$) in TiO_2-treated cells with all treatments at both time points. Significant interaction effects were observed for both activation markers with MDP co-stimulation after 3 h ($p < 0.01$). There was also a significant interaction effect ($p < 0.05$) for CD86 expression in PGN-stimulated BMDMs after 3 h + 21 h. The results of Tukey's HSD *post-hoc* test showed that the CD80 expression in *Nod2*$^{m/m}$ cells treated with 100 μg/mL TiO_2 + MDP was significantly higher ($p < 0.001$) compared to WT BMDMs exposed to the same TiO_2 concentration or the control cells (Figure 2.10b).

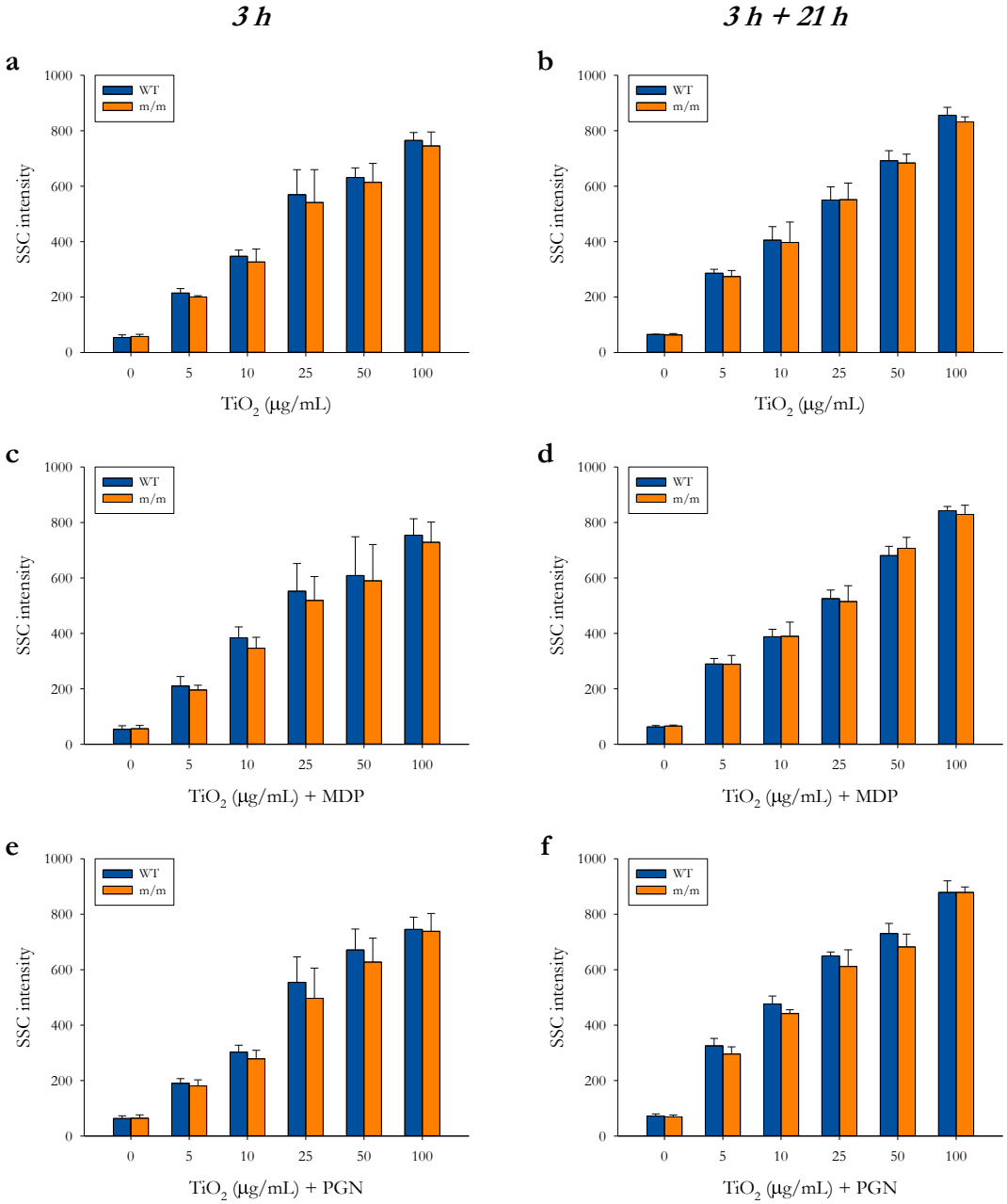

Figure 2.8 *SSC intensity of BMDMs after TiO_2 exposure with or without MDP/PGN co-stimulation.*

Murine WT or *Nod2*$^{m/m}$ (m/m) BMDMs were pre-stimulated for 3 h with LPS (10 ng/mL). Then BMDMs were incubated with TiO_2 particle suspensions at the indicated concentrations without or with MDP or PGN (10 µg/mL respectively) in TCM for 3 h (**a, c, e**) or 3 h followed by further incubation in TCM for 21 h (**b, d, f**). BMDMs were stimulated with TiO_2 alone (**a, b**), TiO_2 + MDP (**c, d**), or TiO_2 + PGN (**e, f**). BMDMs were collected for analysis by flow cytometry after 3 h (**a, c, e**) or 3 h + 21 h incubation (**b, d, f**), and the median SSC intensity of PI^- $F4/80^+$ BMDMs was determined. Shown are results from two independent experiments with three replicates per exposure condition respectively; means ± SD; n = 6. Results were compared with two-way ANOVA (Table 2.3).

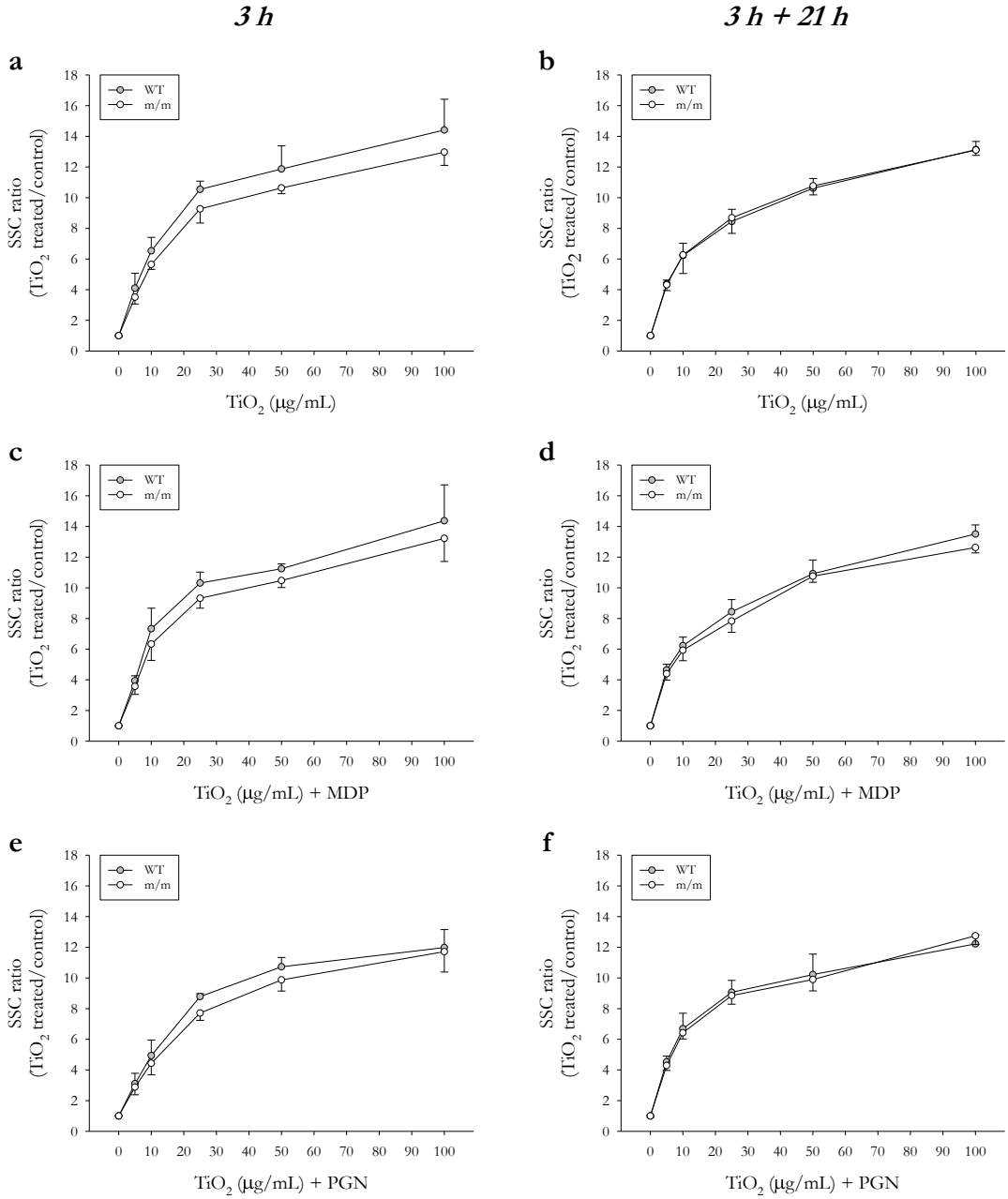

Figure 2.9 *Relative SSC increase of TiO_2-exposed BMDMs compared to unstimulated controls with or without MDP/PGN co-stimulation.*

Murine WT or *Nod2*$^{m/m}$ (m/m) BMDMs were pre-stimulated for 3 h with LPS (10 ng/mL). Then BMDMs were incubated with TiO_2 particle suspensions at the indicated concentrations without or with MDP or PGN (10 µg/mL respectively) in TCM for 3 h (**a, c, e**) or 3 h followed by further incubation in TCM for 21 h (**b, d, f**). BMDMs were stimulated with TiO_2 alone (**a, b**), TiO_2 + MDP (**c, d**), or TiO_2 + PGN (**e, f**). BMDMs were collected for analysis by flow cytometry after 3 h (**a, c, e**) or 3 h + 21 h incubation (**b, d, f**), and the median SSC intensity of PI^- $F4/80^+$ BMDMs was determined. Shown are results from two independent experiments with three replicates per exposure condition respectively; means ± SD; n = 6. Results were compared with two-way ANOVA (Table 2.3).

Table 2.4 *Two-way ANOVA results for CD80 and CD86 expression comparison of murine BMDMs exposed to TiO_2 with or without MDP/PGN co-stimulation.*

Cell surface molecule	***Incubation time (h)***	***Co-stimulation***	**p-*value*[1]**		
			Genotype	***TiO_2***	***Interaction***
CD80	*3*	-	< 0.001	< 0.05	0.72
		MDP	< 0.001	0.40	< 0.01
		PGN	< 0.01	< 0.001	0.82
	3 + 21[2]	-	0.96	< 0.001	0.18
		MDP	< 0.001	< 0.001	0.14
		PGN	0.09	< 0.001	0.40
CD86	*3*	-	< 0.001	< 0.001	0.93
		MDP	< 0.001	< 0.001	< 0.001
		PGN	< 0.001	< 0.001	0.44
	3 + 21[2]	-	0.97	< 0.001	0.94
		MDP	0.36	< 0.001	0.95
		PGN	< 0.001	< 0.001	< 0.05

[1]Statistical comparison with two-way ANOVA with *Nod2* genotype (WT/*Nod2*$^{m/m}$) and TiO_2 concentration (0/5/10/25/50/100 µg/mL TiO_2) as factors. [2]Incubation for 3 h with TiO_2 and respective co-stimulant followed by 21 h incubation in TCM alone.

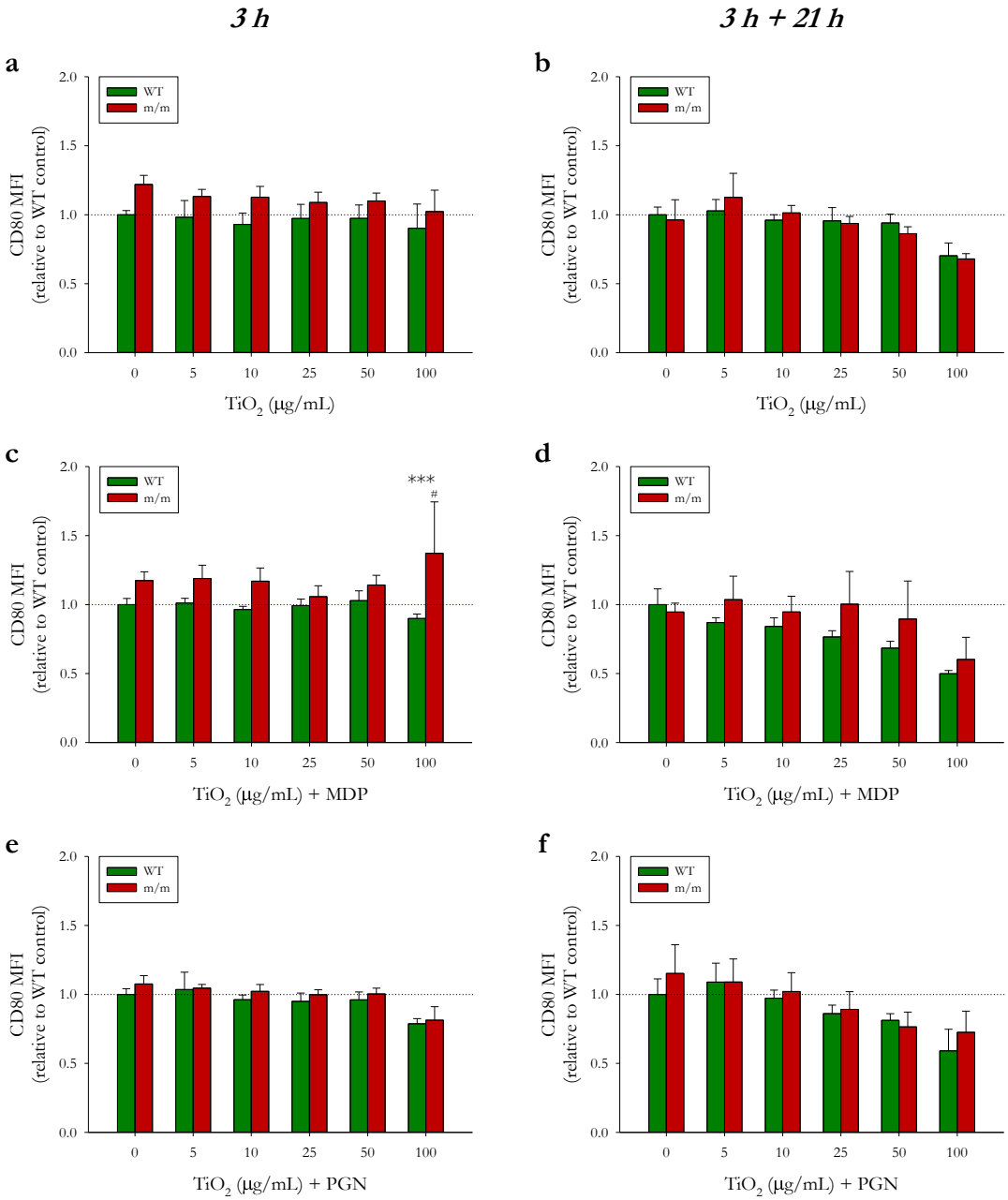

Figure 2.10 *CD80 expression of BMDMs after TiO_2 exposure with or without MDP/PGN co-stimulation.*
Murine WT or *Nod2$^{m/m}$* (m/m) BMDMs were pre-stimulated for 3 h with LPS (10 ng/mL). Then BMDMs were incubated with TiO_2 particle suspensions at the indicated concentrations without or with MDP or PGN (10 µg/mL respectively) in TCM for 3 h (**a, c, e**) or 3 h followed by further incubation in TCM for 21 h (**b, d, f**). BMDMs were stimulated with TiO_2 alone (**a, b**), TiO_2 + MDP (**c, d**), or TiO_2 + PGN (**e, f**). BMDMs were collected for analysis by flow cytometry after 3 h (**a, c, e**) or 3 h + 21 h incubation (**b, d, f**), and the CD80 MFI of PI^- $F4/80^+$ BMDMs was determined. Plots depict relative changes compared to WT control cells (dashed line). Shown are results from two independent experiments with three replicates per exposure condition respectively; means ± SD; $n = 6$. Results were compared with two-way ANOVA (Table 2.4). (**c**) Pairwise group comparisons with Tukey's HSD test; $^{***}p < 0.001$ = significant differences between WT and *Nod2$^{m/m}$* BMDMs exposed to the same TiO_2 concentration; $^{\#}p < 0.05$ = significant differences between BMDMs exposed to TiO_2 and unexposed WT BMDMs.

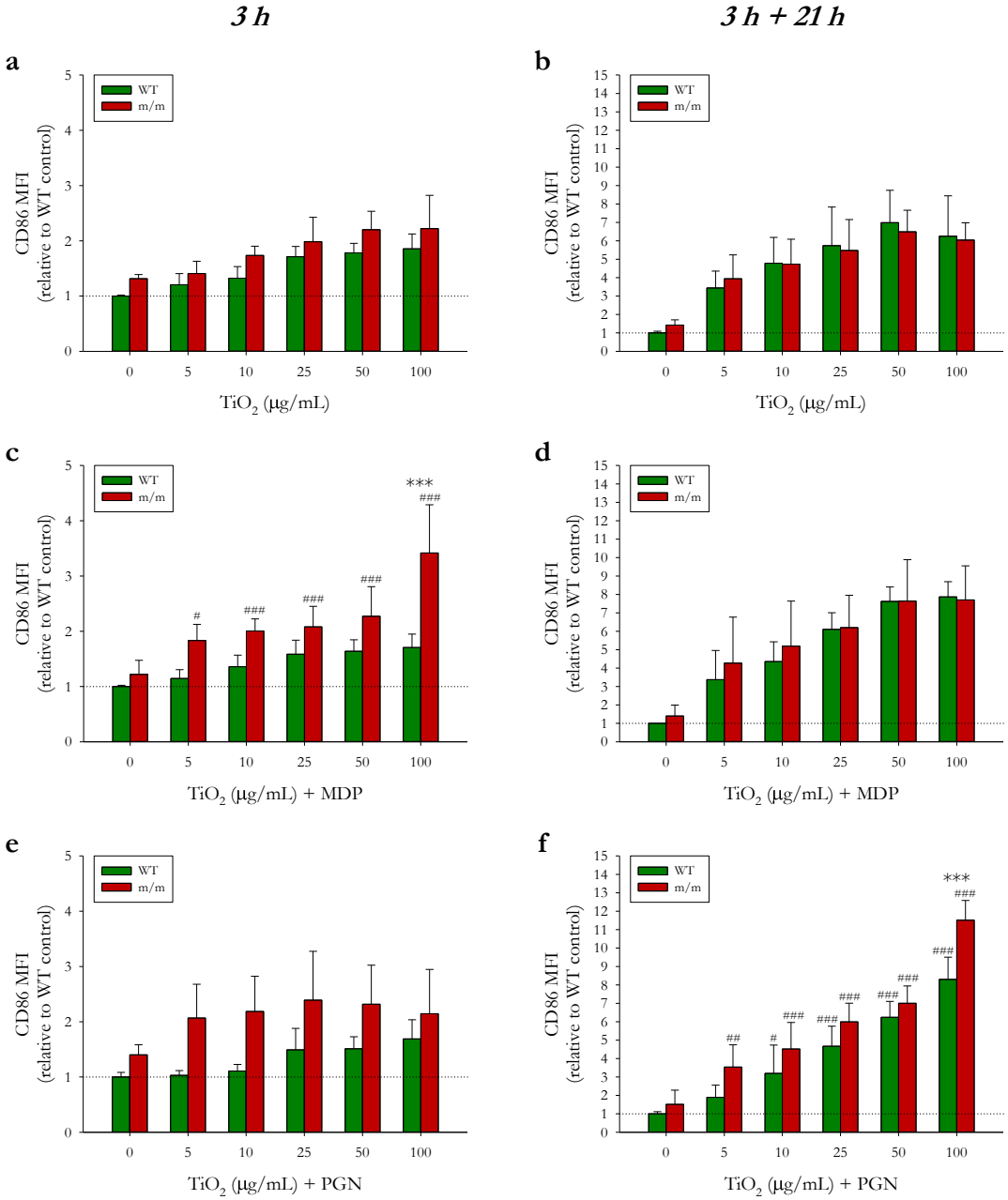

Figure 2.11 *CD86 expression of BMDMs after TiO_2 exposure with or without MDP/PGN co-stimulation.*
Murine WT or *Nod2*$^{m/m}$ (m/m) BMDMs were pre-stimulated for 3 h with LPS (10 ng/mL). Then BMDMs were incubated with TiO_2 particle suspensions at the indicated concentrations without or with MDP or PGN (10 µg/mL respectively) in TCM for 3 h (**a, c, e**) or 3 h followed by further incubation in TCM for 21 h (**b, d, f**). BMDMs were stimulated with TiO_2 only (**a, b**), TiO_2 + MDP (**c, d**), or TiO_2 + PGN (**e, f**). BMDMs were collected for analysis by flow cytometry after 3 h (**a, c, e**) or 3 h + 21 h incubation (**b, d, f**), and the CD86 MFI of PI^- $F4/80^+$ BMDMs was determined. Plots depict relative changes compared to WT control cells (dashed line). Shown are results from two independent experiments with three replicates per exposure condition respectively; means ± SD; $n = 6$. Results were compared with two-way ANOVA (Table 2.4). (**c, f**) Pairwise group comparisons with Tukey's HSD test; $^{***}p < 0.001$ = significant differences between WT and *Nod2*$^{m/m}$ BMDMs exposed to the same TiO_2 concentration; $^{\#}p < 0.05$, $^{\#\#}p < 0.01$, $^{\#\#\#}p < 0.001$ = significant differences between BMDMs exposed to TiO_2 and unexposed WT BMDMs.

In both cases with a significant interaction effect for relative CD86 expression the *Nod2*$^{m/m}$ BMDMs that were exposed to 100 μg/mL TiO_2 expressed significantly more ($p < 0.001$) CD86 compared to the WT cells that were exposed to the same TiO_2 concentration (Figure 2.11b, f). All cells from *Nod2*$^{m/m}$ mice that were exposed to TiO_2 in the presence of MDP showed a significantly higher ($p < 0.05$) relative CD86 MFI after 3 h. In contrast, cells derived from WT mice did not show significantly increased expression of CD86 under the same circumstances (Figure 2.11b). However, this genotype effect for MDP co-stimulation was not observed after 3 h+ 21 h stimulation unlike with PGN co-stimulation. In the latter case, there was both a genotype and an interaction effect after 3 h + 21 h incubation. Analysis with Tukey's HSD *post-hoc* test also showed that nearly all particle-exposed cells, except WT cells treated with 5 μg/mL TiO_2, had significantly elevated ratios ($p < 0.05$) of CD86 MFI compared to untreated WT cells (Figure 2.11f).

2.4.5 Cytokine secretion by bone marrow-derived macrophages after exposure to titanium dioxide

The results of this study showed that TNF-α secretion was significantly affected ($p < 0.001$) by genotype, except with MDP or PGN co-stimulation at the 3 h + 21 h time point (Table 2.5). In cases with a significant genotype difference, the secretion of TNF-α by *Nod2*$^{m/m}$ cells was significantly elevated compared to WT cells (Figure 2.12). The levels of TNF-α in the supernatant of treated cells were also significantly affected ($p < 0.001$) by TiO_2 particle concentration for treatment with TiO_2 alone after 3 h and 3 h + 21 h and with MDP co-stimulation for the 3 h + 21 h time point. In the first two cases, TNF-α secretion increased with increasing TiO_2 concentration. However, when BMDMs were incubated for 3 h + 21 h with TiO_2 + MDP, TNF-α secretion was highest for 25 μg/mL TiO_2 and decreased again for higher TiO_2 concentrations (Figure 2.12e). No interaction effects were detected with the statistical analysis (Table 2.5). Visual comparison of the graphs showed that TNF-α levels were much higher for incubation with TCM and bacterial antigens compared to incubation with TCM alone, and PGN co-stimulation induced greater TNF-α secretion than MDP co-stimulation (Figure 2.12).

Unlike for TNF-α, the IL-1β concentration increased significantly ($p < 0.001$) with increasing TiO_2 concentration for all treatments and time points, except for TiO_2 + PGN co-stimulation for 3 h + 21 h (Figure 2.13). Cells from *Nod2*$^{m/m}$ mice produced significantly more ($p < 0.01$) IL-1β compared to WT cells when they were co-stimulated with bacterial antigens (Table 2.5) at both time points. An interaction was observed for stimulation with

Table 2.5 *Two-way ANOVA results for IL-1β and TNF-a secretion comparison of murine BMDMs exposed to TiO_2 with or without MDP/PGN co-stimulation.*

Cytokine	Incubation time (h)	Co-stimulation	p-value[1]		
			Genotype	TiO_2	Interaction
TNF-a	*3*	-	< 0.001	< 0.001	0.16
		MDP	< 0.001	0.34	0.99
		PGN	< 0.001	0.45	0.98
	3 + 21[2]	-	< 0.001	< 0.001	0.86
		MDP	0.38	< 0.001	0.56
		PGN	0.24	0.41	0.92
IL-1β	*3*	-	0.92	< 0.001	1.00
		MDP	< 0.01	< 0.001	0.13
		PGN	< 0.001	< 0.001	< 0.001
	3 + 21[2]	-	0.68	< 0.001	0.89
		MDP	< 0.01	< 0.001	0.55
		PGN	< 0.001	0.13	< 0.01

[1]Statistical comparison with two-way ANOVA with *Nod2* genotype (WT/*Nod2*$^{m/m}$) and TiO_2 concentration (0/5/10/25/50/100 μg/mL TiO_2) as factors. [2]Incubation for 3 h with TiO_2 and respective co-stimulant followed by 21 h incubation in TCM alone.

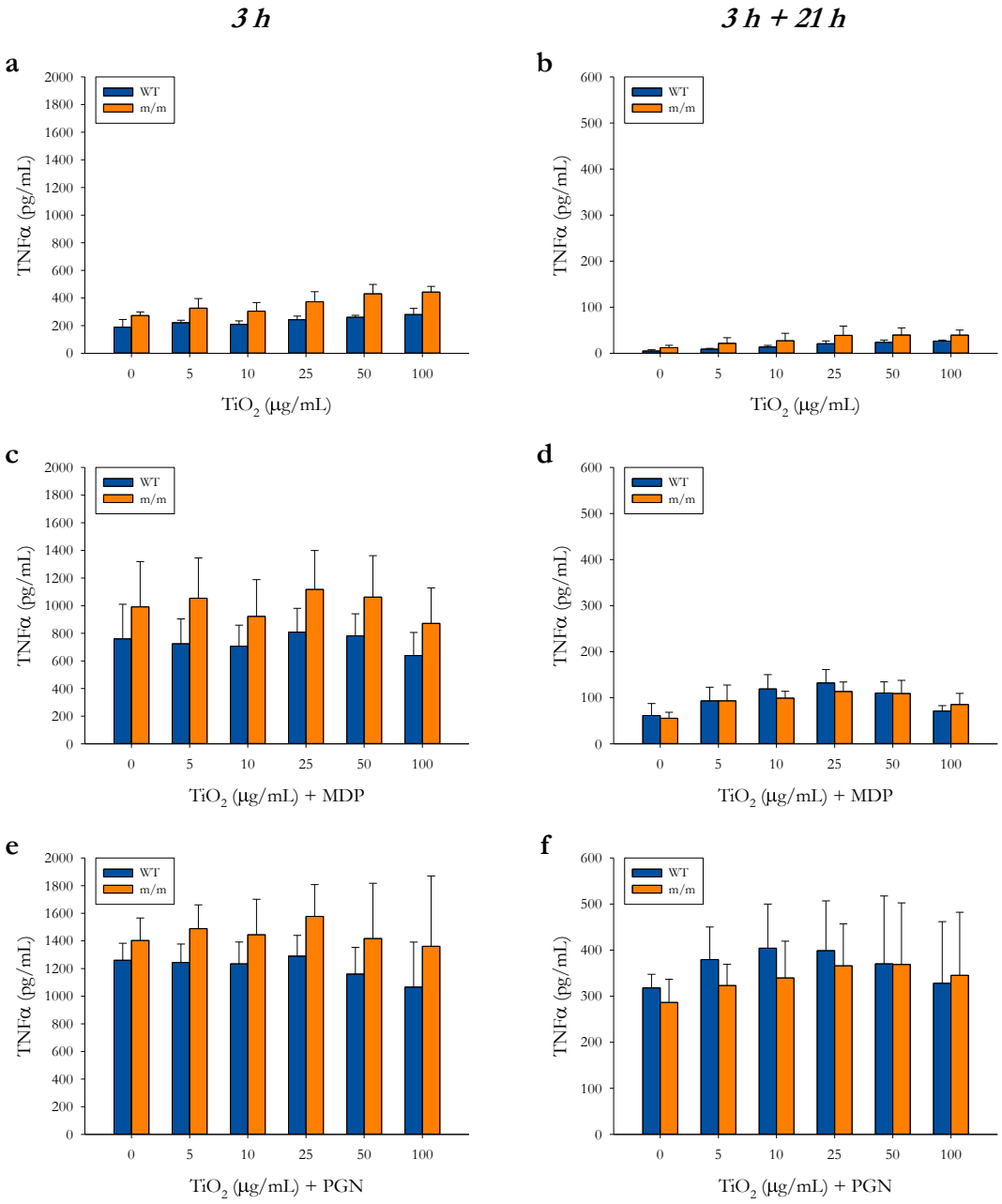

Figure 2.12 *TNF-a secretion by BMDMs after TiO_2 exposure with or without MDP/PGN co-stimulation.*

Murine WT or *Nod2$^{m/m}$* (m/m) BMDMs were pre-stimulated for 3 h with LPS (10 ng/mL). Then BMDMs were incubated with TiO_2 particle suspensions at the indicated concentrations without or with MDP or PGN (10 µg/mL respectively) in TCM for 3 h followed by further incubation in TCM for 21 h. BMDMs were stimulated with TiO_2 alone (**a, b**), TiO_2 + MDP (**c, d**), or TiO_2 + PGN (**e, f**). TNF-α concentration in supernatants collected after 3 h (**a, c, e**) or 3 h + 21 h (**b, d f**) was measured by ELISA. Shown are results from two independent experiments with three replicates per exposure condition respectively; means ± SD; $n = 6$. Results were compared with two-way ANOVA (Table 2.5).

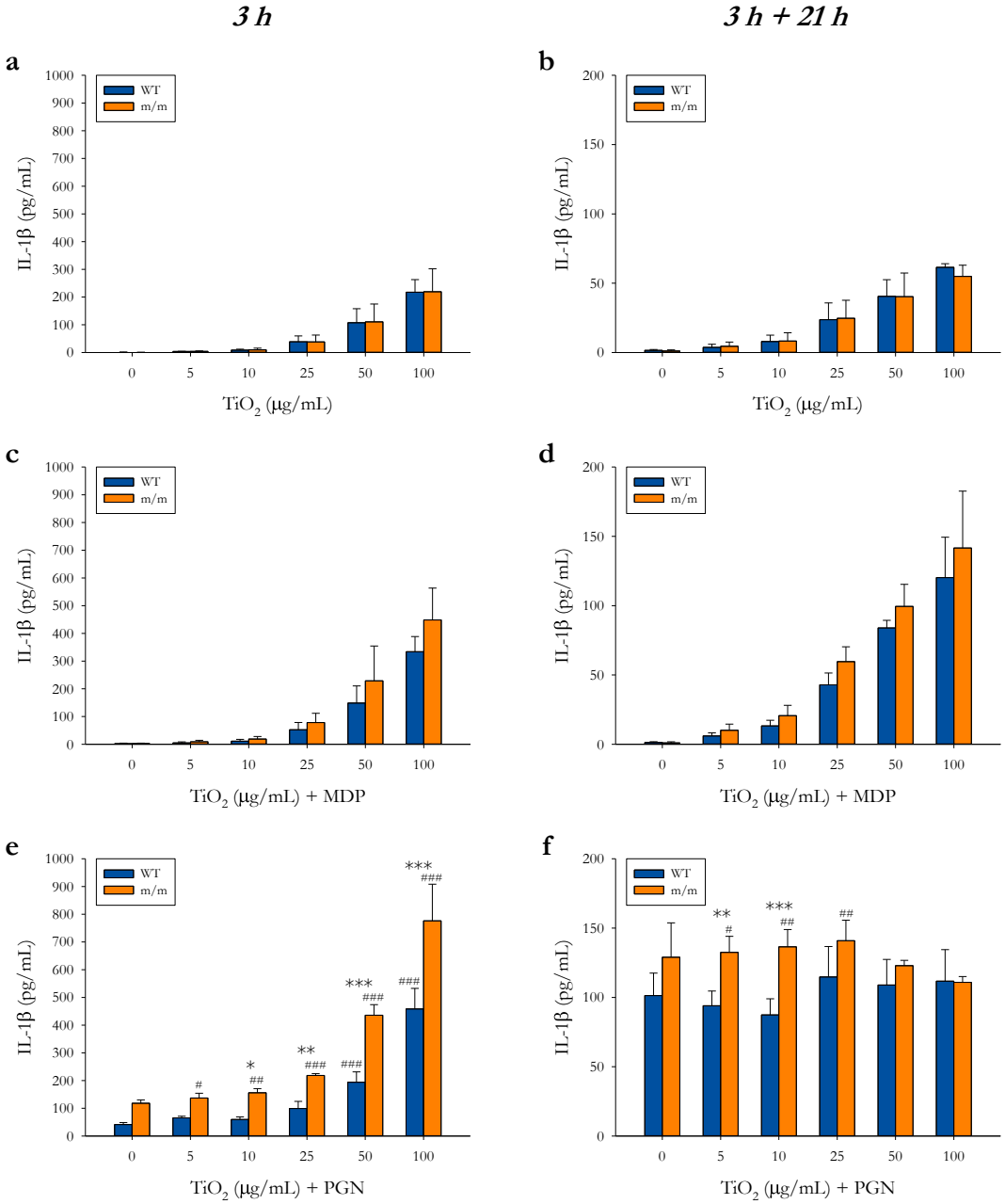

Figure 2.13 *IL-1β secretion by BMDMs after TiO_2 exposure with or without MDP/PGN co-stimulation.*
Murine WT or *Nod2*$^{m/m}$ (m/m) BMDMs were pre-stimulated for 3 h with LPS (10 ng/mL). Then BMDMs were incubated with TiO_2 particle suspensions at the indicated concentrations without or with MDP or PGN (10 µg/mL respectively) in TCM for 3 h followed by further incubation in TCM for 21 h. BMDMs were stimulated with TiO_2 alone (**a, b**), TiO_2 + MDP (**c, d**), or TiO_2 + PGN (**e, f**). IL-1β concentration in supernatants collected after 3 h (**a, c, e**) or 3 h + 21 h (**b, d, f**) was measured by ELISA. Shown are results from two independent experiments with three replicates per exposure condition respectively; means ± SD; $n = 6$. Results were compared with two-way ANOVA (Table 2.5). (**e, f**) Pairwise group comparisons with Tukey's HSD test; $^{*}p < 0.05$, $^{**}p < 0.01$, $^{***}p < 0.001$ = significant differences between WT and *Nod2*$^{m/m}$ BMDMs exposed to the same TiO_2 concentration; $^{\#}p < 0.05$, $^{\#\#}p < 0.01$, $^{\#\#\#}p < 0.001$ = significant differences between BMDMs exposed to TiO_2 and unexposed WT BMDMs.

TiO_2 + PGN at both time points. After 3 h, *Nod2*$^{m/m}$ cells exposed to 10 μg/mL TiO_2 or higher doses produced significantly more ($p < 0.05$) IL-1β compared to WT cells treated with the same amount of TiO_2 (Figure 2.13c). Furthermore, all cells from *Nod2*$^{m/m}$ mice that were treated with TiO_2 secreted significantly more ($p < 0.05$) IL-1β than untreated WT cells. However, with the TiO_2-exposed WT BMDMs there were only significant differences ($p < 0.001$) to the WT control cells for those cells exposed to 50 μg/mL and 100 μg/mL TiO_2. Although there was no effect of TiO_2 concentration with PGN co-stimulation at the 3 h + 21 h time point, there was a significant interaction effect. BMDMs from *Nod2*$^{m/m}$ mice exposed to 5 μg/mL or 10 μg/mL TiO_2 secreted significantly more ($p < 0.01$) IL-1β compared to WT cells stimulated with the same amount of TiO_2 (Figure 2.13f). The secretion of IL-1β from *Nod2*$^{m/m}$ BMDMs was also significantly higher ($p < 0.05$) compared to WT control cells with these two TiO_2 concentrations and with 25 μg/mL TiO_2. In general, cells that were co-stimulated with MDP or PGN secreted more IL-1β compared to cells incubated with TiO_2 particles in TCM alone, and IL-1β secretion was markedly reduced in supernatants collected after 3 h + 21 h compared to the 3 h time point for the same co-stimulation.

2.4.6 Cytokine secretion by human peripheral blood mononuclear cells after exposure to titanium dioxide

No effect of TiO_2 treatment on absolute IL-1β secretion after 3 h and 3 h + 21 h was observed in LPS pre-stimulated PBMCs. This was also the case if the cells were co-stimulated with MDP or PGN (Figure 2.14). Visual comparison of the relative secretion of IL-1β after TiO_2 treatment in comparison to unstimulated control cells showed a trend to increased IL-1β secretion for all conditions after 3 h and a decreased secretion after 3 h + 21 h for MDP and PGN co-stimulation. However, only the latter observation was also statistically significant ($p < 0.05$). Nevertheless, even in this case a pairwise group mean comparison with the Wilcoxon rank sum test did not show statistically significant differences between two individual groups.

The results for both absolute and relative amounts of IL-17 in the supernatants of TiO_2-stimulated PBMCs without or with MDP/PGN co-stimulation are shown in Figure 2.15. With TiO_2 alone or with PGN co-stimulation there were no differences in the absolute levels of IL-17 (Figure 2.15a, c). In contrast, IL-17 was detected at a significantly lower ($p < 0.05$) concentration in PBMCs stimulated with TiO_2 + MDP (Figure 2.15b). Pairwise comparison of the group means showed that cells exposed to 100 μg/mL TiO_2 secreted significantly less ($p < 0.05$) IL-17 than untreated control cells. Comparison of the

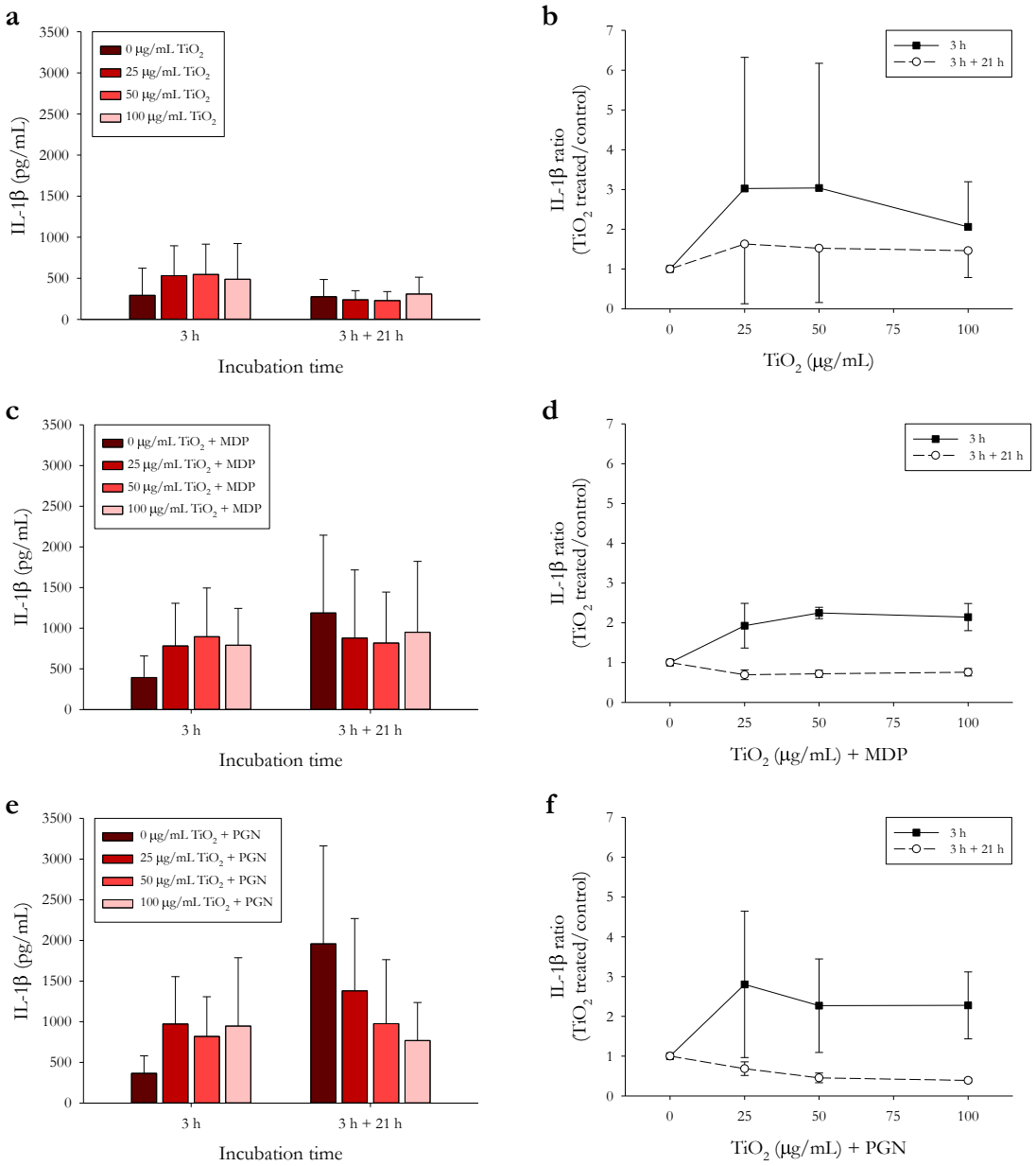

Figure 2.14 *IL-1β secretion by PBMCs after TiO_2 exposure with or without MDP/PGN co-stimulation.*

Human PBMCs were pre-stimulated for 3 h with LPS (10 ng/mL). Then, PBMCs were incubated with TiO_2 particle suspensions at the indicated concentrations without or with MDP or PGN (10 µg/mL respectively) in TCM for 3 h followed by further incubation in TCM for 21 h. PBMCs were stimulated with TiO_2 alone (**a, b**), TiO_2 + MDP (**c, d**), or TiO_2 + PGN (**e, f**). IL-1β concentration in supernatants collected after 3 h or 3 h + 21 h was measured by ELISA. Shown are results from three independent experiments with PBMCs from three different donors; means ± SD; $n = 3$. Results were compared with one-way ANOVA (**a**, 3 h + 21 h; **c**, 3 h; **e**, both time points) or Kruskal-Wallis test (all others).

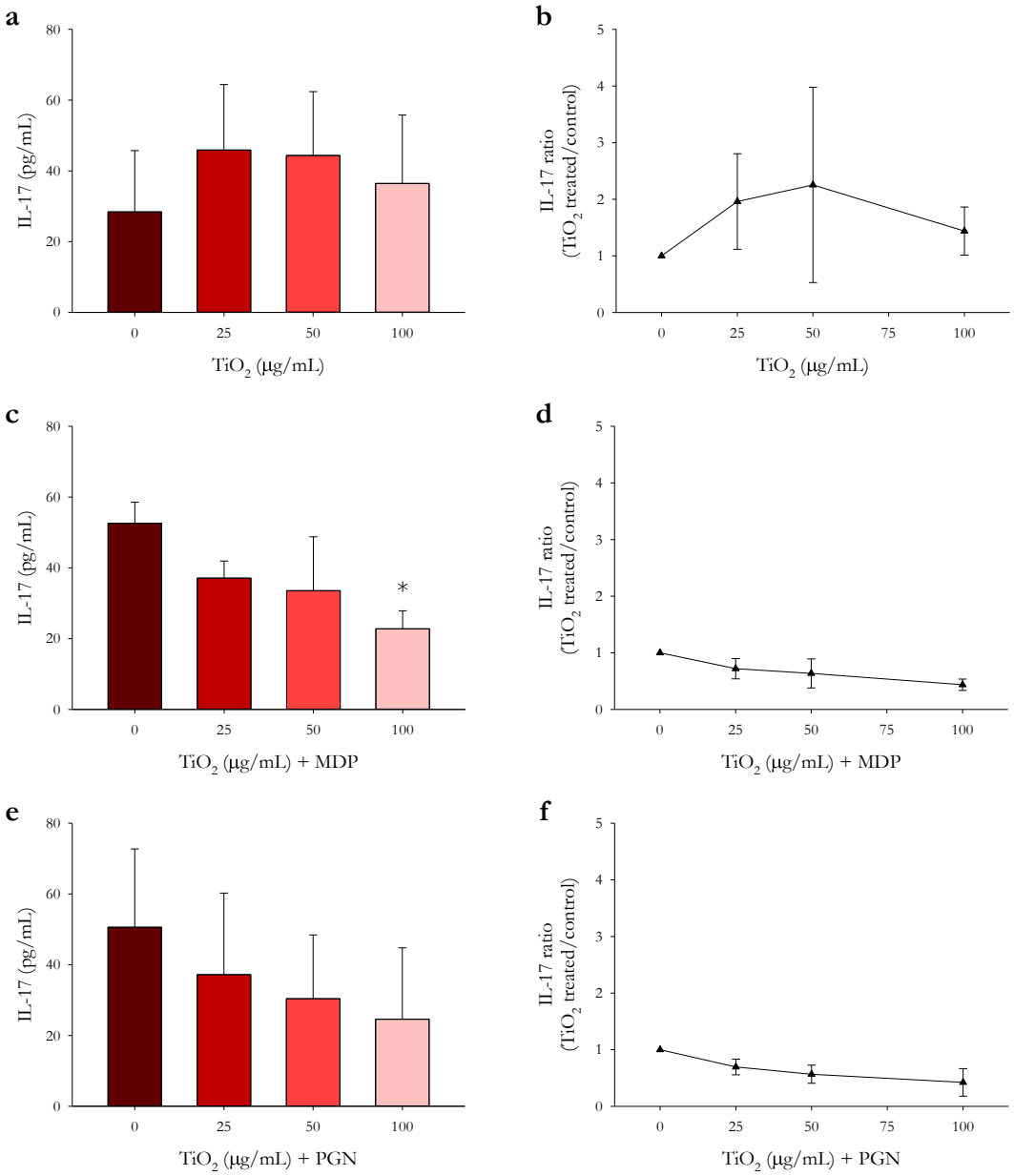

Figure 2.15 *IL-17 secretion by PBMCs after TiO_2 exposure with or without MDP/PGN co-stimulation.*

Human PBMCs were pre-stimulated for 3 h with LPS (10 ng/mL). Then, PBMCs were incubated with TiO_2 particle suspensions at the indicated concentrations without or with MDP or PGN (10 µg/mL respectively) in TCM for 3 h followed by further incubation in TCM for 21 h. Then, PBMCs were stimulated with PHA (10 µg/mL) and further incubated in TCM for 48 h. PBMCs were stimulated with TiO_2 alone (**a, b**), TiO_2 + MDP (**c, d**), or TiO_2 + PGN (**e, f**). IL-17 concentration in supernatants collected after 3 h + 69 h was measured by ELISA. Shown are results from three independent experiments with PBMCs from three different donors; means ± SD; $n = 3$. Results were compared with one-way ANOVA (**a, c, e**) or Kruskal-Wallis test (**b, d, f**). (**c**) Pairwise group comparisons with Tukey's HSD test; $*p < 0.05$ = significant differences between control and TiO_2-treated PBMCs.

relative levels with MDP co-stimulation confirmed the observation of a significant decrease ($p < 0.05$) in IL-17 levels, but in this case the pairwise comparison of group means did not indicate any differences between individual groups. The relative secretion of IL-17 was also significantly decreased ($p < 0.05$) with PGN co-stimulation, but again pairwise group comparison indicated no significant difference between individual groups.

2.5 Discussion

2.5.1 Reassessment of the hypothesis

The results presented in this chapter supported the hypothesis that incubation of phagocytic immune cells with dietary TiO_2 particles activates these cells and induces the production of pro-inflammatory cytokines. This response was increased by simultaneous co-stimulation with the bacterial cell-wall fragments and Nod2 ligands MDP and PGN. Macrophages derived from mice with a CD-like *Nod2* mutation showed an increased activation and IL-1β response after co-stimulation with TiO_2 + MDP/PGN, confirming the hypothesis by Maeda and colleagues that the frameshift *Nod2* variant is a gain-of-function mutation [131].

2.5.2 Suitability of bone marrow-derived macrophages as a model for intestinal macrophages

An important aspect to consider when interpreting the results of the experiments presented in this chapter is the use of BMDMs as model cells for intestinal macrophages. Cell culture studies have been criticised in general, because it is not be possible to accurately model the *in vivo* situation in *in vitro* studies. Ideally, primary intestinal cells would be used if the goal is to investigate specific effects in cell culture [275]. However, primary intestinal macrophages are difficult to isolate from mice, and only a relatively small number of macrophages can be recovered per animal [276]. This means that many animals would be necessary to obtain a sufficient amount of cells for the experiments described in this chapter. For animal ethics reasons, and also because of limited availability of *Nod2*$^{m/m}$ mice, this was not feasible. Alternatively, an immortalised monocyte cell line, e.g. RAW264.7 macrophages, could have been used. Cell lines with macrophage characteristics have been used extensively to study the effects of TiO_2 exposure on macrophages (Table 1.5). Experiments with BMDMs derived from *Nod2*$^{m/m}$ mice were also performed in the study in which the *Nod2*$^{m/m}$ mice were originally described [131]. Furthermore, another study investigated the production of

pro-inflammatory cytokines after TiO_2 and MDP co-stimulation of BMDMs derived from *Nod2*$^{-/-}$ mice [253]. Therefore, it was decided to perform these experiments with BMDMs to be able to compare the data with these two studies.

2.5.3 Cytotoxicity of titanium dioxide

The cytotoxicity of food-grade TiO_2 particles on both WT and *Nod2*$^{m/m}$ macrophages was investigated based on changes in metabolic activity with the commonly used WST-1 assay. The results showed that the TiO_2 particles did not cause a decrease in metabolic activity, even at high concentrations (Figure 2.3). These results are in line with other studies that used the WST-1 assay to assess cytotoxicity of TiO_2 particles with diameters larger than 100 nm [186-188, 199]. For example, TiO_2 particles with diameters from 40 nm to 300 nm for 24 h were not cytotoxic to RAW264.7 macrophages [199]. Another study investigated the effects of three different types of TiO_2 particles, all with average diameters between 250 nm and 450 nm, on RAW264.7 macrophages with the MTS assay, which is another type of tetrazolium salt assay closely related to the WST-1 assay [201]. The metabolic activity of the macrophages was not affected by any of the three types of particles, even at high particle concentrations.

A second study also investigated potential cytotoxic effects of anatase TiO_2 particles with sizes between 350 nm to 500 nm in TCM on RAW264.7 cells with the MTS assay [198]. In contrast to the study by Xiong and colleagues, the metabolic activity was lower for macrophages that were treated with 100 μg/mL TiO_2 particles for 12 h to 24 h, but not for 6 h. The result reported by Sohaebuddin and colleagues for the 24 h time point is also in contrast to the results from other studies in which no cytotoxicity of TiO_2 particles was observed after 24 h incubation [186, 188, 199]. However, the result for the 6 h time point from the study by Sohaebuddin and colleagues is in agreement with the observation from the current study that a relatively short incubation time with anatase TiO_2 particles did not affect metabolic activity of macrophages.

Other researchers have used the WST-1 assay to investigate cytotoxic effects of TiO_2 particles on immortalised intestinal epithelial cell lines. One study showed that the effect on metabolic activity in colon carcinoma cells was dependent on exposure time [186]. Incubation with TiO_2 particles with an average diameter of 320 nm for 24 h or 48 h had no impact on metabolic activity, but incubation for 72 h led to a decrease in metabolic activity. Gerloff and co-workers published two studies that compared the effect of different types of TiO_2 particles on Caco-2 cells [187, 188]. Metabolic activity was only negatively affected by

TiO_2 particles with a primary particle size in the nanometre range, but not by anatase TiO_2 particles with an average diameter of 215 nm.

Although there was no detectable effect of TiO_2 particle concentration on metabolic activity, it was observed that BMDMs derived from *Nod2*$^{m/m}$ mice had lower metabolic activity relative to untreated WT control cells. It had been shown previously that key cellular signalling processes were not affected in *Nod2*$^{m/m}$ mice [131]. However, it cannot be excluded that this mutation affected the cells from these knock-in mice in a way that decreased their viability. In line with this is the observation that during the bone marrow collection consistently fewer cells were obtained from *Nod2*$^{m/m}$ mice (see Appendix B).

Furthermore, the cell viability was determined with PI staining and analysis by flow cytometry (Figure 2.4). Using the trypan blue exclusion assay, Palomäki and colleagues could not detect differences in cell viability between RAW264.7 macrophages and control cells that were both treated with rutile TiO_2 particles (average primary particle size 35 nm) [197]. A more sensitive method to assess cell viability is staining with PI and determining the number of cells that are negative for PI. This is often used in conjunction with annexin-V (A5) staining which allows distinguishing early apoptotic (PI^- $A5^+$), late apoptotic (PI^+ $A5^+$), and dead cells (PI^+ $A5^-$). For the experiments reported in this chapter only staining with PI was performed because the flow cytometer that was used for analysis was able to detect signals in four channels. The other three channels were used to detect the macrophage marker F4/80 and the activation molecules CD80 and CD86, respectively. Therefore, it is possible that early apoptotic cells, i.e. cells that would be PI^- $A5^+$, were not detected in these experiments. However, it has been shown with PI and A5 double staining of J774A.1 macrophages which were incubated with 100 μg/mL TiO_2 (average particle size 220 nm) that most non-viable cells were PI^+ [195]. Only a small fraction of the non-viable cells was PI^- $A5^+$. Möller and colleagues reported that the cell viability was approximately 85 % after 24 h of incubation with TiO_2. In another study in which RAW264.7 macrophages were incubated for 20 h with 100 μg/mL anatase TiO_2 particles (average particles size 350 nm to 500 nm in TCM) and the non-viable cells were also assessed with PI and A5 staining the cell viability was approximately 50 % [198]. Incubation with TiO_2 alone lead to increased apoptosis, but early and late apoptotic cells were not distinguished. In contrast to these two studies that detected a decrease in cell viability after TiO_2 incubation, no increased cell death of RAW264.7 macrophages was detected by PI staining in two other studies after exposure to 10 μg/mL and up to 100 μg/mL TiO_2, respectively [200, 201]. The differences between the first two

and the second two studies might be due to different particle types used, i.e. rutile/anatase or a mixture of both.

Palomäki and co-workers noted that TiO_2 particles were more cytotoxic to murine APCs derived from bone marrow than to cultured RAW264.7 macrophages [197]. This observation could explain why in the current study exposure to TiO_2 particles caused a decrease in cell viability for all treatments and at both time points. Staining with PI showed that the viability of primary cells from humans, namely PBMCs, was also decreased after incubation with just 5 μg/mL anatase TiO_2 for 24 h [215, 217]. However, there was no decrease in cell viability after TiO_2 exposure for human macrophages derived from PBMCs [218]. The latter study was one of the few studies in which cell viability was investigated with PI and A5 staining after exposure to a range of particles in concentrations up to 50 μg/mL TiO_2. Both apoptosis and the amount of dead cells increased with increasing particle concentrations, but the levels were not different to the control cells even for the highest TiO_2 concentrations. The observation that increasing TiO_2 concentrations resulted in decreased cell viability is in agreement with the results from this study (Figure 2.4).

The baseline viability in the current study was higher in cells recovered after 3 h + 21 h treatment, but the decline in viability was similar compared with the 3 h time point. A possible explanation for the higher baseline viability at the later time point is that the cells have recovered from the acute treatment with TiO_2 and started to proliferate in the fresh TCM. This is in line with the observation of de Berardis and colleagues that the cell growth of a colon carcinoma cell line was not affected by stimulation with TiO_2 for up to 72 h [186].

When the results of the WST-1 assay (Figure 2.3) and PI staining (Figure 2.4) were visually compared, it was observed that the results from the two assays did not correspond to each other. Although it could be expected that the observed decrease in cell viability, as assessed by PI staining, would result in a decrease in metabolic activity, as assessed by the WST-1 assay, this does not necessarily have to be the case because the two assays measure fundamentally different parameters (personal communication with Dr Mark McCann, AgResearch, Palmerston North, NZ). A possible explanation why no reduction in metabolic activity was observed after BMDMs were incubated with TiO_2 particles (Figure 2.3) whereas cell viability decreased with increasing particle concentrations (Figure 2.4) could be that although less viable cells were present at higher particle concentrations these live cells had a higher metabolic activity. This could have been the case because more TCM, and therefore nutrients, per live cell was available at higher TiO_2 concentrations. The results from this study

also corresponded to a previous study that did not observe decreased metabolic activity with the WST-1 assay after exposure of cultured macrophages to TiO_2 particles [199]. A decreased cell viability of TiO_2-exposed cultured macrophages according to PI staining has also been reported previously [195, 218].

2.5.4 Uptake of titanium dioxide by cultured cells

It has been demonstrated that TiO_2 particles accumulate in macrophages from human PPs of the terminal ileum. The presence of TiO_2 has been confirmed by microscopy, and the cells have been identified as macrophages based on morphology [56, 144, 147, 162] and cell surface marker expression [162]. It has also been shown that macrophages derived from human PBMCs were able to take up food-grade TiO_2 *in vitro* by phagocytosis [218]. Butler and colleagues verified particle uptake by microscopy and flow cytometry. Macrophages that were incubated with 5 μg/mL TiO_2 showed a large number of internalised particles. Treatment of the macrophages with increasing concentrations of TiO_2 resulted in a concentration dependent increase in the SSC intensity. Stringer and colleagues were the first to demonstrate that uptake of TiO_2 particles positively correlated with an increased granularity which could be measured by assessing the SSC intensity by flow cytometry [277]. They also showed that incubation with higher particle concentrations were linked to even further increases in SSC intensity. Since then, others have used this method to study TiO_2 particle uptake by different cell lines [198, 260, 264, 266, 278]. Treatment of cells with increasing particle concentrations always resulted in higher SSC intensities [260, 264, 266, 278]. Sohaebuddin and colleagues did not report any values, but they showed a FSC *versus* SSC dot plot of TiO_2-treated RAW264.7 macrophages that were incubated with 100 μg/mL TiO_2 and which had a much higher SSC intensity compared to untreated cells [198]. All of these studies are in line with the observations from this study that SSC intensities increased with increasing particle concentrations (Figure 2.8). Zucker and co-workers also calculated the SSC ratio between TiO_2-treated and control cells, e.g. a ratio of approximately '10' was calculated for 30 μg/mL [266]. The SSC intensity ratios from this study (Figure 2.9) corresponded to the results from Zucker and colleagues.

A decrease in FSC has been observed with increasing particle concentrations in this study (Figure 2.7). This is in line with results reported by Zucker and colleagues and Sohaebuddin and co-workers [198, 266]. In contrast, Suzuki and colleagues did not report such a relationship [264]. However, it has been suggested that the FSC is not only a measurement for cell size, but that it can also be influenced negatively by the presence of internal structures

like particles that were taken up by phagocytosis [266]. Therefore, the reduced FSC of TiO_2-treated BMDMs can be interpreted as another indirect measurement for TiO_2 uptake.

It has previously been demonstrated indirectly that TiO_2 particles are taken up by phagocytosis in this study. For instance, when PBMCs were pre-treated with increasing concentrations of the phagocytosis inhibitor cytochalasin D the uptake of fluorescently labelled TiO_2 particles was reduced in a concentration dependent manner [215]. Bone marrow-derived DCs (BMDCs), another type of primary murine phagocytic cells that can be obtained by culturing bone marrow cells with growth factors, pre-treated with cytochalasin D also had decreased SSC intensities after TiO_2 incubation [260]. TiO_2 uptake by phagocytosis was dependent on scavenger receptors [215]. Pre-treatment of hamster alveolar macrophages with cytochalasin D also decreased the SSC intensity despite the fact that TiO_2 particles were still attached to the outside of the cells as shown by microscopy [277].

In another study about the impact of dietary TiO_2 on phagocytic cells, Butler and colleagues compared TiO_2 internalisation between PBMC-derived macrophages from healthy donors and patients with CD [218]. No difference in SSC intensity was observed between the two groups after 24 h treatment with TiO_2 at different concentrations. This result is consistent with the observation from this study that there were no differences between WT and *Nod2*$^{m/m}$ BMDMs treated with TiO_2 alone for 3 h + 21 h (Table 2.3). However, when the BMDMs were incubated for 3 h with TiO_2 without or with bacterial antigens or for 3 h + 21 h with TiO_2 + MDP the cells from *Nod2*$^{m/m}$ mice had lower relative SSC ratios (Table 2.3 & Figure 2.9). This could be an indication for reduced phagocytic activity of the cells that bear a CD-associated mutation. Butler and colleagues also investigated phagocytic activity of macrophages after TiO_2 + LPS stimulation for 24 h. The phagocytic activity was not altered by the presence of TiO_2, and macrophages from CD patients responded no differently than control cells. However, CD patients were not screened for *NOD2* mutations in the study by Butler and co-workers, so it is possible that the macrophages had a WT *NOD2* gene because CD-associated polymorphisms in *NOD2* are only present in approximately half of the patients [59, 71].

It has also been reported that the phagocytic activity of murine J774A.1 macrophages decreased when the cells were incubated with 100 μg/mL TiO_2 particles with a diameter of 220 nm for 24 h [195]. The reduced phagocytic activity was not due to lower viability of the TiO_2-treated cells, so it is likely that the maximum phagocytic capacity was reached after 24 h phagocytosis of TiO_2 particles. Therefore, it might also be possible that BMDMs from

Nod2$^{m/m}$ mice might not have a decreased phagocytic activity, but instead a decreased capacity to internalise exogenous material compared to WT BMDMs. However, it has been shown that monocytes from CD patients had a greater phagocytic capacity compared to cells from healthy controls [279]. According to the FSC results from this study, BMDMs from *Nod2*$^{m/m}$ mice appeared larger than macrophages from WT mice after 3 h + 21 h (Figure 2.7). Thus, the capacity of *Nod2*$^{m/m}$ cells to take up TiO_2 particles should at least be equal to or even greater than that of WT macrophages. This could explain why there was no difference in the SSC ratio between WT and *Nod2*$^{m/m}$ cells after 3 h + 21 h, at least for cells treated with TCM alone and TCM + PGN (Figure 2.9).

2.5.5 Activation marker expression after exposure to titanium dioxide

In addition to cell viability and particle uptake, the expression of two classical APC co-stimulatory molecules, namely CD80 and CD86, was also investigated by flow cytometry. Although it was expected that both markers were up-regulated after stimulation with TiO_2 (see below), this was only the case for CD86 (Figure 2.11). In contrast, the CD80 MFI decreased at higher particle concentrations (Figure 2.10). A reason for these conflicting results could lie in the different and independent expressions of the co-stimulatory molecules on BMDMs. For instance, it has been demonstrated that activated human PBMCs express CD86 earlier than CD80 after *in vitro* stimulation [280]. Therefore, it is possible that the time points which were chosen to analyse the expression of the co-stimulatory molecules were not suitable to detect CD80. Furthermore, it is possible that BMDMs generally do not express detectable levels of CD80 after stimulation. However, a study that investigated the functions of BMDMs generated from cryopreserved bone marrow cells showed that CD80 expression was up-regulated after LPS stimulation of both fresh and cryopreserved BMDMs [258].

Two studies reported activation marker expression of murine APCs after TiO_2 exposure [197, 260]. Palomäki and colleagues showed that the expression of major histocompatibility complex class II and CD40, two other commonly used cell surface molecules that are up-regulated in activated cells, was increased on RAW264.7 macrophages that were stimulated for 24 h with TiO_2 (primary particle size range 30 nm to 40 nm) [197]. The frequency of CD86 was also higher on cells exposed to TiO_2 for 24 h compared to control cells. The expression of CD40 and CD86 was further increased when the macrophages were incubated for 48 h whereas the expression of major histocompatibility

complex class II remained constant compared to the 24 h time point. The expression of CD80 was not investigated by Palomäki and colleagues. It should be noted that no statistical analysis of the results was reported because only results of one experiment were shown. Nevertheless, the study by Palomäki and co-workers provides valuable information about the activation of APCs after TiO_2 stimulation. The increase in cell surface activation marker expression is in line with the findings from this study regarding the increased expression of CD86 with increasing TiO_2 concentration. The finding by Palomäki and colleagues that the expression of CD86 increased over time in TiO_2-treated macrophages could also observed in the current study (Figure 2.11).

In the study by Winter and co-workers, BMDCs were exposed to two different kinds of TiO_2 particles for 18 h, and the expressions of CD80 and CD86 were investigated [260]. Only BMDCs exposed to nanosized TiO_2 (primary particle size range 20 nm to 80 nm) induced expression of the co-stimulatory molecules whereas anatase TiO_2 (primary particle size range 40 nm to 300 nm) had no effect. These results are in contrast to the findings from this study in which stimulation with anatase TiO_2 led to increased CD86 expression (Figure 2.11). A possible explanation for this discrepancy is that Winter and co-workers performed experiments with BMDCs whereas in the current study BMDMs were used. Even though both cell types are APCs, BMDCs might respond differently to TiO_2 particle stimulation than BMDMs.

2.5.6 Pro-inflammatory cytokine secretion after exposure to titanium dioxide

The secretion of two pro-inflammatory cytokines mainly produced by macrophages, TNF-α and IL-1β, was investigated after TiO_2 stimulation of WT and *Nod2*$^{m/m}$ BMDMs. One of the most common sources of these cytokines in the intestine are macrophages, and both cytokines are involved in the pathogenesis of IBD [43]. Stimulation with TiO_2 particles in TCM alone led to a dose-dependent increase in TNF-α secretion by BMDMs (Figure 2.12a). Several studies have investigated TNF-α secretion by RAW264.7 macrophages after TiO_2 treatment, and the results of most of these studies were in agreement with the observations from this study. For example, stimulation with increasing amounts of TiO_2 particles in various forms led to increased TNF-α release after 24 h [197, 201]. In contrast, Xia and co-workers could not detect any effect on TNF-α secretion after stimulation with 10 μg/mL TiO_2 particles for 6 h [200]. A possible explanation for this discrepancy might be the low dose used by Xia and co-workers and/or the short incubation time of 6 h. However, in the

current study incubation for 3 h already induced TNF-α release by the BMDMs (Figure 2.12a). Such a rapid response in TNF-α secretion upon 3 h TiO_2 stimulation has also been reported in another study with RAW264.7 macrophages [196]. It should be noted that in all experiments with RAW264.7 macrophages there was no co- or pre-stimulation with LPS as in this study, which could also account for some of the differences. The decision to compare TNF-α secretion after short-term LPS pre-stimulation in the current study was supported by a study which found that co-stimulation with LPS alone resulted in detectable TNF-α release by human THP-1 monocytes [191].

Furthermore, the results from this study showed that co-stimulation with MDP or PGN caused an increase of TNF-α release that was not influenced by TiO_2 co-stimulation (Figure 2.12c, d). This implies that the pathways which lead to increased secretion of TNF-α after stimulation with particles or bacterial antigens are independent, not synergistic. Interestingly, after incubation for 3 h + 21 h, TiO_2 particles had no effect on TNF-α secretion from BMDMs that were co-stimulated with PGN (Figure 2.12f). There was, however, an effect on cells that have been co-incubated for 3 h + 21 h with TiO_2 particles and MDP (Figure 2.12d). These results imply that MDP and PGN induce TNF-α secretion *via* different mechanisms. Furthermore, macrophages from *Nod2*$^{m/m}$ mice secreted more TNF-α compared to WT BMDMs after 3 h both without and with MDP/PGN co-stimulation (Table 2.5). Although Maeda and colleagues showed that the production of TNF-α mRNA was higher in MDP-stimulated BMDMs from *Nod2*$^{m/m}$ mice compared to control mice, this was not matched by elevated secretion of TNF-α by *Nod2*$^{m/m}$ cells [131]. Moreover, Maeda and co-workers showed that both mRNA production and secretion of TNF-α was similar in untreated and PGN-stimulated WT and *Nod2*$^{m/m}$ BMDMs. In contrast to these findings, Tsay and colleagues reported an increased expression of TNF-α mRNA in peritoneal macrophages from *Nod2*$^{m/m}$ mice that were incubated with *Pseudomonas aeruginosa* compared to WT macrophages [281]. The finding by Tsay and colleagues is in agreement with the results from the current study that the secretion of TNF-α after 3 h is elevated in BMDMs from *Nod2*$^{m/m}$ mice compared to WT mice (Table 2.5). Interestingly, Hsu and co-workers reported that there was no difference in TNF-α secretion between WT and *Nod2*$^{-/-}$ BMDMs after co-stimulation with TiO_2 and MDP for 6 h [253]. This discrepancy between cells from *Nod2*$^{m/m}$ mice and *Nod2*$^{-/-}$ mice indicates that the function of Nod2 is not abrogated in *Nod2*$^{m/m}$ mice like it is in *Nod2*$^{-/-}$ mice. Instead, the *Nod2* frameshift variant is a gain-of-function mutation as postulated by Maeda and colleagues [131].

This is even more evident in the results for IL-1β secretion from *Nod2*$^{m/m}$ macrophages. As mentioned previously, Maeda and colleagues have shown that MDP stimulation of *Nod2*$^{m/m}$ macrophages resulted in increased IL-1β mRNA expression and protein secretion [131], which has been confirmed in this study (Figure 2.13). Increased IL-1β secretion from LPS-primed BMDMs correlated positively with increased TiO_2 concentration, regardless of *Nod2* genotype and co-stimulation. However, when the cells were co-stimulated with TiO_2 + MDP, *Nod2*$^{m/m}$ macrophages secreted more IL-1β than WT macrophages after incubation for 3 h or 3 h + 21 h (Table 2.5). The increased IL-1β response of *Nod2*$^{m/m}$ BMDMs to MDP is in line with the observations by Maeda and colleagues. However, no IL-1β was detected in the supernatant of cells stimulated with MDP without TiO_2 particles in this study (Figure 2.13c). A possible explanation for this discrepancy to the results from Maeda and colleagues might be the different stimulation times with MDP. In the current study the cells were stimulated for 3 h with TiO_2 + MDP followed by 21 h incubation with TCM whereas in the study by Maeda and colleagues the cells were stimulated for 24 h with MDP.

Another difference between the results reported in this chapter compared to the work by Maeda and colleagues was the response of *Nod2*$^{m/m}$ macrophages to PGN. Similar to the results for MDP there was a concentration-dependent increase of IL-1β in the supernatants of TiO_2 + PGN stimulated cells after 3 h (Figure 2.13e). At this time point, BMDMs from *Nod2*$^{m/m}$ mice secreted more IL-1β compared to WT mice (Table 2.5). Such a difference was not reported by Maeda and colleagues [131]. It should be noted, however, that there was only a difference after co-stimulation with 10 μg/mL TiO_2 or higher TiO_2 concentrations. Hence, the observation that BMDMs from *Nod2*$^{m/m}$ mice did not secrete increased amounts of IL-1β after stimulation with PGN alone is in agreement with the results from Maeda and colleagues. After 3 h + 21 h only supernatants from *Nod2*$^{m/m}$ BMDMs stimulated with 5 μg/mL and 10 μg/mL TiO_2 + PGN had a higher concentration of IL-1β compared to supernatants from WT cells (Figure 2.13f). Although still relatively much IL-1β was secreted at this time point, the influence of the factor 'TiO_2 concentration' was not significant (Table 2.5). This suggests that IL-1β secretion after prolonged exposure to PGN is mediated by a different pathway compared to stimulation with TiO_2 alone or TiO_2 + MDP. A possible mechanism would be through TLR2-mediated signalling because it has been shown that TLR2 is a receptor for PGN [282]. Tsay and co-workers also reported increased IL-1β mRNA expression by macrophages derived from *Nod2*$^{m/m}$ mice after bacterial stimulation [281].

Several studies reported production of IL-1β by APCs after incubation with TiO_2 particles when the cell were pre-stimulated with LPS [191, 253, 260]. Similar to their findings on TNF-α secretion by LPS stimulated THP-1 monocytes, Morishige and co-workers demonstrated that LPS pre-stimulation was necessary for TiO_2-induced IL-1β release [191]. Furthermore, the amount of secreted IL-1β was influenced by the TiO_2 form used, but all investigated TiO_2 particle types led to elevated IL-1β in the supernatants of cells exposed to high TiO_2 concentrations. In contrast, in another study in which murine BMDCs were pre-stimulated with LPS and exposed to two different forms of TiO_2 an increased secretion of IL-1β was only detected for cells exposed to mixed anatase and rutile TiO_2 particles with a primary size range from 20 nm to 80 nm [260]. The second type, anatase TiO_2 with a primary particle size range from 40 nm to 300 nm, did not elicit an increased IL-1β response. The TiO_2 particles that were used in this study seem to correspond to the second type of TiO_2 particles (Figure 2.2). However, a detailed particle description was missing in the publication by Winter and colleagues, which makes a direct comparison of the results difficult. Nevertheless, the different results regarding TiO_2 stimulation of phagocytic cells with anatase TiO_2 particles could be due to differences in cytokine production of TiO_2-exposed BMDMs and BMDCs.

Hsu and colleagues reported that BMDMs from *Nod2*$^{-/-}$ mice that were pre-treated with LPS and stimulated with TiO_2 + MDP secreted less IL-1β compared to BMDMs from WT controls [253]. Similar to the differences in TNF-α secretion observed in the same study, this result is in contrast to the finding from the current study that IL-1β release was increased after TiO_2 stimulation (Figure 2.13). Again, this indicates that *Nod2*$^{-/-}$ and *Nod2*$^{m/m}$ mice are different types of mouse models, and that results obtained with one model cannot be applied directly to the other model.

The IL-1β production by PBMCs was also assessed after incubation with TiO_2 without or with MDP/PGN to compare the results of TiO_2-exposed murine BMDMs to previously published results of TiO_2-treated primary human cells. It should be noted that it was only possible to conduct three independent experiments with PBMCs from different donors during the course of this study, and the variability after TiO_2 stimulation between the cells from different donors was high (Figure 2.14). This high variability might have obscured potential effects of the TiO_2 particles. The cells that are primarily responsible for IL-1β secretion in mixed populations of PBMCs are monocytes [283], and the percentage of monocytes in PBMCs can vary from 3 % to 7 % [284]. Thus, it would be useful to normalise IL-1β secretion according to the monocytes frequency for each individual donor. However,

such data was not available at the time the experiments were conducted, and the monocyte frequencies cannot be obtained retrospectively because all cryopreserved PBMCs have since been used in other assays (personal communication with Dr Laetitia Pele, Medical Research Council Human Nutrition Research, Cambridge, UK).

Therefore, the data could only be normalised to the secretion of IL-1β by non-stimulated control cells (Figure 2.14b, d, f). This showed that the relative IL-1β secretion appeared to increase with increasing TiO_2 concentration for the 3 h time point and seemed to decrease with MDP and PGN co-stimulation for the 3 h + 21 h time point. Statistical analysis showed that there was a group difference at a significance level of 0.05 for relative IL-1β concentration in the supernatants of cells stimulated with TiO_2 + PGN after 3 h + 21 h. However, a subsequently performed pairwise comparison indicated that there were no differences between any two groups at the selected significance level of 0.05.

It should be pointed out that cryopreserved PBMCs were used in the experiments, and TCM containing 10 % dimethyl sulfoxide was used during cryopreservation to prevent the formation of cell membrane-damaging ice crystals during the freezing process [285]. It can be argued that the presence of dimethyl sulfoxide might have had an effect on cytokine production by PBMCs stimulated with LPS and TiO_2 particles without or with bacterial antigens because it has been shown that incubation of LPS-stimulated PBMCs with 1 % dimethyl sulfoxide increased the production of IL-1β [286]. However, the reported augmentation of IL-1β secretion by dimethyl sulfoxide is controversial, and it has been shown that dimethyl sulfoxide attenuated IL-1β maturation in LPS-stimulated BMDMs through inhibition of the NLRP3 inflammasome [287]. Moreover, after the cryopreserved PBMCs were thawed the cells were washed in TCM to remove any dimethyl sulfoxide. Furthermore, the PBMCs were incubated overnight in TCM after thawing to ensure the cells were rested before they were stimulated with LPS and TiO_2 without or with MDP/PGN. It has been shown that using rested cells for stimulation experiments with particles is important because non-rested cells displayed higher baseline IL-1β levels than cells that were rested for 24 h before stimulation with calcium phosphate particles [288]. Therefore, the effect, if any, of dimethyl sulfoxide on IL-1β secretion by PBMCs in this study was most likely negligible.

An increase in IL-1β secretion after 3 h+ 21 h stimulation with TiO_2 had been expected based on previously published studies [215, 216]. The contrary observation in this study (Figure 2.14a) might have been due to increased cell death after prolonged cell culture of primary cells, which was enhanced by stimulation with TiO_2. Cell viability was not investigated in the course of these experiments, but it has been reported before that primary

human cells exhibited high cell death after incubation with TiO_2 particles and LPS for 24 h [215, 217]. The observed decrease in IL-17 secretion with MDP and PGN co-stimulation after incubation for 3 h + 69 h would also support this hypothesis (Figure 2.15).

The secretion of both TNF-α and IL-1β by BMDMs stimulated with TiO_2 without or with bacterial antigens was also lower for the 3 h + 21 h time points compared to the respective 3 h time points (Figures 2.12 & 2.13). As discussed in the previous paragraph, it might have been expected to detect higher amounts of cytokines in supernatants collected at a later time point. For example, it has been shown that the secretion of IL-1β by LPS pre-stimulated human peripheral blood monocytes increased exponentially between 2 h and 10 h after LPS pre-stimulation, and it levelled of between 10 h and 20 h [289]. Another study demonstrated that the concentrations of both IL-1β and TNF-α in the supernatants of LPS pre-stimulated human PBMCs reached a maximum after 12 h and remained constant until 24 h [290]. In these studies the supernatants were collected from different cells at the different time points. Thus, the cytokines measured in the supernatants collected at the 24 h time point represented the amount of cytokines that were released into the TCM over a period of 24 h since the initial pre-stimulation with LPS. In contrast, in this study the supernatants were collected from the same cells at both the 3 h and the 3 h + 21 h time points. Therefore, the cytokines detected at the later time point had been secreted only since the collection of the supernatants at the earlier time point. This could explain why the cytokine concentrations were consistently lower for the 3 h + 21 h time point in this study. Nevertheless, it would be interesting to investigate the kinetics of IL-1β secretion by BMDMs after stimulation with TiO_2 alone or with MDP/PGN in future studies.

2.5.7 Conclusion

In summary, it has been shown that exposure of BMDMs to TiO_2 increased cell activation as shown by elevated expression of CD86 in a TiO_2 concentration-dependent manner. Cells from *Nod2*$^{m/m}$ mice exhibited a higher activation phenotype than cells from WT mice, and for both types of cells the expression of CD86 increased with MDP/PGN co-stimulation. This observation was in line with the increased production of both TNF-α and IL-1β after stimulation with TiO_2 in TCM alone. However, a particle-dependent increase after co-incubation with bacterial antigens was only noticeable for IL-1β. The increased amount of IL-1β released by *Nod2*$^{m/m}$ BMDMs compared to WT cells confirmed the finding from Maeda and colleagues and supported the 'gain-of-function' hypothesis for the

NOD2 1,007fs mutation [131]. However, in the current study the same results were obtained with PGN co-stimulation, which is in contrast to the findings by Maeda and colleagues. Variations in the stimulation protocols might account for these differences, and the results presented in this chapter are in line with the hypothesis that MDP can be generated in the cytosol after internalisation of PGN.

Previous results of increased IL-1β release by human PBMCs after TiO_2 exposure could not be repeated due to the limited number of samples available for this study. Although there was a relative decrease of IL-17 after TiO_2 and MDP/PGN co-stimulation, this result has to be confirmed in additional studies because it could have been due to increased cell death after the relatively long culture of PBMCs.

In conclusion, the results from this chapter supported the hypothesis that uptake of dietary TiO_2 particles by macrophages induced a pro-inflammatory response, which was augmented by bacterial antigens. Cells from *Nod2*$^{m/m}$ mice were susceptible to co-stimulation with TiO_2 particles and MDP/PGN.

These results indicated that intake of TiO_2 particles with the diet and subsequent uptake by macrophages in lymphoid tissues of the small intestine could disturb intestinal homeostasis in WT and *Nod2*$^{m/m}$ mice *in vivo*. This might cause CD-like intestinal inflammation especially in *Nod2*$^{m/m}$ mice that responded more to co-stimulation with TiO_2 and bacterial antigens than WT mice.

Chapter 3 Exposure of wild-type mice to dietary titanium dioxide

3.1 Introduction

Environmentally-derived exogenous particles, including TiO_2, were detected in human PPs, which are organised lymphoid tissues in the small intestinal tract [56, 144, 147]. These particles were observed predominantly at the base of PPs or in the submucosa in close association with PPs [56, 161]. The cells that contain TiO_2 were characterised as mature macrophages based on the expression of the cell surface molecule CD68 [162]. It has been speculated that these exogenous particles are taken up into the body *via* the oral route primarily from the diet [56, 147].

Another hypothesis is that they could also be airborne particles that enter the body by inhalation and reach the PPs after they are taken up by alveolar macrophages in the lung which are expectorated and swallowed [144].

Few animal studies have investigated the distribution of TiO_2 particles after oral gavage. For example, in rats it has been shown that after a daily dose of 12.5 mg/kg body weight for 10 d, the TiO_2 accumulated mainly in intestinal and associated lymphoid tissues, especially in PPs [172]. PPs contained the highest amount of particles relative to tissue size. Particles were also detected in liver, spleen and lung, but not in the kidneys or heart. In another study, mice were given a single oral dose of 5,000 mg/kg and after two weeks TiO_2 particles accumulated primarily in liver, spleen, kidneys, and lung tissues [205]. From these observations, the authors concluded that there must have been gastrointestinal uptake of the particles, but this has not been investigated any further. In contrast, another study in which rats received daily oral TiO_2 doses of 260 mg/kg, 521 mg/kg, and 1,042 mg/kg for 13 weeks did not show increased accumulation in liver, spleen, kidney, or brain [291]. The main differences between these animal studies were the frequency of exposure, concentration, and length of TiO_2 administration.

More, albeit indirect, experimental support for a connection between oral TiO_2 intake and gastrointestinal uptake comes from a human study [231]. Healthy volunteers ingested single oral doses of 23 mg or 46 mg anatase TiO_2 with an average particle size of 380 nm in gelatine capsules. This resulted in an increased TiO_2 concentration in the blood over 8 h to 12 h after ingestion which indicated a translocation of TiO_2 particles from the gastrointestinal tract to the blood [231].

Taken together, these studies support the hypothesis that TiO_2 particles which are ingested with processed foods, toothpastes and pharmaceuticals are taken up by PP cells, and that

they can translocate to other organs *via* the blood stream. However, confirming this connection in human studies is practically impossible. Therefore, this question needs to be addressed further using animal models.

3.2 Hypothesis and aims

The hypothesis to be tested in this chapter was that ingested TiO_2 particles from the diet accumulate in phagocytic cells in PPs. From there, the particle-containing cells also translocate to other tissues, e.g. MLNs, *via* efferent lymphatics. The previously reported TiO_2 particle uptake in PPs from humans can be mimicked in mice by feeding a diet to which food-grade TiO_2 has been added.

The aims of the first *in vivo* study were to establish if TiO_2 uptake in PPs can be observed in mice that were exposed to a TiO_2-containing diet, and if so whether and which type of PPs immune cells were affected by this potential uptake. Furthermore, the translocation of TiO_2 particles to MLNs was assessed.

3.3 Materials and methods

3.3.1 Study considerations

For the preparation of the first *in vivo* study several things had to be considered initially because, as far as it was known, a study in which animals were fed a TiO_2-containing diet had not been conducted before. In previous *in vivo* studies in which animals were exposed orally to TiO_2 particles the route of administration was either by gavaging [172, 205, 208, 291] or with the drinking water [203].

The first thing to be considered concerned the amount of TiO_2 that the mice should ingest with the diet. In two short-term *in vivo* studies in which rats and mice were exposed to TiO_2 for 10 d the daily doses were 12.5 mg/kg [172] and 100 mg/kg [208], respectively. Cho and co-workers conducted a long-term study for 13 weeks with rats that were administered daily doses of either 260 mg/kg, 521 mg/kg, or 1,042 mg/kg [291]. In the study by Wang and colleagues a single dose of 5,000 mg/kg was given to mice [205]. Troullier and colleagues used a range of doses from 50 mg/kg to 500 mg/kg in total over 5 d [203]. For this study, it was decided to feed mice daily TiO_2 doses corresponding to either 1 mg/kg, 10 mg/kg, or 100 mg/kg body weight.

The next point concerned the duration of the study. Although accumulation of TiO_2 particles in PPs from humans occurs over the whole life [56, 292] there were practical and financial reasons to limit the duration of the first *in vivo* study to four months. A maximum duration of 18 weeks was chosen because this was considered a sufficient amount of time for the development of any effects resulting from dietary TiO_2 particle intake in mice. Two more time points at 6 weeks and 12 weeks were also selected to investigate potential earlier TiO_2 uptake in PPs.

The final question to address for the study design concerned the sex of the mice. In previous studies females [172], males [203, 208], or both females and males [205] have been used. A factor that influenced the decision of this question for the first *in vivo* study was the planned second *in vivo* study (Chapter 4). It was unknown at the start of the first *in vivo* study which sex the animals would have in the second *in vivo* study because for the latter study the availability of animals depended on the breeding success of the *Nod2*$^{m/m}$ mice. Therefore, it was agreed that both females and males should be used in the first study.

3.3.2 Preparation of titanium dioxide-containing mouse diets

The same food grade TiO_2 particles from Sensient Colors that were used for the *in vitro* experiments in Chapter 2 were used in the first *in vivo* study.

The following equations were used to calculate the required TiO_2 concentrations of the diet:

Equation (1)

$$\textit{Daily } TiO_2 \textit{ intake [mg]} = \textit{Daily } TiO_2 \textit{ dose [mg/kg]} \times \textit{Body weight [kg]}$$

Equation (2)

$$TiO_2 \textit{ content of diet [mg/kg]} = \frac{\textit{Daily } TiO_2 \textit{ intake [mg]}}{\textit{Daily food intake [kg]}}$$

To calculate the required TiO_2 doses for diets that would expose mice to 1 mg/kg, 10 mg/kg, or 100 mg/kg body weight, the average body weight and food intake had to be estimated. The average body weight was based on data from the Mouse Phenome Database [293] that reported body weights of female and male C57BL/6 mice from 4 weeks to 16 weeks. At the age of 14 weeks, which corresponded to the age of the mice at the midpoint of this study after 8 weeks, females had an average body weight of 21.67 g and the average body weight for males was 29.18 g [293]. This equates to a combined average body weight of 25.43 g for female and male mice. For ease of calculation, the average body weight used for calculating

the required TiO_2 content of the diets was rounded down to 25 g. Entering this and the respective targeted relative daily TiO_2 doses of 1 mg/kg, 10 mg/kg, or 100 mg/kg, respectively, in Equation (1) resulted in the values of 0.025 mg, 0.25 mg, and 2.5 mg TiO_2 for the respective daily TiO_2 intake. The average food intake was estimated to be 4 g per day (personal communication with Dr Shelley Edmunds, formerly Plant & Food Research, Auckland, NZ). Using this estimate and the calculated values for the daily TiO_2 intakes in Equation (2) gave the amount of TiO_2 per kg diet. According to this, the requirements for diets that should result in daily doses of 1 mg/kg, 10 mg/kg, or 100 mg/kg body weight were 6.25 mg, 62.5 mg, or 625 mg TiO_2/kg diet, respectively. The well characterised standard rodent diet American Institute of Nutrition (AIN)-76A was selected as basis for the TiO_2-containing diets [294, 295]. The unmodified AIN-76A diet without TiO_2 was used as control diet. All diets were prepared by Research Diets (New Brunswick, NJ, USA). The compositions of the diets are given in Table 3.1.

Homogeneous incorporation of TiO_2 into the diets was confirmed by SEM. With SEM detailed images of sample surfaces with resolution below 100 nm can be obtained. A FEI Quanta 200 environmental scanning electron microscope (Hillsboro, OR, USA) was used for microscopy. The sample for SEM was prepared by fixing an approximately 2 mm × 2 mm × 2 mm piece of the diet containing 625 mg TiO_2/kg on a SEM pin stub specimen mount with an adhesive carbon conductive tab. The sample was then coated with carbon to have an evenly conductive surface for the generation of secondary electrons and to prevent artefacts. Images were acquired by raster-scanning the sample with the electron beam at 20 kV and detecting the emitted secondary electrons. The acquired images were digitally saved.

In addition, the chemical composition of the particles that were detected with SEM were simultaneously assessed with EDS to confirm that the observed particles were indeed TiO_2 particles [56, 147]. EDS can be used to detect the number and energy of X-rays released from a specific area onto which the SEM electron beam has been focused. The resulting EDS spectrum shows the frequency of X-rays of a specific energy. Each peak on the EDS spectrum corresponds to a specific element. The number of peaks per element depends on the number of electron shells of the particular element. The height of each peak indicates how much of the respective element was present in the analysed area. The TEAM EDS Analysis System for SEM software (EDAX, Mahwah, NJ, USA) was used to analyse the elemental composition of the observed particles.

Table 3.1 *Diet compositions according to the manufacturer.*

	***Diet*[1]**							
	Control		***6.25***		***62.5***		***625***	
Macronutrients	***g (%)***	***kcal (%)***	***g (%)***	***kcal (%)***	***g (%)***	***kcal (%)***	***g (%)***	***kcal (%)***
Protein	20	21	20	21	20	21	20	21
Carbohydrate	66	68	66	68	66	68	66	68
Fat	5	12	5	12	5	12	5	12
Total	*91*	*100*	*91*	*100*	*91*	*100*	*91*	*100*
Ingredients	***g***	***kcal***	***g***	***kcal***	***g***	***kcal***	***g***	***kcal***
Casein	200	800	200	800	200	800	200	800
DL-Methionin	3	12	3	12	3	12	3	12
Corn starch	150	600	150	600	150	600	150	600
Sucrose	500	2000	500	2000	500	2000	500	2000
Cellulose	50	0	50	0	50	0	50	0
Corn oil	50	450	50	450	50	450	50	450
Mineral mix[2]	35	0	35	0	35	0	35	0
Vitamin mix[2]	10	40	10	40	10	40	10	40
Choline bitartrate	2	0	2	0	2	0	2	0
TiO_2[3]	0	0	0.00625	0	0.0625	0	0.625	0
FD&C yellow dye #5	0	0	0.05	0	0.025	0	0	0
FD&C red dye #5	0	0	0	0	0.025	0	0.05	0
Total	*1000*	*3902*	*1000.06*	*3902*	*1000.11*	*3902*	*1000.68*	*3902*

[1]AIN-76A rodent diet without (control) or with the respective amount of TiO_2 (mg/kg diet). [2]Obtained from Bio-Serv (Frenchtown, NJ, USA) by Research Diets. [3]Obtained from Sensient Colors (St. Louis, MO, USA) by Research Diets.

3.3.3 Animals and experimental design

All experimental procedures were approved by the Grasslands Animal Ethics Committee in accordance with the New Zealand Animal Welfare Act 1999. The number of animals required for the first *in vivo* study was based on a power analysis performed by senior statistician Dr John Koolaard.

The animals, 144 five weeks old C57BL/6 mice (72 females and 72 males), were transferred from the AgResearch Ruakura Small Animal Colony to the AgResearch Grasslands Small Animal Unit. They were acclimatised to the new environment for one week before the start of the study. The mice were housed individually under the same conditions as described in Section 2.3.2, except that Alpha-dri (Shepherd Specialty Papers) was used as bedding and conventional tissue paper as nesting material. The bedding material was changed once per week. Food and drinking water was provided *ad libitum*, and the health of the mice was checked daily.

At six weeks of age, the mice were randomly assigned to one of the four diets (control diet or diet containing 6.25 mg, 62.5 mg, or 625 mg TiO_2/kg) and one of the three sampling time points after 6, 12, or 18 weeks. The terms 'diet group' and 'sampling group' were used to refer to these groups, respectively. Overall, there were 12 'treatment groups', i.e. one treatment group refers to mice that were fed the same diet and that were sampled at the same time point. There were 12 animals (six females and six males) in each treatment group. Their body weight and feed intake was recorded twice weekly on Tuesdays and Fridays between 8:30 am and 11:30 am. The daily weight gain and food intake was calculated according to the following equations:

Equation (3)

$$\textit{Daily weight gain [g]} = \frac{\textit{(Final body weight [g] − Initial body weight [g])}}{\textit{Number of study days}}$$

Equation (4)

$$\textit{Daily food intake [g]} = \frac{\sum\textit{(Food given [g] − Refusals [g])}}{\textit{Number of study days}}$$

The absolute daily TiO_2 intake in mg was calculated according to Equation (2) by multiplying the daily food intake with TiO_2 concentration of the diet.

The relative daily TiO_2 dose in mg/kg body weight was calculated according to the following two equations:

Equation (5)

$$Total\ TiO_2\ intake\ [mg] = \sum(Food\ given\ [mg] - Refusals\ [mg]) \times TiO_2\ content\ of\ diet\ [mg/kg]$$

Equation (6)

$$Daily\ TiO_2\ dose\ [mg/kg] = \frac{(Total\ TiO_2\ intake\ [mg]/Final\ body\ weight\ [kg])}{Number\ of\ study\ days}$$

3.3.4 Tissue collection

Samples were collected after 6, 12 and 18 weeks from the respective treatment groups. The mice were euthanised with CO_2 asphyxiation and cervical dislocation. The gastrointestinal tract was removed from the abdominal cavity and placed in cold PBS. The small intestine was excised by separating the proximal end of the duodenum from the stomach and at the distal end of the ileum from the caecum. The most distal PP, which was located in the ileum, was excised with approximately 1 mm tissue on either side and embedded for cryosectioning (Section 3.3.6). Cryosectioning is a technique that allows the production of cross-sections in the μm range from fresh, i.e. non-fixed, tissue samples in an atmosphere below 0 °C. Therefore, the respective samples that were required for cryosectioning had to be frozen immediately after collection to preserve tissue integrity. Briefly, an ileal section that included a PP was frozen rapidly on an ice-cold stainless steel bar cooled with dry ice. The frozen tissue was then placed vertical in a 15 mm × 15 mm × 5 mm cryomold (Sakura Finetek, Torrance, CA, USA) on the dry ice-cooled stainless steel bar, and it was carefully immersed in embedding medium for cryosectioning (Tissue Freezing Medium, Electron Microscopy Sciences, Hatfield, PA, USA). All embedded tissues were kept frozen on dry ice until they were transferred to a −80 °C freezer for long-term storage.

Of the 12 animals per group, four mice (two females and two males) were randomly selected, and their two largest MLNs were also embedded for cryosectioning in a similar process as described above for ileal tissue sections. From the other eight mice per group, all remaining PPs and all MLNs were excised. The PPs and MLNs from each mouse were collected in 1 mL cold RPMI 1640 medium containing 100 μg/mL DNaseI (Roche Diagnostics, Mannheim, Germany) and 100 μg/mL LiberaseTL (Roche Diagnostics). The enzymes were added to promote the dissociation of the tissues for the subsequent preparation of single cell

suspensions. The samples were kept on ice for a maximum of 5 h until they were further processed for flow cytometry analysis.

3.3.5 Flow cytometry analysis

Single cell suspensions were prepared from the PPs and MLNs to stain the cells with fluorescently labelled antibodies for the analysis of immune cell populations with flow cytometry. Briefly, the disrupted tissues were incubated for 20 min at 37 °C. The tissue digestion was stopped by adding 10 mM ethylenediamine tetra-acetic acid. The samples were pressed through 70 μm cell strainers with a syringe plunger to obtain single cell suspensions, and then the cells were resuspended in RPMI 1640 and centrifuged for 5 min with 400 *g*. The supernatant was discarded and the cells resuspended in FACS buffer (see Section 2.3.6).

Cells were counted with an improved Neubauer hemocytometer (Hawksley, Lancing, UK) according to standard procedure [257]. Briefly, 10 μL of the cell suspension was mixed with 10 μL 0.4 % trypan blue stain. The clean counting chamber was covered with a haemocytometer cover glass (Hawksley), and approximately 7 μL of the stained cell suspension was added to the chamber. Then, the cells were viewed under an inverted Leica DM IL light microscope (Leica Microsystems, Wetzlar, Germany) in phase contrast with 10× magnification. The live, unstained cells were counted in the four corner squares of the chamber, and the average cell count per square was calculated. The number of cells per mL cell suspension was obtained by multiplying the average cell count per square by '2' (dilution factor) and '10^4' (specific multiplication factor for the haemocytometer). For the subsequent flow cytometry staining approximately 5×10^5 PP cells and approximately 1×10^6 MLN cells were used. A respective volume of the cell suspensions per tissue sample was distributed to two 1.7 μL microcentrifuge tubes, and the PP and MLN cells were collected by centrifuging at 400 *g* for 5 min at 4 °C.

The flow cytometry staining was performed as described in Section 2.3.6. The PP and MLN cell suspensions were first incubated for 15 min on ice with 1 μg/mL anti-mouse CD16/32 fragment crystallisable region receptor blocking antibody (clone 2.4G2; BD Biosciences, Durham, NC,USA), and then for further 15 min on ice with various fluorescently labelled antibodies (all from BD Biosciences), which were titrated before use. The two separate cell suspension samples from each tissue sample were incubated with two different staining panels. For each panel an antibody mastermix was prepared consisting of the three respective antibodies in 50 μL FACS buffer. The antibodies for the first panel were selected to detect the three main lymphocyte populations based on their expression of

specific cell surface molecules, namely $CD4^+$ T cells, $CD8^+$ T cells, and B cells which are positive for CD45R. The mastermix for the first staining panel contained 1.25 μg/mL fluorescein isothiocyanate-labelled rat anti-mouse CD4 (clone H129.19), 1 μg/mL phycoerythrin-labelled rat anti-mouse CD45R (clone RA3-6B2), and 0.5 μg/mL allophycocyanin-labelled rat anti-mouse CD8a (clone 53-6.7). The second panel comprised antibodies for cell surface proteins to identify the two main monocyte populations, namely $CD11b^+$ $CD11c^{-/low}$ macrophages and $CD11c^{high}$ DCs. In addition, the three main PP DC subsets were distinguished based on their expression of CD8 and CD11b. These DC subsets were either $CD8^+$ $CD11b^-$ ($CD8^+$ DCs), $CD8^-$ $CD11b^+$ ($CD11b^+$ DCs), or $CD8^-$ $CD11b^-$ (double-negative DCs). This panel consisted of 1.25 μg/mL fluorescein isothiocyanate-labelled rat anti-mouse CD11b (clone M1/70), 0.5 μg/mL phycoerythrin-labelled Armenian hamster anti-mouse CD11c (clone HL3), and 0.5 μg/mL allophycocyanin-labelled rat anti-mouse CD8a. The antibody mastermixes were added directly to the cells after the incubation with the blocking antibody was finished, and the cells were incubated for further 15 min on ice.

After the staining, the cells were washed once in FACS buffer and then resuspended in 200 μL FACS buffer for analysis. Immediately prior to analysis by flow cytometry, 0.8 μg/mL PI was added to each sample to determine cell viability. The samples were acquired with a FACS Calibur flow cytometer and CellQuest Pro software version 6.0. A minimum of 22,000 total events and 12,000 total events were recorded from all samples stained with the antibody panels for lymphocytes or monocytes, respectively. Samples from eight mice per group were analysed, and both staining panels were used to characterise cell populations of PPs and MLNs. The data were analysed with FlowJo version 9.4.3.

The gating strategy for the flow cytometry data analysis is shown in Figures 3.1 and 3.2. The first step was to select the immune cells based on their FSC and SSC profile, and live cells were identified by plotting the PI fluorescence against the SSC. All cells with PI fluorescence less than $10^{1.1}$ were considered as viable cells (PI^-). The lymphocytes were then selected based on their FSC and SSC expression, which was lower compared to that of monocytes (Figure 3.1c). In contrast, monocytes were specified as the cells that had a higher FSC and SSC compared to that of lymphocytes (Figure 3.2c). The lymphocytes were analysed for expression of either CD4/CD8 or CD45R. The monocytes were divided into macrophages or DCs based on the expression of CD11b and/or CD11c. Monocytes that were $CD11b^+$ $CD11c^{-/low}$ were classified as macrophages, and those that expressed CD11c at a high level ($CD11c^{high}$) were considered to be DCs. The $CD11c^{high}$ DCs were then further

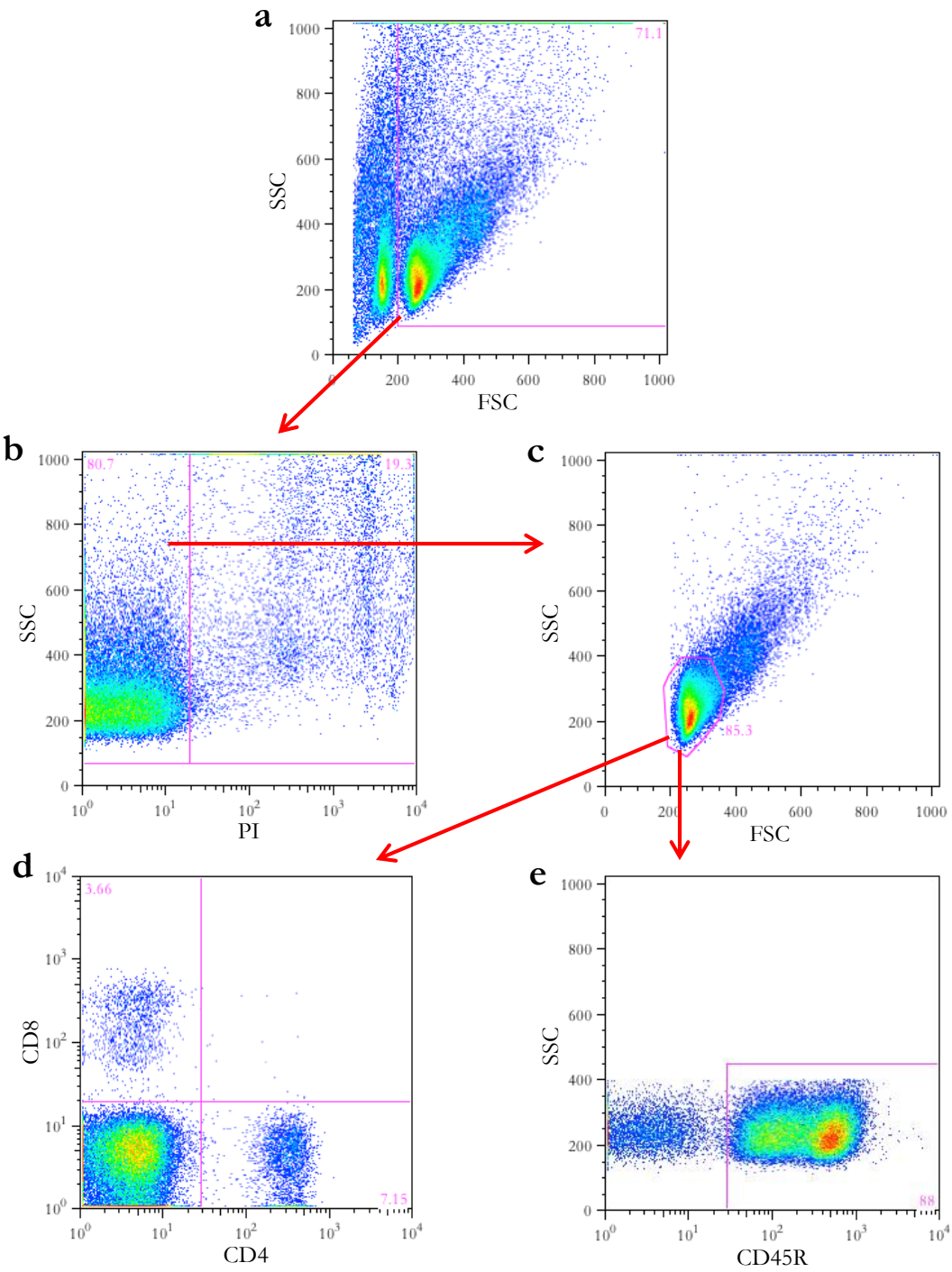

Figure 3.1 *Gating strategy to identify lymphocyte subsets in PPs and MLNs with flow cytometry.*

PP and MLN single cell suspensions were analysed by flow cytometry. Representative analysis plots of PP lymphocytes from a mouse on AIN-76A rodent diet without TiO_2 for 12 weeks are shown. In dot density plots each single event is depicted as a blue dot, and a colour gradient from green to red indicates several events at the same spot. (**a**) Only events with FSC > 200 selected. (**b**) Events with PI fluorescence < $10^{1.1}$ considered PI^-. (**c**) Lymphocytes identified based on lower FSC and SSC intensities compared to monocytes. (**d**) $CD4^+$ T cells identified as $CD4^+$ $CD8^-$ lymphocytes, $CD8^+$ T cells identified as $CD4^-$ $CD8^+$ lymphocytes. (**e**) B cells identified as $CD45R^+$ lymphocytes.

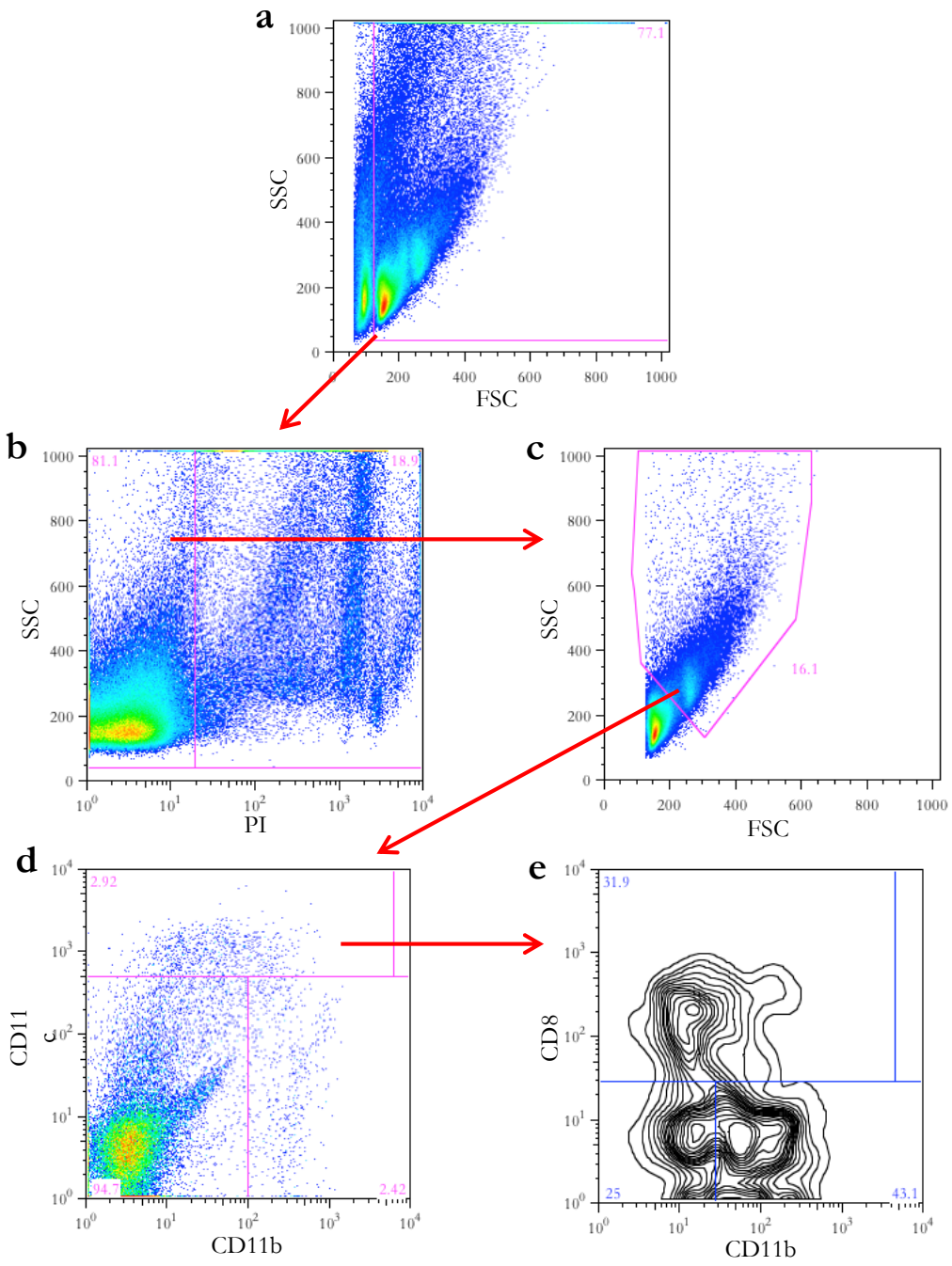

Figure 3.2 *Gating strategy to identify monocyte subsets and DC subpopulations in PPs and MLNs with flow cytometry.*
PP and MLN single cell suspensions were analysed by flow cytometry. Representative analysis plots of PP monocytes from a mouse on AIN-76A rodent diet without TiO_2 for 12 weeks is shown. (**a-d**) Dot density plots: single events depicted in blue, several events indicated by colour gradient from green to red. (**e**) Contour plot: increasing event density indicated by contour lines. (**a**) Only events with FSC > 125 selected. (**b**) Events with PI fluorescence < $10^{1.1}$ considered PI^-. (**c**) Monocytes identified based on higher FSC and SSC intensities compared to lymphocytes. (**d**) Macrophages defined as $CD11b^+$ $CD11c^{-/low}$ monocytes, DCs were defined as $CD11c^{high}$ monocytes. (**e**) $CD8^+$ DCs identified as $CD8^+$ $CD11b^{-/low}$, $CD11b^+$ DCs identified as $CD8^-$ $CD11b^+$, double-negative DCs identified as $CD8^-$ $CD11b^-$.

divided into one of the three subsets described above based on the expression of CD8 or CD11b.

3.3.6 Sample preparation for microscopy

The PPs and MLNs samples that were collected during tissue collection and not used for flow cytometry were processed for microscopy. Cross-sections through the respective tissues were produced with a Leica CM1950 Cryostat microtome (Leica Biosystems, Nußloch, Germany). The tissues were cut at −20 °C and the obtained sections had a thickness of 10 μm. The frozen tissue sections were adhered to pre-cleaned superfrost microscope slides (Thermo Fisher Scientific, Auckland, NZ) at room temperature. Slides that were used for dark field and reflectance confocal microscopy were processed immediately after sectioning (Section 3.3.7). Slides that were used for haematoxylin and eosin (H&E) staining and bright field microscopy (Section 3.3.8) or immunofluorescence staining and confocal microscopy (Section 3.3.10) were processed either immediately or frozen at −80 °C for later processing.

3.3.7 Dark field microscopy

Dark field microscopy is an excellent technique to visualise objects that scatter light, but which have a low contrast in conventional bright field illumination. This technique can be used to observe bacteria, viruses, cytoskeletal filaments like actin, and particles in suspension [296]. Dark field microscopy is also especially useful to detect particulate substances in tissues [297], and this technique has been used to detect TiO_2 particles in histological PPs sections from humans [161]. With dark field illumination only light that is scattered by the sample is detected, and the non-diffracted background light is removed [296]. To use dark field illumination with a conventional light microscope, a dark field condenser annulus is inserted in the light path between the light source and the condenser lens. This annulus will block all light that would normally directly enter the objective, and only some light can pass through a small ring on the outside of the annulus. The condenser lens focuses this remaining light on the sample [297]. Only light that is scattered by the sample will be detected by the objective lens. The resulting image is of reversed contrast, and features of the sample that highly scatter light appear bright whereas the background is black [296]. The refractive TiO_2 particles have a high capacity to scatter light, and thus these particles can be detected as bright white spots when they are observed with dark field illumination [161, 266].

Unstained PP or MLN tissue sections were used to detect TiO_2 particles with dark field microscopy. For this, the sections were fixed immediately after the samples were obtained by cryosectioning in cold 95 % ethanol for 2 min. The slides were then dried at room temperature for at least 30 min. Then, the sections were covered with a coverslip (Thermo Fisher Scientific) using ProLong Gold antifade reagent (Life Technologies, Eugene, OR, USA) as mounting medium. Dark field microscopy images of the unstained sections were acquired with a Zeiss Axiophot microscope (Carl Zeiss, Oberkochen, Germany) and Leica DFC320 camera (Leica Microsystems). The camera was controlled by the Leica Application Suite software version 3.3.0 (Leica Microsystems). The images were saved as 8 bit colour images with a pixel resolution of 2,088 × 1,550. For presentation purposes, the original images were processed with Corel PaintShop Pro version 11.20 (Corel Corporation, Ottawa, Canada). The images were cropped to only include a region of interest. The pixel resolution of the cropped images was 1,500 × 1,500. Brightness and contrast of the dark field images were adjusted by performing histogram stretching with the histogram adjustment function according to standard image processing conventions [297]. The original images were retained for future reference.

3.3.8 Haematoxylin and eosin staining and bright field microscopy

Although dark field microscopy is a good method to detect particulate substances in tissue sections, the observed white spots could also be the result of contamination of the slides with dust. Thus, it has been recommended that tissue sections should also be observed by conventional light microscopy to confirm the presence of pigment in the tissue [161]. With this method, TiO_2 particles can be detected as dark brown granules in the cell cytoplasm [56]. Therefore, some representative PP sections from mice on control diet or diet containing 625 mg TiO_2/kg were used for H&E staining. H&E is one of the most common stains in histology [4].

If the slides were previously frozen at −80 °C, they were removed from the freezer at least 15 min prior to the fixation to acclimatise to room temperature. Otherwise, the sections were removed from the cryostat and fixed immediately in 4 % paraformaldehyde for 10 min at room temperature. The 4 % paraformaldehyde solution was prepared by slowly dissolving paraformaldehyde powder (VWR International, Poole, UK) in PBS at 60 °C. The solution was adjusted to pH 7.2 with sodium hydroxide (VWR International, Phillipsburg, NJ, USA). H&E staining was performed following a standard protocol [298]. Briefly, the fixed sections

were first rehydrated in distilled water, and then they were stained with Meyer's haematoxylin solution (Sigma-Aldrich, St. Louis, MO, USA) for 5 min. A product of haematoxylin binds to DNA and as a result nuclei are stained blue. Excessive haematoxylin stain was removed by gently rinsing the slides in tap water for 15 min followed by a brief rinse in distilled water. Then, the sections were stained with 1 % aqueous Eosin Y solution (Sigma-Aldrich) for 1 min. Eosin Y stains acidic structures, e.g. the cytoplasm, pink to red. To dehydrate the sections, they were immersed two times for 2 min in 95 % ethanol, 100 % ethanol, and xylene (all from Biolab, Scoresby, Australia), respectively. The slides were dried over night at room temperature. On the next day, Permount mounting medium (Fisher Scientific, Fair Lawn, NJ, USA) was added to the slide and the sections were covered with a 22 mm × 40 mm coverslip (Thermo Fisher Scientific).

The H&E stained sections were observed with a Zeiss Axiophot microscope in bright field illumination. Images were captured with a Leica DFC320 camera and the Leica Application Suite software version 3.3.0. Like the dark field images, the bright field images were also saved as 8 bit images with a resolution of 2,088 pixel × 1,550 pixel. The original images were processed for presentation with Corel PaintShop Pro version 11.20 as described above (Section 3.3.7).

3.3.9 Reflectance confocal microscopy and image analysis

Another method to detect TiO_2 particles in tissue sections is by reflectance microscopy with a confocal laser scanning microscope [147]. The same unstained tissue sections that were used for dark field microscopy were also analysed by confocal microscopy with reflectance imaging to assess reflection spots. TiO_2 particles have a high refractive index, and thus scatter the laser light when they are observed with a confocal laser scanning microscope. The backscattered light can then be detected by a photomultiplier tube [299]. The slides were examined with a Leica TCS SP5 confocal laser scanning microscope (Leica Microsystems). The 488 nm argon-ion laser was used for excitation. The reflected light of the TiO_2 particles was detected in the first PMT channel with the gain set to '500' and an offset of '−0.3'. Backscattered light with wavelengths from 485 nm to 490 nm was collected. The reflected light was shown in red on the screen.

To determine the localisation of the TiO_2 particles within the tissue sections, the natural autofluorescence of the tissue was also detected. Unspecific autofluorescence in tissues is mainly caused by extracellular matrix proteins (collagen and elastin), so the morphology of tissues can be observed by detecting this autofluorescence [300]. The tissue sections were

also excited with the 488 nm laser to detect autofluorescence. The autofluorescence was recorded from 505 nm to 550 nm in the PMT2 channel with a gain of '650' and offset of '−0.3'. The autofluorescence signal was visualised in green. The images were acquired with the Leica Confocal Suite software (Leica Microsystems), and the pixel resolution of the images was 1,024 × 1,024 with 8 bits per channel.

To quantify the number of detected reflection spots, the images were first processed with ImageJ version 1.45 (National Institutes of Health, Bethesda, MD, USA). This software was used to select the region of interest for the reflection spot analysis, i.e. the SED areas of the PPs. This was done to exclude reflection spots in the intestinal lumen from further analysis. The number of red reflection spots was analysed in the cropped images with a custom image analysis program that was developed by Mr Paul Smale (AgResearch, Mosgiel, NZ) for this purpose. It was possible to adjust the sensitivity for the detection of the red reflection spots. This was done by changing the 'Threshold' value. To select the optimal threshold for the statistical comparison between the different treatment groups, all images were analysed with the thresholds '10', '20', '30', '40', '50', '60', '70', '80', '90' and '100'. By comparing the number of detected reflection spots between the different thresholds for a selected treatment group, an optimal threshold for the statistical comparison could be determined. The surface areas of the SEDs used for reflection spot analysis were also calculated from the cropped images with ImageJ.

3.3.10 Immunofluorescence staining and confocal microscopy

Immunofluorescence staining of representative PP sections was performed to investigate which immune cell population was mainly associated with the uptake of TiO_2 particles. For this, cross-sections of PP samples were either used directly after cryosectioning, or they were first frozen at −80 °C and used for staining at a later time. In this case, the frozen sections were thawed for 15 min at room temperature prior to fixation. In both cases, the PP sections that were used for immunofluorescence staining were fixed in 4 % paraformaldehyde for 10 min at room temperature. Then, the slides were briefly rinsed three times with 0.1 M Trizma hydrochloride (Sigma-Aldrich, Auckland, NZ) before they were stained with a fluorescently labelled antibody specific for DCs. A staining solution with 2 μg/mL Alexa Fluor 488 Armenian hamster anti-mouse CD11c antibody (clone N418; Biolegend) was prepared in PBS containing 1 % bovine serum albumin. Each tissue section was incubated with 50 μL staining solution overnight at 4 °C. The next day, the slides were rinsed three times in 0.1 M Trizma hydrochloride, and the nuclei stained with 0.2 μg/mL

4',6-diamidino-2-phenylindole (DAPI; Sigma-Aldrich; kindly provided by Dr Gemma Henderson, AgResearch, Palmerston North, NZ) for 15 min at 4 °C. Coverslips were mounted with ProLong Gold antifade mounting medium.

Based on the results from the TiO_2 uptake analysis with reflectance microscopy (Section 3.4.6), representative sections of mice on the diet containing 625 mg TiO_2/kg for 6 weeks were analysed with a Leica TCS SP5 confocal laser scanning microscope using sequential scanning with the 405 nm UV-diode laser and the 488 nm argon-ion laser. DAPI was excited by the 405 nm UV-diode laser, and the resulting emission was detected from 415 nm to 475 nm in the PMT1 channel with a gain of '670' and offset of '−0.1'. The 488 nm laser was used to acquire the light reflected by the TiO_2 particles after excitation with the 488 nm laser. The reflected light was acquired from 485 nm to 490 nm in the PMT2 channel with a gain of '500' and offset of '−0.3' (see Section 3.3.9). The Alexa Fluor 488 dye was also excited by the 488 nm laser. The resulting emission was detected in the PMT3 channel from 505 nm to 595 nm with a gain of '620' and offset of '−0.3'. All images were recorded with a resolution of 1,024 pixels × 1,024 pixels with 8 bit per channel with the Leica Confocal Suite software.

The acquired images were processed with ImageJ version 1.45 as described previously (Section 3.3.7). Brightness and contrast were enhanced by performing histogram stretching for each of the three channels separately as suggested for the processing of multicolour confocal microscopy images [297]. The final image was created as an overlay of the three separately processed images.

3.3.11 Statistical analysis

The statistical analyses were carried out with R version 3.0.0. For all analysis statistical significance was assumed at p less than 0.05. Normal distribution was assessed using the Shapiro-Wilk method, and variance equality was checked using Bartlett's test (Appendix C). The graphs for the figures were produced with SigmaPlot version 12.5.

The averages for age, initial body weight, daily weight gain and daily food intake were compared between the four diet groups with one-way ANOVA, when the data were normally distributed and the variances between the groups were equal, or the Kruskal-Wallis test, when a non-parametric group comparison was required. The mean final body weight was compared with one-way ANOVA between the diet groups with the initial body weight as co-variate. The mean values for daily TiO_2 intake and daily TiO_2 dose were compared with

one-way ANOVA or Kruskal-Wallis test between the three different sampling time groups. In all these cases the averages for females and males were compared separately because it was not the scope of this study to compare differences between sexes.

The averages of the immune cell population percentages were compared with two-way ANOVA with sampling time and diet as factors. In this case the data for females and males were combined to be able to analyse the data in a two-factorial design with 'sampling time' (6, 12, or 18 weeks) as the first factor and 'diet' (control, or 6.25 mg, 62.5 mg, or 625 mg TiO_2/kg diet) as the second factor.

The average numbers of reflection spots for mice on the 625 mg TiO_2/kg diet were compared with a Kruskal-Wallis test between different red thresholds selected for the reflection spot analysis with the custom image analysis software. Based on this analysis, one of the red thresholds was selected to assess the average number of reflection spots per sample. The results of this analysis were compared again with two-way ANOVA with 'sampling time' and 'diet' as factors.

If the statistical analyses indicated a significant difference between groups for the one-factorial analyses or a significant interaction effect for the two-way ANOVA, the respective group means were compared with Tukey's HSD *post-hoc* test.

3.4 Results

3.4.1 Detection of titanium dioxide particles in the diet

Analysis of the diet containing 625 mg TiO_2/kg with SEM showed that particles with a size less than 1 μm were present in the diet (Figure 3.3a). These particles consisted of titanium which was confirmed by EDS (Figure 3.3b).

3.4.2 Performance and titanium dioxide intake

The average values for age at beginning of the study, initial body weight, final body weight, daily weight gain, and daily food intake for all treatment groups are shown in Table 3.2 for female mice and Table 3.3 for male mice. Differences between the respective diet groups were analysed by one-way ANOVA or Kruskal-Wallis test, and the *p*-values are also given in the respective tables. There was no significant age difference between the diet groups of all sampling time points for female and male mice. The average age at the beginning of the study for the combined treatment groups of both females and males was 38 d ± 1 d. The initial

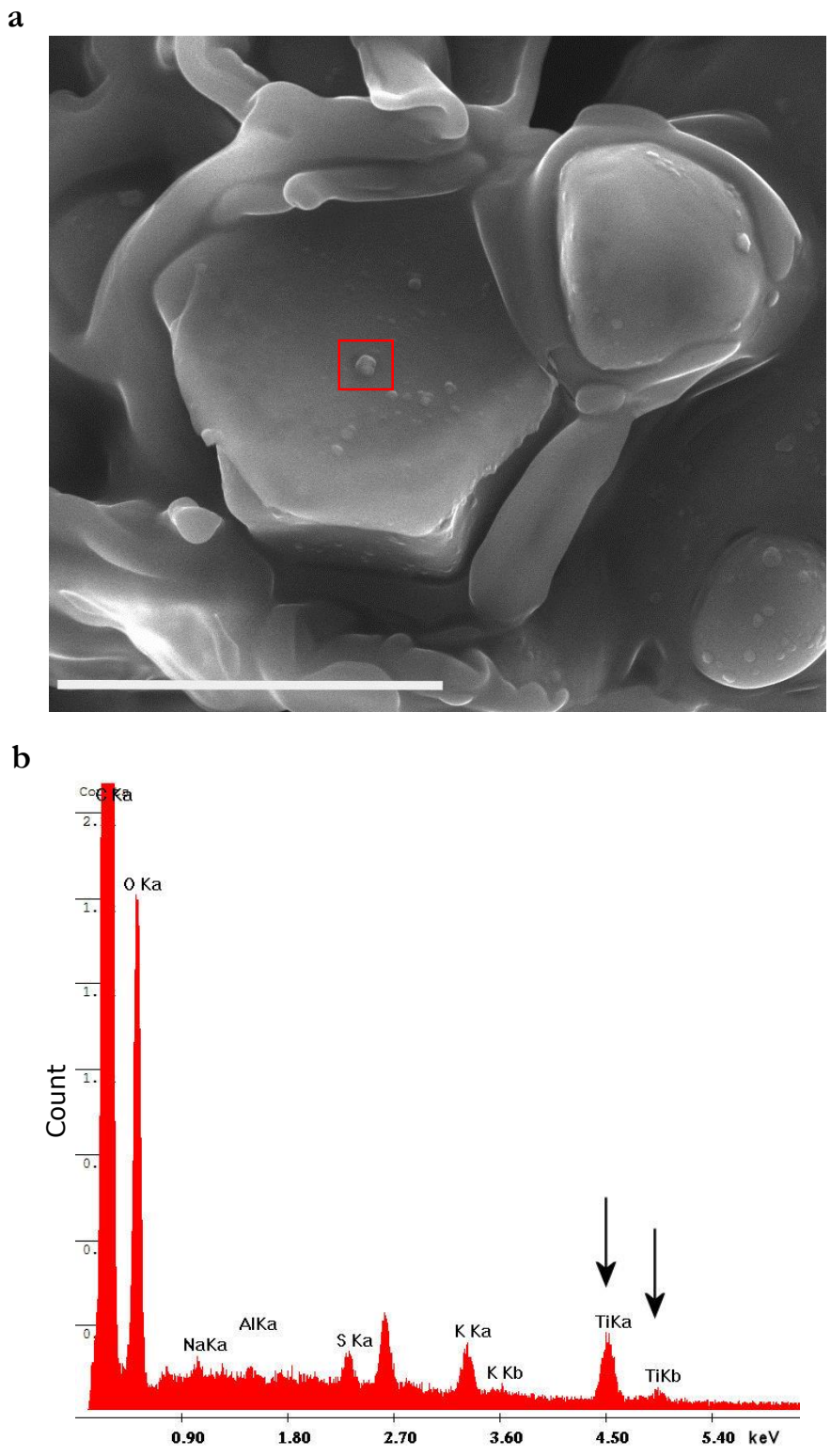

Figure 3.3 *TiO_2 particles in AIN-76A diet containing 625 mg TiO_2/kg.*

TiO_2 particles were identified with SEM in the AIN-76A diet containing 625 mg TiO_2/kg and the presence of titanium was confirmed with EDS. (**a**) Representative SEM image of the diet. Square indicates TiO_2 particle. Scale bar = 20 μm. (**b**) EDS analysis of the particle in the square from (**a**). Arrows point out the characteristic titanium double peak from the analysed particle. The other detected elements are derived from the diet in the background of the particle.

Table 3.2 *Means (± SD) for age, initial and final body weights, daily weight gain, and daily food intake of female WT mice fed a diet with or without TiO_2.*

Parameter	***Weeks***	***Diet[1]***				p-***value[2]***
		Control	***6.25***	***62.5***	***625***	
Age (d)	6	38 ± 1	38 ± 1	38 ± 1	38 ± 1	0.87
	12	38 ± 1	38 ± 1	38 ± 1	38 ± 1	1.00
	18	38 ± 1	38 ± 1	38 ± 1	38 ± 1	0.87
Initial body weight (g)	6	15.0 ± 1.7	15.7 ± 1.1	15.6 ± 0.4	16.0 ± 1.3	0.54
	12	16.4 ± 0.6	16.1 ± 2.1	16.1 ± 0.6	15.8 ± 1.5	0.85
	18	15.6 ± 1.3	15.6 ± 1.1	15.4 ± 1.4	16.0 ± 1.2	0.84
Final body weight (g)[3]	6	18.5 ± 0.7	17.9 ± 1.6	18.5 ± 1.1	18.4 ± 0.6	0.55
	12	19.6 ± 0.4	19.6 ± 0.9	20.0 ± 1.1	19.8 ± 0.8	0.49
	18	20.8 ± 1.5	20.7 ± 1.1	20.4 ± 0.6	21.5 ± 1.1	0.51
Daily weight gain (g)	6	0.09 ± 0.03	0.06 ± 0.05	0.08 ± 0.02	0.06 ± 0.03	0.31
	12	0.04 ± 0.01	0.04 ± 0.03	0.05 ± 0.01	0.05 ± 0.01	0.57
	18	0.04 ± 0.01	0.04 ± 0.01	0.04 ± 0.01	0.05 ± 0.01	0.93
Daily food intake (g)	6	2.64 ± 0.09	2.57 ± 0.26	2.60 ± 0.13	2.59 ± 0.20	0.91
	12	2.54 ± 0.06	2.58 ± 0.20	2.47 ± 0.18	2.51 ± 0.14	0.68
	18	2.63 ± 0.15	2.52 ± 0.18	2.58 ± 0.19	2.47 ± 0.13	0.37

[1]AIN-76A rodent diet without (control) or with the respective amount of TiO_2 (mg/kg diet). [2]Statistical comparison with one-way ANOVA or Kruskal-Wallis test. [3]For statistical comparison of 'final body weight' results 'initial body weight' was used as co-variate.

Table 3.3 *Means (± SD) for age, initial and final body weight, daily weight gain, and daily food intake of male WT mice fed a diet with or without TiO_2.*

Parameter	***Weeks***	***Diet[1]***				p-***value[2]***
		Control	***6.25***	***62.5***	***625***	
Age (d)	6	39 ± 1	38 ± 1	38 ± 1	39 ± 1	0.88
	12	38 ± 1	38 ± 1	39 ± 1	38 ± 1	0.92
	18	38 ± 2	39 ± 1	39 ± 1	39 ± 1	0.99
Initial body weight (g)	6	17.3 ± 3.4	17.5 ± 2.5	18.6 ± 1.2	19.0 ± 1.9	0.47
	12	18.7 ± 1.6	17.4 ± 1.5	18.2 ± 2.0	17.0 ± 1.7	0.31
	18	18.3 ± 1.2	17.9 ± 3.0	16.1 ± 2.6	18.5 ± 1.3	0.19
Final body weight (g)[3]	6	23.0 ± 1.3	22.1 ± 2.3	23.3 ± 1.7	23.2 ± 1.6	0.53
	12	26.0 ± 2.1	24.5 ± 1.2	24.7 ± 1.3	24.8 ± 1.6	0.61
	18	25.4 ± 0.9[a]	26.2 ± 2.1[a,b]	24.3 ± 1.8[a]	28.0 ± 1.5[b]	< 0.01[4]
Daily weight gain (g)	6	0.15 ± 0.07	0.12 ± 0.03	0.12 ± 0.02	0.11 ± 0.03	0.80
	12	0.09 ± 0.02	0.09 ± 0.03	0.08 ± 0.01	0.10 ± 0.03	0.64
	18	0.06 ± 0.01	0.07 ± 0.02	0.07 ± 0.01	0.08 ± 0.01	0.11
Daily food intake (g)	6	2.75 ± 0.12	2.69 ± 0.20	2.81 ± 0.28	2.85 ± 0.21	0.57
	12	2.95 ± 0.34	2.89 ± 0.25	2.75 ± 0.08	2.80 ± 0.16	0.80
	18	2.80 ± 0.23	2.84 ± 0.23	2.66 ± 0.11	2.83 ± 0.23	0.32

[1]AIN-76A rodent diet without (control) or with the respective amount of TiO_2 (mg/kg diet). [2]Statistical comparison with one-way ANOVA or Kruskal-Wallis test. [3]For statistical comparison of 'final body weight' results 'initial body weight' was used as co-variate. [4]Pairwise comparison of group means with Tukey's HSD test; significant differences between groups with different superscript letters; [a/b]$p < 0.05$.

body weights were not significantly different between the respective female and male diet groups of all sampling times. The mean combined body weight of all treatment groups was 18.5 g ± 1.7 g for females and 22.5 g ± 2.6 g for males.

There were no differences between the adjusted final body weight results of the diet groups from all sampling times for females and for the 6-week and 12-week samplings for males (Figures 3.4 & 3.5). At 18 weeks, male mice on the 625 mg TiO_2/kg diet had a significantly higher ($p < 0.05$) average final body weight than mice on both the control and 62.5 mg TiO_2/kg diet (Figure 3.6). There were no significant differences between the respective female and male diet groups of the three different sampling times points for either the daily weight gain or the daily food intake. The average combined weight gain of all treatment groups was 0.06 g/d ± 0.028 g/d for females and 0.10 g/d ± 0.039 g/d for males. The mean food intake per day was 2.56 g ± 0.17 g and 2.72 g ± 0.22 g for the combined treatment groups of the female and male mice, respectively.

The means for daily TiO_2 intakes and daily TiO_2 dose according to sampling group are given in Table 3.4 for female and Table 3.5 for male mice. There were no significant differences between TiO_2 intakes for the different sampling groups of the respective diets for both females and males. All female mice showed significant differences ($p < 0.05$) between the sampling groups in respect to daily TiO_2 dose. For those on the 6.25 mg and 625 mg TiO_2/kg diets the daily dose of the mice that were sampled after 6 weeks was significantly higher ($p < 0.01$) compared to those that were sampled after 18 weeks. For the 62.5 mg TiO_2/kg diet group the 6-weeks sampling group had a significantly higher ($p < 0.05$) daily dose compared to both other sampling groups. The daily TiO_2 doses were not significantly different for male mice on the 6.25 mg and 62.5 mg TiO_2/kg diets, but there was a significant difference ($p < 0.05$) between the sampling groups on the 625 mg TiO_2/kg diet. The mice from this diet group that were sampled after 18 weeks were exposed to a significantly lower ($p < 0.001$) dose compared to those animals that were sampled after 6 weeks.

3.4.3 Effects of dietary titanium dioxide exposure on immune cell populations of intestinal lymphoid tissues

The single cell suspensions of PPs and MLNs were analysed by flow cytometry to assess lymphocyte and monocyte populations as well as three DC subsets. The results were compared with two-way ANOVA with sampling time point and diet as respective factors. The *p*-values of this analysis are reported in Table 3.6. There was no significant interaction

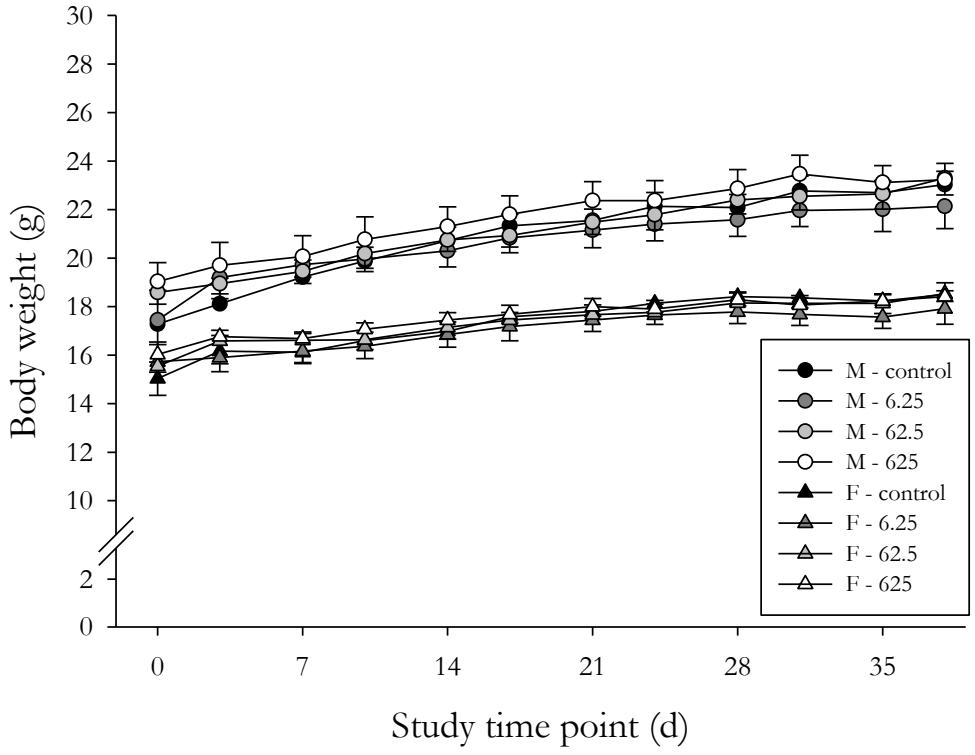

Figure 3.4 *Body weights of WT mice fed a diet with or without TiO_2 for 6 weeks.*

Female (F) and male (M) WT mice were fed AIN-76A rodent diet without TiO_2 (control) or with 6.25 mg, 62.5 mg, or 625 mg TiO_2/kg for 6 weeks. The body weight was recorded twice weekly for 38 d. Shown are means ± SE; n = 6. Results from the last time point were compared separately for females and males with one-way ANOVA (Tables 3.2 & 3.3).

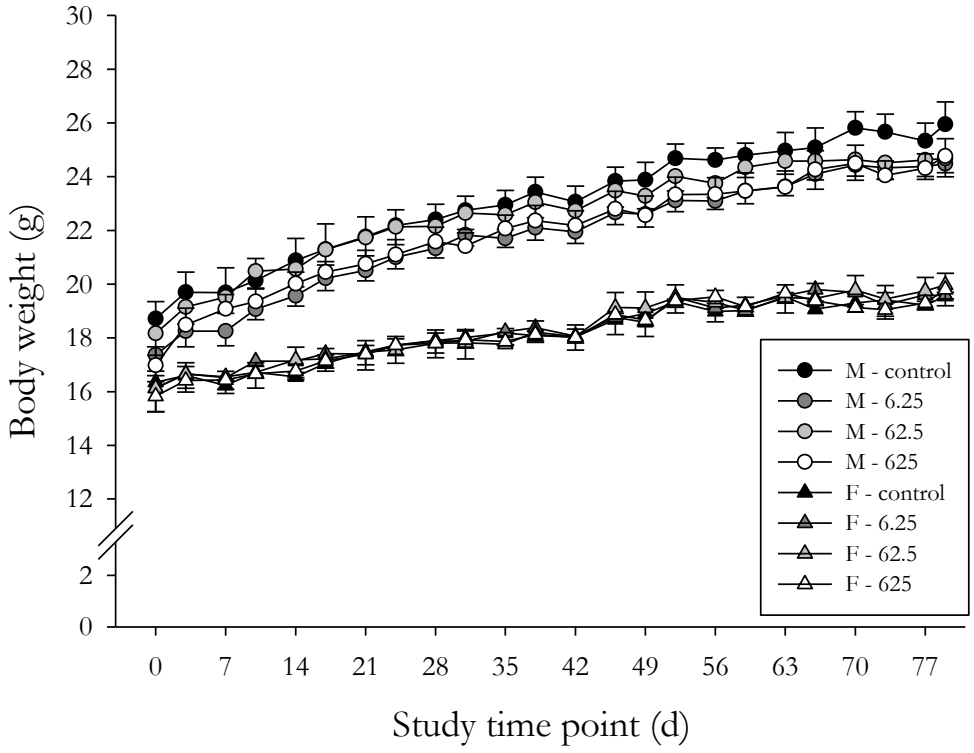

Figure 3.5 *Body weights of WT mice fed a diet with or without TiO_2 for 12 weeks.*

Female (F) and male (M) WT mice were fed AIN-76A rodent diet without TiO_2 (control) or with 6.25 mg, 62.5 mg, or 625 mg TiO_2/kg for 12 weeks. The body weight was recorded twice weekly for 79 d. Shown are means ± SE; n = 6. Results from the last time point were compared separately for females and males with one-way ANOVA (Tables 3.2 & 3.3).

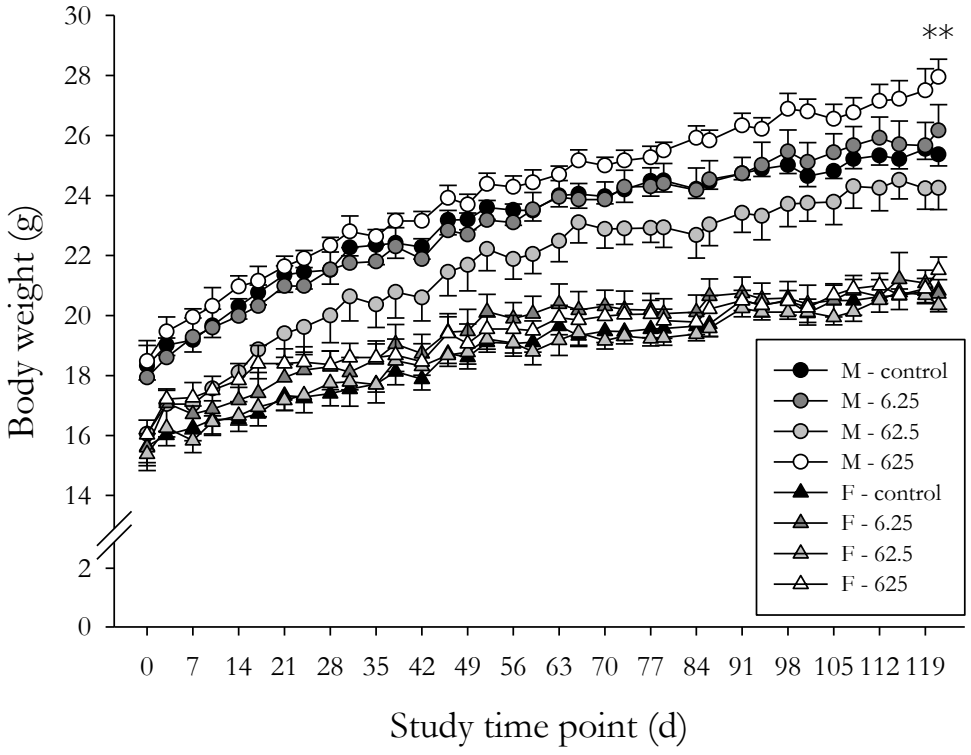

Figure 3.6 *Body weights of WT mice fed a diet with or without TiO_2 for 18 weeks.*

Female (F) and male (M) WT mice were fed AIN-76A rodent diet without TiO_2 (control) or with 6.25 mg, 62.5 mg, or 625 mg TiO_2/kg for 18 weeks. The body weight was recorded twice weekly for 121 d. Shown are means ± SE; $n = 6$. Results from the last time point were compared separately for females and males with one-way ANOVA (Tables 3.2 & 3.3). Significant difference between male diet groups is indicated; $^{**}p < 0.01$.

Table 3.4 *Means (± SD) for daily TiO_2 intake and daily TiO_2 dose of female WT mice fed a diet with TiO_2.*

Parameter	***Diet***[1]	***Weeks***			p-***value***[2]
		6	***12***	***18***	
Daily	6.25	0.016 ± 0.002	0.016 ± 0.001	0.016 ± 0.001	0.89
TiO_2 intake	62.5	0.162 ± 0.008	0.154 ± 0.012	0.161 ± 0.012	0.41
(mg)	625	1.621 ± 0.126	1.569 ± 0.087	1.543 ± 0.081	0.32
Daily	6.25	0.897 ± 0.071^{c}	0.825 ± 0.084^{c,d}	0.759 ± 0.029^{d}	< 0.05[3]
TiO_2 dose	62.5	8.737 ± 0.365^{a}	7.730 ± 0.552^{b}	7.931 ± 0.620^{b}	< 0.05[3]
(mg/kg)	625	88.027 ± 6.886^{c}	79.451 ± 6.708^{c,d}	71.827 ± 4.640^{d}	< 0.01[3]

[1]AIN-76A rodent diet with the respective amount of TiO_2 (mg/kg diet). [2]Statistical comparison with one-way ANOVA or Kruskal-Wallis test. [3]Pairwise comparison of group means with Tukey's HSD test; significant differences between groups with different superscript letters; $^{a/b}p < 0.05$, $^{c/d}p < 0.01$.

Table 3.5 *Means (± SD) for daily TiO_2 intake and daily TiO_2 dose of male WT mice fed a diet with TiO_2.*

Parameter	***Diet*[1]**	***Weeks***			**p-*value*[2]**
		6	***12***	***18***	
Daily	6.25	0.017 ± 0.001	0.018 ± 0.002	0.018 ± 0.002	0.34
TiO_2 intake	62.5	0.176 ± 0.018	0.172 ± 0.005	0.166 ± 0.007	0.38
(mg)	625	1.783 ± 0.133	1.750 ± 0.102	1.768 ± 0.145	0.98
Daily	6.25	0.763 ± 0.049	0.737 ± 0.065	0.682 ± 0.076	0.11
TiO_2 dose	62.5	7.586 ± 0.990	6.965 ± 0.402	6.876 ± 0.516	0.24
(mg/kg)	625	76.827 ± 4.700[a]	70.853 ± 5.564[a,b]	63.335 ± 4.933[b]	< 0.05[3]

[1]AIN-76A rodent diet with the respective amount of TiO_2 (mg/kg diet). [2]Statistical comparison with one-way ANOVA or Kruskal-Wallis test. [3]Pairwise comparison of group means with Tukey's HSD test; significant differences between groups with different superscript letters; [a/b]$p < 0.001$.

Table 3.6 *Two-way ANOVA results for comparisons of immune cell population frequencies in PPs and MLNs of WT mice fed a diet with or without TiO_2.*

Cell subset	***Tissue***	***Population***	***p-value[1]***		
			Time	***Diet***	***Interaction***
Lymphocytes[2]	*PPs*	all	< 0.001	0.75	0.82
		$CD4^+$ T cells	< 0.01	0.78	0.68
		$CD8^+$ T cells	0.14	0.87	0.65
		$CD45R^+$ B cells	0.18	0.66	0.59
	MLNs	all	< 0.05	0.96	0.18
		$CD4^+$ T cells	< 0.01	0.69	0.36
		$CD8^+$ T cells	0.51	0.73	0.43
		$CD45R^+$ B cells	< 0.05	0.96	0.18
Monocytes[3]	*PPs*	all	< 0.001	0.80	0.62
		$CD11b^+$ $CD11c^{-/low}$ MΦ[5]	< 0.001	0.09	0.50
		$CD11c^{high}$ DCs	0.39	0.68	0.22
	MLNs	all	0.10	0.75	0.42
		$CD11b^+$ $CD11c^{-/low}$ MΦ	< 0.001	0.73	0.74
		$CD11c^{high}$ DCs	0.05	0.76	0.53
DCs[4]	*PPs*	$CD8^+$ $CD11b^-$ DCs	< 0.01	0.86	0.22
		$CD8^-$ $CD11b^+$ DCs	< 0.001	0.90	0.61
		$CD8^-$ $CD11b^-$ DCs	< 0.001	0.95	0.83
	MLNs	$CD8^+$ $CD11b^-$ DCs	0.08	0.96	0.89
		$CD8^-$ $CD11b^+$ DCs	< 0.05	0.90	0.99
		$CD8^-$ $CD11b^-$ DCs	< 0.001	0.76	0.92

[1]Statistical comparison with two-way ANOVA with sampling time point (6/12/18 weeks), and diet (AIN-76A diet without TiO_2 or with 6.25/62.5/625 mg TiO_2/kg) as factors. [2]Defined as PI^-, FSC^{low} SSC^{low}. [3]Defined as PI^-, FSC^{high} SSC^{high}. [4]Defined as PI^-, FSC^{high} SSC^{high}, $CD11c^{high}$. [5]Abbreviations specific for this table: MΦ = macrophages.

or diet effect. In some instances, however, there were significant differences ($p < 0.05$) in immune cell composition between the sampling groups. Thus, the average results of the combined diet groups of each sampling time point are reported in Tables 3.7 and 3.8 to highlight differences between the sampling groups.

There were significant differences ($p < 0.05$) in the percentages of lymphocytes and monocytes determined from the total number of acquired live cells (Table 3.6 & Figure 3.7) between the sampling groups in all cases, except for the percentage of monocytes in MLNs. The PPs from the 6-weeks sampling group contained a lower number of lymphocytes and more monocytes compared to the groups sampled after 12 weeks and 18 weeks (Tables 3.7 & 3.8). Less lymphocytes were also observed in the MLNs of the 18-weeks group compared to the other two sampling groups.

The results for the three main lymphocyte populations were reported as average percentages of the total live lymphocytes (Figure 3.8). The percentages of $CD4^+$ T cells in PPs and MLNs were lowest for the 12-weeks sampling group for both tissues (Table 3.7). In MLNs, the number of $CD45^+$ B cells was diminished in mice sampled after 18 weeks compared to the other two time points.

The results for macrophages and DCs were shown as average percentages of the analysed total live monocytes (Figure 3.9). There were no significant differences for the percentage of DCs observed in PPs and MLNs, but the frequencies of macrophages in both tissues were significantly different ($p < 0.001$) between the sampling groups (Table 3.6). There were less macrophages in the tissues from animals sampled after 18 weeks compared to the other two sampling time points (Table 3.8).

The results of the three investigated DC subsets were shown as percentages of the total DC population (Figure 3.10). All subsets, except $CD8^+$ DCs in MLNs, were significantly different ($p < 0.05$) between the sampling groups (Table 3.6). The frequencies of $CD8^+$ DCs in PPs and of $CD11b^+$ DCs in MLNs were lowest for the 6-weeks sampling group and highest for the 18-weeks group (Table 3.8). In contrast the percentages of double-negative DCs in both tissues were highest for the earliest sampling time point. For $CD11b^+$ DCs the highest number for PPs was observed in the 12-weeks group.

Table 3.7 *Mean (± SD) frequencies of lymphocytes and lymphocyte populations in PPs and MLNs from WT mice according to sampling time point.*

Tissue	***Population***	***Weeks***			
		6	***12***	***18***	***Combined***
PPs	Lymphocytes[1]	78.6 ± 4.2	85.1 ± 2.4	82.1 ± 3.5	81.9 ± 4.3
	$CD4^+$ T cells	10.8 ± 2.0	9.6 ± 1.9	11.6 ± 2.6	10.7 ± 2.3
	$CD8^+$ T cells	4.0 ± 1.3	4.7 ± 1.3	4.6 ± 1.6	4.4 ± 1.4
	$CD45R^+$ B cells	83.0 ± 3.2	84.9 ± 3.3	83.7 ± 4.6	84.0 ± 3.8
MLNs	Lymphocytes[1]	83.0 ± 3.2	84.7 ± 3.2	81.8 ± 4.9	83.2 ± 4.0
	$CD4^+$ T cells	30.1 ± 4.3	27.4 ± 2.9	30.7 ± 4.1	29.4 ± 4.0
	$CD8^+$ T cells	23.3 ± 4.8	22.9 ± 2.3	24.1 ± 3.5	23.4 ± 3.6
	$CD45R^+$ B cells	45.5 ± 9.2	47.5 ± 5.6	42.7 ± 7.3	45.2 ± 7.6

[1]Defined as PI^-, FSC^{low} SSC^{low}.

Table 3.8 *Mean (± SD) frequencies of monocytes, monocyte populations, and DC subsets in PPs from WT mice according to sampling time point.*

Tissue	***Population***	***Weeks***			
		6	***12***	***18***	***Combined***
PPs	Monocytes[1]	22.8 ± 6.4	14.7 ± 2.5	16.3 ± 3.0	17.9 ± 5.6
	$CD11b^{+}CD11c^{-/low}$ MΦ[2]	2.0 ± 1.0	2.7 ± 0.9	1.6 ± 0.7	2.1 ± 1.0
	$CD11c^{high}$ DCs	3.7 ± 1.1	4.0 ± 1.1	4.0 ± 1.2	3.9 ± 1.1
	$CD8^{+}$ $CD11b^{-}$ DCs	25.3 ± 6.5	28.7 ± 7.7	31.7 ± 5.2	28.9 ± 7.0
	$CD8^{-}$ $CD11b^{+}$ DCs	34.0 ± 6.6	45.7 ± 7.6	40.4 ± 4.5	40.6 ± 7.8
	$CD8^{-}$ $CD11b^{-}$ DCs	40.7 ± 8.2	25.6 ± 5.3	28.1 ± 4.1	30.6 ± 8.6
MLNs	Monocytes[1]	15.7 ± 3.2	15.0 ± 4.3	17.5 ± 6.4	16.1 ± 4.9
	$CD11b^{+}CD11c^{-/low}$ MΦ	3.7 ± 1.0	4.3 ± 0.7	2.9 ± 0.9	3.7 ± 1.1
	$CD11c^{high}$ DCs	7.1 ± 2.4	8.4 ± 2.9	8.7 ± 2.1	8.1 ± 2.6
	$CD8^{+}$ $CD11b^{-}$ DCs	20.2 ± 5.5	24.1 ± 6.8	20.9 ± 5.8	21.7 ± 6.2
	$CD8^{-}$ $CD11b^{+}$ DCs	46.1 ± 5.6	49.6 ± 5.6	51.1 ± 6.5	49.1 ± 6.3
	$CD8^{-}$ $CD11b^{-}$ DCs	33.7 ± 5.8	26.3 ± 7.6	28.0 ± 4.6	29.2 ± 6.6

[1]Defined as PI^{-}, FSC^{high} SSC^{high}. [2]Abbreviations specific for this table: MΦ = macrophages.

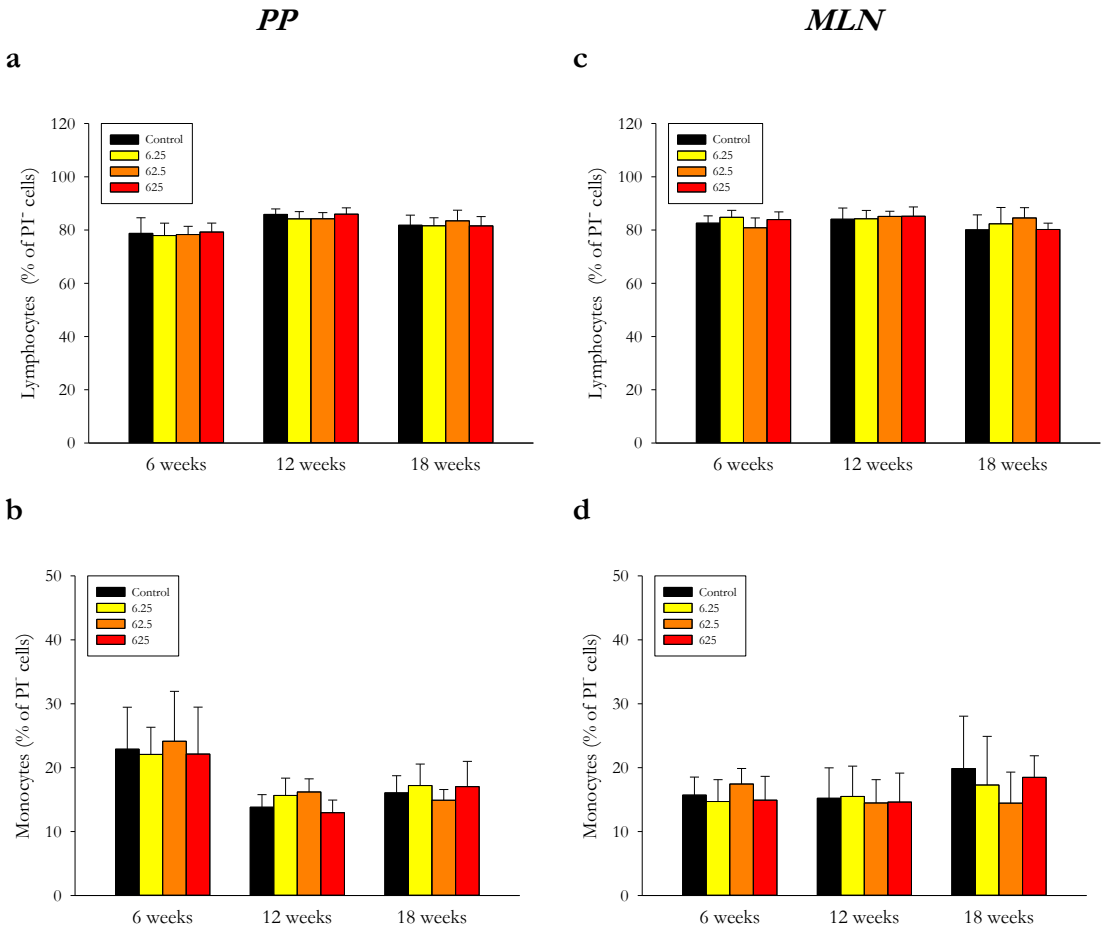

Figure 3.7 *Frequencies of lymphocytes and monocytes in PPs and MLNs from WT mice fed a diet with or without TiO_2.* Female and male WT mice were fed AIN-76A rodent diet without TiO_2 (control) or with 6.25 mg, 62.5 mg, or 625 mg TiO_2/kg for 6, 12, or 18 weeks. Single cell suspensions of PPs (**a, b**) and MLNs (**c, d**) were stained with fluorescently labelled antibodies and PI as live/dead stain. The stained cells were analysed by flow cytometry. The percentages of lymphocytes (**a, c**) and monocytes (**b, d**) from all live cells were determined. Shown are means ± SD; n = 8. Results were compared with two-way ANOVA (Table 3.6).

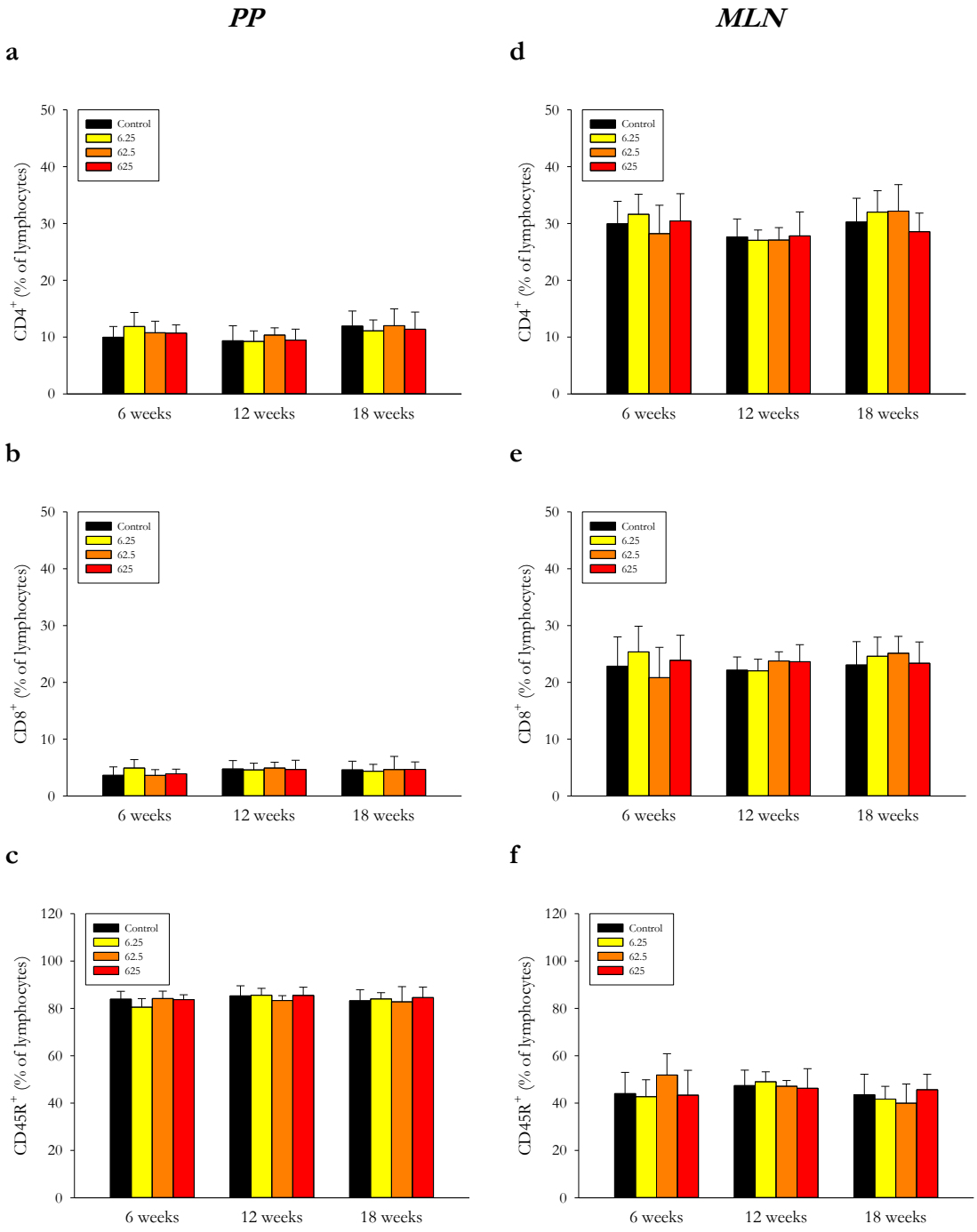

Figure 3.8 *Frequencies of lymphocyte populations in PPs and MLNs from WT mice fed a diet with or without TiO_2.* Female and male WT mice were fed AIN-76A rodent diet without TiO_2 (control) or with 6.25 mg, 62.5 mg, or 625 mg TiO_2/kg for 6, 12, or 18 weeks. Single cell suspensions of PPs (**a-c**) and MLNs (**d-f**) were stained with fluorescently labelled CD4, CD8 and CD45R antibodies and PI as live/dead stain. The stained cells were analysed by flow cytometry. The percentages of $CD4^+$ T cells (**a, d**), $CD8^+$ T cells (**b, e**), and $CD45R^+$ B cells (**c, f**) from all live lymphocytes were determined. Shown are means ± SD; $n = 8$. Results were compared with two-way ANOVA (Table 3.6).

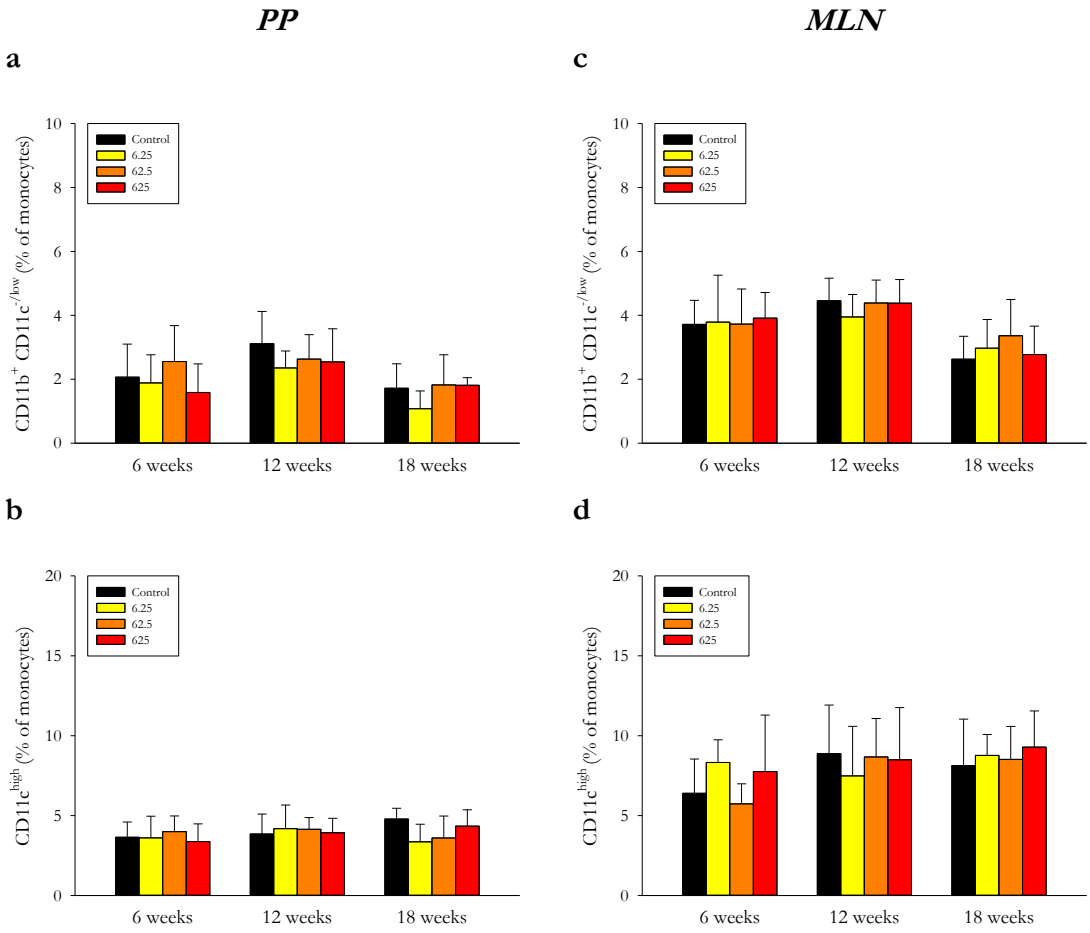

Figure 3.9 *Frequencies of monocyte populations in PPs and MLNs from WT mice fed a diet with or without TiO_2.*
Female and male WT mice were fed AIN-76A rodent diet without TiO_2 (control) or 6.25 mg, 62.5 mg, or 625 mg TiO_2/kg for 6, 12, or 18 weeks. Single cell suspensions of PPs (**a, b**) and MLNs (**c, d**) were stained with fluorescently labelled CD8, CD11b, and CD11c antibodies and PI as live/dead stain. The stained cells were analysed by flow cytometry. The percentages of $CD11b^+$ $CD11c^{-/low}$ macrophages (**a, c**) and $CD11c^{high}$ DCs (**b, d**) from all live monocytes were determined. Shown are means ± SD; n = 8. Results were compared with two-way ANOVA (Table 3.6).

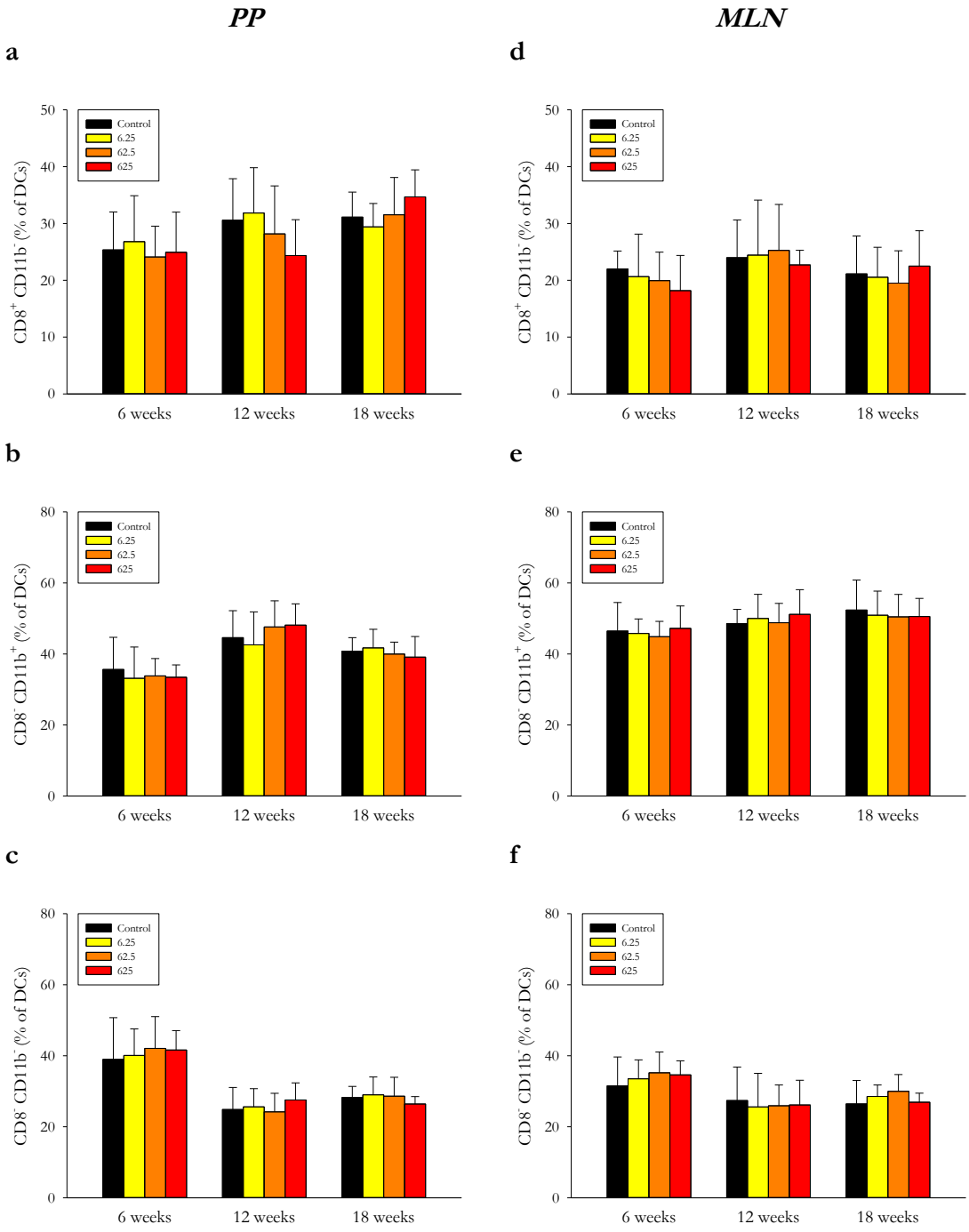

Figure 3.10 *Frequencies of DC subsets in PPs and MLNs from WT mice fed a diet with or without TiO_2.*
Female and male WT mice were fed AIN-76A rodent diet without TiO_2 (control) or with 6.25 mg, 62.5 mg, or 625 mg TiO_2/kg for 6, 12, or 18 weeks. Single cell suspensions of PPs (**a-c**) and MLNs (**d-f**) were stained with fluorescently labelled CD8, CD11b and CD11c antibodies and PI as live/dead stain. The stained cells were analysed by flow cytometry. The percentages of $CD8^+$ $CD11b^-$ DCs (**a, d**), $CD8^-$ $CD11b^+$ DCs (**b, e**), and $CD8^-$ $CD11b^-$ DCs (**c, f**) were determined from all live DCs. Shown are means ± SD; n = 8. Results were compared with two-way ANOVA (Table 3.6).

3.4.4 Observation of titanium dioxide particle uptake in intestinal lymphoid tissues with dark field microscopy

No particles were detected in PP sections from mice on control or 6.25 mg TiO_2/kg diet from all sampling groups (Figure 3.11). Only few white spots were observed in the PPs from mice on the diet containing 62.5 mg TiO_2/kg. In contrast, mice that were exposed to the 625 mg TiO_2/kg diet showed a large number of particles in PPs. Those particles were mainly located in cells of the SED directly below the FAE, but pigment-containing cells were also found in smaller numbers throughout the PP sections. Particle-containing cells were also detected in MLNs (Figure 3.12). They were mainly observed when the animals have been fed a diet with 625 mg TiO_2/kg, but also in some cases in MLNs from mice exposed to 62.5 mg TiO_2/kg diet (Figure 3.12h).

3.4.5 Observation of titanium dioxide particle uptake in Peyer's patches with bright field microscopy

Representative PP samples from animals on control diet and diet containing 625 mg TiO_2/kg were stained with H&E and observed under bright field illumination. The PPs from mice on particle-free control diet did not contain any pigmented cells (Figure 3.13a, c). In contrast, brown granules were detected in larger numbers with higher magnification in the cytoplasm of cells from PPs of mice that received the diet with 625 mg TiO_2/kg (Figure 3.13c-f). Most pigmented cells were observed in the SED (Figure 3.13d), and only some cells at the PP base contained particles (Figure 3.13e, f).

3.4.6 Assessment of titanium dioxide particle uptake in Peyer's patches with reflectance confocal microscopy

Images of the SED areas from all unstained PP sections were obtained with reflectance confocal microscopy at 40× magnification (Figure 3.14a, c). From these images, only the SED area was selected for reflection spot analysis (Figure 3.14b, d). The reflection spots were observed in the same focal plane as the tissue which was observed by acquiring the tissue autofluorescence in a separate channel. Reflection spots were observed to occur most frequently within cells that showed a high autofluorescence (Figure 3.15).

The reflection spot counts from mice on the diet containing 625 mg TiO_2/kg were analysed with different threshold settings. There was significant difference ($p < 0.05$) between the

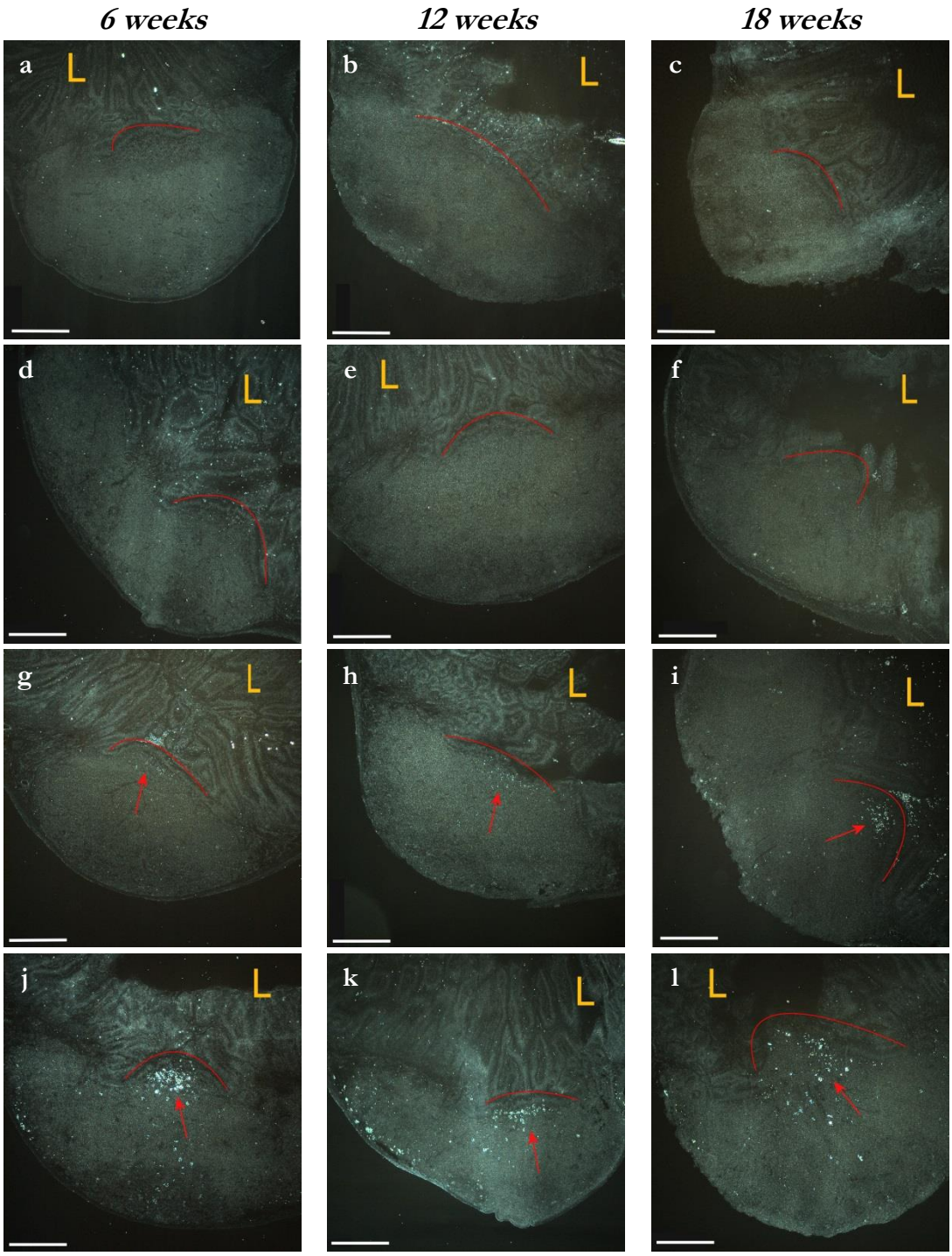

Figure 3.11 *Dark field microscopy images of PP cross-sections from WT mice fed a diet with or without TiO_2.*
Images of PP cross-sections from WT mice on AIN-76A rodent diet without TiO_2 (**a, b, c**) or with 6.25 mg (**d, e, f**), 62.5 mg (**g, h, i**), or 625 mg TiO_2/kg (**j, k, l**) for 6 (**a, d, g, j**), 12 (**b, e, h, k**), or 18 weeks (**c, f, i, l**). Unstained sections were viewed with a light microscope under dark field illumination. Lines indicate FAE. Arrows point out selected TiO_2 particle clusters in SEDs (white). Representative images are shown. Scale bar = 200 µm. L = intestinal lumen.

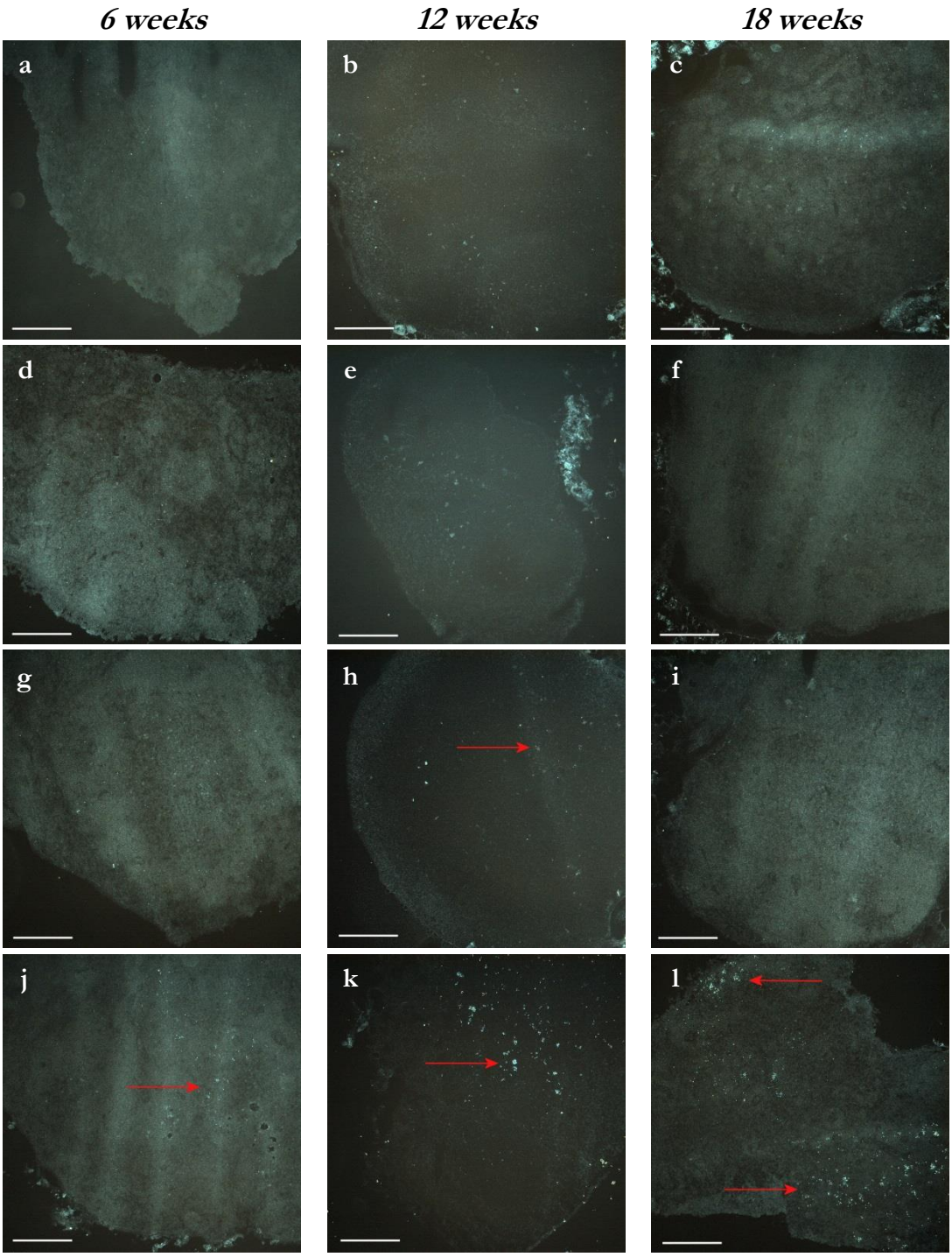

Figure 3.12 *Dark field microscopy images of MLN cross-sections from WT mice fed a diet with or without TiO_2.*
Images of MLN cross-sections from WT mice on AIN-76A rodent diet without TiO_2 (**a, b, c**) or with 6.25 mg (**d, e, f**), 62.5 mg (**g, h, i**), or 625 mg TiO_2/kg (**j, k, l**) for 6 (**a, d, g, j**), 12 (**b, e, h, k**), or 18 weeks (**c, f, i, l**). Unstained sections were viewed with a light microscope under dark field illumination. Arrows point out examples for TiO_2 particle aggregates (white). Representative images are shown. Scale bar = 200 μm.

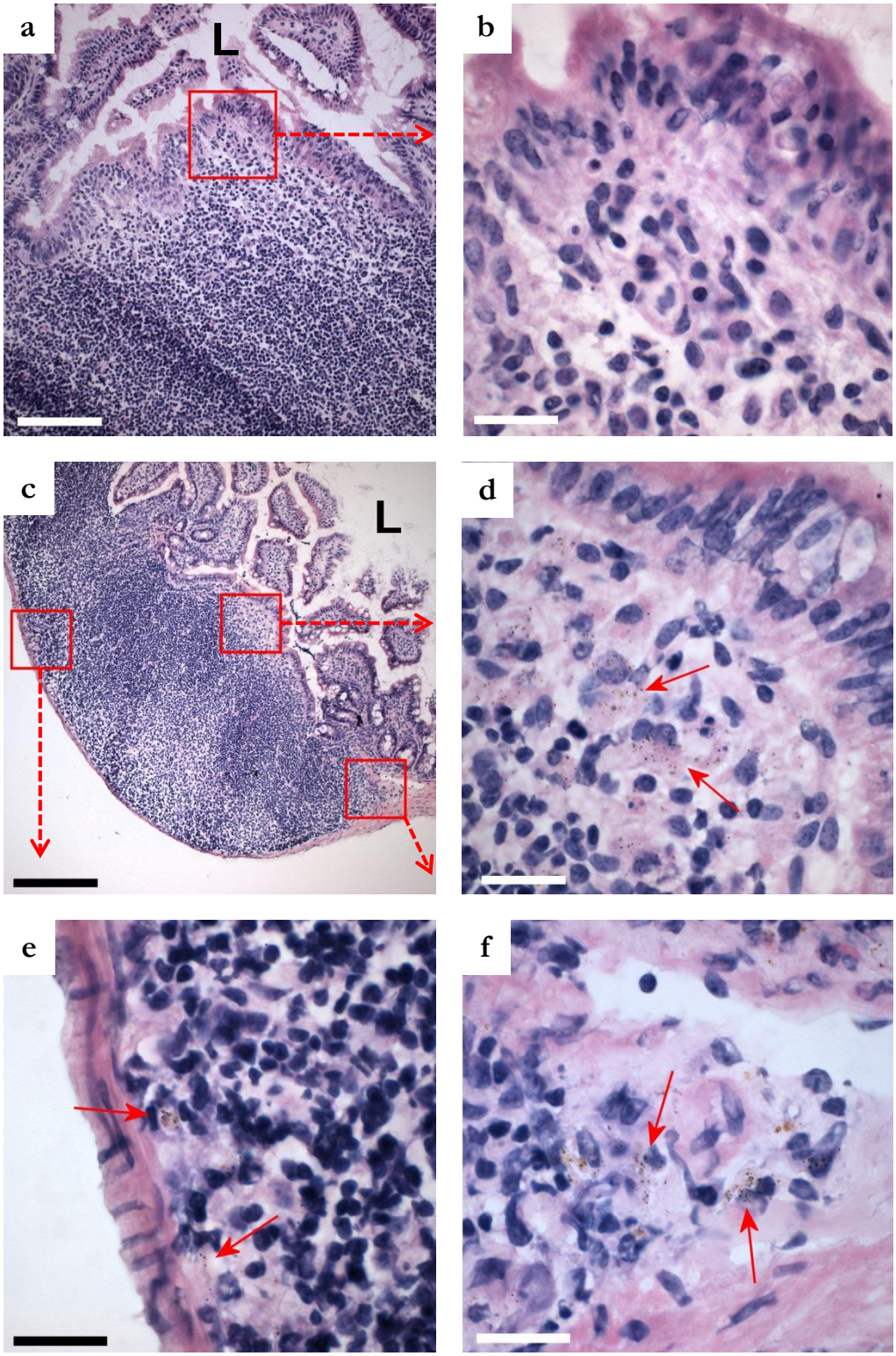

Figure 3.13 *Bright field microscopy images of PP cross-sections from WT mice fed a diet with or without TiO_2.*
Images of PP cross-sections from WT mice on AIN-76A rodent diet without TiO_2 (**a, b**) or with 625 mg TiO_2/kg (**c-f**) for 18 weeks. H&E stained sections were viewed with a light microscope under bright field illumination. Squares and dotted arrows in (**a**) and (**c**) indicate magnified areas shown in (**b**) and (**d-f**), respectively. Complete arrows point out selected TiO_2 particle clusters (brown/dark) in PPs. Representative images are shown. Scale bar = 100 μm (**a, c**)/20 μm (**b, d-f**). L = intestinal lumen.

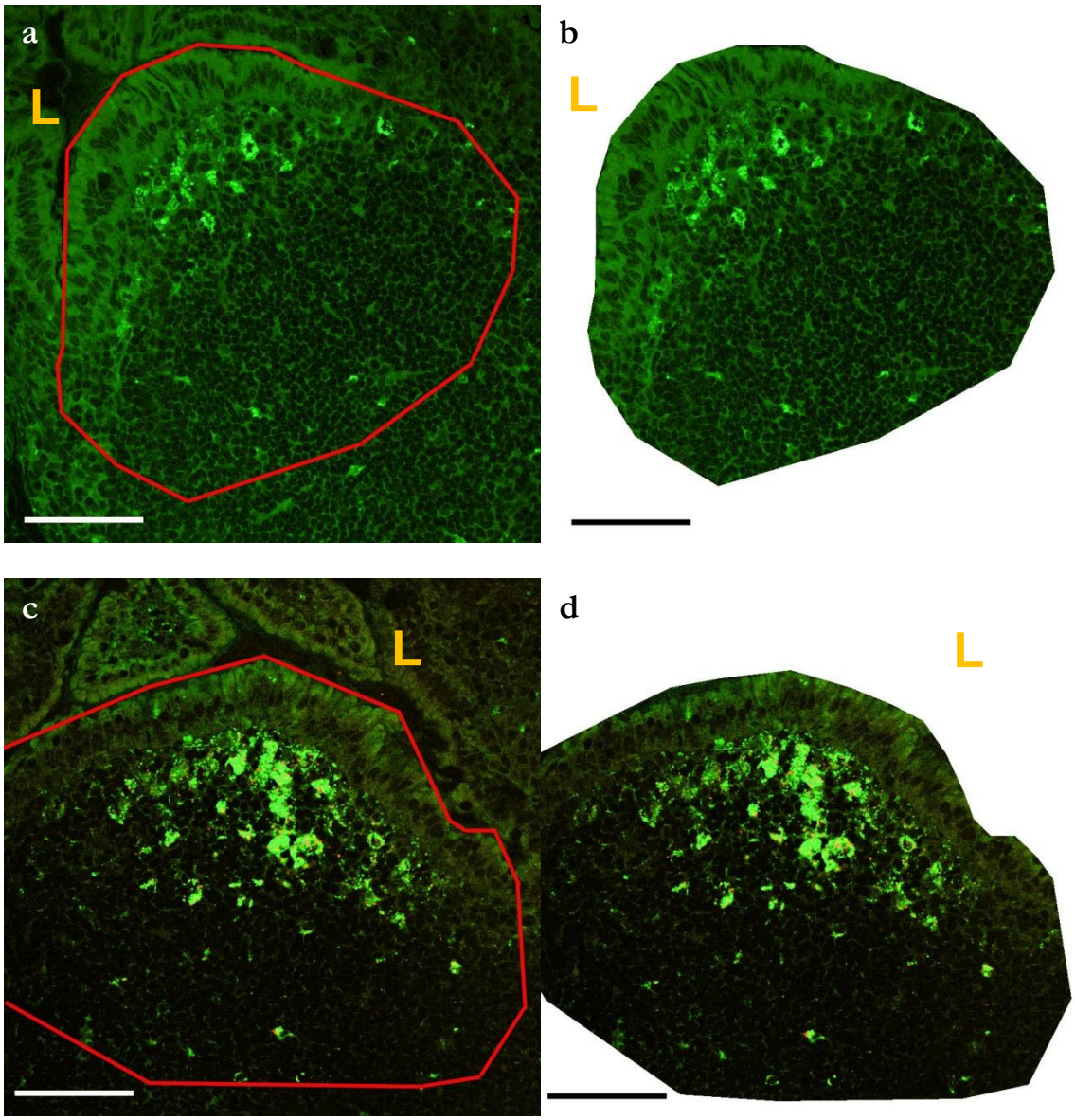

Figure 3.14 *Reflectance confocal microscopy images of PP cross-sections from WT mice fed a diet with or without TiO_2.* Reflectance confocal microscopy images of PP cross-sections from WT mice on AIN-76A rodent diet without TiO_2 (**a, b**) or with 625 mg TiO_2/kg (**c, d**) for 6 weeks. Unstained sections were excited at 488 nm. TiO_2 particle reflection (red) was detected from 485 nm to 490 nm; tissue autofluorescence (green) was detected from 505 nm to 550 nm. (**a, c**) Overview of SED area. Line indicates SED area that was cropped with image analysis software. (**b, d**) Cropped images used for reflection spot analysis. Lines in (**a**) and (**c**) indicate cropped SEDs. Representative images are shown. Scale bar = 75 µm. L = intestinal lumen.

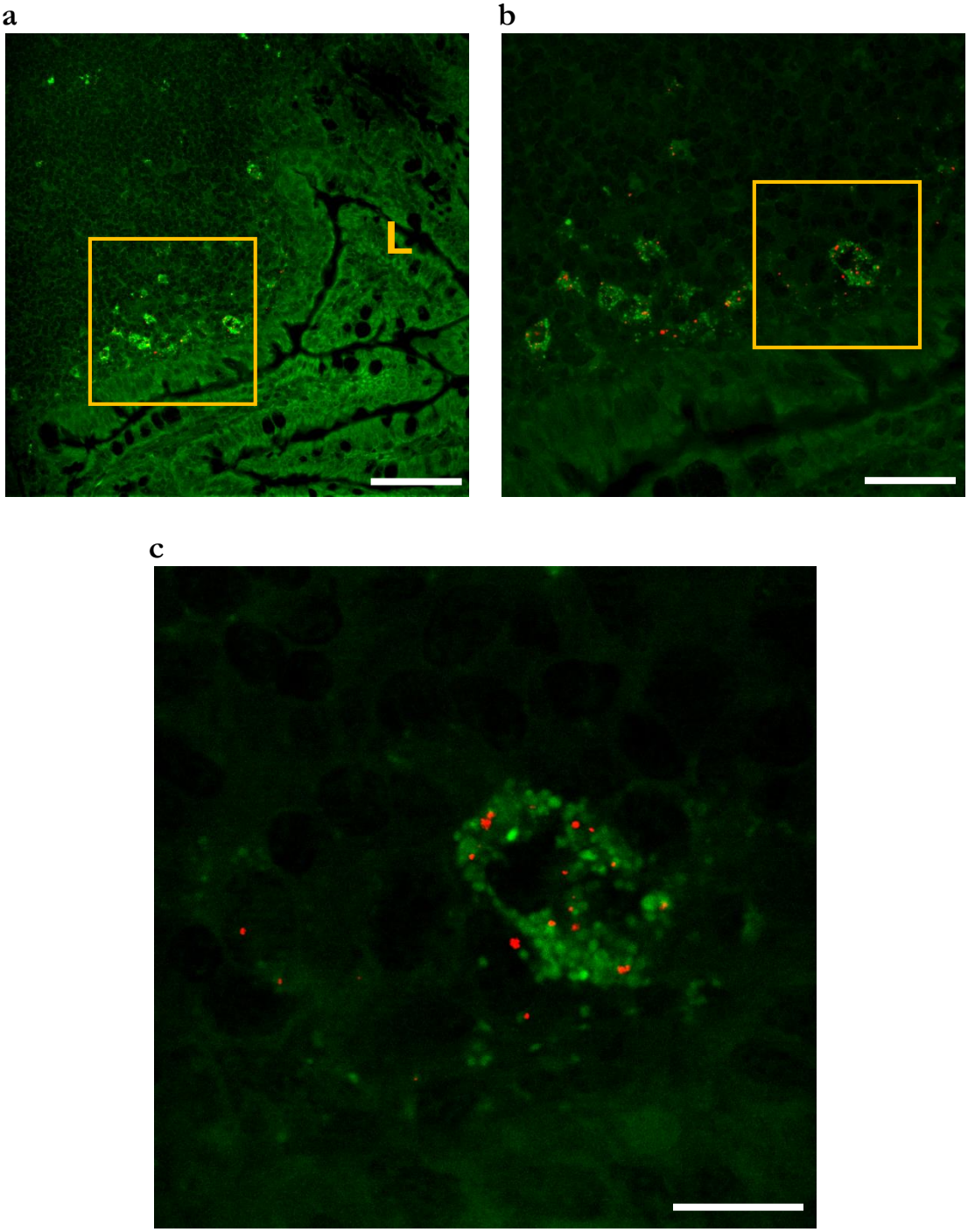

Figure 3.15 *Reflectance confocal microscopy images of the SED area from a WT mouse fed a diet with TiO_2.*

Reflectance confocal microscopy images of a PP cross-section from a WT mouse on AIN-76A rodent diet with 625 mg TiO_2/kg for 6 weeks. Unstained sections were excited at 488 nm. Reflection from TiO_2 particles (red) was detected from 485 nm to 490 nm; tissue autofluorescence (green) was detected from 505 nm to 550 nm. (**a**) Overview of SED area. (**b**) TiO_2 particles-containing autofluorescent cells in SED. (**c**) Detail of an autofluorescent cell with TiO_2 particles. Squares in (**a**) and (**b**) indicate magnified areas shown in (**b**) and (**c**), respectively. Representative images are shown. Scale bar = 75 µm (**a**)/25 µm (**b**)/10 µm (**c**). L = intestinal lumen.

samples depending on the threshold. With a threshold of '20' significantly more ($p < 0.05$) spots were detected by the image analysis software compared to the other thresholds (Figure 3.16a). With this threshold there was also a relatively large standard deviation between the samples from the individual mice. In contrast, the number of detected reflection spots was not significantly different between the other threshold settings, and the standard deviations were also comparable. A threshold setting of '60' was then used to compare the number of reflection spots between the treatment groups (Figure 3.16b). There was a significant interaction effect ($p < 0.05$) between the treatment groups. The results of this pairwise comparison are reported in Table 3.9 for an easier comparison of the statistical results of the pairwise comparisons.

Statistical comparison of the surface areas of the SEDs showed that there was no significant interaction difference. The impact of the diet on SED areas was also not significant (Figure 3.17). However, there was a significant effect ($p < 0.001$) on larger SED areas in all PP sections from mice that were sampled after 6 weeks compared to the SEDs from PPs collected at 12 or 18 weeks.

3.4.7 Titanium dioxide particle uptake by Peyer's patch dendritic cells

Immunofluorescence staining with a marker specific for DCs and confocal microscopy confirmed that the particle-containing cells were DCs. In overview images that were taken at 10× magnification, it was confirmed that $CD11c^+$ cells were mainly located in the SED (Figure 3.18). When focusing on this area, it was observed that most of the $CD11c^+$ cells from the SED contained particles (Figure 3.19), and TiO_2 particles in the SED were always detected in co-localisation with CD11c-expressing cells.

3.5 Discussion

3.5.1 Reassessment of the hypothesis

The results presented in this chapter supported the hypothesis that accumulation of TiO_2 particles in PPs is due to dietary exposure. The TiO_2 particles were also detected in MLN, supporting the assumption that particle-containing cells from PPs translocate to other tissues *via* efferent lymphatics.

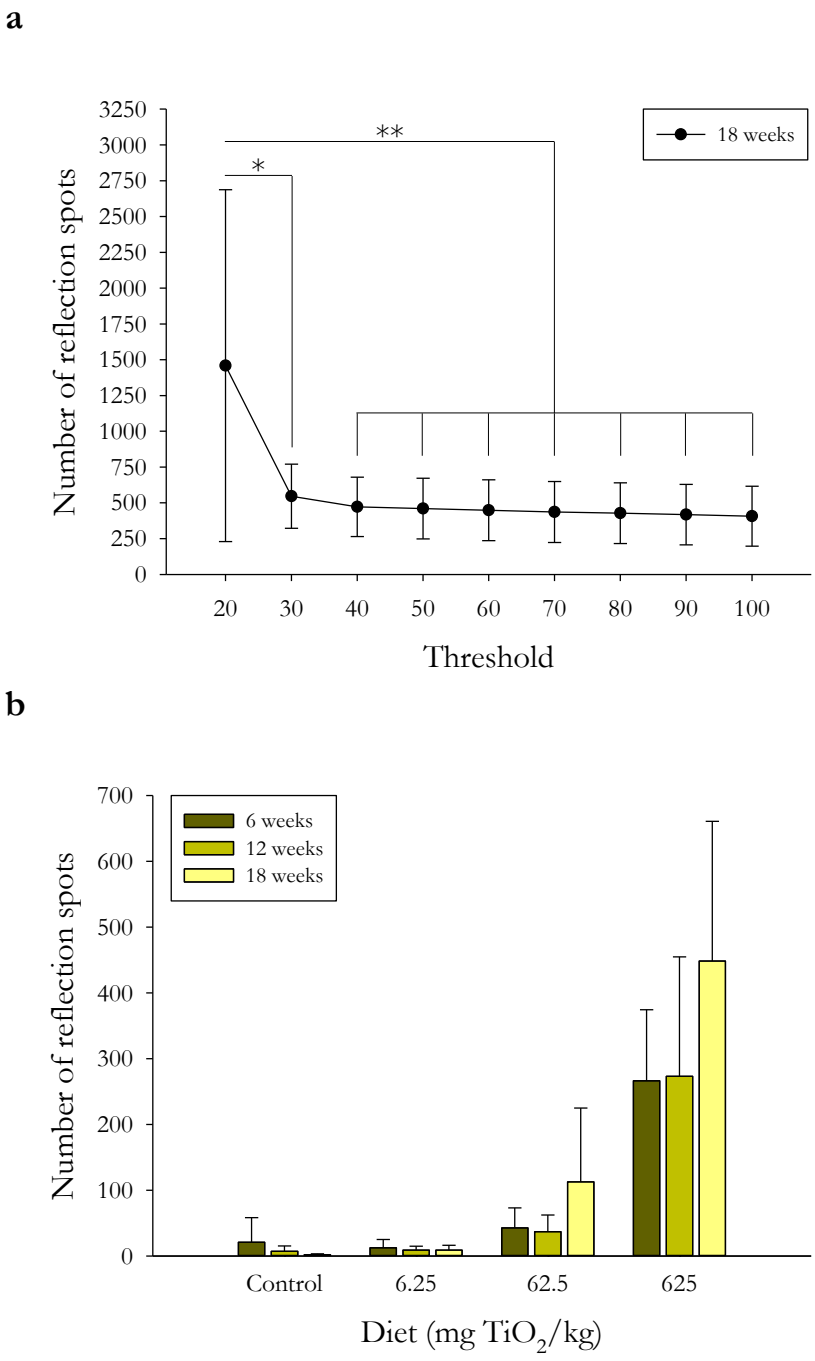

Figure 3.16 *TiO_2 particle uptake in SED areas from WT mice fed a diet with or without TiO_2.*

WT mice were fed an AIN-76A rodent diet without TiO_2 (control) or with 6.25 mg TiO_2/kg, 62.5 mg TiO_2/kg, or 625 mg TiO_2/kg for 6 weeks, 12 weeks or 18 weeks. Unstained PP cross-sections were analysed by reflectance confocal microscopy. The number of reflection spots in SED areas was assessed with image analysis software. (**a**) Detected reflection spots from mice on diet with 625 mg TiO_2/kg for 18 weeks using different red thresholds. (**b**) Number of reflection spots detected with 'Threshold 60'. Shown are means ± SD; n = 7-12. Results were compared with Kruskal-Wallis test (**a**) or two-way ANOVA (**b**). Pairwise group comparisons with Tukey's HSD test. (**a**) Significant differences between 'Threshold 20' and other thresholds are indicated; *$p < 0.05$, **$p < 0.01$. (**b**) p-values reported in Table 3.9.

Table 3.9 *P-value results for pairwise group mean comparisons of the number of TiO_2 particles in SED areas with Tukey's HSD test.*

Diet[1]		***Control***			***6.25***			***62.5***			***625***	
	Weeks	***6***	***12***	***18***	***6***	***12***	***18***	***6***	***12***	***18***	***6***	***12***
Control	12	1.00										
	18	1.00	1.00									
6.25	6	1.00	1.00	1.00								
	12	1.00	1.00	1.00	1.00							
	18	1.00	1.00	1.00	1.00	1.00						
62.5	6	1.00	1.00	1.00	1.00	1.00	1.00					
	12	1.00	1.00	1.00	1.00	1.00	1.00	1.00				
	18	0.60	0.42	0.52	0.50	0.45	0.56	0.90	0.81			
625	6	< 0.001	< 0.001	< 0.001	< 0.001	< 0.001	< 0.001	< 0.001	< 0.001	< 0.05		
	12	< 0.001	< 0.001	< 0.001	< 0.001	< 0.001	< 0.001	< 0.001	< 0.001	< 0.05	1.00	
	18	< 0.001	< 0.001	< 0.001	< 0.001	< 0.001	< 0.001	< 0.001	< 0.001	< 0.001	< 0.01	< 0.05

[1]AIN-76A rodent diet without (control) or with the respective amount of TiO_2 (mg/kg diet).

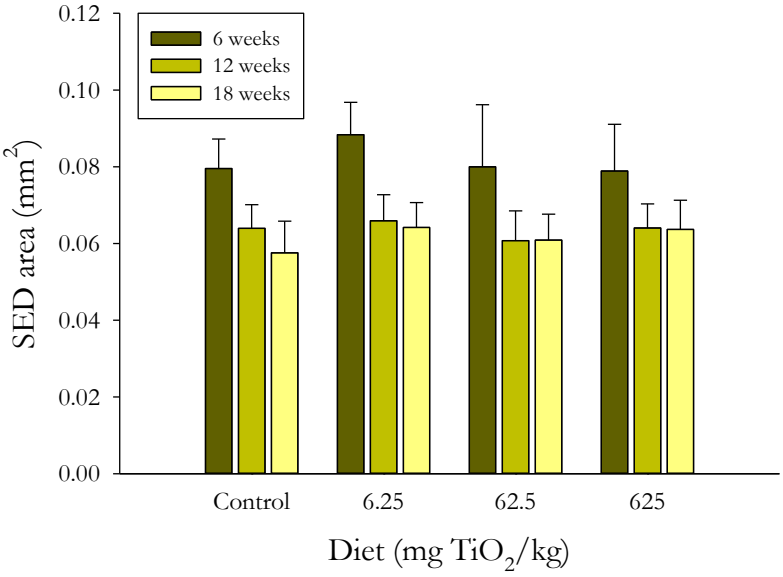

Figure 3.17 *Sizes of SED areas used for TiO_2 particle uptake assessment from WT mice fed a diet with or without TiO_2.* WT mice were fed an AIN-76A rodent diet without TiO_2 (control) or with 6.25 mg TiO_2/kg, 62.5 mg TiO_2/kg, or 625 mg TiO_2/kg for 6 weeks, 12 weeks or 18 weeks. Unstained PP cross-sections were analysed by reflectance confocal microscopy. The sizes of SED areas used for the assessment of detected TiO_2 particles were measured with image analysis software. Shown are means ± SD; n = 7-12. Results were compared with two-way ANOVA.

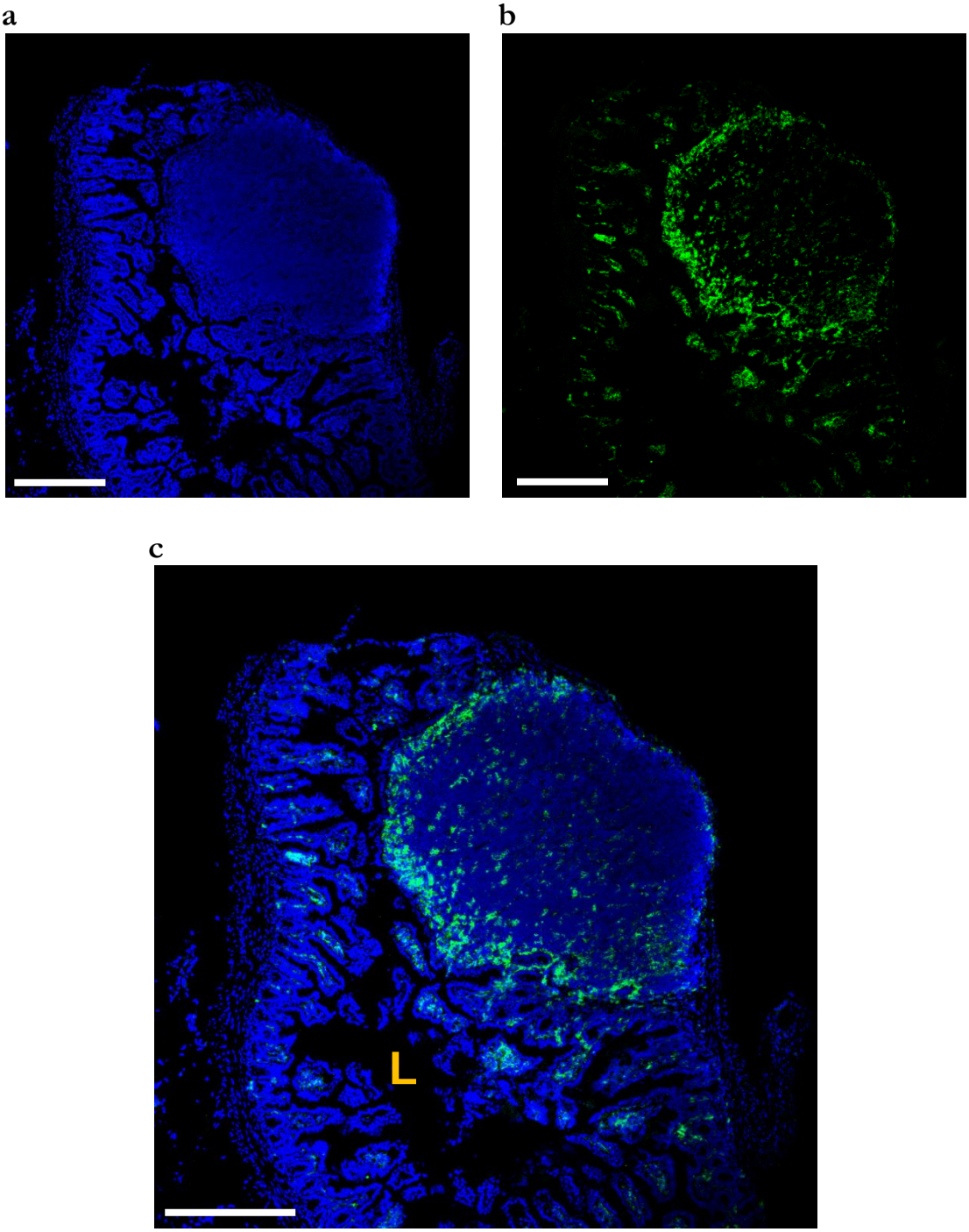

Figure 3.18 *Immunofluorescence confocal microscopy image of a PP cross-section from a WT mouse fed a diet with TiO_2.* Fluorescence confocal microscopy image of a cross-section through the ileum with a PP from a WT mouse on AIN-76A rodent diet with 625 mg TiO_2/kg for 6 weeks. PPs were incubated with Alexa Fluor 488-labelled CD11c (green) and DAPI to stain nuclei (blue). (**a**) DAPI was excited at 405 nm and the emission detected from 405 nm to 475 nm. (**b**) Alexa Fluor 488 was excited at 488 nm and the emission detected from 505 nm to 595 nm. (**c**) Overlay image. Representative images are shown. Scale bar = 250 μm. L = intestinal lumen.

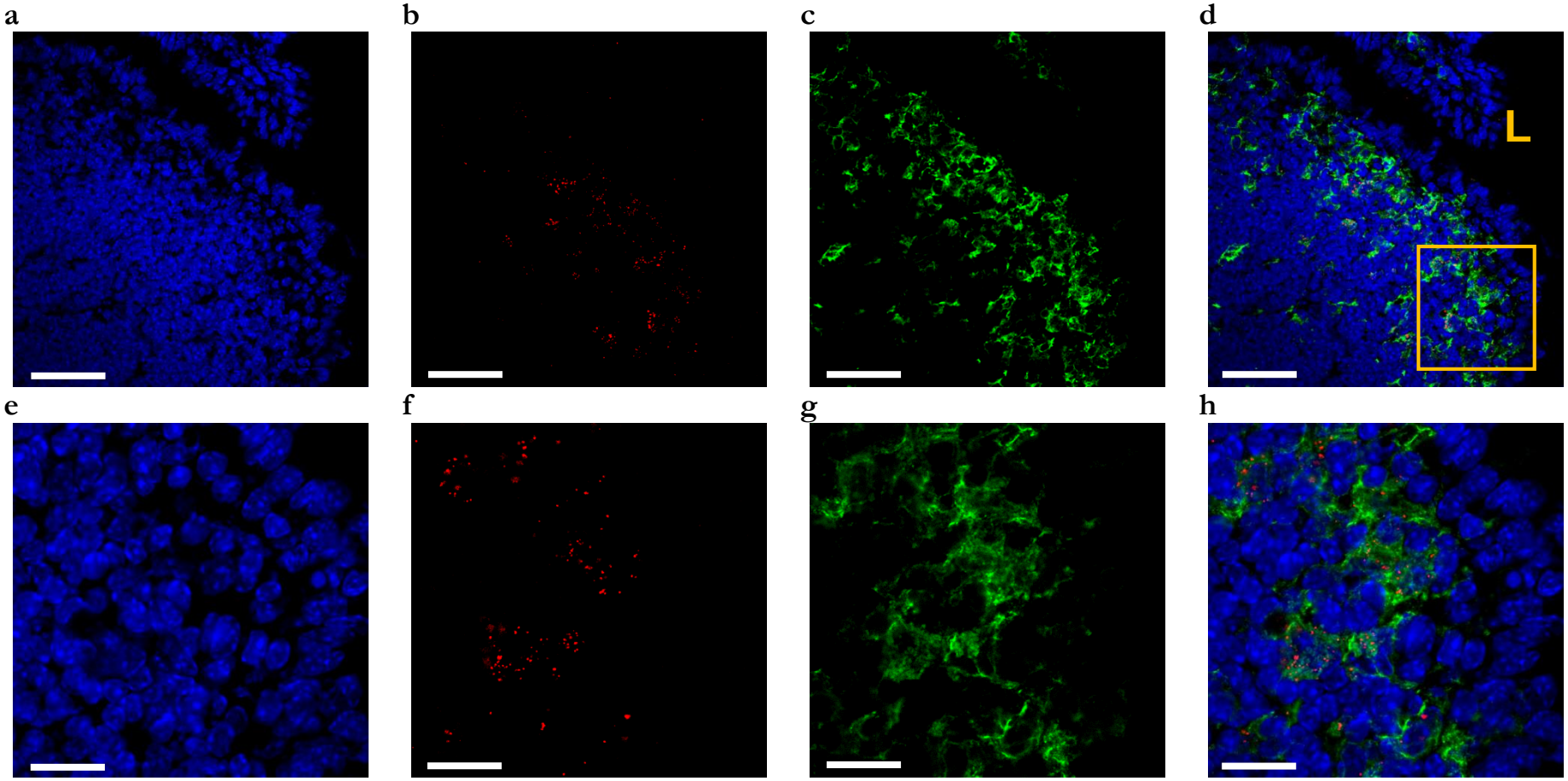

Figure 3.19 *Immunofluorescence confocal microscopy image of the SED area from a mouse fed a diet with TiO_2.*

Fluorescence and reflectance confocal microscopy images of the SED area of a PP cross-section from a WT mouse on AIN-76A rodent diet with 625 mg TiO_2/kg for 6 weeks. PPs were incubated with Alexa Fluor 488-labelled CD11c (green) and DAPI to stain nuclei (blue). (**a, e**) DAPI was excited at 405 nm and the emission detected from 405 nm to 475 nm. (**b, f**) Sections were excited at 488 nm and the reflection from TiO_2 particles (red) was detected from 485 nm to 490 nm. (**c, g**) Alexa Fluor 488 was excited at 488 nm and the emission detected from 505 nm to 595 nm. (**d, h**) Overlay image. Representative images are shown. Scale bar = 50 μm (**a-d**)/25 μm (**e-h**). Square in (**d**) indicates magnified area shown in (**e-h**). L = intestinal lumen.

3.5.2 Titanium dioxide incorporation into the diet

When preparing TiO_2-containing diets it is important that the TiO_2 particles are distributed homogenously throughout the diet. This is difficult to achieve if the diets are prepared in-house [202]. Therefore, it was decided to obtain the diets from Research Diets, a commercial supplier of custom-made animal diets. This company specialises in adding substances to basic animal diets. To check the incorporation of TiO_2 particles, the diet containing 625 mg TiO_2/kg was analysed by SEM and EDS (Figure 3.3), a method that has been used previously to characterise TiO_2 particles [56, 301]. The obtained EDS spectrum showed the characteristic titanium double peak at approximately 4.5 keV (Figure 3.3b) that was also observed in these previous studies.

The presence of TiO_2 particles in the other two TiO_2-containing diets could not be examined because the TiO_2 concentration in these samples was below the detection threshold for particle detection with SEM (personal communication with Mr Douglas Hopcroft, formerly Manawatū Microscopy and Imaging Centre, Massey University, Palmerston North, NZ). An alternative method that allows the detection of trace amounts of TiO_2 in various samples is inductively coupled plasma atomic emission spectroscopy. This method has been widely used to confirm the presence of TiO_2 in biological samples [154, 172, 208, 231]. However, this equipment was not available at AgResearch or Massey University, Palmerston North.

3.5.3 Effects of oral exposure to titanium dioxide on body weights

The body weights observed in this study were in line with the expected body weights for C57BL/6 WT mice as reported in the Mouse Phenome Database created by the Jackson Laboratory [293]. For example, Duriancik and colleagues reported that female and male C57BL/6 mice fed a solid pellets diet had body weights of 19.03 g and 24.77 g, respectively [302]. There were no body weight differences between mice on a control diet compared to mice fed a TiO_2-containing diet for the various exposure durations, except for male mice on a diet containing 625 mg TiO_2/kg for 18 weeks (Table 3.3). The animals from this diet group had higher final body weights compared to mice on a control diet or a diet containing 62.5 mg TiO_2/kg (Figure 3.6). However, it seems unlikely that this result is of biological relevance. Although the mice were assigned randomly to a diet, the male mice on the 62.5 mg TiO_2/kg diet of the 18 weeks sampling time point had the lowest average initial body weight of all groups, and the male mice on the 625 mg TiO_2/kg diet of the 18 weeks

sampling time point had one of the highest. One reason why it is unlikely that the observed body weight differences between male mice of the 18 weeks sampling time point are of biological relevance is that there were no differences between the body weights of male mice from the other two sampling time points (Table 3.3). Furthermore, the body weights of female mice of the 18 weeks sampling time point were similar between the diet groups (Table 3.2).

Moreover, in previous studies in which effects of oral TiO_2 administration were studied with animal models no differences on body weight were observed. For instance, Bu and co-workers conducted a study in which rats received daily doses of TiO_2 from 160 μg/kg to 1,000 μg/kg body weight for 14 d days [209]. Despite the high TiO_2 doses, there were no differences in body weight between the TiO_2-exposed groups and the control group. However, the duration of the study by Bu and co-workers was much shorter than the exposure time in the current study, and effects of TiO_2 particles on the body weights of rats and mice might not be directly comparable. There has also been a long term study with rats and mice that were exposed to TiO_2 in the diet for 103 weeks [202]. The TiO_2 concentrations in the diets were 2.5 % and 5 % which corresponded to 25 g and 50 g TiO_2/kg diet, respectively. There were no body weight differences between both rats and mice of either sex on the TiO_2-containing diets compared to animals on a control diet.

3.5.4 Daily titanium dioxide intake in this study

As described in Section 3.3.2, the concentrations of 6.25 mg, 62.5 mg, and 625 mg TiO_2/kg diet were chosen to ensure approximate daily TiO_2 doses of 1 mg/kg, 10 mg/kg, and 100 mg/kg body weight, respectively. These daily doses were comparable to the range of concentrations used in previous oral TiO_2 administration studies [172, 208, 291]. It was observed that the calculated daily doses were slightly lower than the anticipated daily intakes for both females and males on all three TiO_2-containing diets (Tables 3.4 & 3.5). Furthermore, for females on all TiO_2-containg diets and for males on the diet with 625 mg TiO_2/kg the calculated daily doses decreased with increasing exposure time. The reason for this was that although the body weights of the mice increased throughout the study, the daily food intake (and therefore also the daily TiO_2 intake) remained more or less constant. It was not considered as an issue for this study that the actual daily TiO_2 doses were below the anticipated daily doses and that they were not exactly 1 mg/kg, 10 mg/kg, and 100 mg/kg.

The daily TiO_2 doses were higher for females than for males. While the absolute food intake for female mice was lower compared to male mice, the relative food intake in comparison to body weight was actually higher for females. For example, females on a control diet for 18 weeks had a relative daily food intake of 126.4 mg/kg whereas the corresponding group of male mice had a relative daily food intake of 110.2 mg/kg.

3.5.5 Immune cell populations of murine Peyer's patches

The impact of TiO_2 administration on immune cell populations of PPs and MLNs has been examined. A reason behind the assumption that there could be changes in immune cell subsets after dietary TiO_2 exposure was that uptake of TiO_2 particles by a certain subset could have led to increased apoptosis of these particular cells [215]. Alternatively, as it was expected that APCs would be exposed to TiO_2 and their regulatory function for intestinal homeostasis would be disrupted, their ability to imprint lymphocytes to return to the small intestinal mucosa from the blood might have been impaired [303]. Therefore, TiO_2 exposure of intestinal APCs could have indirectly affected lymphocyte cell populations. However, there were no differences in the examined immune cell subsets between the diet groups even after prolonged dietary administration of TiO_2 (Table 3.6). There were differences between the sampling groups in several of the investigated subsets, but this was most likely caused by natural variation in tissue immune cell populations over time.

The percentages of the cell populations investigated in this study corresponded to those from previous studies. For example, Barreau and co-workers investigated several immune cell populations of PPs in healthy WT mice [304]. Their results showed that PPs comprised approximately 70 % $CD45R^+$ B cells, 20 % $CD3^+$ T cells, and less than 10 % $CD11c^+$ DCs. CD3 is a cell surface molecule which is specifically expressed only by mature T cells. It was decided not to include a CD3 antibody in this study because of limitations in the number of antibodies that could be detected at the same time with the FACSCalibur flow cytometer. Instead lymphocytes were selected based on their FSC and SSC values (Figure 3.1), and T cells distinguished directly according to their expression of CD4 or CD8. In the study by Barreau and colleagues the frequency of $CD4^+$ and $CD8^+$T cells is given as a percentage of $CD3^+$ cells therefore it was not possible to compare the results from their study directly with the results from this study. However, Barreau and colleagues also reported that the number of $CD4^+$ T cells was approximately twice as high as the number of $CD8^+$ T cells, which was similar to the results from this study (Figure 3.8). Similarly, the number of B cells observed

in this study corresponded to results reported by Duriancik and colleagues who described that B cells represented approximately 80 % of all PPs immune cells [302].

For the comparison of monocytes and their sub-populations, the flow cytometry acquisition parameters were changed to be able to better select monocytes that have higher FSC and SSC values compared to lymphocytes (Figure 3.2). Monocytes that expressed the cell surface marker CD11b but not the DC-specific antigen CD11c were defined as macrophages. It was not possible to use the F4/80 antibody, which was used in the flow cytometry experiments with BMDMs (Section 2.3.6), because it has been shown that F4/80 is not expressed by PPs macrophages [305]. However, immunohistochemistry of mouse PPs has shown that $CD11b^+$ $CD11c^{-/low}$ cells are present in PPs and are most likely macrophages [306]. The DC subsets found in PPs have been described in detail by Iwasaki and Kelsall with immunohistochemistry and flow cytometry [307, 308]. Based on their results, the frequencies of the three PP DC populations $CD8^+$ DCs, $CD11b^+$ DCs, and double-negative DCs were analysed in this study. According to Iwasaki and Kelsall, the relative frequencies of the three subsets from the total DC population were approximately 30 % in both PPs and MLNs [308]. This corresponded to the frequencies detected in this study for both types of tissue (Figure 3.10).

3.5.6 Titanium dioxide particle uptake in Peyer's patches

The uptake of TiO_2 particles by cells of PPs and MLNs was examined by dark field microscopy. Other studies have used this method before to investigate TiO_2 particle uptake in cells or tissues. For example, Powell and colleagues have employed this technique to visualise TiO_2 particles in histological sections of human PPs [161, 162]. In PPs from mice on the diet that contained 625 mg TiO_2/kg, large numbers of TiO_2 particles were visible in the SED regions, but reflectance spots were also observed dispersed throughout the follicle and along the base (Figure 3.11). Many TiO_2 particles were also present in MLNs from these mice (Figure 3.12). In contrast, no TiO_2 was detected in PPs and MLNs from mice on the diet containing 6.25 mg TiO_2/kg, and only some TiO_2 particles were visible in the SEDs and MLNs of mice fed a diet containing 62.5 mg TiO_2/kg. This result is comparable to an *in vitro* study, in which intracellular TiO_2 uptake was also investigated by dark field microscopy [266]. The amount of TiO_2 taken up by the cells increased according to the particle concentration to which the cells were exposed in the TCM. Translocation of TiO_2 particles to from PPs to MLNs after oral administration has also been demonstrated previously for rats [172].

To investigate the distribution of the TiO_2 particles in PPs after dietary exposure in more detail, tissue sections from mice fed the diet containing 625 mg TiO_2/kg were stained with H&E and compared to stained sections from mice on control diet. The H&E stained sections were then observed under bright field illumination. Previous studies have shown that with this method aggregates of TiO_2 particles could be detected as granular brown pigment [56, 161]. This analysis confirmed the presence of TiO_2 particles in PPs as observed by dark field microscopy. Again, most particles were detected in the SEDs of TiO_2-exposed mice, whereas mice on a control diet had no granular pigment in the corresponding PP locations (Figure 3.13).

TiO_2 particles can also be detected by confocal microscopy using reflectance. This method has been employed by Powell and colleagues in their studies of TiO_2 particles in human PPs [147, 161, 162]. This detection method was also used in an *in vitro* study that investigated the uptake of TiO_2 particles by intestinal epithelial cells [189]. The advantage of detecting TiO_2 particles in tissues by reflectance confocal microscopy over dark field and bright field microscopy lies in the different way that images are acquired in confocal microscopy. The details of confocal microscopy images are all obtained from one plane within the tissue section [299]. The simultaneous detection of reflectance spots and tissue autofluorescence by confocal microscopy indicated that the TiO_2 particles were indeed localised within the tissue (Figure 3.15). In the dark field and bright field images it would have been possible that the detected particles were artefacts, e.g. dust particles, introduced during sample preparation. However, the abundant presence of particles in PPs from mice fed a diet containing 625 mg TiO_2/kg already indicated that the observed particles were not contaminants but indeed TiO_2 particles located within the tissue.

The observation that the TiO_2 particles accumulated primarily in the SED area was in contrast to previous studies that investigated the occurrence of TiO_2 particles in human PPs [56, 161, 219]. In these studies TiO_2 particles were consistently detected exclusively at the base of PPs. Furthermore, the particle-containing cells in humans were characterised by immunohistochemistry as mature macrophages [162]. In contrast, the immunofluorescence results from this study indicated that the particles were mainly taken up by DCs (Figure 3.19). This discrepancy could be explained by the different locations in which the TiO_2 particles were observed in human PPs compared to murine PPs. Immunohistochemistry has shown that the SED area contains large numbers of $CD11c^+$ DCs, but no $F4/80^+$ macrophages [306, 307]. Moreover, preliminary data from Powell and colleagues indicated that also in humans TiO_2 particles can be detected in DCs in the SED area (personal communication with

Dr Jonathan Powell, Medical Research Council Human Nutrition Research, Cambridge, UK).

It has been shown that the three PP DC subsets have different locations within the PP [307]. DCs that are present in the SED are usually either $CD11b^+$ DCs or double-negative DCs. The IFRs also contain DCs which are mainly $CD8^+$ DCs or double-negative DCs. As most TiO_2 particles were detected in the SED area it is probable that the DC subsets that contain the particles are either $CD11b^+$ DCs or double-negative DCs. It has been reported that the three DC subsets differed in their capacities to stimulate immune responses [308, 309]. Although the subsets expressed similar levels of major histocompatibility complex class II and the co-stimulatory molecules CD80 and CD86, they secreted different cytokines as a reaction to antigen exposure [308]. $CD11b^+$ DCs secreted mostly the anti-inflammatory and regulatory T cell-associated cytokine IL-10 whereas $CD8^+$ DCs and double-negative DCs secreted predominantly the pro-inflammatory and Th 1 T cell-associated cytokine IL-12. Uptake of TiO_2 particles by these DCs could disturb their inherent response to intestinal antigens, and this could lead to disturbances in intestinal immune homeostasis. It would be of interest to investigate whether TiO_2 particles were taken up specifically by one of the DC subset, or if all subsets contained TiO_2 particles equally. A previous study showed that fluorescent thiol-organosilica particles with diameters from 100 nm to 925 nm accumulated in $CD11b^+$ DCs in the SED areas after oral administration in C57BL/6 WT mice [310]. These findings imply that it is also the $CD11b^+$ DC subset that would be mostly affected by TiO_2 particles. This could impair the capacity of these cells to induce immune tolerance to innocuous antigens derived from the diet or commensal microbiota. The consequence could be an exacerbated pro-inflammatory reaction in response to otherwise harmless antigens. In cases with a genetic predisposition to develop intestinal inflammation, e.g. in people with mutations in the *NOD2* gene, this could represent the environmental component which triggers the development of CD.

3.5.7 Conclusion

In conclusion, the results from the first *in vivo* study supported the hypothesis that the observed TiO_2 particle uptake in PPs in humans can be mimicked in mice by feeding the animals a TiO_2-containg diet. The results showed for the first time that ingestion of TiO_2 particles with the diet results in particle uptake in small intestinal lymphoid tissues. Therefore, the hypothesis that TiO_2 particles accumulate in human PPs because of dietary TiO_2 particles that have been added to processed foods, toothpastes, and pharmaceuticals seems to be valid.

Furthermore, in this study it has been shown that most TiO_2 particles in murine PPs were located in DCs in the SED area. This observation could be expected for dietary particles in human PPs as well, but it has not yet been reported.

The accumulation of TiO_2 particles in DCs in the SED area and translocation to MLNs might affect intestinal homeostasis. Although WT mice did not show any adverse reaction based on performance, it is possible that *Nod2*$^{m/m}$ mice develop CD-like intestinal inflammation after prolonged exposure to TiO_2 particles with the diet.

Chapter 4 Exposure of wild-type mice and mice with a Crohn's disease-like *Nod2* gene variant to dietary titanium dioxide

4.1 Introduction

Since the discovery that the exogenous particles TiO_2 and aluminium-containing silicates accumulate in human PPs, there has been speculation about potential detrimental effects of these dietary particles on intestinal homeostasis [56]. Specifically, a connection between intestinal uptake of exogenous dietary particles and the development of CD has been suggested. This hypothesis has been based on the observation that dietary particles accumulate in the same region of the small intestine which is mostly affected by CD, namely the terminal ileum [56, 147]. The cells that contained the dietary particles were identified as macrophages [147, 161, 162].

Intestinal macrophages isolated from patients with IBD showed a higher rate of apoptosis and secreted more pro-inflammatory IL-1β upon stimulation with a TiO_2-LPS conjugate compared to macrophages obtained from patients without IBD [217]. Furthermore, macrophages derived *in vitro* from PBMCs from patients with CD released increased amounts of the pro-inflammatory cytokine TNF-α after co-stimulation with TiO_2 + LPS compared to cultured cells from healthy controls [218].

However, a connection between reduced oral intake of exogenous particles and disease remission in CD patients was not confirmed in a dietary intervention study [233]. Therefore, a possible connection between exogenous dietary particle intake and CD seems to be more complex than initially anticipated. For example, exogenous dietary particles might only be involved in the initiation of disease, but their presence or absence would not have an impact on disease progression once intestinal inflammation has been established [143]. Moreover, intestinal uptake of exogenous dietary particles might only affect people with a genetic susceptibility for the development of CD [55, 233].

The most common genetic risk factors that are associated with CD are mutations in the *NOD2* gene, and the most common *NOD2* variant is a frameshift mutation that leads to a truncated protein [59, 60]. A mouse model with a homologous mutation in the *Nod2* gene has been created, and these $Nod2^{m/m}$ mice can be used to study effects of this CD-associated mutation *in vivo* [131]. $Nod2^{m/m}$ mice did not develop spontaneous intestinal inflammation if kept under conventional conditions. However, they were more susceptible to chemically-induced colitis with DSS than WT mice which indicated that the presence of a truncated Nod2 protein had a negative effect on intestinal homeostasis.

4.2 Hypothesis and aims

The hypothesis to be tested in this chapter was that dietary exposure to TiO_2 leads to the development of intestinal inflammation in *Nod2*$^{m/m}$ mice due to an increased pro-inflammatory response of the *Nod2*$^{m/m}$ mice to TiO_2 particles and adsorbed antigens from the intestinal lumen.

The aims of the second *in vivo* study were to investigate TiO_2 particle uptake in PPs from WT and *Nod2*$^{m/m}$ mice after feeding a TiO_2-containing diet. Furthermore, the development of intestinal inflammation was assessed with histology. In addition, possible mucosal uptake of TiO_2 particles in non-PPs regions of the small intestine was evaluated.

4.3 Materials and methods

4.3.1 Study considerations

The experimental design of the second *in vivo* study had to be modified compared to the first *in vivo* study (Chapter 3) because only a limited number of *Nod2*$^{m/m}$ mice were available. This was due to breeding difficulties, which is a common problem in genetically modified mice, especially on the C57BL/6 background [311]. Only female mice were included in the second study.

The TiO_2 concentration of the diet for the second *in vivo* study was selected based on the results from Chapter 3. At a concentration of 625 mg TiO_2/kg diet, a significant accumulation of TiO_2 was observed in PPs (Table 3.9 & Figure 3.16). The animals which were fed this diet showed no adverse effects based on daily health monitoring and their performance compared to mice on the control diet (Table 3.2 & Figure 3.6).

As a consequence of the limited availability of female *Nod2*$^{m/m}$ mice with similar age for the second *in vivo* study, only one sampling time point after 18 weeks was chosen for consistency with the maximum TiO_2-feeding period in the first *in vivo* study.

4.3.2 Experimental design, diets, and animals

All animal experiments were approved by the Grasslands Animal Ethics Committee according to the New Zealand Animal Welfare Act 1999.

The second study had a 2 × 2 factorial design in which the first factor represented the *Nod2* genotype (WT or *Nod2*$^{m/m}$ mice) and the second factor the diet (control or TiO_2 diet). In this context, the term 'group' was used to refer to a group of mice that had the same genotype and were fed the same diet, i.e. either WT or *Nod2*$^{m/m}$ mice on either control or TiO_2 diet. Thus, there were four groups in the second *in vivo* study. The term 'genotype' was used to specify either WT or *Nod2*$^{m/m}$ mice irrespective of the type of diet they were fed, and the term 'diet group' was used for WT and *Nod2*$^{m/m}$ mice together receiving either the control or TiO_2 diet. The study design and the required minimum number of animals per group were discussed with senior statistician Dr John Koolaard.

The TiO_2 particles for the TiO_2-containing diet came from the same batch obtained from Sensient Colors as those particles used for the *in vitro* and first *in vivo* studies (Sections 2.3.1 & 3.3.2). The AIN-76A control diet without TiO_2 and AIN-76A diet with 625 mg TiO_2/kg were again prepared by Research Diets according to the previous specifications (Table 3.1).

Ten female WT and *Nod2*$^{m/m}$ mice were transferred from the AgResearch Ruakura Small Animal Colony to the AgResearch Grasslands Small Animal Unit. The mice were kept under the same conditions as described previously (Section 3.3.3). Five mice of each genotype were randomly assigned to either the control or TiO_2 diet. The animals were housed individually to monitor health, body weight, and food intake. The health of the mice was checked daily. Body weight and food intake were measured twice weekly.

In addition to the second *in vivo* study, several characteristics were also recorded from the mice that were used for bone marrow cell collection (Chapter 2). This data provided information about intrinsic differences between WT and *Nod2*$^{m/m}$ mice on a standard rodent diet. The recorded characteristics included body weight immediately prior to euthanasia, number of PPs along the small intestine, and lengths of ileum and colon. The housing conditions of these mice were described in Section 2.3.2.

In addition, ten female WT and *Nod2*$^{m/m}$ mice, respectively, were acquired from the AgResearch Ruakura Small Animal Colony in two batches. The mice were fed a standard rodent diet (LabDiet), so they were not exposed to TiO_2 with the diet. The animals were housed in groups up to five as described in Section 2.3.3. These TiO_2-unexposed mice were used for the assessment of monocytes, monocyte populations, and DC subsets from PPs with flow cytometry because no spare PP samples were available from the mice of the second *in vivo* study.

4.3.3 Tissue collection and sample preparation

At the end of the study after 18 weeks the mice were sacrificed with CO_2 asphyxiation and cervical dislocation. The intestinal tract was transferred to cold PBS (Life Technologies) in a Petri dish, and approximately 3 mm long pieces of the distal ileum and proximal colon were collected in 10 % formalin (Thermo Fisher Scientific). These tissues were used for the preparation of H&E stained cross-sections for histology.

At least three approximately 3 mm long ileum sections containing a PP and one 3 mm section of the distal ileum were embedded for cryosectioning (see Section 3.3.4) to assess TiO_2 particle uptake.

For the cell population assessment, all PPs were obtained from the unexposed WT and *Nod2*$^{m/m}$ mice. The PP samples were collected in cold RPMI 1640 medium with 100 μg/mL DNaseI and 100 μg/mL LiberaseTL until the samples were processed for flow cytometry staining (Section 4.3.5).

4.3.4 Histology of ileum and colon

The formalin-fixed ileum and colon sections were processed for histology by Ms Evelyn Lupton (Massey University, Palmerston North, NZ). Briefly, the sections were embedded in paraffin, and 10 μm thick cross-sections were obtained by cutting the embedded tissues with microtome. Three cross-sections from the central part of each sample were transferred to a microscopy slide and stained with H&E.

The stained tissue sections were analysed under bright field illumination with an Olympus BX50 microscope (Olympus Corporation, Tokyo, Japan). A histology score was assigned to each sample based on a scoring system developed by Mrs Kelly Armstrong (AgResearch, Palmerston North, NZ). According to this system, a score of '0' was assigned when the section had a completely normal appearance. A higher score, up to a maximum of '10', could be given when aberrant characteristics and tissue damage were observed in the tissue sections. A score from '1' to '3' would indicate only slight changes from a normal appearance, a score from '4' to '6' would signify moderate changes, a score from '7' to '9' would be given when high deviations from the normal appearance were observed, and finally a score of '10' could mean that the whole section would be distorted. To make the scoring system more robust against personal interpretations, the final score was based on the systematic observation of several characteristics. Tissue sections were always examined for the following characteristics: crypt hyperplasia, aberrant crypts, crypt injury, crypt loss,

goblet cell loss, presence of lymphoid aggregates, crypt abscesses, submucosal thickening, and loss of surface enterocytes. The first three characteristics were useful to assess the morphology of the crypts in detail, whereas the remaining characteristics applied to the appearance of the tissue sections in general. A separate score from '1' to '10' was given for each characteristic. The final histology score was obtained by dividing the sum of the individual scores by the number of characteristics. The ileum and colon sections were scored separately for each mouse. The sections were scored blindly.

As any scoring system is inevitably subjective a more objective approach to assess tissue injury was additionally undertaken. For this purpose, images were recorded at 40× magnification with a ColorView III camera (Olympus Soft Imaging Solutions) and the analySIS^{B} image acquisition software version 5.0 (Olympus Soft Imaging Solutions). These images were then used to measure the lengths of the intestinal crypts of the ileum and colon and of the villi in the ileum with ImageJ version 1.45. Crypt and villi lengths can be correlated to intestinal injury [249]. Five randomly selected crypts or villi from one section per slide were measured, and the average crypt length for each mouse was calculated from these measurements. In addition, images were also recorded for presentation purposes as described above. All images were saved with a resolution of 2,576 pixels × 1,932 pixels. The quality of the images that were selected for presentation in this chapter were enhanced by performing histogram stretching with Corel PaintShop Pro version 11.20 as described in Section 3.3.7.

4.3.5 Dark field and reflectance confocal microscopy

Unstained, 10 μm PP cross-sections were prepared as described in Section 3.3.6. These sections were used to assess TiO_2 particle uptake with dark field microscopy and reflectance confocal microscopy as described previously (Sections 3.3.7 & 3.3.9).

In addition, 10 μm cross-sections of the embedded ileal tissues were prepared as described in Section 3.3.6. The sections were observed with dark field microscopy as described in Section 3.3.7 to assess the presence of TiO_2 particles in the small intestinal mucosa.

4.3.6 Flow cytometry analysis

Single cell suspensions were prepared from the PPs of WT and *Nod2*$^{m/m}$ mice on a standard rodent diet. The cells were stained with fluorescently labelled antibodies and analysed with flow cytometry as described previously (Section 3.3.5). To analyse monocyte populations and DC subsets, the cells were stained with 1.25 μg/mL fluorescein isothiocyanate-labelled rat

anti-mouse CD11b, 0.5 μg/mL phycoerythrin-labelled Armenian hamster anti-mouse CD11c, and 0.5 μg/mL allophycocyanin-labelled rat anti-mouse CD8a. For the assessment of cell viability, 0.8 μg/mL PI was added to each sample before analysis.

The samples were analysed with a FACS Calibur flow cytometer using the CellQuest Pro software version 6.0. At least 40,000 events were acquired from each sample. FlowJo version 9.4.3 was used to analyse the data as previously described for monocytes (see Figure 3.2).

4.3.7 Statistical analysis

All statistical calculations were performed with R version 3.0.0. The normality of the data was checked with the Shapiro-Wilk test. The variance homogeneity for comparisons between two sets of samples or the four groups was checked with the *F*-test or Bartlett's test, respectively (Appendix D). SigmaPlot version 12.5 was used to create the graphs for all figures.

All parameters that were obtained from WT and *Nod2*$^{m/m}$ mice used for bone marrow cell collection had equal variances. The average age and number of PPs were not normally distributed, so the results for these two parameters were compared with the nonparametric Wilcoxon test. The results for body weight and lengths of small intestine and colon were normally distributed, and the two-sample comparisons were performed with Student's *t*-test. In addition, the Pearson correlation coefficient between age and either body weight, small intestine length, or colon length was assessed separately for WT and *Nod2*$^{m/m}$ mice.

For the parameters of the TiO_2 exposure study there were no significant differences between the variances of all groups, except for the age of the mice. All results were distributed normally. The means of the four groups were compared with two-way ANOVA, except for the average final body weight which were compared by a modified two-way ANOVA using the initial body weight as a co-variate. The data for daily TiO_2 intake and TiO_2 dose, which were normally distributed and had equal variances, were compared with Student's *t*-test between the genotypes of the mice on TiO_2 diet.

The results between the groups from the histology analyses and TiO_2 uptake assessment were also compared by two-way ANOVA. The data for the ileum and colon histology scores had equal variances, but were not normally distributed. The data for the lengths of villi and crypts of the ileum were distributed normally and the variances were equal. However, the variances for colon crypt length were different between the groups, and the data did not to follow a

normal distribution. The data for the number of reflection spots in the PP SEDs neither followed a normal distribution nor showed variance equality between the groups. In contrast, the data for SED areas were both normally distributed, and all groups had equal variances. As mentioned in Section 2.3.9, there was no alternative for conducting two-way ANOVAs in these cases. As long as the data is interpreted carefully within the biological context, it is possible to perform parametric analysis even if some requirements are not fulfilled [273].

The variances of the data from the flow cytometry analysis were distributed equally with the exception of monocytes and DCs. However, only the data for monocytes and $CD11b^+$ macrophages were normally distributed. The results for monocytes were compared with Student's *t*-test and all other results with the Wilcoxon rank sum test.

Dot density plots were used for the figures to show the distribution of the individual results and the means, except in the graphs showing the body weight and body weight changes over time in which the results were plotted as means ± SE.

4.4 Results

4.4.1 Body weight and intestinal characteristics of wild-type mice and mice with a Crohn's disease-like *Nod2* gene variant on a standard diet

Several characteristics were recorded from the WT and $Nod2^{m/m}$ mice that were used for bone marrow cell collection (see Section 2.3.2). The average age at tissue sampling was not significantly different, with 94 d ± 18 d and 95 d ± 17 d for WT and $Nod2^{m/m}$ mice, respectively. The body weight of WT mice was 20.29 g ± 1.36 g, and the body weight of $Nod2^{m/m}$ mice was 18.11 g ± 1.74 g (Figure 4.1a). These averages were significantly different ($p < 0.001$). The number of PPs was not significantly different between the two groups (Figure 4.1b).

The average lengths of the small intestines were also similar between the two groups, with 32.5 cm ± 3.3 cm for WT mice and 32.7 cm ± 3.9 cm for $Nod2^{m/m}$ mice (Figure 4.2a). In contrast, the average lengths of the colons were significantly different ($p < 0.05$), with 6.8 cm ± 0.7 cm for WT mice and 6.4 cm ± 0.9 cm for $Nod2^{m/m}$ mice (Figure 4.2b).

An increase in body weight was positively correlated with older age for both WT and $Nod2^{m/m}$ mice (Figure 4.1a). The Pearson correlation coefficients were 0.65 and 0.77 for WT and

a

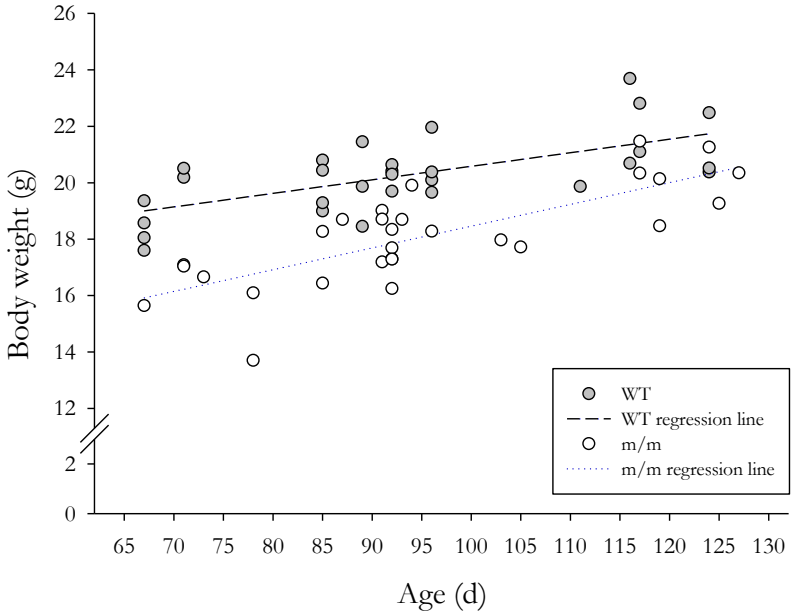

b

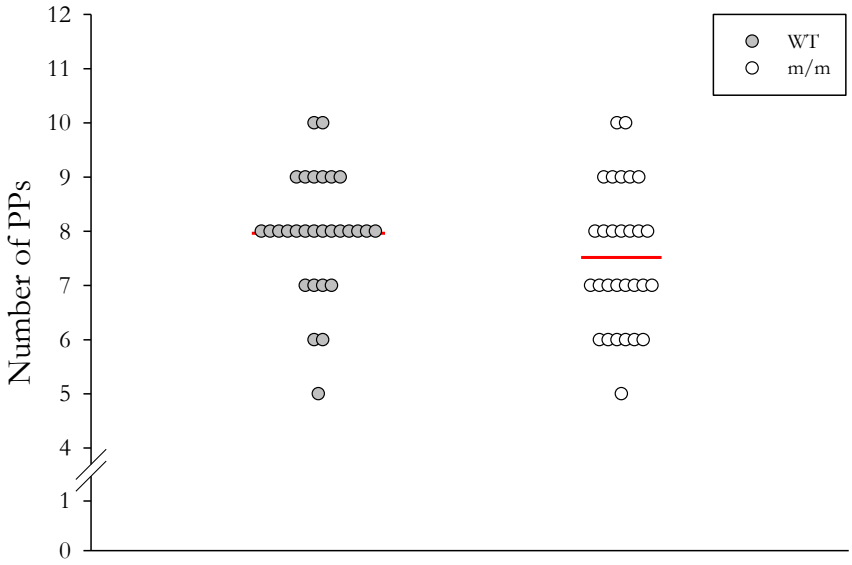

Figure 4.1 *Body weights and numbers of PPs of WT and* Nod2$^{m/m}$ *mice fed a standard rodent diet.*

The body weights and numbers of PPs of female WT and *Nod2$^{m/m}$* (m/m) mice that were used for bone marrow cell collection (see Section 2.3.3) were recorded at sampling. (**a**) Live body weight of each individual mouse were plotted against age; regression lines are indicated for WT (dashed) and *Nod2$^{m/m}$* mice (dotted). (**b**) Number of PPs of each individual mouse were plotted according to genotype; means are indicated by red lines. n = 29. Results for the number of PPs per genotype were compared with Wilcoxon rank sum test.

a

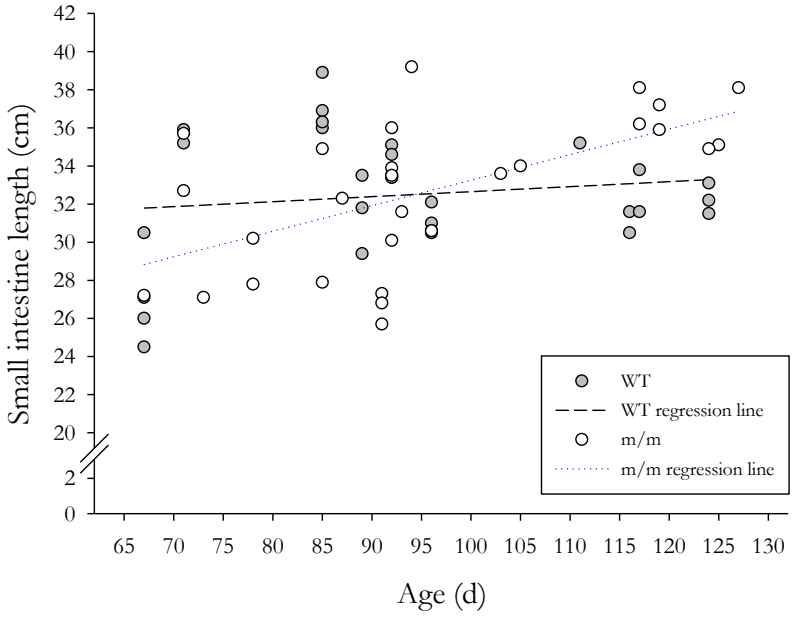

b

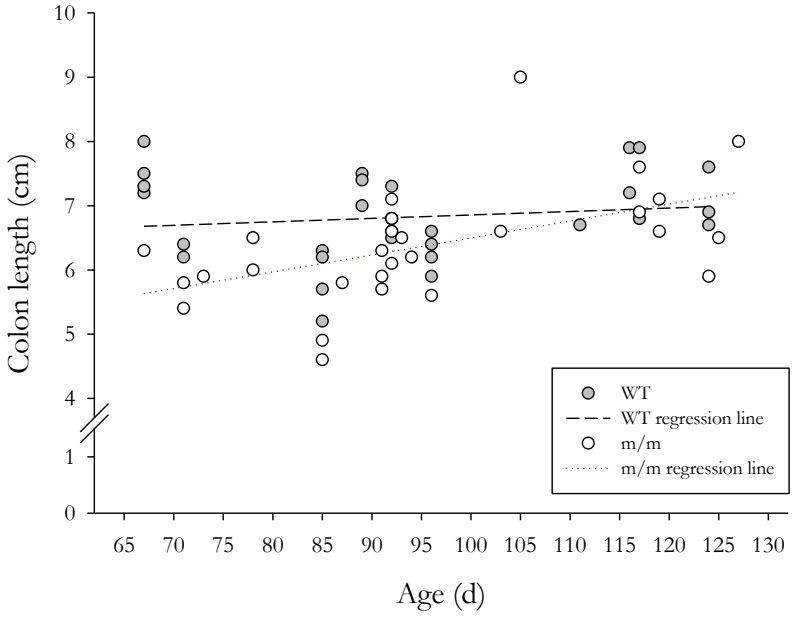

Figure 4.2 *Small intestine and colon lengths of WT and* Nod2$^{m/m}$ *mice fed a standard rodent diet.*

The lengths of the small intestines and colons of female WT and *Nod2$^{m/m}$* (m/m) mice that were used for bone marrow cell collection (see Section 2.3.3) were recorded at sampling. Small intestine length (**a**) and colon length (**b**) of each individual mouse were plotted against age. Regression lines are indicated for WT (dashed) and *Nod2$^{m/m}$* mice (dotted); $n = 29$.

Nod2$^{m/m}$ mice, respectively. These increases were significantly different from zero ($p < 0.001$). The correlation coefficients for age and small intestine length or colon length were 0.15 and 0.14, respectively, for WT mice (Figure 4.2) which indicates that there was no correlation between older age and increasing intestinal length for WT mice. However, there was a positive correlation between age and both intestinal lengths for *Nod2*$^{m/m}$ mice (Figure 4.2) with Pearson correlation coefficients of 0.60 for small intestine length and 0.52 for colon length. In both cases, the slopes of the corresponding regression lines were significantly different from zero ($p < 0.01$).

4.4.2 Performance and titanium dioxide intake

The age and initial body weight of the mice in all four groups was similar at the start of the study (Table 4.1). The body weight of all groups increased over the course of the study, and there were no significant interaction effects for both overall body weight and relative change in body weight at the final recording time point (Table 4.1 & Figure 4.3).

The average daily body weight gain was also similar between all groups (Table 4.1). However, the final body weight, overall body weight change and daily body weight gain was significantly ($p < 0.05$) higher for WT mice compared to *Nod2*$^{m/m}$ mice when the results between the genotypes were compared independently of the diet (Table 4.1).

There was no significant difference for the average daily food intake between the groups or between genotypes. However, mice on a TiO_2-containing diet regardless of the genotype had a significantly lower ($p < 0.01$) average daily food intake. The average daily TiO_2 intake and TiO_2 dose were not significantly different between the groups (Table 4.2).

The number of PPs, and lengths of the small intestine and colon were also recorded at sampling, and the results of the statistical analysis are presented in Table 4.3. There were no significant differences regarding the number of PPs (Figure 4.4a). The effect of diet on the lengths of the small intestines was significant ($p < 0.05$) with longer small intestines in mice on the control diet compared to mice on the TiO_2 diet, but there was no significant interaction effect (Figure 4.4b). In contrast, a significant interaction effect ($p < 0.05$) was observed for the colon lengths (Figure 4.4c). However, after a pairwise comparison with Tukey's HSD *post-hoc* test was carried out no significant differences between any two groups could be detected. Nevertheless, there was a trend to a significant difference ($p = 0.06$) between the colon lengths of WT and *Nod2*$^{m/m}$ mice on a control diet because of the longer colon lengths of WT mice.

Table 4.1 *Means (± SD) for age, initial and final body weight, body weight change, daily weight gain, and daily food intake of female WT and Nod2$^{m/m}$ mice fed a diet with or without TiO_2.*

Parameter	***Control diet***[1]		***TiO_2 diet***[1]		**p-*value*[2]**		
	WT	**Nod2$^{m/m}$**	***WT***	**Nod2$^{m/m}$**	***Genotype***	***Diet***	***Interaction***
Age (d)	45 ± 3	48 ± 4	44 ± 6	46 ± 6	0.29	0.48	0.74
Initial body weight (g)	16.9 ± 1.0	15.2 ± 1.2	15.5 ± 1.8	15.8 ± 1.5	0.30	0.55	0.14
Final body weight (g)[3]	21.7 ± 1.0	19.0 ± 1.6	20.3 ± 1.6	18.3 ± 1.6	< 0.01	0.14	0.62
Body weight change (%)	128.8 ± 6.4	125.2 ± 12.6	131.8 ± 11.3	115.9 ± 3.3	< 0.05	0.46	0.16
Daily weight gain (g)	0.04 ± 0.007	0.03 ± 0.014	0.04 ± 0.010	0.02 ± 0.004	< 0.01	0.25	0.25
Daily food intake (g)	2.77 ± 0.18	2.57 ± 0.20	2.46 ± 0.14	2.41 ± 0.16	0.14	< 0.01	0.35

[1]AIN-76A rodent diet without (control) or with 625 mg TiO_2/kg. [2]Statistical comparison with two-way ANOVA with *Nod2* genotype (WT/*Nod2$^{m/m}$*) and diet (control/625 mg TiO_2/kg) as factors. [3]For statistical comparison of 'final body weight' results 'initial body weight' was used as co-variate.

a

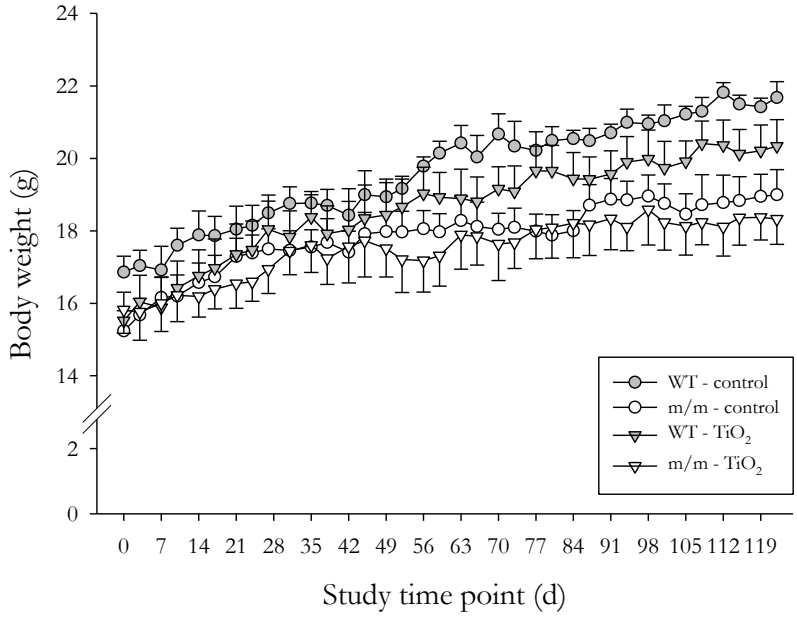

b

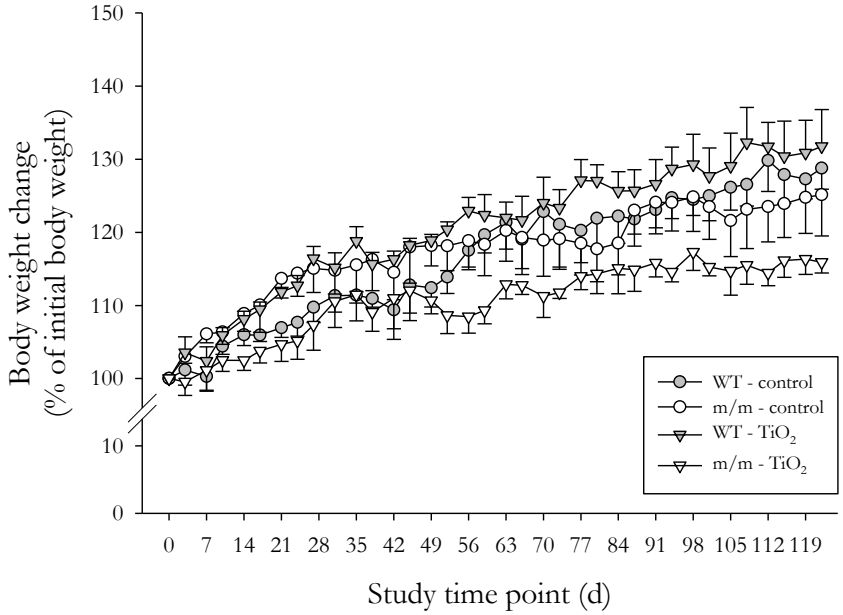

Figure 4.3 *Body weights and weight changes relative to initial body weight of WT and* Nod2$^{m/m}$ *mice fed a diet with or without TiO_2 for 18 weeks.*

Female WT and *Nod2$^{m/m}$* (m/m) mice were fed AIN-76A rodent diet without (control) or with 625 mg TiO_2/kg for 18 weeks. The body weights were recorded twice weekly for 122 d. (**a**) Changes in body weight over time. (**b**) Changes in body weight relative to initial body weight over time. Shown are means ± SE; n = 5. Results from the last time point were compared with two-way ANOVA (Table 4.1).

Table 4.2 *Means (± SD) for daily TiO_2 intake and daily TiO_2 dose of female WT and $Nod2^{m/m}$ mice fed a diet with 625 mg TiO_2/kg.*

Parameter	***WT***	**Nod2$^{m/m}$**	**p-*value*[1]**
Daily TiO_2 intake (mg)	1.538 ± 0.087	1.509 ± 0.102	0.64
Daily TiO_2 dose (mg/kg)	75.821 ± 4.650	82.891 ± 5.930	0.08

[1]Statistical comparison with Student's *t*-test.

Table 4.3 *Two-way ANOVA results for comparisons of intestinal parameters of female WT and Nod2$^{m/m}$ mice fed a diet with or without TiO_2*

Parameter	**p-*value*[1]**		
	Genotype	***Diet***	***Interaction***
Number of PPs	0.42	0.42	0.63
Small intestine length	0.30	< 0.05	0.13
Colon length	0.10	0.30	< 0.05
Ileum histology score	0.25	0.77	1.00
Colon histology score	0.30	< 0.01	0.42
Ileum crypt length	0.72	0.06	0.26
Ileum villi length	0.12	0.68	0.54
Colon crypt length	0.36	< 0.05	0.06
Reflection spots analysis group comparison	< 0.01	< 0.001	< 0.01
SED areas comparison	< 0.01	0.23	< 0.05

[1]Statistical comparison with two-way ANOVA with *Nod2* genotype (WT/*Nod2*$^{m/m}$) and diet (AIN-76A diet with/without 625 mg TiO_2/kg) as factors.

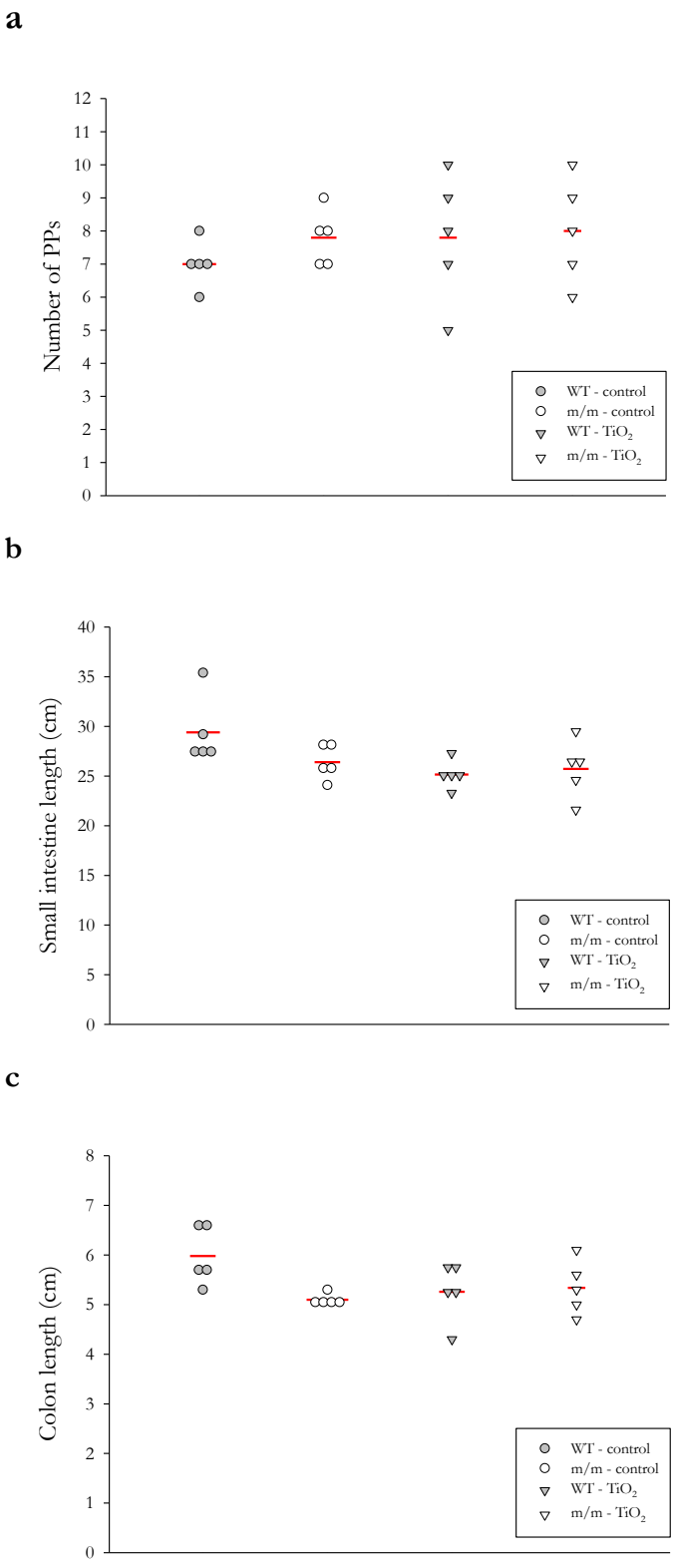

Figure 4.4 *Numbers of PPs and small intestine and colon lengths of WT and* Nod2$^{m/m}$ *mice fed a diet with or without TiO_2 for 18 weeks.*

Female WT and *Nod2$^{m/m}$* (m/m) mice were fed AIN-76A rodent diet without (control) or with 625 mg TiO_2/kg for 18 weeks. Number of PPs (**a**), small intestine length (**b**), and colon length (**c**) of each individual mouse were plotted according to group; means are indicated by red lines; n = 5. Results were compared with two-way ANOVA (Table 4.3).

4.4.3 Bright-field microscopy and histology of ileum and colon cross-sections

Representative images of H&E stained ileum and colon cross-sections are shown in Figures 4.5 and 4.6, respectively. The overall appearance of the tissue sections between the four groups was similar.

This was confirmed by the respective histology scores for ileum and colon for which no significant interaction effects were observed (Table 4.3 & Figure 4.7). However, the colon histology scores were significantly higher ($p < 0.01$) for mice on TiO_2 diet irrespective of genotype (Figure 4.7b).

There were no significant differences for ileum crypt and villi lengths (Table 4.3 & Figure 4.8) and no significant interaction difference for colon crypt length (Table 4.3 & Figure 4.9). Of note, the colon crypt lengths of mice on the TiO_2 diet were significantly ($p < 0.05$) increased compared to mice on control diet.

4.4.4 Assessment of titanium dioxide particle uptake in Peyer's patches and the ileal mucosa

TiO_2 particle uptake in PPs was confirmed with dark field microscopy. Both WT and *Nod2*$^{m/m}$ mice contained TiO_2 particles as shown in the representative images (Figure 4.10).

Statistical analysis of the number of TiO_2 particles in PPs, as determined from the reflection spot analysis with confocal microscopy, and the SED areas indicated that there were significant interaction differences between the groups for both (Table 4.3). Pairwise group comparisons of the number of reflection spots showed that the SED of WT mice on the TiO_2 diet contained significantly more ($p < 0.01$) TiO_2 particles than all other groups (Figure 4.11). The number of reflection spots in the SED of *Nod2*$^{m/m}$ mice on the TiO_2 diet was also significantly higher ($p < 0.05$) compared to the control groups. The SED area that was analysed for reflection spots was significantly larger ($p < 0.05$) in WT mice exposed to TiO_2 compared to both *Nod2*$^{m/m}$ mice groups (Figure 4.12). However, there was no difference between the SED areas of *Nod2*$^{m/m}$ mice on the TiO_2 diet and the control diet.

In addition, unstained ileal tissue cross-sections from mice on the TiO_2 diet were also observed with dark field illumination. Many TiO_2 particles were observed in the intestinal lumen (Figure 4.13). However, only few TiO_2 particles were detected in the mucosa of WT and *Nod2*$^{m/m}$ mice.

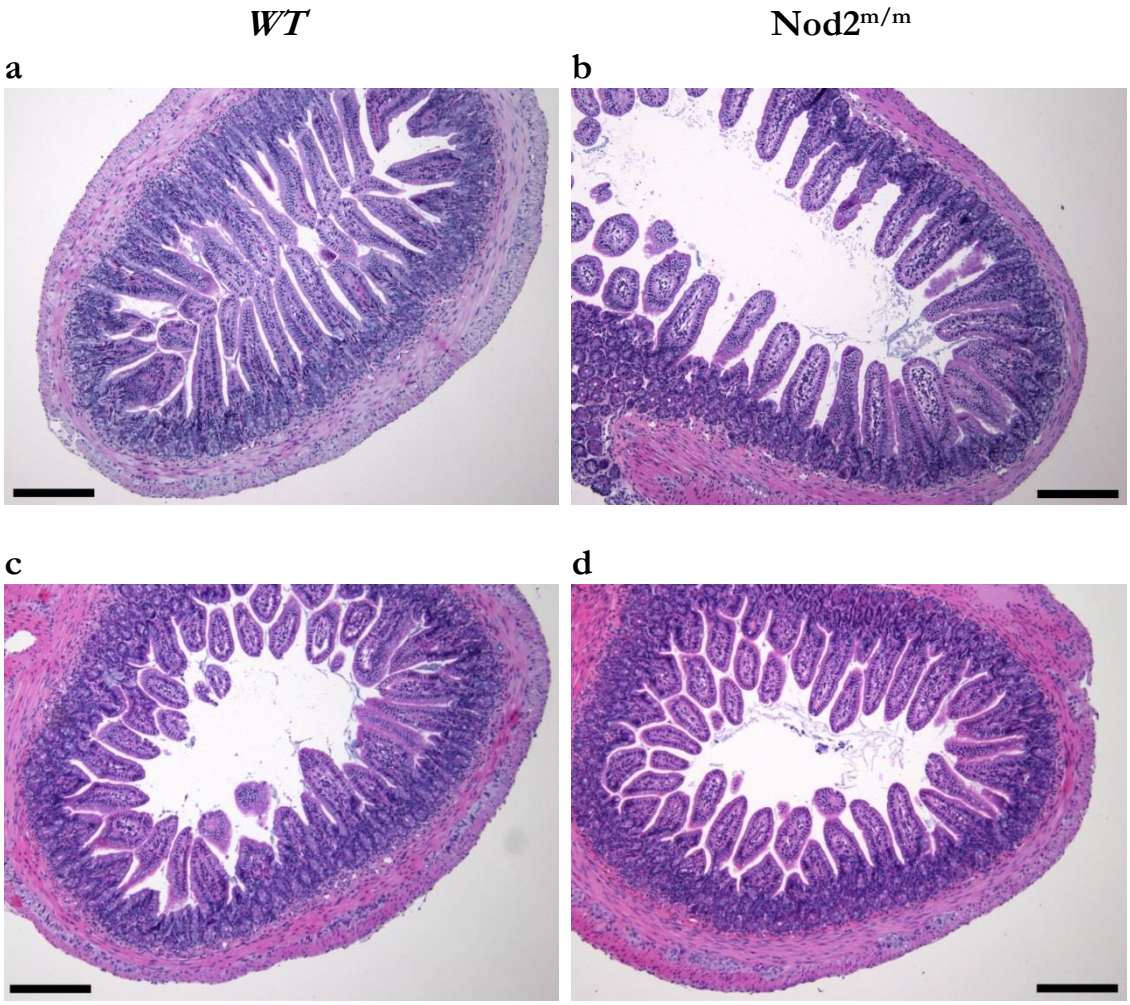

Figure 4.5 *Bright field microscopy images of ileum cross-sections from WT and* Nod2$^{m/m}$ *mice fed a diet with or without* TiO_2 *for 18 weeks.*

Images of ileum cross-sections from female WT and *Nod2$^{m/m}$* mice on AIN-76A rodent diet without (**a, b**) or with 625 mg TiO_2/kg (**c d**) for 18 weeks. H&E stained sections were viewed with a light microscope under bright field illumination to determine the histology score (Figure 4.7), and the villi and crypt lengths (Figure 4.8). Representative images from WT (**a, c**) and *Nod2$^{m/m}$* mice (**b, d**) are shown. Scale bar = 200 μm.

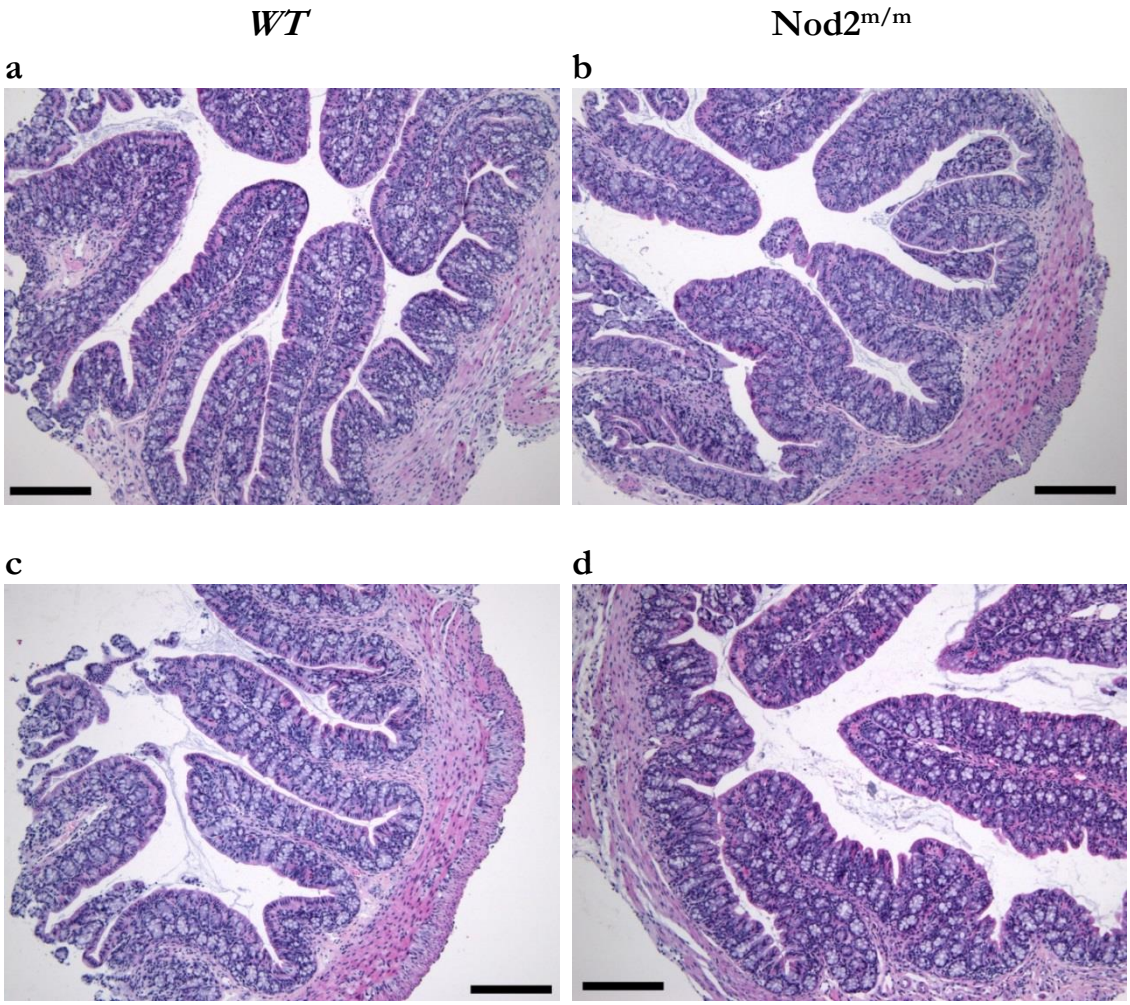

Figure 4.6 *Bright field microscopy images of colon cross-sections from WT and* Nod2$^{m/m}$ *mice fed a diet with or without* TiO_2 *for 18 weeks.*

Images of colon cross-sections from female WT and *Nod2$^{m/m}$* mice on AIN-76A rodent diet without (**a, b**) or with 625 mg TiO_2/kg (**c d**) for 18 weeks. H&E stained sections were viewed with a light microscope under bright field illumination to determine the histology score (Figure 4.7). Representative images from WT (**a, c**) and *Nod2$^{m/m}$* mice (**b, d**) are shown. Scale bar = 200 μm.

a

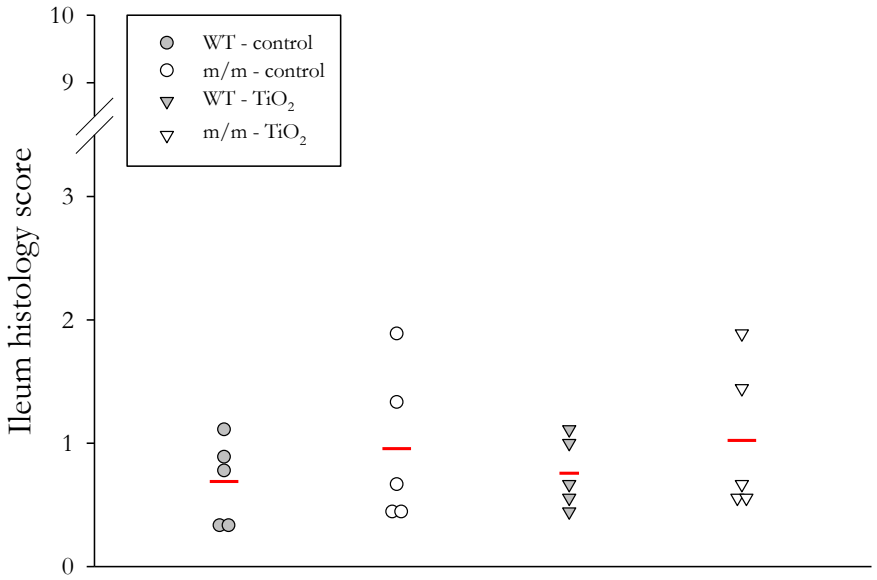

b

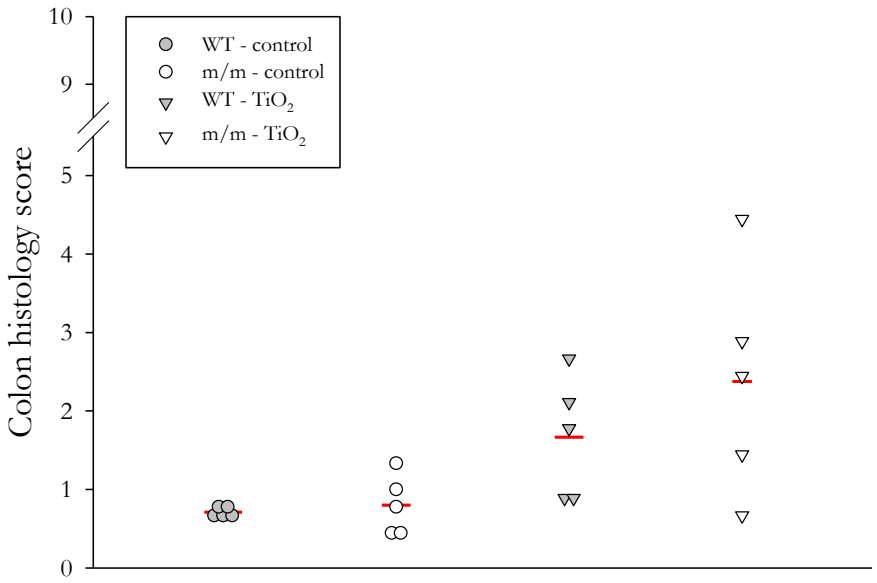

Figure 4.7 *Ileum and colon histology scores of WT and* Nod2$^{m/m}$ *mice fed a diet with or without TiO_2 for 18 weeks.* Female WT and *Nod2$^{m/m}$* (m/m) mice were fed AIN-76A rodent diet without (control) or with 625 mg TiO_2/kg for 18 weeks. Histology scores were determined from H&E stained cross-sections. Histology scores of ileum (**a**) and colon (**b**) of each individual mouse were plotted according to group; means are indicated by red lines; $n = 5$. Results were compared with two-way ANOVA (Table 4.3).

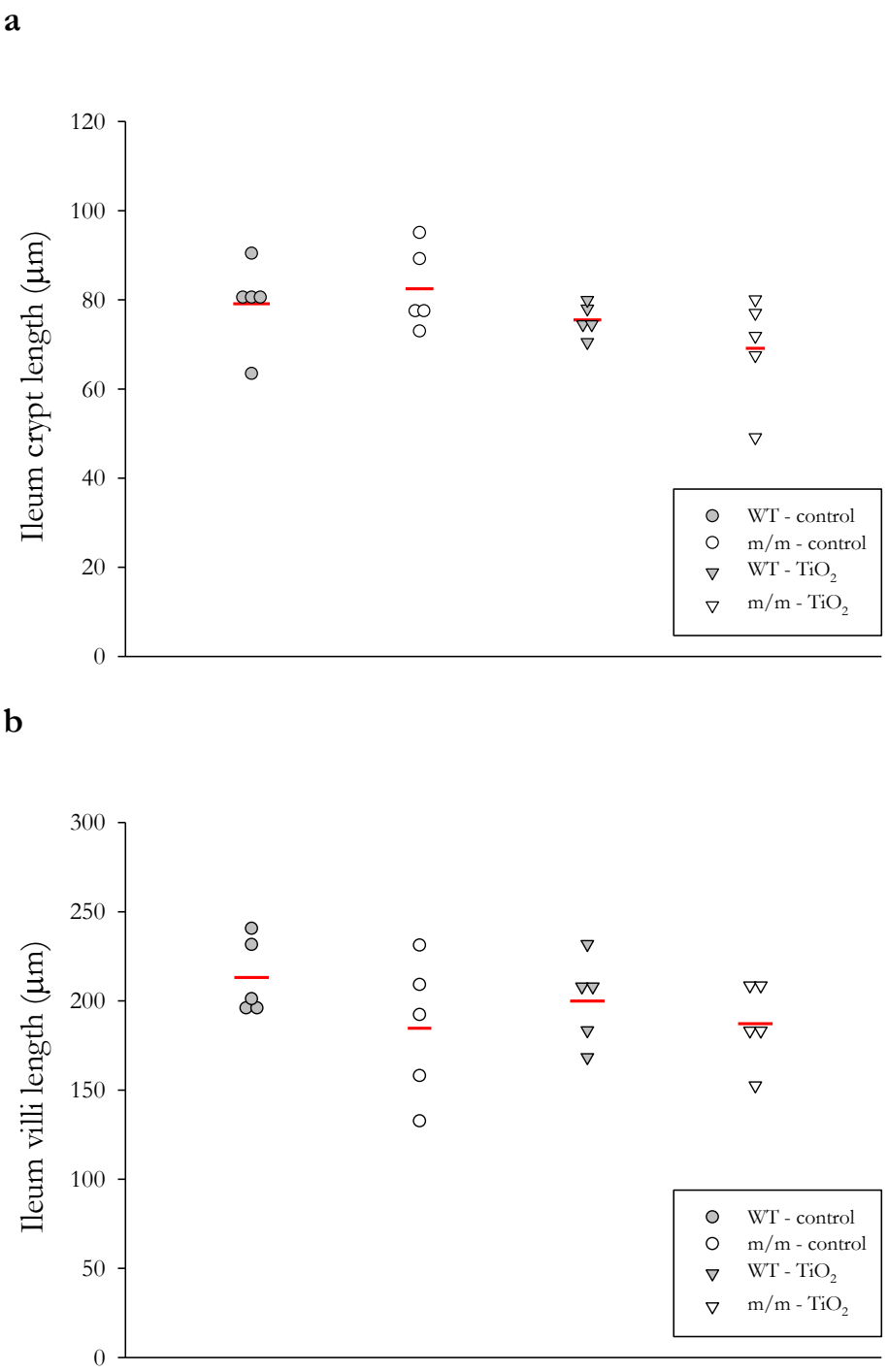

Figure 4.8 *Lengths of crypts and villi in the ileum from WT and* Nod2$^{m/m}$ *mice fed a diet with or without TiO_2 for 18 weeks.* Female WT and *Nod2$^{m/m}$* (m/m) mice were fed AIN-76A rodent diet without (control) or with 625 mg TiO_2/kg for 18 weeks. Images of H&E stained ileum cross-sections were acquired with a light microscope. Lengths of crypts (**a**) and villi (**b**) of each individual mouse were measured with image analysis software and plotted according to group; means are indicated by red lines; n = 5. Results were compared with two-way ANOVA (Table 4.3).

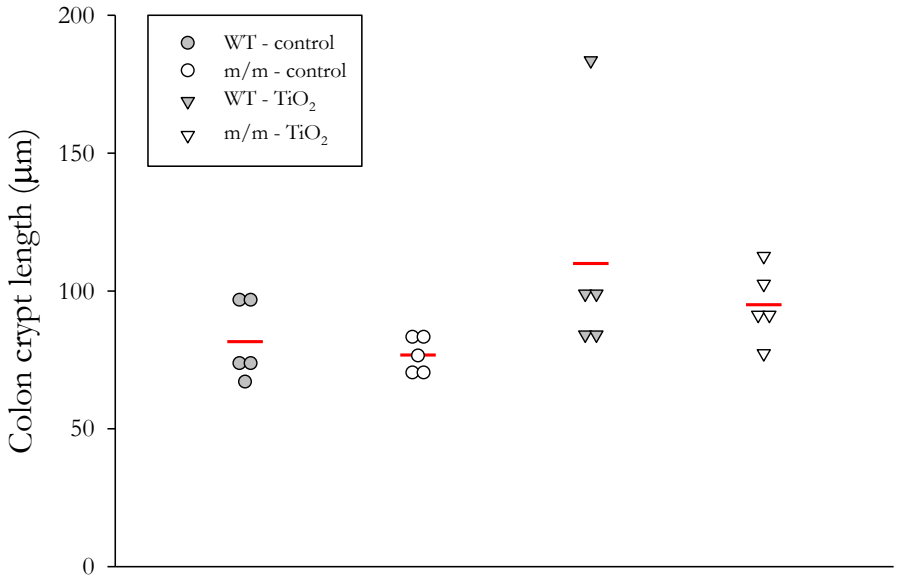

Figure 4.9 *Lengths of crypts in the colon from WT and* Nod2$^{m/m}$ *mice fed a diet with or without TiO_2 for 18 weeks.* Female WT and *Nod2$^{m/m}$* (m/m) mice were fed AIN-76A rodent diet without (control) or with 625 mg TiO_2/kg for 18 weeks. Images of H&E stained colon cross-sections were acquired with a light microscope. Length of crypts of each individual mouse were measured with image analysis software and plotted according to group; means are indicated by red line; $n = 5$. Results were compared with two-way ANOVA (Table 4.3).

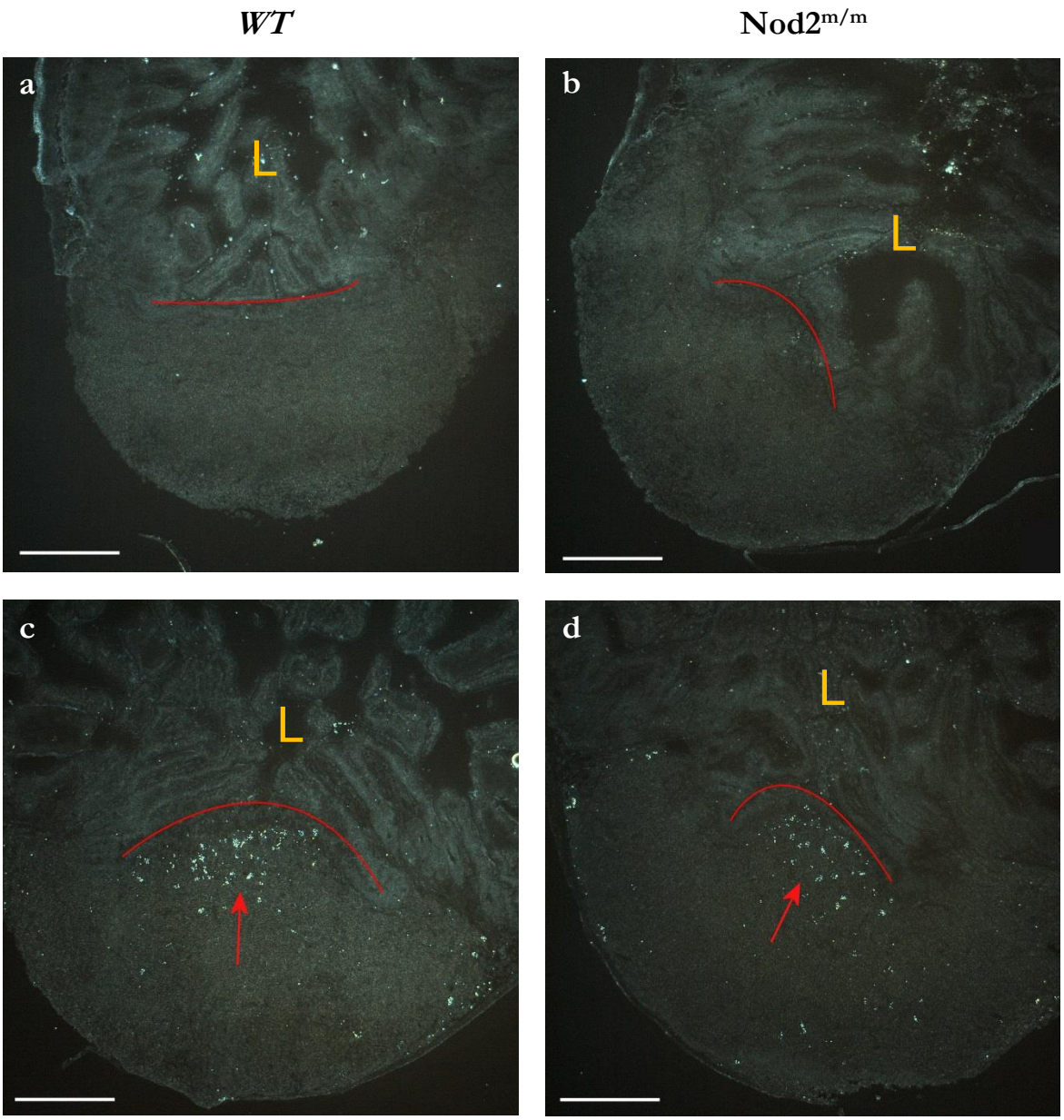

Figure 4.10 *Dark field microscopy images of PP cross-sections from WT and* Nod2$^{m/m}$ *mice fed a diet with or without* TiO_2 *for 18 weeks.*

Images of PP cross-sections from female WT and *Nod2$^{m/m}$* mice on AIN-76A rodent diet without (**a, b**) or with 625 mg TiO_2/kg (**c, d**) for 18 weeks. Unstained sections were viewed with a light microscope under dark field illumination. Lines indicate FAE. Arrows point out selected TiO_2 particle clusters in SEDs (white). Representative images from WT (**a, c**) and *Nod2$^{m/m}$* mice (**b, d**) are shown. Scale bar = 200 µm. L = intestinal lumen.

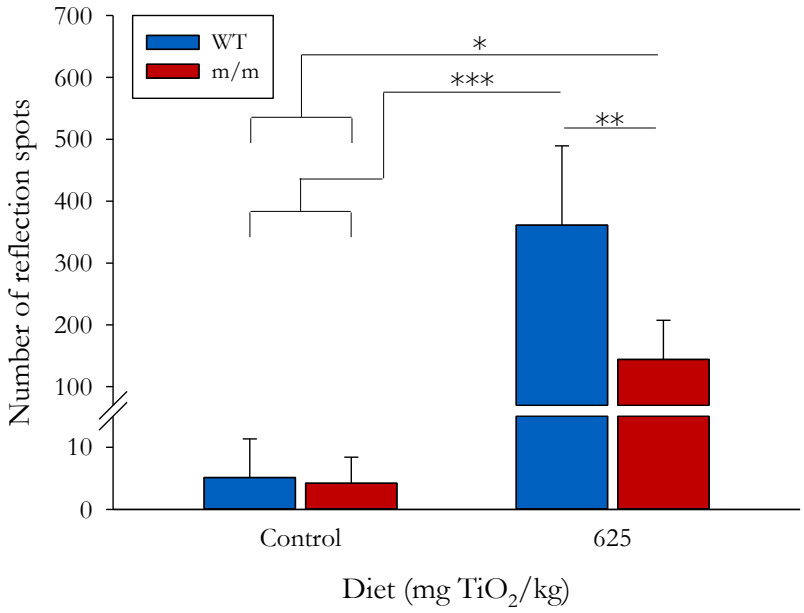

Figure 4.11 *TiO_2 particle uptake in SED areas from WT and* $Nod2^{m/m}$ *mice fed a diet with or without TiO_2 for 18 weeks.* Female WT and *$Nod2^{m/m}$* (m/m) mice were fed an AIN-76A rodent diet without (control) or with 625 mg TiO_2/kg for 18 weeks. Unstained 10 μm thick PP sections were analysed by reflectance confocal microscopy. The number of reflection spots in PP SEDs was assessed with image analysis software. Shown are means ± SD; $n = 5$. Results were compared with two-way ANOVA. *P*-values were calculated with Tukey's HSD test and significant differences between groups are indicated; *$p < 0.05$, **$p < 0.01$, ***$p < 0.001$.

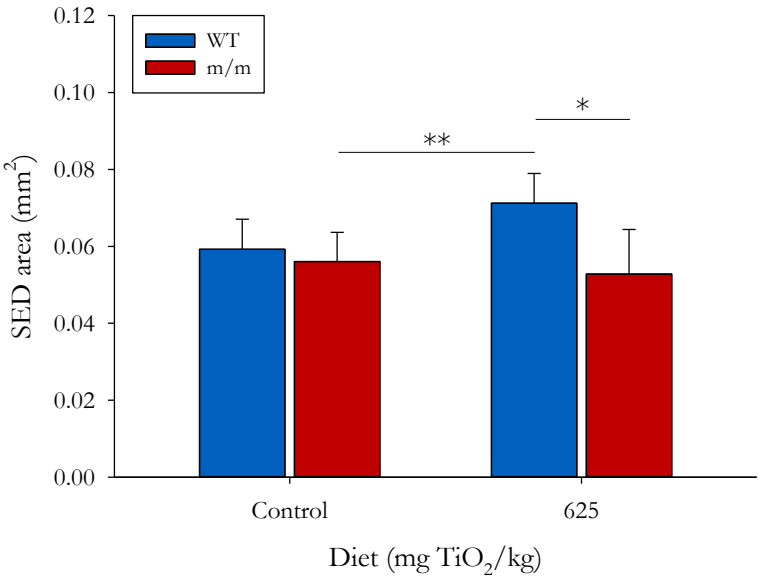

Figure 4.12 *Sizes of SED areas used for TiO_2 particle uptake assessment from WT and* Nod2$^{m/m}$ *mice fed a diet with or without TiO_2 for 18 weeks.*

Female WT and *Nod2$^{m/m}$* (m/m) mice were fed an AIN-76A rodent diet without (control) or with 625 mg TiO_2/kg diet for 18 weeks. Unstained 10 µm thick PP sections were analysed by reflectance confocal microscopy. The area of SEDs used for red spot counting was measured with image analysis software. Shown are means ± SD; n = 5. Results were compared with two-way ANOVA. *P*-values were calculated with Tukey's HSD test and significant differences between groups are indicated; *$p < 0.05$, **$p < 0.01$.

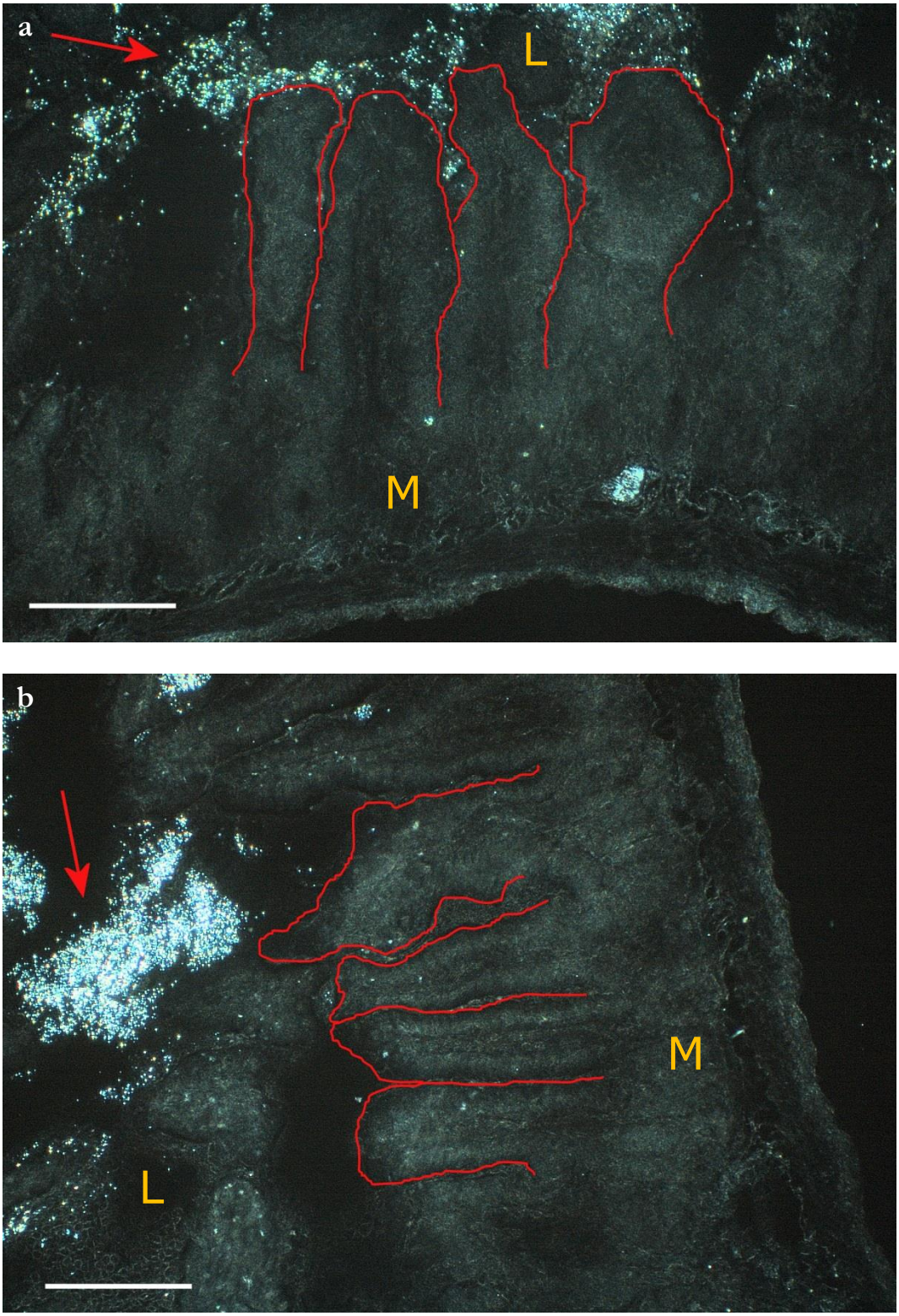

Figure 4.13 *Dark field microscopy images of ileum cross-sections from WT and* Nod2$^{m/m}$ *mice fed a diet with or without* TiO_2 *for 18 weeks.*

Images of ileum cross-sections from female WT and *Nod2$^{m/m}$* mice on AIN-76A rodent diet with 625 mg TiO_2/kg for 18 weeks. Unstained sections were viewed with a light microscope under dark field illumination. Lines indicate villi. Arrows point out TiO_2 particles (white spots) in lumen. Representative images from WT (**a**) and *Nod2$^{m/m}$* mice (**b**) are shown. Scale bar = 200 μm. L = lumen, M = mucosa.

4.4.5 Monocyte populations of Peyer's patches from wild-type mice and mice with a Crohn's disease-like *Nod2* gene variant on a standard diet

The frequencies of monocytes and monocyte populations, including DC subsets, in PPs from WT and *Nod2*$^{m/m}$ mice are shown in Figures 4.14 and 4.15. There were no significant differences between WT and *Nod2*$^{m/m}$ mice on a standard rodent diet.

4.5 Discussion

4.5.1 Reassessment of the hypothesis

The results presented in this chapter did not support the hypothesis that *Nod2*$^{m/m}$ mice develop intestinal inflammation as a consequence of TiO_2 particle accumulation in PPs. Furthermore, the uptake of TiO_2 particles was lower in *Nod2*$^{m/m}$ mice compared to WT mice. Possible reasons for this observation will be discussed in Section 4.5.3.

4.5.2 Considerations about the performance of mice with a Crohn's disease-like *Nod2* gene variant

The *Nod2*$^{m/m}$ mice on the TiO_2 diet had the lowest average body weight of all groups and showed the lowest body weight increase over the course of the study (Figure 4.3). However, the mean final body weight, body weight change, and daily weight gain of *Nod2*$^{m/m}$ mice on the control diet were not different from the other three groups (Table 4.1). Nevertheless, there was a genotype effect for these three parameters which indicated that *Nod2*$^{m/m}$ mice had a lower body weight performance than WT mice. The body weights of *Nod2*$^{m/m}$ mice on a standard rodent diet, which were used for *in vitro* experiments (see Chapter 2), were also lower compared to age matched WT mice (Figure 4.1a). Taken together, these findings suggest that *Nod2*$^{m/m}$ mice have a lower average body weight than WT mice. In addition, the *Nod2*$^{m/m}$ mice from the *in vitro* studies also had shorter colons than age matched WT mice (Figure 4.2b). These observations could be interpreted as indicators of a disturbed intestinal homeostasis in *Nod2*$^{m/m}$ mice.

However, if the intestinal function was impaired in *Nod2*$^{m/m}$ mice, this was not obvious from aberrances in the intestinal tract. No differences in histological parameters that would have indicated the presence of intestinal inflammation were observed between the groups from

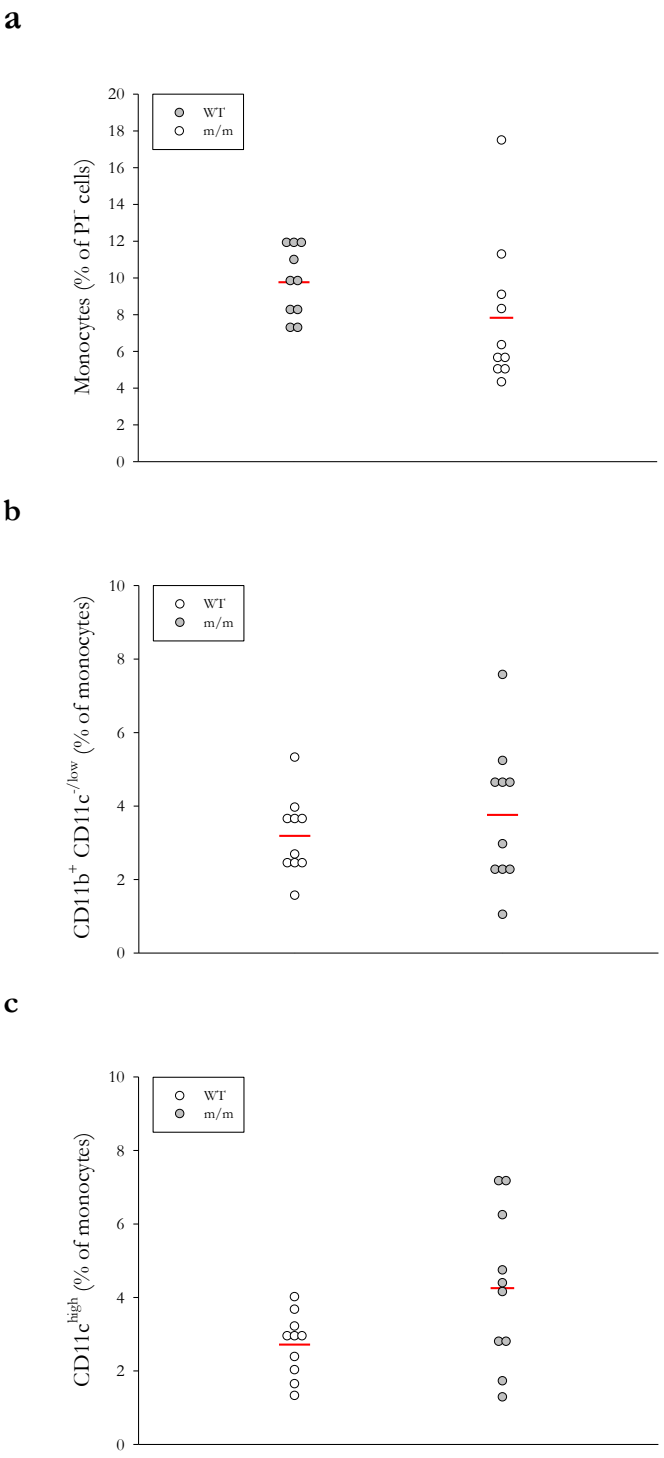

Figure 4.14 *Frequencies of monocytes and monocyte populations in PPs from WT and* Nod2$^{m/m}$ *mice on a standard rodent diet.* Single cell suspensions of PPs from female WT and *Nod2$^{m/m}$* (m/m) mice on standard rodent diet were stained with fluorescently labelled antibodies and analysed by flow cytometry. Percentages of monocytes from all live cells (**a**) and of CD11b^{+} CD11c$^{-/low}$ macrophages (**b**) or CD11c^{high} DCs (**c**) from all live monocytes were determined. Results of each individual mouse were plotted according to genotype; means are indicated by red lines; shown are combined results of two independent experiments; n = 10. Results were compared with Student's *t*-test (**a**) or Wilcoxon rank sum test (**b, c**).

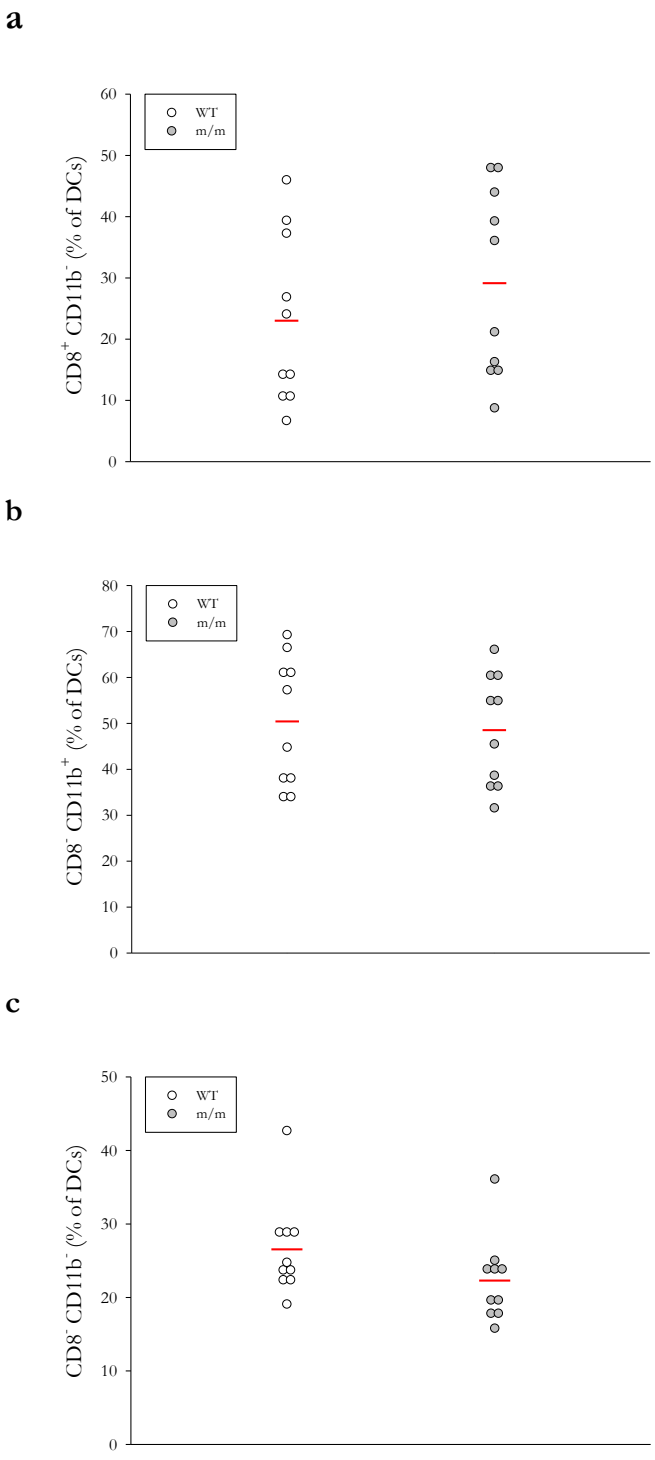

Figure 4.15 *Frequencies of DC subsets in PPs from WT and* Nod2$^{m/m}$ *mice on a standard rodent diet.*

Single cell suspensions of PPs from female WT and *Nod2$^{m/m}$* (m/m) mice on standard rodent diet were stained with fluorescently labelled antibodies and analysed by flow cytometry. Percentages of CD8^{+} CD11b^{-} DCs (**a**), CD8^{-} CD11b^{+} DCs (**b**), and CD8^{-} CD11b^{-} DCs (**c**) from all live DCs were determined. Results of each individual mouse were plotted according to genotype; means are indicated by red lines; shown are combined results of two independent experiments; n = 10. Results were compared with Wilcoxon rank sum test.

the second *in vivo* study (Figure 4.7). The lengths of crypts in the ileum and colon and of the villi in the ileum were also similar between the groups (Figures 4.8 & 4.9). In case of inflammation in the intestine, it would be expected that the histology scores would be higher and crypt lengths would be increased in affected mice compared to control mice without intestinal inflammation [249].

Although statistical analysis of the colon lengths showed an interaction effect between genotype and diet in the second *in vivo* study (Table 4.3), the subsequently performed pairwise group comparison did not reveal significant differences between any two groups. There was only a trend to a significant difference between WT and *Nod2*$^{m/m}$ mice both on control diet. The reason why the significant difference observed with ANOVA was not confirmed with pairwise group comparison could be that the Tukey's HSD method, which was used for pairwise group comparison, is a more conservative statistical method [272]. If a more liberal pairwise group comparison test would have been used, e.g. Fisher's Least Significant Difference test, the difference between WT and *Nod2*$^{m/m}$ mice both on control diet might have been statistically significantly different (personal communication with Ms Catherine Lloyd-West). This assumption was supported by the finding that colon lengths between WT and *Nod2*$^{m/m}$ on a standard rodent diet were significantly different (Figure 4.2b).

In contrast to the colon lengths, there was no interaction effect regarding the small intestine lengths. However, there was a diet effect for the latter. Mice on the control diet had longer small intestines than mice on the TiO_2 diet (Figure 4.4b). This result was likely a statistical effect, rather than a 'real' diet effect, which might have been caused by an outlier value in the group of WT mice on a control diet. Correspondingly, WT and *Nod2*$^{m/m}$ on a standard rodent diet had similar small intestine lengths (Figure 4.2a).

There was also a diet effect on the daily food intake in the second *in vivo* study. Animals that were fed a TiO_2-containing diet had a lower food intake than mice on a control diet (Table 4.1). This result was in contrast to the first *in vivo* study in which no differences were observed between the diet groups of the respective sampling time points (Section 3.4.2; Table 3.2). These contradictory results could potentially be clarified through another *in vivo* study.

In the original study in which the generation of the *Nod2*$^{m/m}$ mice had been described, it was mentioned that conventionally housed *Nod2*$^{m/m}$ mice did not develop intestinal inflammation spontaneously [131]. The other available mouse model with a modification of the *Nod2* gene, the *Nod2*$^{-/-}$ mouse model, also did not show spontaneous intestinal abnormalities [98, 125].

In contrast to *Nod2*$^{-/-}$ mice, however, *Nod2*$^{m/m}$ mice had an increased susceptibility to DSS-induced colitis compared to WT mice [131]. Therefore, it was expected that the *Nod2*$^{m/m}$ mouse model would be better suited to investigate the influence of dietary TiO_2 particles on the development of intestinal inflammation in the presence of a *Nod2* mutation.

4.5.3 Titanium dioxide particle uptake in Peyer's patches of mice with a Crohn's disease-like *Nod2* gene variant

The number of PPs was similar between both WT and *Nod2*$^{m/m}$ mice kept under conventional conditions for the *in vitro* studies as well as all the groups in the second *in vivo* study (Figures 4.1b & 4.4a). In their report about the generation of *Nod2*$^{m/m}$ mice, Maeda and colleagues have not indicated if they observed different numbers of PPs in *Nod2*$^{m/m}$ mice. However, Barreau and colleagues have investigated the numbers of PPs in *Nod2*$^{-/-}$ mice and found that they had more PPs compared to WT mice [304].

The uptake of TiO_2 particles in PPs was investigated by dark field microscopy and reflectance confocal microscopy. The results showed that most TiO_2 particles were located in the SED areas in both WT and *Nod2*$^{m/m}$ mice (Figure 4.10). This observation was similar to the results from the first *in vivo* study (Sections 3.4.4 & 3.4.6; Figures 3.11 & 3.16). However, in the second *in vivo* study the total amount of TiO_2 particles was lower in PPs from *Nod2*$^{m/m}$ mice compared to WT mice (Figure 4.11). This finding was unexpected because it has been reported that the transcellular permeability of PPs and the translocation of microorganisms from the lumen into PPs was increased in *Nod2*$^{-/-}$ mice compared to WT mice [304, 312]. Furthermore, *Nod2*$^{-/-}$ mice contained more M cells in the FAE compared to WT mice [304]. If this was also the case in *Nod2*$^{m/m}$ mice, it would be expected to detect an increased amount of TiO_2 particles in PPs of *Nod2*$^{m/m}$ mice compared to WT mice.

Taken together, the findings that *Nod2*$^{m/m}$ mice had equal number of PPs and fewer particles in the SED area compared to WT mice indicate that there are fundamental differences in intestinal function between *Nod2*$^{m/m}$ and *Nod2*$^{-/-}$ mice. This would also explain why *Nod2*$^{m/m}$ mice showed increased susceptibility to DSS-induced colitis [131] whereas there was no difference between *Nod2*$^{-/-}$ and WT mice after treatment with DSS [125].

Several possibilities could explain the reduced amount of TiO_2 particles in PPs of *Nod2*$^{m/m}$ mice. For instance, there might be a difference in the number of M cells between *Nod2*$^{m/m}$ and WT mice. Unlike for *Nod2*$^{-/-}$ mice, however, the amount of M cells in the FAE of *Nod2*$^{m/m}$ mice would be reduced compared to WT mice. It has been shown that the number

of M cells decreased with increasing age in mice [313]. The uptake of fluorescent latex particles with a diameter of 200 nm in PPs was impaired in older mice. However, in the second *in vivo* study the age of *Nod2*$^{m/m}$ and WT mice was similar, so a reduced number of M cells because of an older age of *Nod2*$^{m/m}$ mice seems to be an unlikely explanation.

Another possibility could be that the function of M cells in the FAE of *Nod2*$^{m/m}$ mice is reduced compared to WT mice. It has been reported that the transport capacity of M cells could be up-regulated by the presence of bacteria in the intestinal lumen [314]. This result suggested that disturbances in the intestinal microbiota could affect M cell function. Indeed, it has been reported that the intestinal microbial profile of *Nod2*$^{-/-}$ mice differed from WT mice [315-317]. However, the intestinal microbiota of *Nod2*$^{m/m}$ mice has not yet been investigated.

A third possibility could be that there are differences in PPs immune cells, specifically DCs, between *Nod2*$^{m/m}$ and WT mice. As shown previously (Section 3.4.7), TiO_2 particles were taken up by DCs in the SED area. Differences in PP immune cells have been reported for WT and *Nod2*$^{-/-}$ mice, e.g. an increased frequency of CD4$^+$ T cells *Nod2*$^{-/-}$ mice [304, 312]. It is possible that the number of DCs in the SED area of *Nod2*$^{m/m}$ mice was reduced compared to WT mice. Therefore, less phagocytic cells that can take up TiO_2 particles would be available. A reduced number of cells in the SED area of *Nod2*$^{m/m}$ mice was also suggested by the smaller SED area in these mice compared to WT mice. To further investigate the possibility of a reduced number of APCs in the SED area of *Nod2*$^{m/m}$ mice compared to WT mice, the frequencies of PP monocyte populations were compared between healthy *Nod2*$^{m/m}$ and WT mice on a conventional diet. It was necessary to obtain further animals for this investigation because no spare PPs were available from the second *in vivo* study. The results from this additional investigation indicated that the frequencies of PP monocytes, macrophages, DCs, or DC subsets did not differ between *Nod2*$^{m/m}$ and WT mice kept under conventional conditions.

Lelouard and colleagues have recently investigated DC subsets from the SED area in more detail [182, 183]. They showed that lysozyme-expressing CD11c$^+$ CD11b$^+$ DCs from the SED had a higher phagocytic activity *in vitro* compared to CD11c$^+$ cells that did not express lysozyme [182]. Moreover, lysozyme-expressing DCs were able to extend dendrites through pores in M cells, and this enabled them to sample particulate antigens directly in the intestinal lumen [183]. The formation of the transepithelial dendrites was mediated through a particular cell adhesion molecule. Therefore, another possible explanation for the decreased amount of TiO_2 particles in the SED of *Nod2*$^{m/m}$ mice compared to WT mice that was observed in

this study would be that the formation of these dendrites is reduced in *Nod2*$^{m/m}$ mice, e.g. through impaired expression of the necessary adhesion molecule.

A recent study examined the amount of exogenous particles in PPs from children with IBD [292]. Overall, 42 % of the children showed accumulation of exogenous particles in PPs. However, less children with CD had exogenous particles in their PPs compared to children with UC or non-IBD patients. This result is in line with the observation from the second *in vivo* study that *Nod2*$^{m/m}$ mice had less TiO_2 particles in PPs. Hummel and colleagues hypothesised that the numbers of cells containing exogenous particles in children affected by CD might be reduced because these cells became activated and migrated from PPs to MLNs or the LP where they initiated a pro-inflammatory immune response.

4.5.4 Titanium dioxide particle uptake across the intestinal epithelium

Increased translocation of TiO_2 particle-containing DCs from PPs to other sites of the gastrointestinal tract would be another explanation why there were less TiO_2 particles in the SED of *Nod2*$^{m/m}$ mice. Unfortunately, MLNs were not collected during the sampling of the second *in vivo* study to investigate the translocation of TiO_2 particles in *Nod2*$^{m/m}$ mice. However, a section of the ileum adjacent to a PPs was collected to investigate the presence of TiO_2 in the intestinal mucosa. Although many studies have examined intestinal particle uptake across PPs (reviewed in [318]), some studies also showed that particles could be taken up across the intestinal epithelium. For example, Desai and colleagues compared the uptake of biodegradable particles with a size of approximately 100 nm between ileal PPs and non-PP tissues *in situ* with an intestinal loop model in rats [319]. Although this model showed that more particles were taken up in PPs, a considerable amount of particles was also present in non-PP tissues. Theoretically, TiO_2 particles could cross the intestinal epithelial barrier by transcytosis through enterocytes [189], or by persorption through gaps created in the intestinal epithelium by apoptotic enterocytes [169]. The latter case has been demonstrated for gold nanoparticles of various sizes after oral administration in the small intestine of mice [170].

Analysis of the samples obtained during the second *in vivo* study from mice fed a TiO_2-containing diet showed that some TiO_2 particles were present in the mucosa of WT and *Nod2*$^{m/m}$ mice (Figure 4.13). However, in both cases the number of particles in the LP was much smaller compared to the amount of TiO_2 observed in the SED areas of

PPs (Figure 4.10). Therefore, particle uptake across the epithelium of the small intestine seems to be a less important way for particulate substances to gain access to the intestinal mucosa compared to uptake across the FAE.

Although relative particle uptake across the non-PP intestinal epithelium might be low, the absolute uptake could however be of biological relevance [219]. The intestinal epithelium has a much larger surface area compared to the combined surface areas of FAE in the small intestine. Nevertheless, it cannot be excluded that the particle-containing cells observed in the intestinal mucosa were originally located in PPs and migrated to the LP after uptake of TiO_2 particles in the SED area.

4.5.5 Conclusion

To summarize, the results presented in this chapter suggest that a mutation in the *Nod2* gene did not increase the susceptibility to develop intestinal inflammation in response to TiO_2 particle uptake in PPs. However, limitations in using models to investigate human diseases, in general, or in the *Nod2*$^{m/m}$ mouse model, in particular, might have masked potential negative effects of TiO_2 particles on intestinal function. Using additional mouse models for CD or conducting another human dietary intervention study might be options to continue research on this topic in the future. The limitations and possibilities for further research will be discussed in more detail in Chapter 6.

In addition, more investigations could be carried out with *Nod2*$^{m/m}$ mice exposed to dietary TiO_2 as a consequence of the results from the second *in vivo* study. For instance, it should be clarified why the uptake of TiO_2 particles in PPs from *Nod2*$^{m/m}$ mice was lower compared to WT mice. Immunofluorescence staining with M cell specific markers, e.g. *Ulex europaeus* agglutinin-I [182], could be used to clarify whether this was the consequence of a reduced number of M cell in the FAE. Furthermore, the intestinal permeability of *Nod2*$^{m/m}$ mice could be assessed by measuring the FITC-labelled dextran flux *in vitro* using an Ussing chamber [304]. Moreover, the composition of the intestinal microbiota could be compared between *Nod2*$^{m/m}$ and WT mice by sequencing microbial ribosomal ribonucleic acid genes of intestinal content samples [317].

Although WT and *Nod2*$^{m/m}$ mice on a TiO_2-containing diet did not develop intestinal inflammation according to histological assessment, exposed mice might nevertheless be affected on the molecular level. Thus, dietary TiO_2 intake might be reflected in changes of urine metabolite concentrations of exposed individuals.

Chapter 5 Effects of dietary titanium dioxide on urine metabolite profiles of wild-type mice and mice with a Crohn's disease-like *Nod2* gene variant

5.1 Introduction

Currently, the precise diagnosis of CD and UC is complicated and requires invasive clinical procedures that can cause discomfort for the patients. Therefore, the use of biomarkers that can be measured in samples that can be obtained with no or minimal discomfort, e.g. urine, serum, plasma or faeces, would be useful for the diagnosis of IBD [320]. Biomarkers are parameters that are associated with specific biological processes, e.g. the development or progression of diseases, and that can be objectively measured [321].

There is increasing interest to use metabolomics, also known as metabolic profiling, for the study of disease-associated biomarkers [321, 322], including IBD [320]. Metabolomics has been defined as the study of metabolites, i.e. small molecules with a molecular weight less than 1 kDa, in a biological sample [320-322]. The term 'metabolome' refers to all metabolites that are present in a specific sample [322].

For diagnostic purposes, metabolites are usually measured in urine, serum, plasma, or faeces. Various biomarkers that distinguish CD and/or UC patients from healthy controls have been identified in all of these sample types with metabolomics [323-328]. For example, the amount of formate was increased and the levels of p-cresol and hippurate decreased in urine samples from CD patients compared to healthy controls [327].

Urine samples are useful for IBD diagnostics because the sample collection is non-invasive and consecutive samples can be obtained from the same patient without great difficulties to monitor disease progression and response to treatment [320]. An advantage of using metabolomics for the identification of disease-associated biomarkers in clinical diagnostics is the possibility to perform high-throughput analyses with low associated costs per sample [321].

The most common analytical methods to detect metabolites in biological samples are nuclear magnetic resonance spectroscopy (NMR) and mass spectrometry [320]. The latter is usually used together with sample separation methods, such as gas chromatography mass spectrometry (GC-MS) or liquid chromatography mass spectrometry (LC-MS). The metabolite analysis can be targeted, when defined metabolites are investigated in a specific sample, or untargeted, when a profile of all detectable metabolites in a given sample is obtained. Untargeted metabolomics can be useful to identify metabolic pathways that are affected by specific disorders like IBD [320, 329].

Metabolomics has been applied to studies with animal models of IBD. For instance, mice that developed colitis after treatment with DSS showed differences in serum metabolites compared to untreated mice [330]. Another commonly used mouse model for CD is the *Il10*$^{-/-}$ mouse strain, which does not express the anti-inflammatory cytokine IL-10 [50, 331]. Differences in urine metabolites of *Il10*$^{-/-}$ mice with active colitis were detected by NMR and GC-MS analysis compared to WT mice without inflammation. For example, the levels of trimethylamine, fucose, xanthurenic acid and 5-aminovaleric acid were increased in urine of *Il10*$^{-/-}$ mice compared to WT controls [332-334].

Further analysis of urine samples from *Il10*$^{-/-}$ and WT mice with LC-MS by Otter and colleagues confirmed the association between an elevated level of xanthurenic acid, which is a product of the tryptophan catabolism, and CD-like inflammation in *Il10*$^{-/-}$ mice [335]. The level of xanthurenic acid glucuronide, a precursor of xanthurenic acid, was correspondingly decreased in urine samples from *Il10*$^{-/-}$ mice with colitis. Furthermore, the amount of 2,5,7,8-tetramethyl-2-(2'-carboxyethyl)-6-hydroxychroman, a vitamin E degradation product, was increased in urine samples from these mice.

The studies with animal models showed that metabolomics can successfully be used to differentiate mice with colonic inflammation from healthy control animals based on their urine metabolite profiles. The biomarkers discovered in these animal studies highlighted new metabolic pathways that are affected by the presence of colon inflammation and which might be of relevance for the clinical diagnostics of IBD in the future.

Metabolomics is also a useful tool in toxicology, and it has been used extensively to study drug toxicity [336]. One metabolomics study investigated the impact of oral TiO_2 administration to rats for 14 d [209]. Analysis of urine and serum metabolites by NMR showed changes in energy and amino acid metabolism after TiO_2 exposure. Increased concentrations of phenylacetylglycine and hippurate in urine of TiO_2 exposed rats also indicated impacts of TiO_2 on the intestinal microbiota as the precursors to these two metabolites are produced by commensal bacteria. So far, effects of exposure to dietary TiO_2 particles on metabolic pathways has been investigated neither in humans nor in mice.

5.2 Hypothesis and aims

The hypothesis to be tested in this chapter was that intake of a diet containing TiO_2 particles leads to systemic metabolic changes, and the urine metabolite profiles of mice on TiO_2-containing diets will be different compared to mice on a TiO_2 particle-free diet. Furthermore,

it was expected that *Nod2*$^{m/m}$ mice will show differences in their urine metabolite profiles compared to WT mice, regardless of dietary TiO_2 intake, due to effects on metabolic pathways as a result of the introduced frameshift mutation in the *Nod2* gene.

The aims of this chapter were to analyse urine samples collected during the first and second *in vivo* studies with LC-MS and to compare the results statistically. If differences exist, metabolites that discriminate the respective groups should be identified based on database searches and comparisons with previous metabolomics studies.

5.3 Materials and methods

5.3.1 Metabolomics analysis workflow

A diagram about the workflow for metabolomics analysis, which highlights the main steps in general [320, 329] and the corresponding steps for the studies from this dissertation in particular, is presented in Figure 5.1.

5.3.2 Animals and urine collection

The animal studies, including the procedure for spot urine collection, were approved by the Grasslands Animal Ethics Committee in compliance with the New Zealand Animal Welfare Act 1999.

Spot urine samples were collected from the mice during the course of the two animal studies. Urine was chosen as the sample type to assess potential metabolic changes after feeding TiO_2-containing diets. The advantage of urine samples compared to other potential sample types, e.g. plasma, was that the sample collection could be performed non-invasively. Thus, several samples could be obtained from the same animal over the course of the study, which was of relevance for the second *in vivo* study. All samples were collected at 10 am ± 1 h on the respective collection days.

During the first *in vivo* study (Chapter 3), urine samples were obtained from female and male WT mice after they were fed one of three TiO_2-containing diets or a control diet for 6 weeks, 12 weeks, and 18 weeks just before the mice were sacrificed for tissue collection (see Section 3.3.3). During the second *in vivo* study (Chapter 4), urine samples were collected from female WT and *Nod2*$^{m/m}$ mice on a TiO_2-containing or control diet on the first day of the study and then every four weeks until the end of the study after 18 weeks (see Section 4.3.2).

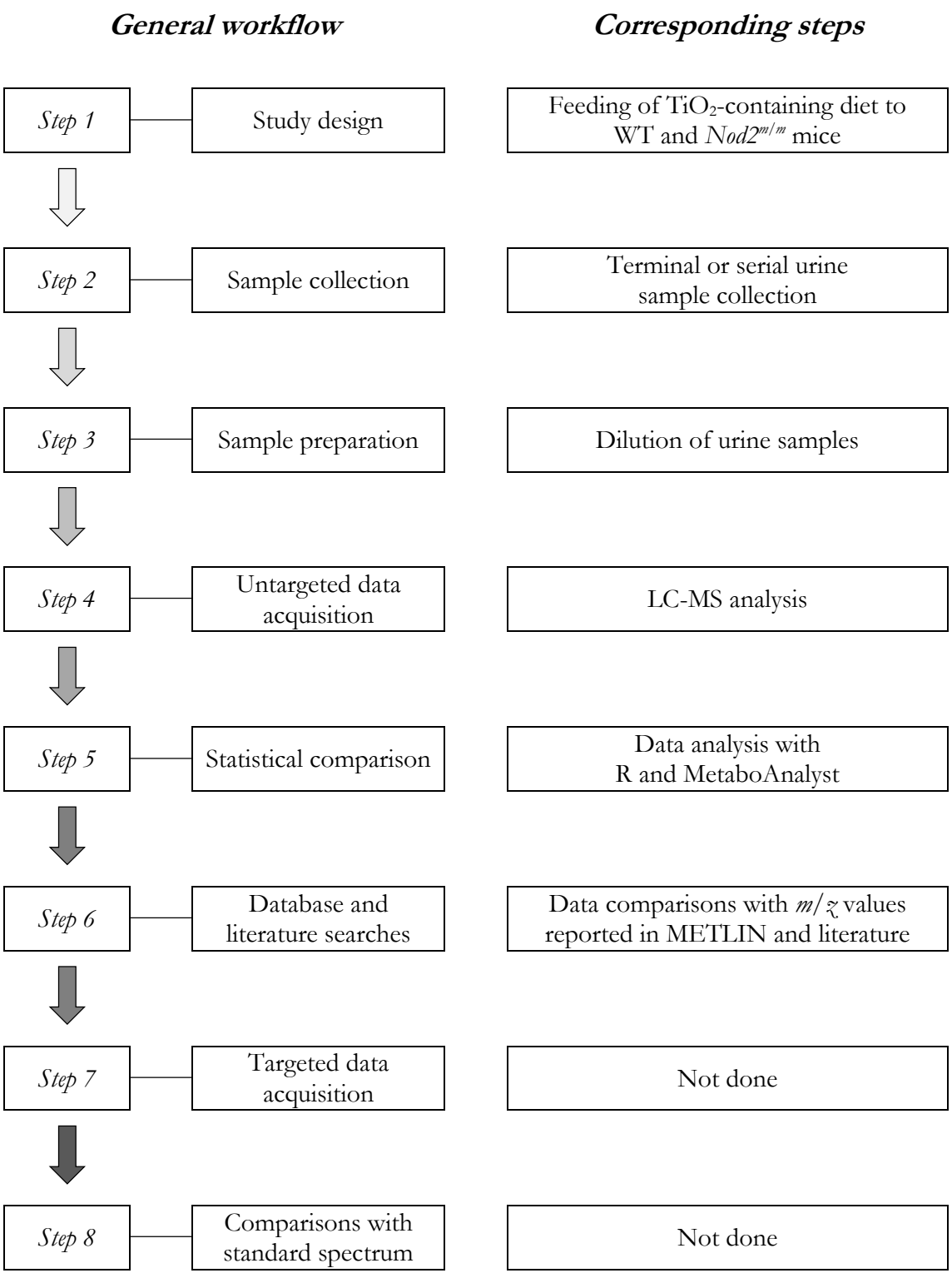

Figure 5.1 *Overview of the workflow for metabolomics studies.*

This diagram shows the main steps of an untargeted metabolomics analysis workflow and highlights the corresponding steps for the metabolomics analysis of the mouse urine samples from this dissertation.

In total, five sets of samples were taken in week 1, 5, 9, 13, and 18 during this second *in vivo* study.

For the spot urine collection, the mice were placed with their back over a clean Petri dish lid. The mice were held at the tail with one hand while gentle pressure was exerted on their lower back with the other hand to stimulate urination. Released urine was taken up from the Petri dish with a 100 µL volume pipette and transferred to a 1.7 mL microcentrifuge tube. The samples were immediately frozen in liquid nitrogen, and they were subsequently transferred to a −80 °C freezer for long term storage.

5.3.3 Sample preparation

The samples were defrosted and centrifuged at 12,000 *g* for 10 s to precipitate particulate substances, if present. A 4 µL aliquot from each sample was transferred to a glass insert for mass spectrometry vials with a capacity of 250 µL and diluted with 200 µL 0.1 % (volume/volume) formic acid (Thermo Fisher Scientific) in distilled water. The insert was placed into a 2 mL mass spectrometry vial and sealed with a specific membranous cap for mass spectrometry vials. All samples were kept on ice until the sample preparation was finished.

In addition, a combined urine sample of all mice from each study was prepared as a LC-MS analysis quality control sample. For this, 4 µL urine from each mouse was added to a 2 mL mass spectrometry vial. The pooled urine sample was mixed by pipetting, and 4 µL were transferred to a glass insert and diluted with 200 µL 0.1 % formic acid. The samples were stored at −20 °C until they were required for LC-MS analysis.

5.3.4 Liquid chromatography mass spectrometry analysis

The samples of the two studies were analysed by LC-MS on a Q Exactive Mass Spectrometer (Thermo Fischer Scientific). It has been suggested that LC-MS represents the best analysis method to investigate changes in urine metabolites, especially in the case of spot urine samples collected from mice where only a small volume is available for analysis [337]. For analysis by LC-MS, the molecules in liquid samples are first separated by high-performance liquid chromatography before they are analysed on the mass spectrometer. Mass spectrometry is a measurement of the mass-to-charge (m/z) ratio of charged molecules, so the molecules have to be ionised before analysis. For LC-MS, this is commonly performed by electrospray ionisation If the molecules are analysed with this method in negative mode

the resulting molecular ions usually lack a proton ($[M-H]^-$ ion), and if the analysis is performed in positive mode molecular ions are usually formed by addition of a proton ($[M+H]^+$ ion). Otter and colleagues have developed a method to analyse diluted mouse urine samples by direct infusion LC-MS, and this method was used to analyse the samples from both animal studies of this dissertation [335].

All samples belonging to the same study were analysed together at the same time. The samples were first analysed in negative electrospray ionisation mode followed by analysis in positive ionisation mode. The run order of the samples was randomised. A pooled urine sample was run after approximately every 11th to 14th sample, so that the performance of the instrument over the whole run could be checked later by comparing the ion spectra of the combined urine samples. A Luna C18 column (Phenomenex, Torrence, CA, USA) with a size of 150 mm × 2 mm (5 μm particle size) was used to separate the metabolites. At the beginning of each run, at least five samples of distilled water were run to remove any residuals left in the LC-MS column from the previous run.

For the analysis, 5 μL of sample was injected using a Thermo Surveyor pump (Thermo Fisher Scientific) and auto-sampler (Thermo Fisher Scientific). Initially, the flow from the column was diverted to a waste container for 30 s, and after this the sample was directed to the mass spectrometer electrospray source. First, the samples were loaded onto the column with 0.1 % formic acid in distilled water for 1.5 min at 300 μL/min. The metabolites were then eluted off the column with a linear gradient of 0 % to 70 % acetonitrile (Merck, Palmerston North, NZ) containing 0.1 % formic acid. The initial solvent was then restored with a linear gradient over 30 s, and the column re-equilibrated. The source ion voltage was −4,000 V, and the capillary temperature was 275 °C. The spectra of ions from 50 m/z to 2,000 m/z were recorded with the Xcalibur software (Thermo Fisher Scientific).

5.3.5 Data analysis

The original LC-MS data files were in the proprietary 'raw' file format. To analyse the data with open source software, they had to be converted to 'mzXML' files. This file conversion was performed with the MSConvert program, which is integrated in the open source software ProteoWizard version 3.0 [338, 339] using the filter setting 'Peak Picking' with 'MS Level' set to '1'. The 'mzXML' files were subsequently analysed in R version 3.0.3 with the xcms package version 1.38.0 [340]. The commands used for this analysis were provided by Dr Wayne Young (AgResearch, Palmerston North, NZ) and are listed in Appendix E.

Briefly, the first step was to pre-process the data files with the function 'xcmsSet'. This function identified ion peaks according to default settings for low resolution LC-MS data. Next, the peaks from the different samples were grouped across the samples with the 'group' function using default settings. Then, the function 'retcor' was used to align the peaks by correcting for the drift in retention time from sample to sample. After the retention time correction the peaks were grouped again with the 'group' function. Finally, missing peaks were filled with the function 'fillPeaks'. A peak intensity table, which is a list of all detected ions with their peak values for the respective samples, was created with the 'peakTable' function, and the list was exported as a 'csv' file.

The statistical data analysis was also carried out in R, and the code is given in Appendix E. First, the data was normalised using the median fold change method to account for differences in sample concentration. The concentrations of metabolites in urine can vary depending on the volume. It has been shown that normalisation of the data according to the median fold change is the preferred normalisation method for urine samples to reduce concentration-induced variation between samples [341]. Because metabolomics data has a large dynamic range, it was also necessary to perform a logarithmic transformation. The statistical comparison was then carried out using a non-parametric multivariate ANOVA (MANOVA) provided by the R package vegan version 2.0-10 [342]. The statistical comparison for the first *in vivo* study was performed as a three-way MANOVA with 'sex', 'urine collection time point', and 'diet' as factors. For the second *in vivo* study, the groups were also compared with a three-way MANOVA this time with '*Nod2* genotype', 'urine collection time point', and 'diet' as factors.

Further statistical analysis was carried out online with MetaboAnalyst 2.0 [343-345]. The LC-MS peak intensity tables in 'csv' file format were uploaded on the website, and the MetaboAnalyst program provided several data processing and analysis options which were all based on R packages [346]. The first step was to filter the data to remove non-informative values. The 'interquantile range' method was used to identify peaks that had similar intensities for all samples, and these peaks were excluded from the dataset for further analysis. Then the data were normalised by median and transformed logarithmically. Furthermore, the 'Pareto' data scaling option was selected to adjust the highly variable mass spectrometry data for a more accurate comparison.

Next, the clustering of samples into the respective groups in those cases in which the statistical analysis indicated the presence of significant differences between groups was visualised with partial least squares discriminant analysis (PLS-DA). This method is a

multivariate analysis method that is commonly used for metabolomics data [320]. Another multivariate analysis method is principal component analysis. Both methods can be used to display variations in large datasets with many variables by transforming the data and plotting the samples according to the components that represent the largest possible variability within the data. In contrast to principal component analysis, PLS-DA is a supervised method in which prior information about the sample groups is considered for the data transformation and the plotting of the components [345]. Three-dimensional PLS-DA plots, which show the three components that contribute most to the variability of the dataset, were selected to visualise the relationships between significantly different groups.

A list of discriminant ions that were responsible for the separation of the specified groups were obtained by selecting the 'ANOVA' entry under the 'Statistics' menu.

MetaboAnalyst also provided an option for pairwise group comparisons between individual ions with significant differences. Tukey's HSD *post-hoc* analysis was selected, and the significance level was set to less than 0.05.

5.3.6 Database searching and comparison with literature

The list of discriminant ions included all metabolites with a significant ($p < 0.05$) *p*-value that had been calculated by one-way ANOVA. An additional *p*-value that was adjusted for multiple comparisons with the false discovery rate (FDR) method was also listed for each ion. Only discriminant ions with FDR adjusted *p*-value less than 0.05 were considered for further analysis. Potential metabolites for these ions were identified by database searching and comparisons with previously described urine metabolites affected by various conditions. When isotopes were detected those with the larger m/z value were excluded from the database and literature comparisons.

The METLIN metabolite database [347, 348] was used to compare the m/z values for statistically significant ions with m/z values of metabolites available on this database. The METLIN database is currently the most comprehensive database available for metabolomics studies, and it contains information to more than 10,000 distinct metabolites [329]. A mass tolerance of 0.01 Da was selected for the database search, so that only $[M\text{-}H]^-$ ions or $[M+H]^+$ ions with a mass that closely matched the experimentally determined m/z value were shown. The m/z values of the metabolites obtained with these settings were then compared to the m/z values of the significantly different positive and negative discriminant ions,

respectively. Ions with expected m/z values ± 0.005 to the detected m/z values were considered as potential metabolites.

More information about their nature was obtained by checking for information on these metabolites in another comprehensive metabolomics database, the human metabolome database [349, 350], and/or by conducting internet searches with the web search engine Google (www.google.com; Google, Mountain View, CA, USA).

Statistically significant ions were also compared to previously described discriminating metabolites from studies that compared urine samples from either CD patients and healthy controls [327, 328], *Il10*$^{-/-}$ mice displaying colonic inflammation and healthy WT mice [332, 333, 335], or rats orally exposed to TiO_2 and unexposed controls [209].

5.4 Results

5.4.1 Urine metabolite profile comparisons of wild-type mice exposed to dietary titanium dioxide

The number of urine samples per group collected from mice during the first *in vivo* study is given in Table 5.1. In eight instances it was not possible to collect urine samples from mice even after repeated attempts.

Statistical analysis of the LC-MS results from the first *in vivo* study with a three-way MANOVA showed that there was no significant interaction between the three factors 'sex', 'sampling group', and 'diet' (Table 5.2). However, if the samples were grouped according to 'sex' alone there was a significant difference ($p < 0.01$ for both negative and positive mode), which could also be seen in the PLS-DA plots (Figure 5.2).

There was also a significant interaction effect ($p < 0.05$ for both negative and positive mode) between 'sex' and 'sampling group'. The PLS-DA plots showed that the samples from the 6 weeks sampling group did not overlap with the samples from the 18 weeks sampling group (Figure 5.3). Only samples from female mice were selected to be analysed with PLS-DA for this because in the subsequent study with WT and *Nod2*$^{m/m}$ mice only female mice were used.

Table 5.1 *Number of urine samples per respective group collected from mice for metabolomics studies at different time points.*

				Samples per group collected in week						
Study	***Sex***	***Genotype***	***Diet[1]***	***1***	***5***	***6***	***9***	***12***	***13***	***18***
1[2]	*Female*	*WT*	control			6		6		5
			6.25			6		6		4
			62.5			6		6		4
			625			6		6		6
	Male	*WT*	control			6		6		6
			6.25			6		6		6
			62.5			6		6		4
			625			5		6		6
2[3]	*Female*	*WT*	control	5	4		5		4	5
			625	5	5		5		5	5
	Female	Nod2$^{m/m}$	control	5	5		5		5	5
			625	5	5		5		5	5

[1]AIN-76A rodent diet without (control) or with the respective amount of TiO_2 (mg/kg diet). [2]Terminal urine samples collected once from the indicated number of animal per group prior to euthanasia. [3]Serial urine samples collected repeatedly from the indicated number of animals per groups over the course of the study.

Table 5.2 *MANOVA results for comparisons of urine metabolite profiles from WT mice fed a diet with or without TiO_2.*

LC-MS analysis mode	***Statistical factor(s)***	**p-*value*[1]**
Negative	Sex	< 0.01
	Weeks	< 0.05
	Diet	0.26
	Sex × weeks	< 0.05
	Sex × diet	0.39
	Weeks × diet	0.17
	Sex × weeks × diet	0.42
Positive	Sex	< 0.01
	Weeks	0.16
	Diet	0.23
	Sex × weeks	< 0.05
	Sex × diet	0.20
	Weeks × diet	0.20
	Sex × weeks × diet	0.38

[1]Statistical comparison with non-parametric MANOVA with sex (female/male), urine collection time point (6/12/18 weeks), and diet (AIN-76A diet without TiO_2 or with 6.25/62.5/625 mg TiO_2/kg) as factors.

a

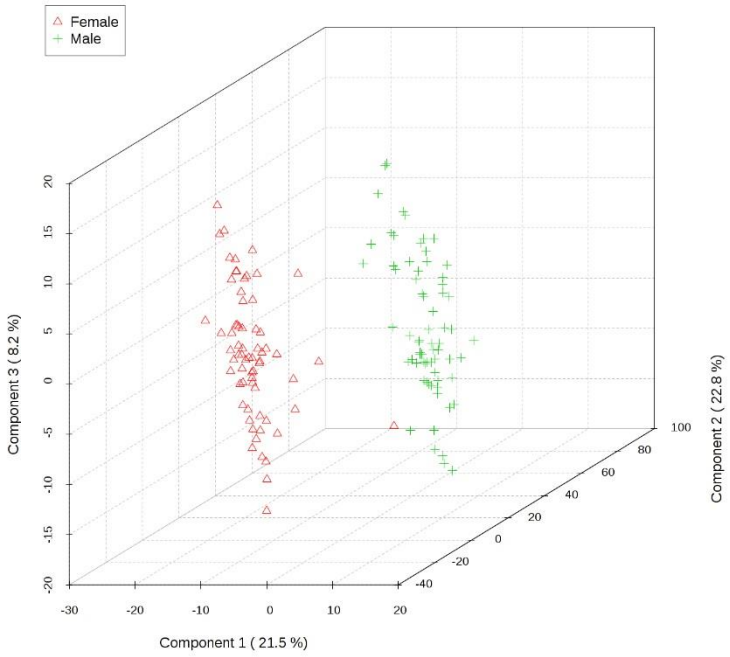

b

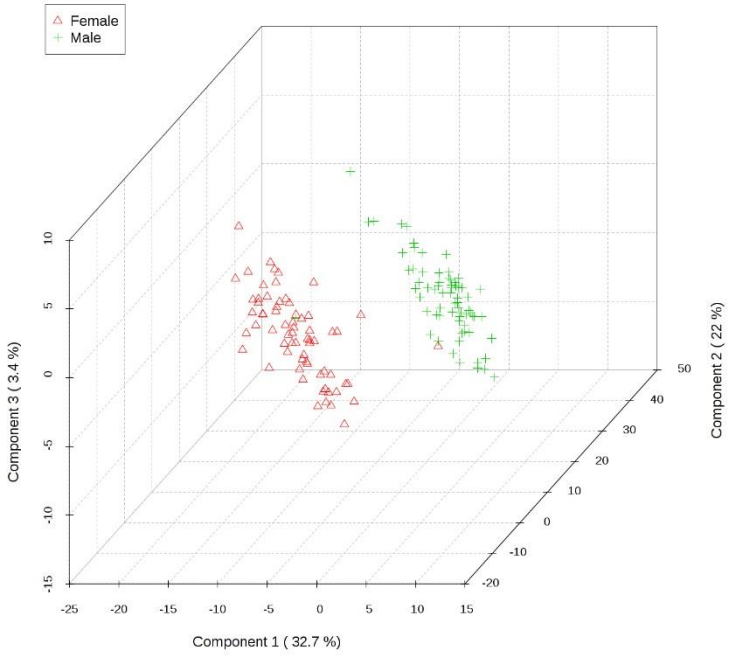

Figure 5.2 *PLS-DA plots of negative and positive ion profiles detected in urine samples from WT mice fed a diet with or without TiO_2 analysed according to sex.*

Female and male WT mice were fed AIN-76A rodent diet without or with 6.25 mg, 62.5 mg, or 625 mg TiO_2/kg. Terminal urine samples were collected after 6 weeks, 12 weeks, or 18 weeks immediately prior to euthanasia. Metabolite profiles were obtained with LC-MS. Data analysis was performed with R and MetaboAnalyst. Shown are three-dimensional PLS-DA plots of negative (**a**) and positive (**b**) discriminant ions with samples grouped according to sex; n = 67/69 (females/males).

a

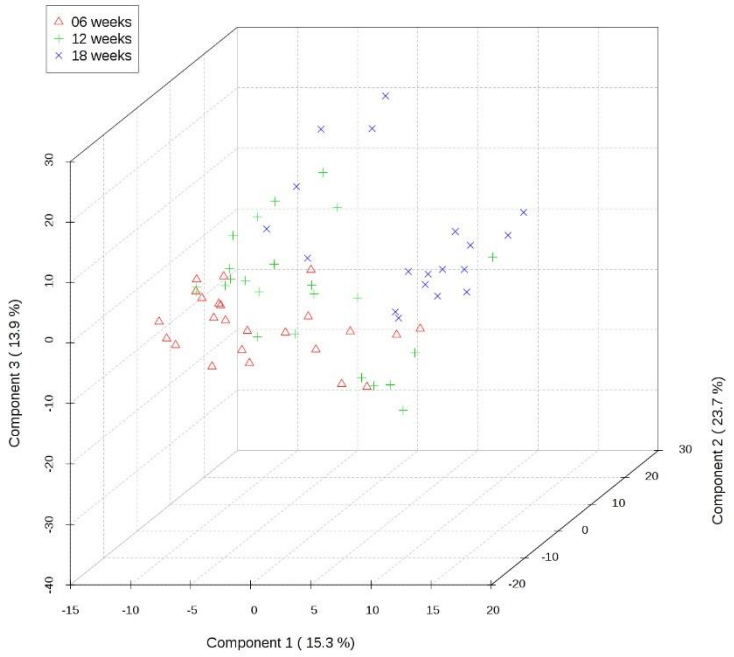

b

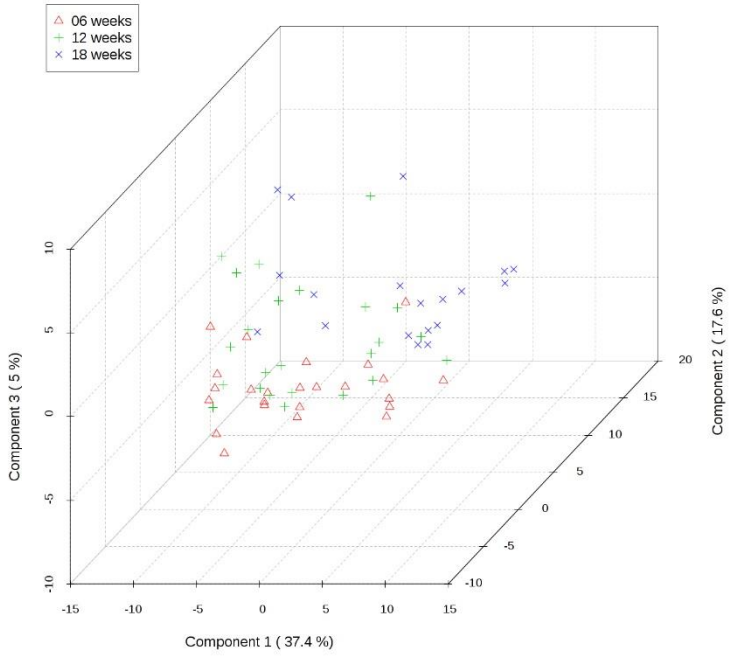

Figure 5.3 *PLS-DA plots of negative and positive ion profiles detected in urine samples from female WT mice fed a diet with or without TiO_2 analysed according to urine collection time point.*

Female WT mice were fed AIN-76A rodent diet without or with 6.25 mg, 62.5 mg, or 625 mg TiO_2/kg. Terminal urine samples were collected after 6 weeks, 12 weeks, or 18 weeks immediately prior to euthanasia. Metabolite profiles were obtained with LC-MS. Data analysis was performed with R and MetaboAnalyst. Shown are three-dimensional PLS-DA plots of negative (**a**) and positive (**b**) discriminant ions with samples grouped according to urine collection time point; n = 24/24/19 (6/12/18 weeks).

5.4.2 Urine metabolite profile comparisons of wild-type mice and mice with a Crohn's disease-like *Nod2* gene variant exposed dietary titanium dioxide

The number of urine samples per group obtained during the second *in vivo* study is given in Table 5.1. Except for two instances, it was possible to collect samples from all mice of the four different groups at each urine collection.

The LC-MS results from the second *in vivo* study were analysed with a three-way MANOVA, and there was a significant interaction ($p < 0.01$ for negative mode, $p < 0.05$ for positive mode) between the three factors '*Nod2* genotype', 'urine collection time point', and 'diet' (Table 5.3). There were also significant differences when the samples were compared between genotypes ($p < 0.01$ for both negative and positive mode), time points ($p < 0.01$ for negative mode, $p < 0.05$ for positive mode), or diets ($p < 0.05$ for positive mode) alone.

Correspondingly, the PLS-DA plots according to genotype alone showed that the two groups were separated based on their urine metabolites, irrespective of urine collection time points and diets (Figure 5.4). When the samples were plotted with PLS-DA according to urine collection time points alone, the samples that were collected in week 1 appeared distinct from all others (Figure 5.5). However, the separation between the samples collected at the other time points was less pronounced.

The significant differences between the control and TiO_2 diet groups alone in positive mode could also be visualised by PLS-DA (Figure 5.6). However, there was no significant diet effect in negative mode, so no PLS-DA plot was generated for this factor alone.

The urine metabolite profiles of the last time point at week 18 were selected for further analysis with PLS-DA to visualise differences between the groups that were expected based on the significant interaction between all three factors. The PLS-DA plots showed that samples from *Nod2*$^{m/m}$ mice on control diet were separated from the other three groups in both ionisation modes (Figure 5.7). In contrast, samples from WT mice on control diet could not be distinguished from the TiO_2 groups according to their PLS-DA scores.

Table 5.3 *MANOVA results for comparisons of urine metabolite profiles from female WT and Nod2$^{m/m}$ mice fed a diet with or without TiO_2.*

LC-MS analysis mode	***Statistical factor(s)***	**p-*value*[1]**
Negative	Genotype	< 0.01
	Week	< 0.01
	Diet	0.06
	Genotype × week	0.54
	Genotype × diet	0.13
	Week × diet	0.24
	Genotype × week × diet	< 0.01
Positive	Genotype	< 0.01
	Week	< 0.05
	Diet	< 0.05
	Genotype × week	0.70
	Genotype × diet	0.24
	Week × diet	0.16
	Genotype × week × diet	< 0.05

[1]Statistical comparison with non-parametric MANOVA with *Nod2* genotype (WT/*Nod2*$^{m/m}$), urine collection time point (week 1/5/9/13/18), and diet (AIN-76A diet with/without 625 mg TiO_2/kg) as factors.

a

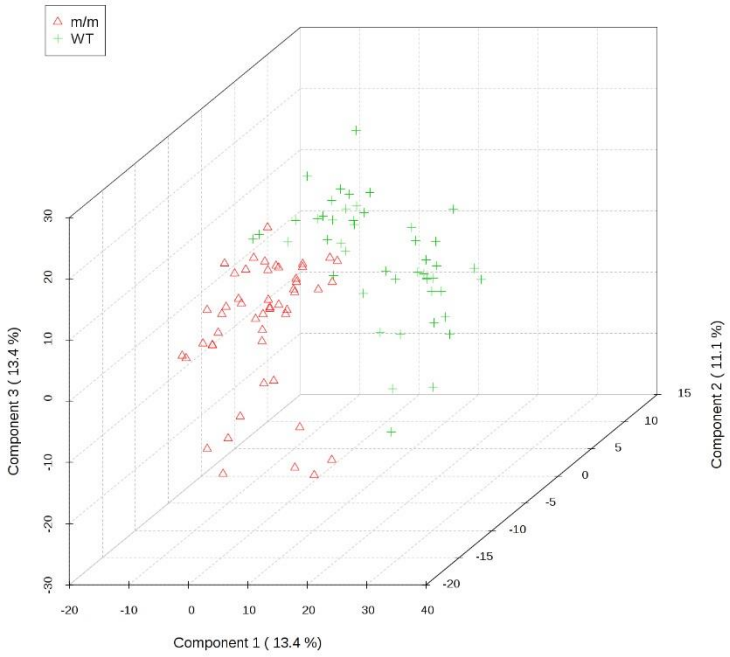

b

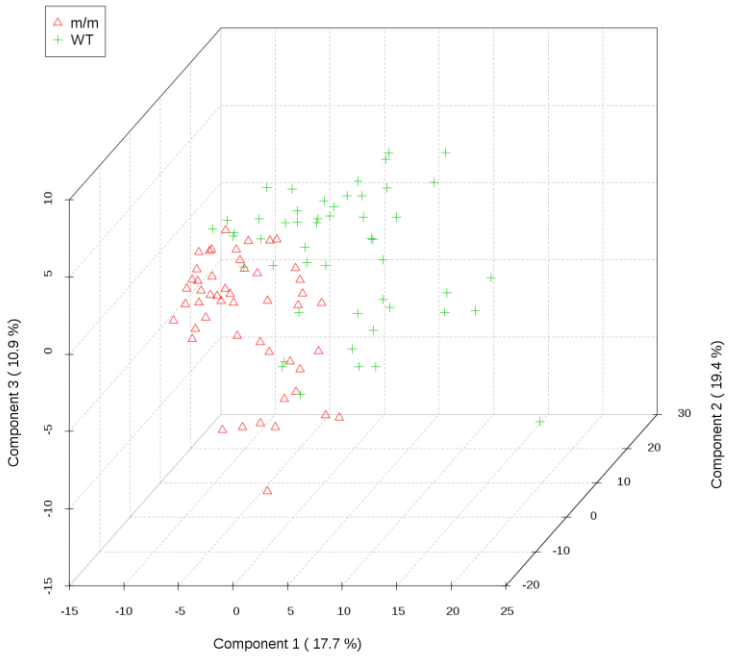

Figure 5.4 *PLS-DA plots of negative and positive ion profiles detected in urine samples from WT and* Nod2$^{m/m}$ *mice fed a diet with or without TiO_2 analysed according to* Nod2 *genotype.*

Female WT and *Nod2$^{m/m}$* (m/m) mice were fed AIN-76A rodent diet without or with 625 mg TiO_2/kg for 18 weeks. Serial urine samples were collected throughout the study from the same animals. Metabolite profiles were obtained with LC-MS. Data analysis was performed with R and MetaboAnalyst. Shown are three-dimensional PLS-DA plots of negative (**a**) and positive (**b**) discriminant ions with samples grouped according to *Nod2* genotype; n = 48/50 (WT/*Nod2$^{m/m}$* mice).

a

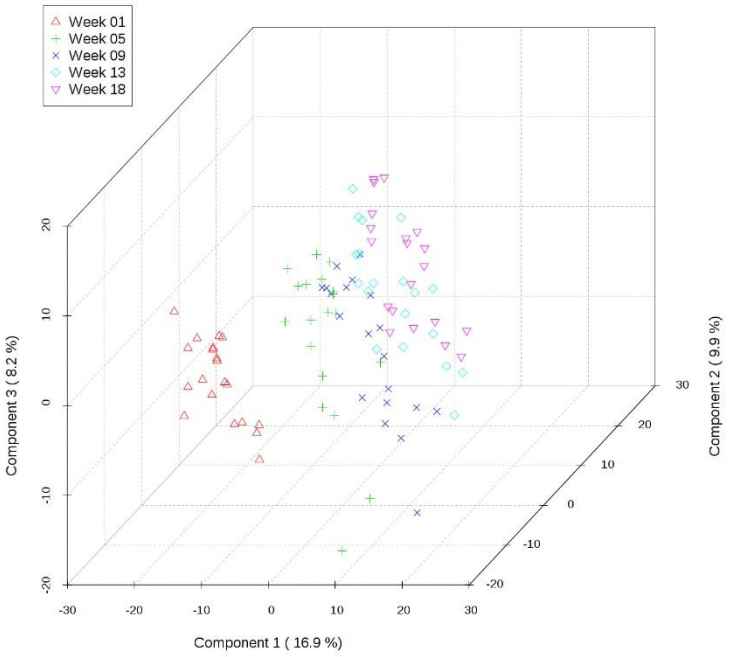

b

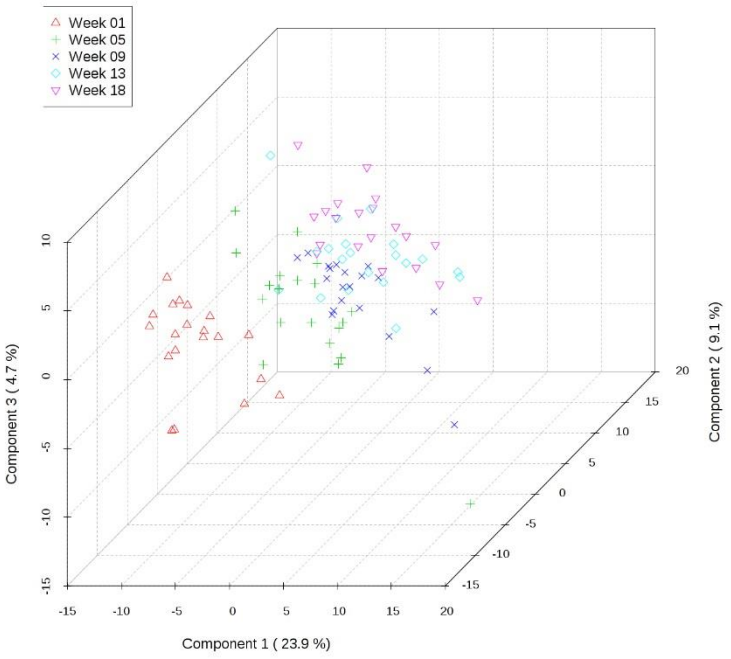

Figure 5.5 *PLS-DA plots of negative and positive ion profiles detected in urine samples from WT and* Nod2$^{m/m}$ *mice fed a diet with or without* TiO_2 *analysed according to urine collection time point.*

Female WT and *Nod2$^{m/m}$* (m/m) mice were fed AIN-76A rodent diet without or with 625 mg TiO_2/kg for 18 weeks. Serial urine samples were collected throughout the study from the same animals. Metabolite profiles were obtained with LC-MS. Data analysis was performed with R and MetaboAnalyst. Shown are three-dimensional PLS-DA plots of negative (**a**) and positive (**b**) discriminant ions with samples grouped according to urine collection time point; n = 20/19/20/19/20 (week 1/5/9/13/18).

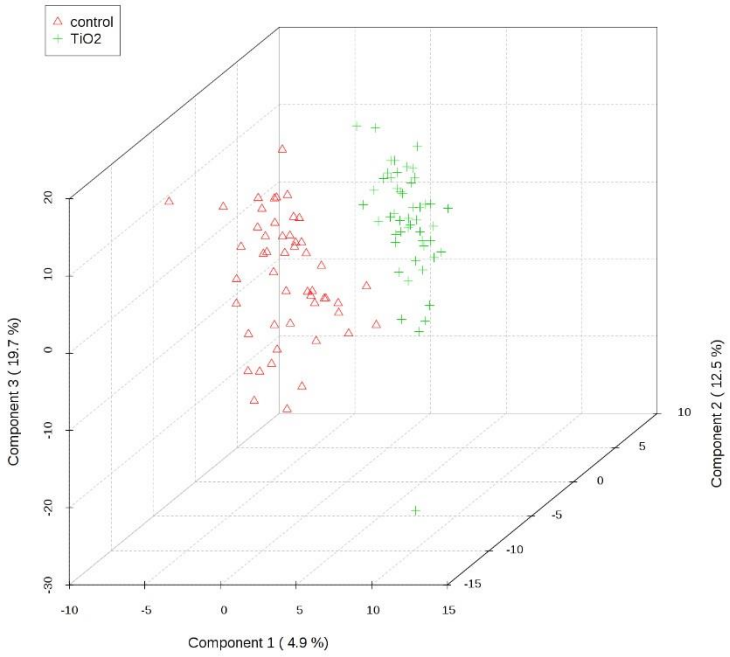

Figure 5.6 *PLS-DA plot of positive ion profiles detected in urine samples from WT and* Nod2$^{m/m}$ *mice fed a diet with or without TiO_2 analysed according to diet.*

Female WT and *Nod2$^{m/m}$* (m/m) mice were fed AIN-76A rodent diet without (control) or with 625 mg TiO_2/kg for 18 weeks. Serial urine samples were collected throughout the study from the same animals. Metabolite profiles were obtained with LC-MS. Data analysis was performed with R and MetaboAnalyst. Shown is a three-dimensional PLS-DA plot of positive discriminant ions with samples grouped according to diet; n = 48/50 (control/TiO_2 diet).

a

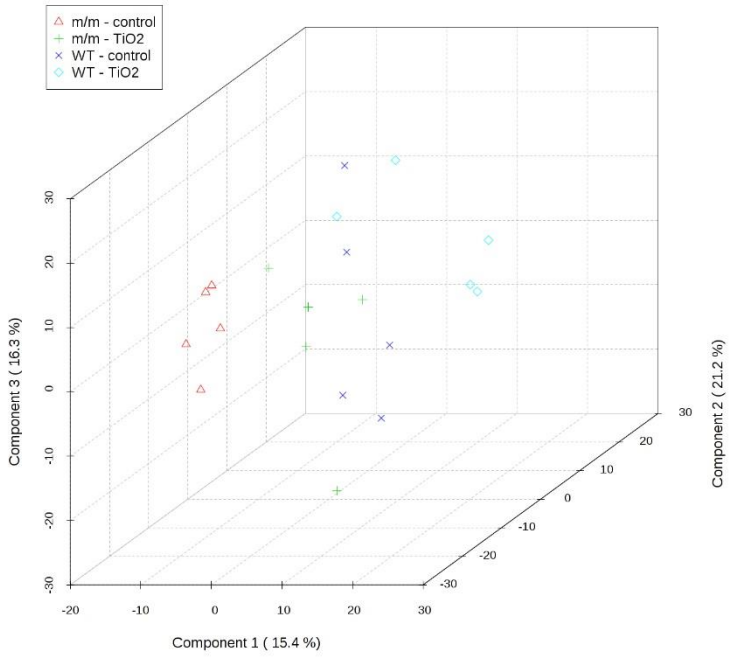

b

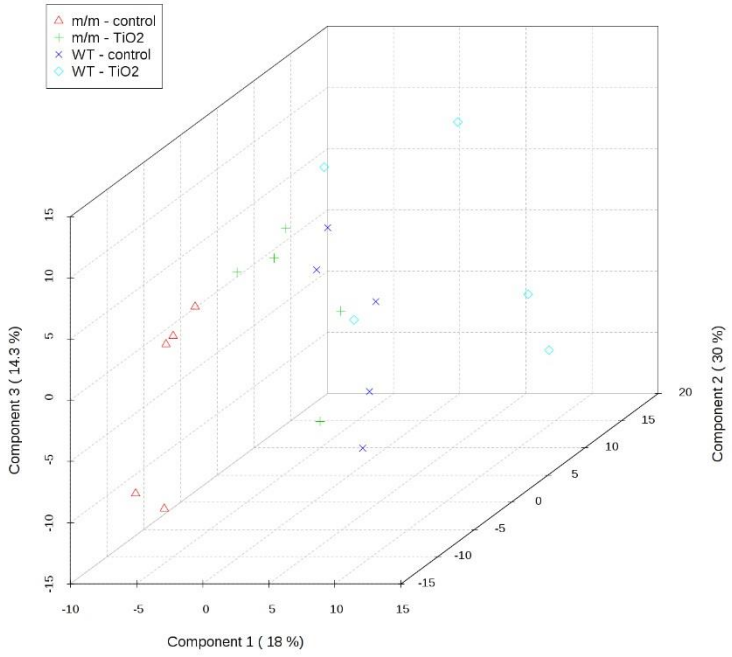

Figure 5.7 *PLS-DA plots of negative and positive ion profiles detected in urine samples from WT and* Nod2$^{m/m}$ *mice fed a diet with or without* TiO_2 *for 18 weeks analysed according to* Nod2 *genotype and diet.*

Female WT and *Nod2*$^{m/m}$ (m/m) mice were fed AIN-76A rodent diet without (control) or with 625 mg TiO_2/kg for 18 weeks. Serial urine samples were collected throughout the study from the same animals. Metabolite profiles were obtained with LC-MS. Data analysis of samples collected in week 18 was performed with R and MetaboAnalyst. Shown are three-dimensional PLS-DA plots of negative (**a**) and positive (**b**) discriminant ions with samples grouped according to *Nod2* genotype and diet; $n = 5$.

5.4.3 Discriminant ions in urine samples from wild-type mice and mice with a Crohn's disease-like *Nod2* gene variant exposed dietary titanium dioxide

The lists of discriminant ions that were responsible for the significant differences between *Nod2*$^{m/m}$ and WT mice after 18 weeks feeding of a control or TiO_2-containing diet comprised 177 negative ions and 283 positive ions. However, the number of ions from these lists that were significantly different, i.e. with an FDR less than 0.05, between the groups was much lower with 20 negative ions and 13 positive ions (Tables 5.4 and 5.5).

Pairwise comparisons showed how the levels of individual ions varied between two groups at a time. The ions detected in negative mode were affected differently by genotype and diet (Table 5.4). However, one trend was that the levels of the negative ions in urine samples from *Nod2*$^{m/m}$ mice on a control diet were significantly lower ($p < 0.05$) compared to both *Nod2*$^{m/m}$ and WT mice on a TiO_2-containing diet. In contrast, positive ions were affected more similarly by genotype and diet, and their levels were mostly significantly higher ($p < 0.05$) in urine samples from WT mice on a control diet compared to the other three groups (Table 5.5). Urine samples from WT and *Nod2*$^{m/m}$ mice on a TiO_2-containing diet had similar metabolite levels.

The results of comparisons of the detected m/z values from the significantly different discriminant ions with expected m/z values of $[M-H]^-$ metabolites and $[M+H]^+$ metabolites listed in the METLIN database are presented in Tables 5.6 and 5.7, respectively. Additionally, the detected m/z values of the significantly different discriminant ions were compared to reported m/z values of urine metabolites from the literature (Table 5.8).

Two corresponding significantly different discriminant ions were the negative ion m/z 204.0662 (Table 5.6) and the positive ion m/z 206.0811 (Table 5.7). The results of a METLIN database search suggested the same seven metabolites with close m/z values for both ions. Of those metabolites, the only two possible ones were 3-indolelactic acid and 5-methoxyindolacetic acid, both of which had expected values of m/z 204.0666 and m/z 206.0812 for the $[M-H]^-$ ion and $[M+H]^+$ ion, respectively. The reason why these two metabolites were likely candidates was that both have been previously detected in urine samples of WT mice and humans [351, 352]. Both ions are end products of tryptophan catabolism (Figure 5.8).

Table 5.4 *Significantly different negative discriminant ions in urine samples from female WT and Nod2$^{m/m}$ mice fed a diet with or without TiO_2 for 18 weeks and pairwise group comparisons.*

[M-H]⁻ ion (m/z)[2]	*Time (s)*	*WT control* - Nod2$^{m/m}$ *control*	*WT control* - *WT TiO_2*	*WT control* - Nod2$^{m/m}$ *TiO_2*	*WT TiO_2* - Nod2$^{m/m}$ *control*	*WT TiO_2* - Nod2$^{m/m}$ *TiO_2*	Nod2$^{m/m}$ *control* - Nod2$^{m/m}$ *TiO_2*
180.0296	309.2	↑[1]	n.s.	↑	n.s.	n.s.	n.s.
198.0666	348.0	↓	↓	↓	n.s.	n.s.	n.s.
202.0674	430.7	↓	n.s.	↓	↓	n.s.	n.s.
204.0662[a]	390.5	↑	↑	↑	n.s.	n.s.	n.s.
205.0695[a]	389.8	↑	↑	↑	n.s.	n.s.	n.s.
210.0770	400.0	↓	↓	n.s.	n.s.	n.s.	n.s.
230.0570	429.5	↑	n.s.	n.s.	↑	n.s.	↓
275.0963	434.7	n.s.	↓	↓	↑	n.s.	↓
291.0912	387.8	n.s.	n.s.	↑	↑	n.s.	↓
298.0504	333.0	↓	n.s.	↓	↓	n.s.	n.s.
312.0663	361.0	↓	n.s.	↓	↓	n.s.	n.s.
320.0962	283.1	n.s.	↓	↓	↑	n.s.	↓
351.2180	420.5	↑	n.s.	n.s.	↑	n.s.	↓
380.1751	341.4	n.s.	↓	↓	↑	n.s.	↓
433.2079	349.6	n.s.	↓	↓	↑	n.s.	↓
439.1613[b]	391.1	↑	↑	n.s.	↓	n.s.	n.s.
440.1646[b]	391.1	↑	↑	n.s.	↓	n.s.	n.s.
461.1096	456.1	↑	n.s.	n.s.	↑	↑	n.s.
507.2239	422.3	↑	n.s.	n.s.	↑	n.s.	↓
514.2343	373.2	↑	↑	n.s.	n.s.	n.s.	↓

[1]Significant differences obtained by pairwise comparisons of respective groups with Tukey's HSD *post-hoc* test with a significance level of $p < 0.05$; arrows indicate changes in metabolite levels of first group compared to second group of the respective pairwise comparisons: ↑ = increase; ↓ = decrease; n.s. = not significant.

[2]Same uppercase letters indicate ions are isotopes.

Table 5.5 *Significantly different positive discriminant ions in urine samples from female WT and Nod2$^{m/m}$ mice fed a diet with or without TiO_2 for 18 weeks and pairwise group comparisons.*

[M+H]$^+$ ion (m/z)[2]	*Time (s)*	*WT control* - Nod2$^{m/m}$ *control*	*WT control* - *WT TiO_2*	*WT control* - Nod2$^{m/m}$ *TiO_2*	*WT TiO_2* - Nod2$^{m/m}$ *control*	*WT TiO_2* - Nod2$^{m/m}$ *TiO_2*	Nod2$^{m/m}$ *control* - Nod2$^{m/m}$ *TiO_2*
105.0701	182.8	↑[1]	↑	↑	n.s.	n.s.	n.s.
130.0647	311.4	↑	↑	↑	n.s.	n.s.	n.s.
176.0705	371.9	↑	↑	↑	n.s.	n.s.	n.s.
206.0447	232.8	↑	↑	↑	n.s.	n.s.	n.s.
206.0811	331.5	↑	↑	↑	n.s.	n.s.	n.s.
218.0929	347.3	↑	↑	↑	↑	n.s.	↓
233.0919[a]	311.3	↑	↑	↑	n.s.	n.s.	n.s.
234.0952[a]	311.3	↑	↑	↑	n.s.	n.s.	n.s.
250.1224	372.8	↑	n.s.	↑	n.s.	n.s.	n.s.
263.1330	255.5	↑	↑	↑	n.s.	n.s.	n.s.
322.1104	237.9	↑	↓	↓	↑	n.s.	↓
384.1146	188.6	↑	↑	↑	n.s.	n.s.	n.s.
526.2928	610.8	↑	n.s.	n.s.	↑	n.s.	↓

[1]Significant differences obtained by pairwise comparisons of respective groups with Tukey's HSD *post-hoc* test with a significance level of $p < 0.05$; arrows indicate changes in metabolite levels of first group compared to second group of the respective pairwise comparisons: ↑ = increase; ↓ = decrease; n.s. = not significant.
[2]Same uppercase letter indicates ions are isotopes.

Table 5.6 *Results of the METLIN database queries for potential metabolites of negative discriminant ions.*

Detected **m/z**	***Number of ions***[1]	***Expected ions*** ***(*****m/z ± 0.0005 to detected** **m/z*****)***	***Expected*** **m/z**
180.0296	5	-	
198.0666	2	-	
202.0674	5	-	
204.0662[2]	7	Cinnamoylglycine	204.0666
		Gentianamine	204.0666
		N-(3-hydroxypropyl)phthalamide	204.0666
		3-Indolelactic acid	204.0666
		5-Methoxyindoleacetic acid	204.0666
		Methyl 1-methoxy-1H-indole-3-carboxylic acid	204.0666
		Swietendin B	204.0666
210.0770	8	Enicoflavine	210.0772
		3-O-Methyl-L-DOPA[3]	210.0772
		Methyldopa	210.0772
		3-Methoxytyrosine	210.0772
		6-Maleimidocaproic acid	210.0772
230.0570	0	n/a[3]	
275.0963	29	-	
291.0912	7	-	
298.0504	1	-	
312.0663	7	Albendazole (II)	312.0660
		Albendazole-β-hydroxysulphone	312.0660
		Albendazole-γ-hydorxysulphone	312.0660
320.0962	17	-	
351.2180	134	All 134 ions with *m/z* 351.2177	351.2177
380.1751	20	-	
433.2079	222	-	
439.1613	119	-	
461.1096	72	-	
507.2239	161	Acetyl-T2 toxin	507.2236
		Cafamarine	507.2236
		Gibberllin A37 glucosyl ester	507.2236
		Mozambioside	507.2236
514.2343	72	-	

[1]Number of $[M-H]^-$ ions returned by the METLIN database after searching for ions with similar *m/z* values by entering the detected *m/z* value with a tolerance of 0.01 Da. [2]Ion in boldface is discussed in the text. [3]Abbreviations specific for this table: DOPA = dihydroxyphenylalanine, n/a = not applicable.

Table 5.7 *Results of the METLIN database queries for potential metabolites of positive discriminant ions.*

Detected **m/z**	***Number of ions***[1]	***Expected ions*** ***(*****m/z** ***± 0.0005 to detected*** **m/z*****)***	***Expected*** **m/z**
105.0701	9	Styrene	105.0699
130.0647	6	Isoquinoline	130.0651
		3-Methylene-indolenine	130.0651
		Quinoline	130.0651
176.0705[2]	13	N-Acetylindoxyl	176.0706
		7-Amino-4-methylcoumarin	176.0706
		Gentianine	176.0706
		5-Hydroxyindoleacetaldehyde	176.0706
		Hydroxymethyl indol-3-yl keton	176.0706
		3-Hydroxy-2-methyl-1H-quinolin-4-one	176.0706
		3-Indoleacetic acid	176.0706
		3-Indoleglycolaldehyde	176.0706
		1-Methoxy-1H-indole-3-carboxaldehyde	176.0706
		2-Methylquinoline-3,4-diol	176.0706
		3-Methyl-quinolin-2,8-diol	176.0706
206.0447	2	6-Hydroxykynurenic acid	206.0448
		Xanthurenic acid	206.0448
206.0811	7	Cinnamoylglycine	206.0812
		Gentianamine	206.0812
		N-(3-hydroxypropyl)phthalamide	206.0812
		3-Indolelactic acid	206.0812
		5-Methoxyindoleacetic acid	206.0812
		Methyl 1-methoxy-1H-indole-3-carboxylic acid	206.0812
		Swietendin B	206.0812
218.0929	6	Acetylhydrazinopthalazinone	218.0924
233.0919	6	Nalidixic acid	233.0921
		Oxabetrinil	233.0921
		Phenobarbital	233.0921
250.1224	6	Cysteine lysine/lysine cysteine/lysyl-cysteine/cysteinyl-lysine	250.1220
		Lansiumamide A	250.1226
263.1330	33	-	
322.1104	17	-	
384.1146	17	Succinoadenosine	384.1150
526.2928	54	LysoPE[4](22:6(4Z,7Z,10Z,13Z,16Z,19Z)/0:0)	526.2928
		LysoPE(0:0/22:6(4Z,7Z,10Z,13Z,16Z,19Z))	526.2928
		PE(22:6(4Z,7Z,10Z,13Z,16Z,19Z)/0:0)	526.2928

[1]Number of $[M+H]^+$ ions returned by the METLIN database after searching for ions with similar m/z values by entering the detected m/z value with a tolerance of 0.01 Da. [3]Ions in boldface are discussed in the text. [4]Abbreviations specific for this table: PE = phosphoethanolamine.

Table 5.8 *Significantly different metabolites identified in studies comparing urine samples from CD patients and healthy controls, Il10$^{-/-}$ mice with intestinal inflammation and healthy WT control mice, or rats orally exposed to TiO_2 and unexposed rats.*

Comparison	***Metabolite***	***Change[1]***	***[M-H]$^-$ ion (m/z)[2]***	***[M+H]$^+$ ion (m/z)[2]***	***References***
CD patients	p-Cresol	↓	107.0502	109.0648	[327]
versus	Formate	↑	44.9982	47.0128	[327]
healthy	Hippurate	↓	178.0510	180.0655	[327]
controls	N-Methylhistamine	↑	124.0880	126.1026	[328]
Il10$^{-/-}$ *mice*	5-Aminovaleric acid	↑	116.0717	118.0863	[333]
with colitis	α-CEHC glucoronide[6]	↓	453.1761[3]	-[4]	[335]
versus	Fucose	↑	163.0669	165.0757	[332-334]
healthy	Trimethylamine	↑	58.0662	60.0808	[334]
WT mice	**Xanthurenic acid[5]**	↑	204.0302	206.0448	[332, 333, 335]
	Xanthurenic acid glucuronide	↓	380[3]	382.0774[3]	[335]
Rats after	Acetate	↑	59.0139	61.0284	[209]
oral TiO_2	Betaine	↓	16.1717	118.0863	[209]
exposure	Choline	↓	102.0924	104.1070	[209]
versus	Citrate	↑	191.0197	193.0343	[209]
unexposed rats	Citrulline	↑	174.0884	176.1030	[209]
	Hippurate	↑	178.0510	180.0655	[209]
	Histidine	↑	154.0622	156.0768	[209]
	D-3-Hydroxybutyrate	↓	103.0401	105.0546	[209]
	α-Ketoglutarate	↑	145.0142	147.0288	[209]
	Lactate	↓	89.0244	91.0390	[209]
	Leucine	↓	130.0874	132.1019	[209]
	Methionine	↓	148.0438	150.0583	[209]
	Phenylacetylglycine	↑	192.0666	194.0812	[209]
	Pyruvate	↓	87.0088	89.0233	[209]
	Taurine	↑	124.0074	126.0219	[209]
	Threonine	↓	118.0510	120.0655	[209]
	Trimethylamine-N-oxide	↑	74.0611	76.0757	[209]

[1]Arrows indicate changes in metabolite levels of first group compared to second group: ↑ = increase; ↓ = decrease. [2]Expected *m/z* values according to METLIN database. [3]Metabolite not in METLIN database, *m/z* value according to [335]. [4]No $[M+H]^+$ ion reported. [5]Metabolite in boldface is discussed in the text. [6]Abbreviations specific for this table: α-CEHC glucoronide = 2,5,7,8-Tetramethyl-2-(2'-carboxyethyl)-6-hydroxychroman glucuronide.

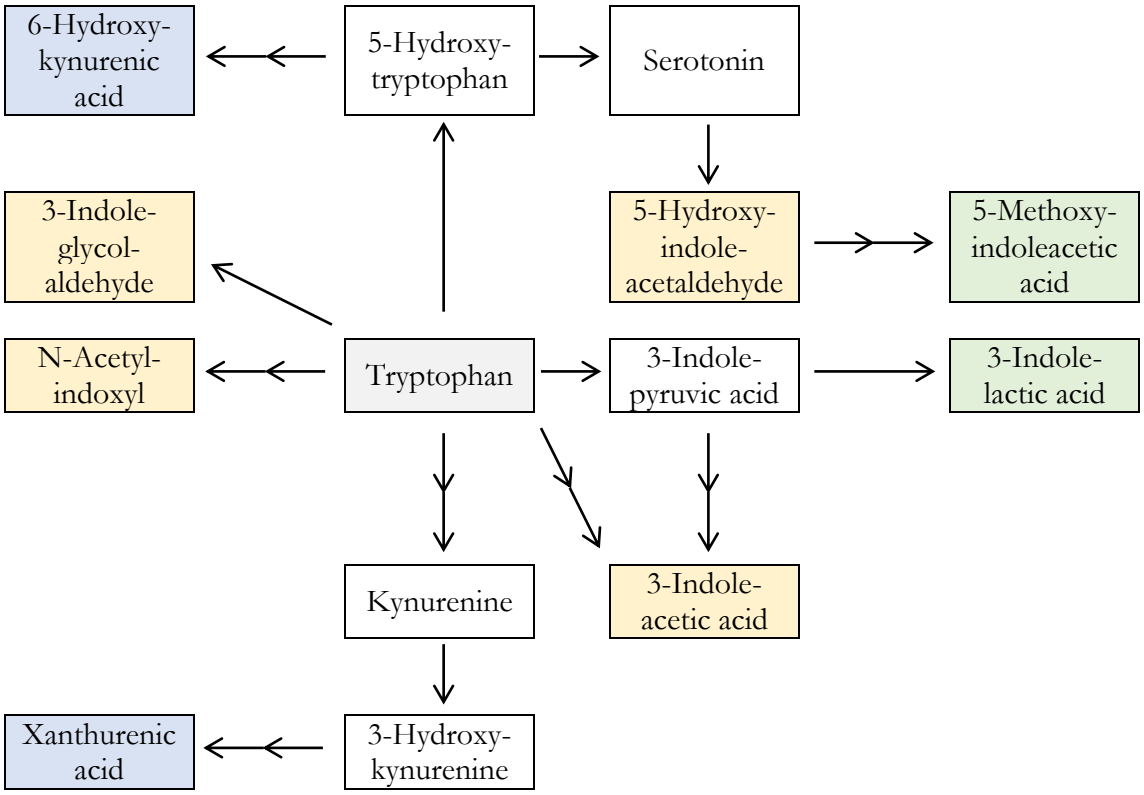

Figure 5.8 *Overview of selected tryptophan catabolism pathways.*

This diagram shows selected metabolites of several tryptophan catabolism pathways and highlights metabolites potentially corresponding to detected ions. Putative candidates for the negative ion m/z 204.0662 and the positive ion m/z 206.0811 are shaded green; putative candidates for the negative ion m/z 174.0554 and the positive ion m/z 176.0705 are shaded yellow; putative candidates of the negative ion m/z 204.0297 and the positive ion m/z 206.0447 are shaded blue. Single arrows indicate enzyme-mediated metabolite conversions; double arrows indicate enzyme-mediated metabolite conversions *via* intermediate metabolites. Pathways adapted from the Kyoto Encyclopedia of Genes and Genomes [353].

In contrast, even though the other five closely matched metabolites have the same expected m/z values as 3-indolelactic acid and 5-methoxyindolacetic acid they are not associated with the urine metabolome. Cinnamoylglycine, gentianamine, methyl 1-methoxy-1H-indole-3-carboxylic acid, and swietendin B are all phytochemical compounds derived from cinnamon (*Cinnamomum verum*), gentian (*Gentiana turkestanorum*), Japanese horseradish (*Wasabia japonica*), and mahogany (*Swietenia macrophylla*), respectively. The seventh metabolite, N-(3-Hydroxypropyl)phthalamide, is a synthetic chemical compound. Pairwise comparison of the groups showed that the levels of both the negative ion and the positive ion were significantly ($p < 0.05$) higher in WT mice on a control diet compared to the other three groups (Figure 5.9).

Another significantly different discriminant ion detected in positive mode with the m/z value 176.0705 (Table 5.7) had a corresponding negative ion at m/z 174.0554. However, the FDR of the negative ion was greater than 0.05, therefore it does not appear in the list of discriminant ions obtained in negative mode (Table 5.4). The same list of 13 metabolites was obtained after conducting a search in the METLIN database with these two detected m/z values, which indicated that both ions could indeed correspond to the same metabolite. Four of the matching $[M+H]^+$ metabolites, namely N-acetylindoxyl, 5-hydroxyindoleacetaldehyde, 3-indoleacetic acid, and 3-indoleglycolaldehyde had expected m/z values of 176.0706, and they were all metabolites of tryptophan catabolism (Figure 5.8).

Seven other $[M+H]^+$ metabolites also had expected values of m/z 176.0706. These were 7-amino-4-methylcoumarin, an antibacterial and antifungal compound isolated from the fungus *Xylaria sp.*, hydroxymethyl indol-3-yl ketone, an alkaloid produced by the fungus *Lactarius deliciosus*, 3-hydroxy-2-methyl-1H-quinolin-4-one, a microbial quinoline derivate, and 1-methoxy-1H-indole-3-carboxaldehyde and gentianine, which are phytochemical compounds found in root vegetables and blue gentian (*Gentiana acaulis*), respectively. It was not possible to find out the source for two metabolites, 3-methyl-quinolin-2,8-diol and 2-methylquinoline-3,4-diol, but queries of the human metabolome database indicated that these two metabolites have not been detected in urine samples before. The remaining two metabolites obtained by the database search had expected m/z values that differed by more than 0.0005 from the m/z values of the detected ions. The level of the positive ion m/z 176.0705 was significantly higher ($p < 0.05$) in urine samples from WT mice on a control diet compared to all other groups, and urine samples from WT mice on a control diet had a significantly increased ($p < 0.05$) level of the negative ion m/z 174.0554 compared to $Nod2^{m/m}$ mice on a control diet (Figure 5.10).

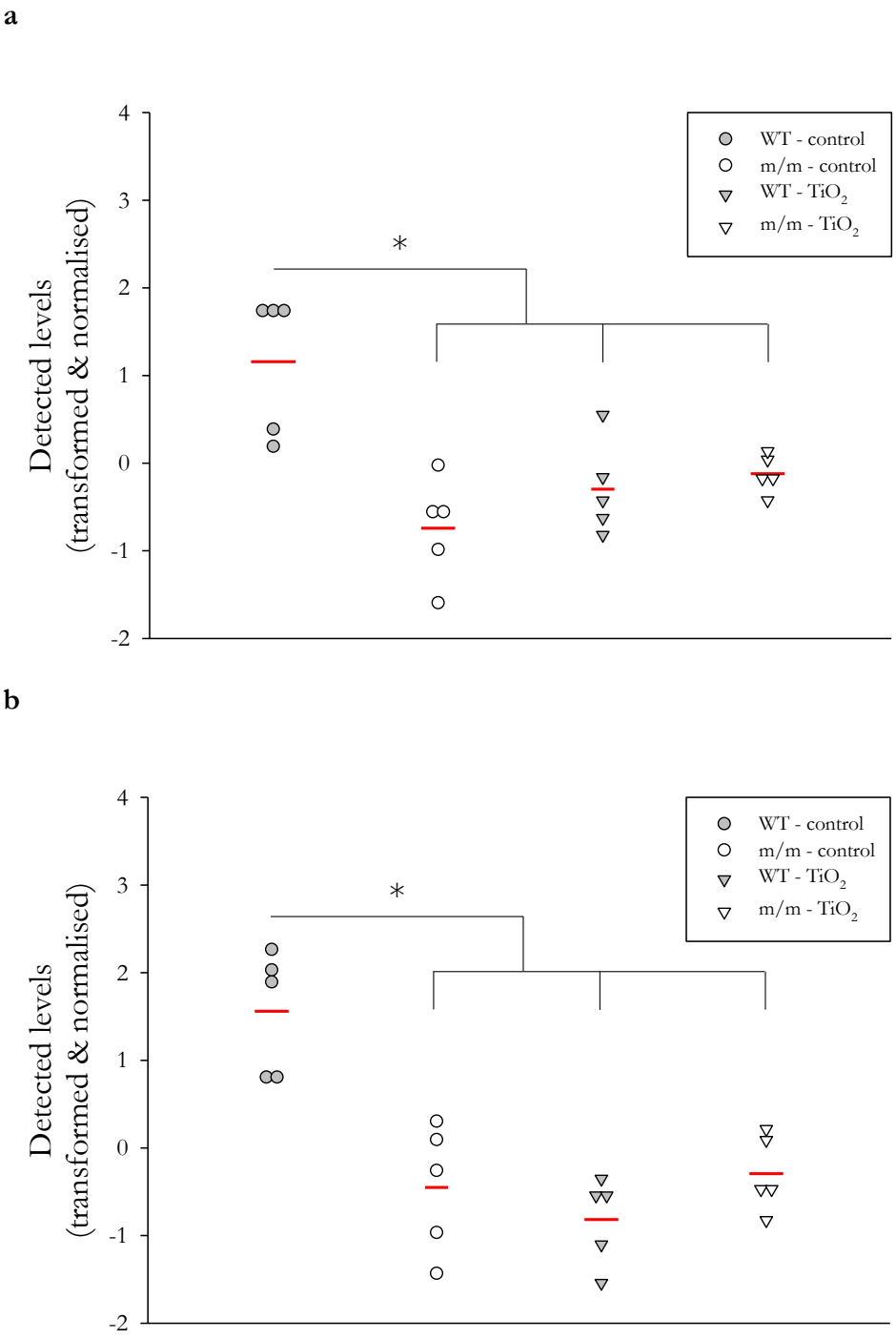

Figure 5.9 *Comparisons of the levels for the negative ion* m/z *204.0662 and the positive ion* m/z *206.0811 detected in urine samples from WT and* Nod2$^{m/m}$ *mice fed a diet with or without* TiO_2.

Female WT and *Nod2*$^{m/m}$ (m/m) mice were fed a diet without (control) or with TiO_2 for 18 weeks. Urine samples were collected in week 18. Metabolite profiles were obtained with LC-MS. Data analysis was performed with R and discriminant ions were identified with MetaboAnalyst. Data were normalised by median and transformed logarithmically. Levels of the negative ion *m/z* 204.0662 (**a**) and the positive ion *m/z* 206.0811 (**b**) of each individual mouse were plotted according to group; means are indicated by red lines; $n = 5$. Results were compared with one-way ANOVA. Pairwise group comparisons with Tukey's HSD test; $*p < 0.05$.

a

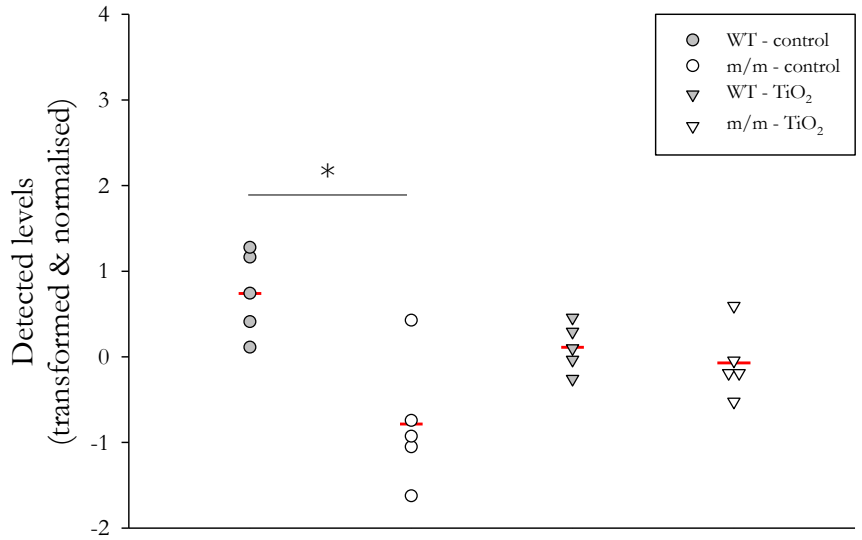

b

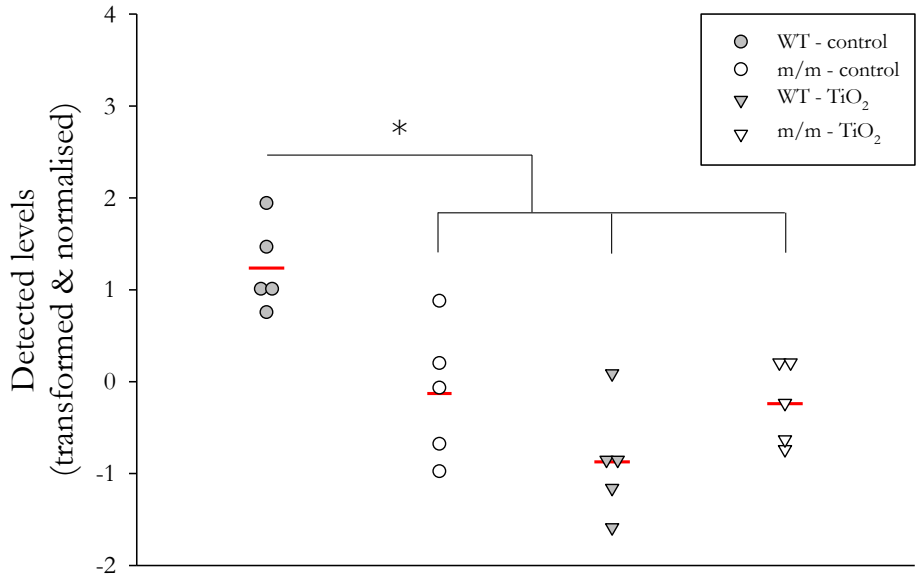

Figure 5.10 *Comparisons of the levels for the negative ion* m/z *174.0554 and the positive ion* m/z *176.0705 detected in urine samples from WT and* Nod2$^{m/m}$ *mice fed a diet with or without* TiO_2.

Female WT and *Nod2*$^{m/m}$ (m/m) mice were fed a diet without (control) or with TiO_2 for 18 weeks. Urine samples were collected in week 18. Metabolite profiles were obtained with LC-MS. Data analysis was performed with R and discriminant ions were identified with MetaboAnalyst. Data were normalised by median and transformed logarithmically. Levels of the negative ion m/z 174.0554 (**a**) and the positive ion m/z 176.0705 (**b**) of each individual mouse were plotted according to group; means are indicated by red lines; $n = 5$. Results were compared with one-way ANOVA. Pairwise group comparisons with Tukey's HSD test; $*p < 0.05$.

A query of the METLIN database for the positive ion m/z 206.0447 showed that only two $[M+H]^+$ metabolites, namely xanthurenic acid and 6-hydroxykynurenic acid, had expected m/z values similar to the detected m/z value that fitted the search criteria (Table 5.7). Both compounds are products of tryptophan catabolism (Figure 5.8).

An elevated level of xanthurenic acid in urine was previously described for *Il10*$^{-/-}$ mice with intestinal inflammation (Table 5.8). However, in the present study the level of the positive ion m/z 206.0447 was significantly higher in urine samples from WT mice on a control diet compared to all three other groups (Table 5.5 & Figure 5.11). A corresponding negative ion with a detected m/z value of 204.0297 was also present in the general list of discriminant negative ions, but its FDR value was greater than 0.05. The corresponding $[M-H]^-$ metabolites to this ion were again xanthurenic acid and 6-hydroxykynurenic acid, both of which had expected m/z values of 204.0302 according to the METLIN database. Pairwise group comparison of this ion showed that its level was only significantly ($p < 0.05$) higher in urine from WT mice on a control diet compared to *Nod2*$^{m/m}$ mice on a control diet.

Several fragments of xanthurenic acid have been identified previously [335]. To narrow down the choice between xanthurenic acid and 6-hydroxykynurenic acid further, the lists of negative and positive discriminant ions have been screened for these xanthurenic acid fragments. In the general list of negative discriminant ions one of the fragments was present. Its m/z value was 160.0408 and it had the same retention time (285.4 s) as the potential negative ion for xanthurenic acid with the m/z value 204.0297. The level of this ion was significantly ($p < 0.05$) higher in urine from WT mice compared to both groups of *Nod2*$^{m/m}$ mice.

No further detailed metabolite comparisons were undertaken with the remaining discriminant ions where the m/z values of the matched metabolites had a difference greater than 0.0005. In cases in which the m/z values differed by less than 0.0005 from detected m/z values, but there were no corresponding molecules of the opposite ionisation mode in the complete list of discriminant ions, no further comparisons were carried out either.

None of the identified metabolites in urine of rats that were orally exposed to TiO_2 were detected in this study based on the reported m/z values for the respective $[M-H]^-$ ions or $[M+H]^+$ ions (Table 5.8).

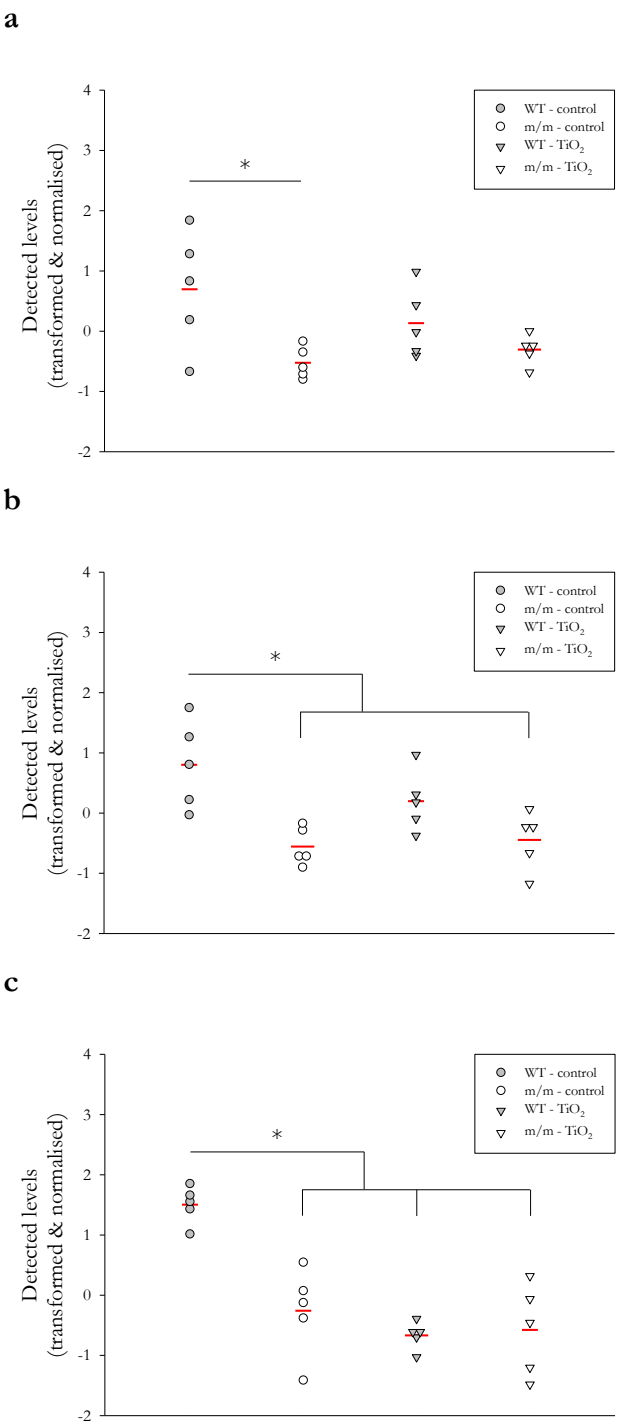

Figure 5.11 *Comparisons of the levels for the negative ions* m/z *204.0297 and* m/z *160.0408 and the positive ion* m/z *206.0447 detected in urine samples from WT and* $Nod2^{m/m}$ *mice fed a diet with or without* TiO_2.

Female WT and *Nod2*$^{m/m}$ (m/m) mice were fed a diet without (control) or with TiO_2 for 18 weeks. Urine samples were collected in week 18. Metabolite profiles were obtained with LC-MS. Data analysis was performed with R and discriminant ions were identified with MetaboAnalyst. Data were normalised by median and transformed logarithmically. Levels of the negative ions *m/z* 204.0297 (**a**) and *m/z* 160.0408 (**b**) and the positive ion *m/z* 206.0447 (**c**) of each individual mouse were plotted according to group; means are indicated by red lines; $n = 5$. Results were compared with one-way ANOVA. Pairwise group comparisons with Tukey's HSD test; $*p < 0.05$.

5.5 Discussion

5.5.1 Reassessment of the hypothesis

The results presented in this chapter support the hypothesis that dietary TiO_2 particle uptake in the intestine leads to systemic metabolic changes. In the second *in vivo* study, the urine levels of several metabolites were different between WT mice on a control diet and WT mice on a TiO_2-containing diet. The urine metabolite profiles were also distinct between *Nod2*$^{m/m}$ mice regardless of the type of diet and WT mice on a control diet.

5.5.2 Considerations about the factors of the statistical analyses

The results of the first *in vivo* study showed that females and males can be clearly distinguished based on their metabolite profiles, and this separation was irrespective of diet (Table 5.2). This confirmed the results of a previous study in which urine samples from female and male WT mice of the Alpk:ApfCD strain were analysed with LC-MS [354]. The observed differences between urine metabolite profiles of female WT mice seemed to reflect differences in the metabolism of mice over time. A difference between urine collection time points was also noticed in the second *in vivo* study in which the samples from the first urine collection time point could be clearly distinguished from the samples collected at the other time points (Figure 5.5). It should be stressed that the samples from the first *in vivo* study represented terminal urine samples collected immediately before tissue collection whereas the samples from the second *in vivo* study were serial urine samples collected every four weeks from the same animals. Differences between time points of serial urine samples have been described in a metabolomics study with *Il10*$^{-/-}$ and WT mice [332]. Previous studies have shown that urine metabolic profiles could also be separated depending on the time of the day at which they were collected [332, 354]. During both the first and second *in vivo* study, the urine samples were collected at approximately the same time of the day in a randomised order. Therefore, it is unlikely that variations in metabolite concentrations during the day had any influence on observed variations in urine metabolite concentrations.

In the second *in vivo* study, the effects of a TiO_2-containing diet on the urine metabolite profiles of WT and *Nod2*$^{m/m}$ mice were investigated. Although no inflammation was observed by histological assessment of ileum and colon tissue sections from WT and *Nod2*$^{m/m}$ mice after TiO_2-administration (Figures 4.6-4.9), their urine metabolite profiles differed from the respective groups on a control diet (Figure 5.7).This is consistent with the findings by Bu

and colleagues who observed changes in urine and serum metabolite profiles of rats that were orally exposed to TiO_2 despite a lack of histopathological changes in liver, heart, kidney, and brain [209].

That the first *in vivo* study did not indicate any statistical differences between metabolite profiles of mice on a control diet compared to mice on TiO_2-containing diets is not in contrast to the findings from the second *in vivo* study. It is likely that the strong influences of the factors 'sex' and 'urine collection time point' on urine metabolites obscured the more subtle effects of dietary TiO_2 particles in the first *in vivo* study.

It should be noted that metabolite concentrations in urine are variable and dependent on many factors, e.g. hydration status and recent urine output [355]. To account for such differences, in this study the data was normalised according to the median fold change method, which has been shown to be the most relevant statistical normalisation method for urine samples [341]. However, it has been suggested that several normalisation approaches should be combined for studies that compare metabolite concentrations between urine samples [355]. A commonly used method is normalisation according to creatinine levels, which correlate well to the total urine volume [355, 356]. This additional normalisation method could be applied in future metabolomics studies that compare urine metabolite profiles between different groups.

5.5.3 Dietary titanium dioxide particles and tryptophan metabolism

The urine levels of potential tryptophan metabolites were reduced in WT mice on a TiO_2-containing diet as well as in both groups of *Nod2*$^{m/m}$ mice compared to WT mice on a control diet (Figures 5.9-5.11). For animals, tryptophan is an essential amino acid which cannot be synthesised *de novo* and thus has to be taken up with the diet [357]. Therefore, a possible explanation for reduced urine levels of tryptophan metabolites would be a reduced food intake by the groups with lower potential tryptophan metabolites. Indeed, WT and *Nod2*$^{m/m}$ mice on the TiO_2-containing diet had lower food intakes than WT and *Nod2*$^{m/m}$ mice on the control diet (Table 4.1). There was no difference between the food intakes of WT and *Nod2*$^{m/m}$ mice when the mice were compared according to 'genotype', yet the levels of the investigated ions were always reduced in *Nod2*$^{m/m}$ mice. Therefore, it seems unlikely that reduced food intake is the reason for the observed decrease in potential tryptophan metabolites. Another reason could be that the tryptophan metabolism was reduced in WT

mice fed a TiO_2-containing diet and both groups of *Nod2*$^{m/m}$ mice because of either an increased requirement of tryptophan for protein biosynthesis or malabsorption of amino acids in the gastrointestinal tract [320]. Interestingly, it has been observed that IBD patients had higher concentrations of amino acids in faecal extracts compared to healthy controls [324, 325].

Apart from its function as an amino acid for protein biosynthesis, tryptophan is also the precursor molecule for several metabolites, including the neurotransmitter serotonin (Figure 5.8). Another tryptophan-derived metabolite is kynurenine, which is synthesised by indoleamine 2,3-dioxygenase in many tissues in response to pro-inflammatory stimuli [358]. Kynurenine and several of its metabolites, including xanthurenic acid, have important functions in the regulation of the immune response, e.g. induction of apoptosis in Th1 cells and generation of regulatory T cells [357, 359, 360]. An increased urine level of xanthurenic acid was positively correlated with an increased amount of kynurenine in the plasma of *Il10*$^{-/-}$ mice [332]. Thus, a potential decrease in xanthurenic acid in WT mice on a TiO_2-containing diet or *Nod2*$^{m/m}$ mice could indicate a decrease in kynurenine and kynurenine metabolites. This decrease might disturb immune homeostasis, and specifically the induction of immune tolerance, after pro-inflammatory stimuli in these cases.

Different mechanisms might be involved in TiO_2-exposed WT and *Nod2*$^{m/m}$ mice that would lead to a reduction of the potential tryptophan metabolites. DCs are the main cell type responsible for T cell tolerance induction *via* kynurenine metabolites [357]. As shown earlier in this dissertation, DCs are also the cells that take up TiO_2 particles in PPs (Section 3.4.5; Figure 3.19). It is possible that this uptake of TiO_2 particles has an impact on intracellular biochemical pathways, including the tryptophan metabolism. Oral TiO_2 exposure affected serum and urine levels of several amino acids in rats [209]. However, Bu and colleagues did not observe an effect on tryptophan or tryptophan metabolites. A possible explanation for the reduction of tryptophan metabolites in *Nod2*$^{m/m}$ mice would be a defect in cellular processes of APCs from these mice. For example, BMDM cells from *Nod2*$^{m/m}$ mice produced more IL-1β in response to MDP [131]. As mentioned in the paragraph above, kynurenine and its metabolites are involved in the induction of regulatory T cells. Barreau and co-workers have shown that *Nod2*$^{-/-}$ mice have fewer $CD4^+$ T cells in PPs [304]. Although this has not been investigated in detail by Barreau and colleagues, it is likely that these $CD4^+$ T cells comprise regulatory T cells. Therefore, it can be speculated that a decrease in regulatory T cells in the GALT is due to a decrease in tryptophan metabolites.

5.5.4 Metabolomics studies of mouse models for inflammatory bowel disease

Metabolomics studies with *Il10*$^{-/-}$ mice with colonic inflammation have shown that the level of xanthurenic acid was increased in the urine of this mouse model for IBD [332, 333, 335]. This finding is in line with observations that colonic gene expression of indoleamine 2,3-dioxygenase and the plasma level of kynurenine were increased in patients with CD [361, 362]. In contrast, in this study the decrease of a metabolite that could be xanthurenic acid was observed in the urine of *Nod2*$^{m/m}$ mice compared to WT mice (Table 5.7 & Figure 5.11). This finding would indicate that the metabolite profiles of *Nod2*$^{m/m}$ mice do not correspond to those of CD patients. However, no study has yet been carried out to compare the level of xanthurenic acid in urine samples from CD patients and healthy controls, but it has been reported that the plasma level of xanthurenic acid was similar between CD patients and healthy controls [361].

Of note, there were no differences in the urine levels of the investigated discriminant ions between *Nod2*$^{m/m}$ mice on a control diet compared to *Nod2*$^{m/m}$ mice on a TiO_2-containing diet (Figures 5.9-5.11) although a separation based on genotype and diet was observed in the PLS-DA plots (Figure 5.7). The separation of the two *Nod2*$^{m/m}$ mice groups in the PLS-DA plots was due to discriminant ions that did not correspond to metabolites from the METLIN database or previous metabolomics publications (Tables 5.4 & 5.5).

It has been shown that different WT mouse strains have differences in their urine metabolite profiles [354]. Some of the observed differences in urine metabolites of *Il10*$^{-/-}$ mice have also been ascribed to differences between mouse strains rather than the effect of intestinal inflammation [333]. Originally, *Il10*$^{-/-}$ mice were created with embryonic stem cells from the WT mouse strain 129P2, and they were backcrossed later with C57BL/6 WT mice. However, the region flanking the modified *Il10* gene remained of 129P2 origin, and exerted influence on the phenotype of *Il10*$^{-/-}$ mice [363]. Several of the urine metabolites that discriminated *Il10*$^{-/-}$ from WT mice have been associated with genes from the flanking region of the *Il10* gene [333]. It is unlikely that a similar strain influence might underline the observed differences between urine metabolic profiles of WT and *Nod2*$^{m/m}$ mice on a control diet because *Nod2*$^{m/m}$ mice have originally been created on a C57BL/6 background.

5.5.5 Conclusion

Overall, the results from the second *in vivo* study showed that uptake of dietary TiO_2 particles can have an effect on the urine metabolomes of WT and *Nod2*$^{m/m}$ mice, and these changes can be assessed by metabolomics.

The next steps in the metabolomics analysis workflow would be to perform targeted tandem mass spectrometry on selected samples from the second *in vivo* study with high levels of the metabolites of interest and of commercial standards for the respective metabolites (Figure 5.1) [329]. The data from the samples could then be compared side-by side with the mass spectra of the commercial standard samples, in this case the various tryptophan catabolites. Thus, the investigated discriminant ions could be identified unequivocally with this procedure.

Furthermore, the samples from these two studies or additional samples from future studies in which mice were fed dietary TiO_2 could be analysed with additional metabolomics platforms, e.g. GC-MS and NMR. The advantage of including more analytical techniques would be to cover a wider range of metabolites that cannot be detected with LC-MS, e.g. lipids [337].

In addition, the metabolites of other sample types, like plasma or faeces, could be investigated in future studies to obtain a more complete picture of the metabolic pathways on the level of the whole organism that might be affected by dietary TiO_2 intake. The results obtained from such studies might be useful in the assessment of biomarkers that would be indicative of metabolic changes as a reaction to intestinal uptake of dietary TiO_2 particles.

Chapter 6 General discussion

6.1 Summary of the main findings

The purpose of this dissertation was to elucidate a potential connection between exogenous TiO_2 particles and the development of intestinal inflammation in WT and *Nod2*$^{m/m}$ mice. The *Nod2*$^{m/m}$ mouse model was used to investigate if such a connection would be relevant in the presence of a *Nod2* mutation that is similar to the most common *NOD2* variant associated with CD.

In Chapter 2 it has been demonstrated that food-grade TiO_2 particles were taken up by cultured BMDMs from WT and *Nod2*$^{m/m}$ mice, and this led to macrophage activation and secretion of pro-inflammatory IL-1β in a concentration dependent manner. Moreover, TiO_2 exposure together with the bacterial cell wall components MDP and PGN induced an increased release of IL-1β compared to incubation with TiO_2 particles in TCM alone, but no such effect on TNF-α secretion was observed. Therefore, food-grade TiO_2 particles seem to specifically induce the production of IL-1β *in vitro*.

In the first *in vivo* study, described in Chapter 3, the uptake of dietary TiO_2 particles in PPs from the ileum of WT mice was examined. The immune cell composition of PPs was not affected by feeding TiO_2 diets although a large number of particles could be observed in PPs from mice exposed to the highest TiO_2 dose. The particles accumulated primarily in the SED where they could be observed within DCs that are abundantly present in this PP area. Furthermore, TiO_2 particles were also observed in MLNs. Therefore, intake of exogenous dietary TiO_2 particles leads to the uptake of those particles in GALT by APCs, which are crucial for the maintenance of intestinal homeostasis.

In the second *in vivo* study, described in Chapter 4, it has been shown that *Nod2*$^{m/m}$ mice did not develop intestinal inflammation either spontaneously or in response to dietary TiO_2. In line with the observations from WT mice, TiO_2 particles were present in the SED areas of ileal PPs from *Nod2*$^{m/m}$ mice, but not in the small intestinal mucosa. However, the number of TiO_2 particles in PPs was lower in *Nod2*$^{m/m}$ mice compared to WT mice. Therefore, TiO_2 particles would have had less of an effect on intestinal homeostasis in *Nod2*$^{m/m}$ mice than in WT mice on quantitative grounds.

In Chapter 5 the metabolite profiles of urine samples from WT and *Nod2*$^{m/m}$ mice collected during the first and second *in vivo* studies were assessed with LC-MS. No differences between the groups of female and male WT mice were observed in the first *in vivo* study. In the second *in vivo* study, there was an effect of genotype, urine collection time point, and diet on the

detected metabolite levels of female WT and *Nod2*$^{m/m}$ mice. Specifically, potential products of the tryptophan catabolism decreased in WT mice on a TiO_2-containing diet compared to WT mice. Therefore, gastrointestinal uptake of dietary TiO_2 particles has effects on the metabolism of WT and *Nod2*$^{m/m}$ mice that can be detected through the assessment of metabolite profiles in urine samples.

6.2 General discussion

6.2.1 Exposure of cultured macrophages to titanium dioxide

The purpose of the experiments described in Chapter 2 with BMDMs from WT and *Nod2*$^{m/m}$ mice was to determine how these phagocytic immune cells would respond to treatment with food-grade TiO_2 particles with or without additional co-stimulation with the Nod2 ligands MDP and PGN. Previous studies that examined the distribution of TiO_2 particles in human intestinal tissues have shown that the cells which contained TiO_2 particles were macrophages at the base of PPs in the ileum [56, 147, 162].

Effects of TiO_2 particles on cell line-derived human and murine macrophages have been investigated in previous studies (see Table 1.5). Although the impact of TiO_2 particles on primary murine macrophages has not yet been examined, the effects of TiO_2 particles on cytokine production and phagocytosis of primary human macrophages derived from PBMCs has been assessed. Butler and co-workers showed that TiO_2 particle uptake by PBMC-derived macrophages was positively correlated with increasing TiO_2 concentration [218], and this result was confirmed in this study (Figure 2.8). Butler and colleagues also detected increased amounts of TNF-α after incubation with food-grade TiO_2 particles, but they did not examine the expression of activation markers or the production of IL-1β.

However, an earlier study by Powell and colleagues has shown that LPS-treated human PBMCs secreted increased amounts of IL-1β after TiO_2 incubation [216]. Elevated intestinal levels of IL-1β are a characteristic feature of CD [44, 45, 364]. In this study, it has been shown that food-grade TiO_2 particles also induced the secretion of IL-1β by macrophages from WT mice, which was even more pronounced in BMDMs derived from *Nod2*$^{m/m}$ mice (Figure 2.13).

6.2.2 Inflammasome-mediated secretion of interleukin-1β

The secretion of IL-1β is a tightly regulated multi-step process. Initially, a precursor form of IL-1β, pro-IL-1β, is produced that is subsequently processed to mature IL-1β by inflammasomes [365]. Inflammasomes are multi-protein complexes that are located in the cytoplasm. Several types of inflammasomes have been characterised so far. Typically, they consist of a protein belonging to the NLR family, the adaptor protein apoptosis-associated speck-like protein containing a CARD (ASC), and caspase-1 [223].

One of the best characterised inflammasomes to date is the NLRP3 inflammasome. The domain architecture of NLRP3 is similar to that of NOD2, which is also a member of the NLR family, with a central nucleotide-binding oligomerisation domain and a carboxy-terminal LRR. In contrast to NOD2, however, NLRP3 contains an amino-terminal pyrin domain [366]. ASC interacts with NLRP3 *via* its pyrin domain and links it to caspase-1, a cysteine protease [367]. Activation of caspase-1 by inflammasome assembly is necessary for the formation of mature IL-1β from pro-IL-1β [221].

In the context of this study, it is of interest that *NLRP3* has recently been described as a susceptibility gene for CD [368]. Unlike mutations in *NOD2*, however, the most prevalent *NLRP3* allele among humans has been described as a risk factor for the development of CD. It has been hypothesised that the presence of SNPs in the *NLRP3* gene were protective factors because they lead to a decrease in NLRP3 inflammasome activity. Consistent with this finding, it has been observed that *NLRP3* gene expression was increased in the mucosa from CD patients and colons from mice with chemically induced colitis [368]. These findings suggested that NLRP3 inflammasome activity and subsequent IL-1β release play an important role in the development of intestinal inflammation.

The NLRP3 inflammasome can be activated by exogenous factors, such as microbial products or viruses, or by endogenous signals that occur during injury and metabolic stress, e.g. high concentrations of extracellular ATP or glucose [223, 369]. It also has been shown that the NLRP3 inflammasome can be activated by various particulate substances, including gout-associated uric acid crystals [370], silica [371-373], asbestos [371], and calcium phosphate particles [374]. The secretion of IL-1β by human and mouse macrophages and DCs after incubation with TiO_2 particles *in vitro* has also been ascribed to NLRP3 activation [260, 373]. Additionally, intranasal administration of TiO_2 caused pulmonary inflammation with elevated levels of pro-inflammatory cytokines, including IL-1β [373]. Therefore, it is likely that activation of the NLRP3 inflammasome also plays a part in the

secretion of IL-1β by BMDMs after incubation with TiO_2 [222]. This possibility should be investigated further in future studies, e.g. by measuring IL-1β secretion of cells obtained from mice deficient in either Nlrp3, Asc, or caspase-1 after stimulation with TiO_2 particles.

How the NLRP3 inflammasome is activated by so many different signals is currently still unclear. Suggested mechanisms include potassium efflux through the purinergic receptor P2X ligand-gated ion channel [375, 376], lysosomal damage [372], and generation of ROS [371]. However, these mechanisms might not be mutually exclusive and several signals might be required for NLRP3 activation [220, 223, 369]. It would be interesting to study the mechanisms for TiO_2-induced IL-1β release in more detail in the future.

Furthermore, it has also shown that the NLRP3 inflammasome can be activated by MDP [377]. Thus, MDP seems to have a dual role in regulating IL-1β synthesis. First, detection of MDP by NOD2 initiates the transcription of pro-IL-1β *via* the NF-κB pathway, and subsequently mature IL-1β is produced upon MDP-mediated activation of NLRP3 [259, 378]. Moreover, it has been suggested that the expression of NLRP3 is dependent on NF-κB [379]. Therefore, NLRP3 inflammasome activity could additionally be regulated indirectly by MDP and NOD2. Thus, facilitated delivery of MDP that is conjugated to TiO_2 particles might increase both pro-IL-1β and NLRP3 production through the activation of the NOD2 and NF-κB pathway. As cells from *Nod2*$^{m/m}$ mice show increased secretion of IL-1β in response to MDP [131] and TiO_2 + MDP/PGN as demonstrated in this study (Figure 2.13), it might be possible that the transcription of *NLRP3* mRNA is increased under these circumstances. This could be investigated with quantitative real-time polymerase chain reaction in further studies.

In addition to NOD2 and NLRP3, it has been shown that MDP is also sensed by NLRP1, another NLR family member that is involved in inflammasome formation [380]. In contrast to NLRP3, NLRP1 contains an additional carboxy-terminal CARD domain in addition to the amino-terminal pyrin domain. Therefore, it can activate caspase-1 independently of ASC. Engagement of the NLRP1 inflammasome also leads to release of IL-1β, but the physiological role of MDP-sensing by NLRP1 is still under debate [381]. It has also been suggested that NLRP1 and NOD2 can interact through their CARDs, and this activation is responsible for MDP-induced IL-1β processing by the NLRP1 inflammasome [253]. These studies suggest that intracellular MDP might be recognised by more proteins than just NOD2, and this could contribute to the increased pro-inflammatory response in conjunction with TiO_2 exposure *in vitro*.

6.2.3 Other cytokines and chemokines associated with Crohn's disease

TNF-α and IL-17 are other important pro-inflammatory cytokines that are elevated in the mucosa of CD patients [44, 251]. Secretion of TNF-α by murine BMDMs and IL-17 by human PBMCs after exposure to food-grade TiO_2 particles with or without MDP/PGN co-stimulation was also investigated in the experiments described in Chapter 2 (Figures 2.12 & 2.15). However, many more cytokines have been implicated in CD that either enhance or suppress immune function [43, 382].

In addition to IL-1β and TNF-α, APCs secrete the pro-inflammatory cytokines IL-6, IL-12, IL-18 and IL-23. Effector T cells of the Th1 lineage also produce TNF-α and IL-6, and additionally IFN-γ, which activates macrophages and induces epithelial cell death [31]. In contrast, Th17 cells produce IL-17 and IL-21, which have mainly pro-inflammatory effects [41, 383]. However, they also secrete IL-22 which may exert beneficial effects on the epithelial barrier [384]. Furthermore, regulatory T cells are abundant in the intestinal mucosa where they secrete the anti-inflammatory cytokine IL-10 [385]. They are also present in the mucosa of CD patients [386]. However, it seems that the anti-inflammatory function of regulatory T cells in the mucosa of CD patients is insufficient compared to the increased activity of effector Th cells [382].

It would be of interest to study the secretion of additional cytokines with relevance for intestinal homeostasis after stimulation of primary immune cells with TiO_2 particles *in vitro*. Both pure cultures of primary APCs, like murine BMDMs, as well as mixed immune cell populations, like human PBMCs, could be used for such experiments. For example, Ashwood and colleagues have shown that co-stimulation of PBMCs with TiO_2 particles and LPS enhanced the release of IL-6 [215].

Chemokines are another class of molecules that are important in the regulation of the immune system by directing the recruitment of immune cells to specific sites in tissues [387]. Therefore, they play a crucial role in the maintenance of intestinal homeostasis in addition to cytokines. Ashwood and colleagues have also investigated the release of two chemokines, namely MIP-1α and MCP-1, by TiO_2-treated PBMCs with LPS co-stimulation [215]. The production of MIP-1α was increased and the secretion of MCP-1 decreased after TiO_2 + LPS stimulation. These somewhat contradictory results highlight the need for further studies about the relationship between TiO_2 exposure, with or without additional co-stimulation with bacterial antigens, and the induction of chemokines by immune cells.

6.2.4 Advantages of research with animal models

Despite important insights that can be gained from *in vitro* and *ex vivo* TiO_2-stimulation assays of immune cells, there are nevertheless limitations in translating the results obtained from these studies to the situation of exogenous dietary particle uptake by intestinal phagocytes in humans [163].

On the other hand, it is problematic to conduct dietary intervention studies with humans to study consequences of oral TiO_2 intake on intestinal health. For example, there are many difficulties associated with the recruitment of a large number of suitable participants, like CD patients with homozygous mutations in the *NOD2* gene and age and sex matched healthy controls. Another limitation is the collection of tissue samples from participants especially if this requires invasive procedures. Therefore, animal models provide an option to study the basic principles of the effects of TiO_2 particles on intestinal health in a controlled environment *in vivo*.

Mice were used as an animal model in the studies described in Chapters 3 and 4 because they have been frequently used in studies that investigate gastrointestinal function [388, 389]. Other common animal models in nutritional research are rats, pigs, and dogs. Although all animal models have a different structure of the gastrointestinal tract compared to humans, each model can be of relevance for studying certain aspects of human gastrointestinal biology [390].

It has been suggested that pigs are the most useful model in respect to studying the function of PPs because the distribution of PPs along the small intestinal tract is more similar between pigs and humans than for example between mice and humans [391].

However, mice have several advantages over pigs as animal models especially regarding experimental costs when a large number of animals is required or the study is conducted over a long period of time. Moreover, studies with mice are logistically easier to carry out, and the handling of the animals and required manipulations, e.g. weighing, is more convenient. A further advantage of mice over other animal models is that many genetically manipulated strains are available that are deficient in specific genes or have mutations that are homologous to human mutations, such as the *Nod2*$^{m/m}$ mouse model [392]. Therefore, it is possible to study effects of specific genes or gene variants during nutritional manipulation. This is especially relevant in the context of IBD/CD in which both genetic and environmental components are important for disease development [393].

6.2.5 Limitations of mice with a Crohn's disease-like *Nod2* gene variant as a model for Crohn's disease

It has been suggested that only people with a genetic predisposition that is associated with an increased risk to develop CD, e.g. mutations in the *NOD2* gene, are affected by the exposure to exogenous dietary particles [163]. However, investigating a possible connection between CD-susceptible genotypes and the uptake of exogenous dietary particle by intestinal immune cells is difficult in humans. Therefore, the development of the *Nod2*$^{m/m}$ mouse model provided a good opportunity to study potential effects of TiO_2 particles on intestinal function in more detail. Nevertheless, this genetically modified mouse model has some limitations.

Firstly, although mutations in the *NOD2* gene have shown the highest association with CD [80, 86], only a small number of CD patients carry the 1,007fs mutations. It has been estimated that between 2.5 % and 6.5 % are homozygous for this mutation and between 11 % and 19 % are heterozygous. The 1,007fs mutation is nevertheless the most common *NOD2* variant among CD patients, and it represents the highest genetic risk factor for the development of CD. It has been estimated that the likelihood to develop CD is increased by 1.5 to 2.6 for heterozygous carriers and 17.6 to 42.1 for homozygous individuals [58, 60]. Furthermore, the presence of two alleles of this gene variant was only observed in CD patients, but never in healthy controls [58-60].

Despite the well-documented connection between the 1,007fs mutation in humans and the development of CD, *Nod2*$^{m/m}$ mice failed to develop spontaneous intestinal inflammation [131]. The results from this study have shown that dietary exposure to TiO_2 particles for a prolonged time also did not lead to the development of intestinal inflammation in this mouse model (Figures 4.5-4.9).

In a 'Corrections and Clarifications' letter published in 2011, Maeda and colleagues reported that the mutation that was introduced in the *Nod2* gene to create the *Nod2*$^{m/m}$ mouse model might not accurately reflect the human 1,007fs variant [394]. In particular, the *Nod2*$^{m/m}$ mouse model contains a duplication of the 3'-end of the WT *Nod2* locus, which includes the region that was targeted by the mutation. However, Maeda and co-workers were confident that the results obtained with the *Nod2*$^{m/m}$ mouse model are valid [394], and the main finding concerning the control of IL-1β expression by Nod2 has been confirmed in two subsequent studies [253, 395]. Nevertheless, in future studies that investigate the role of dietary TiO_2 in intestinal function it might be useful to consider using other mouse models of CD instead of, or in addition to the *Nod2*$^{m/m}$ model.

6.2.6 Alternative mouse models for Crohn's disease

A possible alternative to the *Nod2*$^{m/m}$ model would be the *Nod2*$^{-/-}$ mouse model [98, 125]. In this model no functional Nod2 protein is expressed, and therefore this model might be more representative of the situation that other mutations in the *NOD2* gene also contribute to increased CD susceptibility [59]. This model could be useful for investigating the effects of dietary TiO_2 on intestinal homeostasis in the absence of Nod2-regulated IL-1β production. Similar to *Nod2*$^{m/m}$ mice, however, *Nod2*$^{-/-}$ mice housed under conventional conditions did not develop spontaneous intestinal inflammation [125].

In contrast, inoculation of *Nod2*$^{-/-}$ mice with the opportunistic bacterial pathogen *Helicobacter hepaticus* resulted in intestinal inflammation with a similar phenotype to CD [396]. Under these circumstances, *Nod2*$^{-/-}$ mice developed inflammation primarily in the ileum with Th1-like gene expression and cytokine production. Furthermore, *Nod2*$^{-/-}$ mice that were exposed to *H. hepaticus* had an increased number of PPs compared to similarly treated WT mice. Moreover, the PPs and MLNs were enlarged in *Nod2*$^{-/-}$ mice that were infected with *H. hepaticus*. These observations suggest that this model could be suitable to investigate whether dietary TiO_2 particles contribute to the initiation and progression of inflammation in the gastrointestinal tract.

In this context, it is of interest that the background strain of the mouse model can affect susceptibility to intestinal inflammation. For example, mice of the strain C3H/He were more susceptible to DSS-induced colitis than C57BL/6 mice, which showed an intermediate susceptibility compared to other strains [397]. As already mentioned before (Section 5.1), another commonly used animal model for studying intestinal inflammation is the *Il10*$^{-/-}$ mouse model [50]. *Il10*$^{-/-}$ mice on a BALB/c background, which is another WT mouse strain, developed more severe enterocolitis than on a C57BL/6 background [398]. The *Nod2*$^{m/m}$ mice that were used in this study have been bred on a C57BL/6 background because they were originally developed on this WT strain [131]. A project is currently in progress at the AgResearch Ruakura Small Animal Colony to backcross the C57BL/6 *Nod2*$^{m/m}$ mice onto a BALB/c background to investigate whether the mice will develop spontaneous intestinal inflammation on this background strain. If successful, these BALB/c *Nod2*$^{m/m}$ mice could be used in future studies of dietary TiO_2 administration.

When the *Il10*$^{-/-}$ mouse model was originally described it was shown that these mice developed spontaneous enterocolitis affecting also the crypts and villi of the ileum and resulting in diminished GALT [50]. These changes in the intestinal tract occurred when the

animals were kept under conventional conditions, but no or only mild symptoms were observed when *Il10*$^{-/-}$ mice were raised under specific pathogen free conditions [50, 399]. This highlights the role of the commensal intestinal microbiota in disease initiation in this model [400]. Furthermore, colonisation with only one specific commensal intestinal bacterium, namely *Enterococcus faecalis*, was sufficient to trigger colitis in germ-free *Il10*$^{-/-}$ mice [401]. Intestinal inflammation in *Il10*$^{-/-}$ mice that occurred under conventional conditions was erratic and differed considerably between individual animals in terms of disease location and severity [50]. In contrast, when 5 weeks old *Il10*$^{-/-}$ mice were inoculated with cultures of *E. faecalis* and *Enterococcus faecium*, the animals developed a more consistent intestinal inflammation at 12 weeks of age [399]. These results might be of relevance for the *Nod2*$^{m/m}$ mouse model, and it might be possible to elicit spontaneous inflammation in these mice after challenging them with commensal microbes. However, in a preliminary study in which *Nod2*$^{m/m}$ were inoculated with *E. faecalis* and *E. faecium* cultures no intestinal inflammation could be established (personal communication with Dr Matthew Barnett, AgResearch, Palmerston North, NZ). It would be worth to continue studies that aim to establish spontaneous intestinal inflammation in *Nod2*$^{m/m}$ mice because if this was successful such a modified *Nod2*$^{m/m}$ mouse model could be used in further studies with dietary TiO_2 particles.

Alternatively, the effect of dietary TiO_2 on initiation and progression of intestinal inflammation could be investigated in *Il10*$^{-/-}$ mice housed under both conventional and specific pathogen/germ-free conditions. However, the defect in the production of the important regulatory cytokine IL-10 in this mouse model would make it difficult to extrapolate findings from such studies to the situation observed in CD patients. It has been shown that the number of IL-10-producing regulatory T cells was not diminished in the intestinal mucosa of CD patients [386], and treatment of CD patients with recombinant IL-10 had no positive effects on disease progression [402]. In fact, even detrimental effects of IL-10 therapy have been reported [403].

Intestinal inflammation can also be induced with chemical agents [404]. The two substances which are most commonly used for this type of studies are DSS polymers and the hapten 2,4,6-trinitrobenzenesulfonic acid (TNBS). Oral administration of DSS in drinking water to mice for several days induces acute or chronic colitis, depending on the DSS concentration, that is mediated by the immune system [405, 406]. Therefore, this model would be suitable to investigate the role of intestinal macrophages and DCs to dietary TiO_2 in an inflammatory milieu. Intrarectal instillation of TNBS in ethanol also induces colitis in susceptible mouse strains [304, 407, 408]. This model is characterised by a T cell-mediated immune response

with a Th1-associated cytokine signature, which would allow investigating the role of TiO_2 particles in CD-like intestinal inflammation. It has been shown that *Nod2*$^{m/m}$ mice are more susceptible to DSS-induced colitis than WT mice [125], and *Nod2*$^{-/-}$ mice developed more severe intestinal inflammation with TNBS compared to WT mice [304]. However, both models affect primarily the colon and not the small intestine, which is the site where TiO_2 particles are mainly taken up by intestinal cells in Peyer's patches. Furthermore, both chemicals supposedly lead to inflammation because of a disturbed epithelial barrier [407, 409]. Accordingly, studies in which these models were used to investigate the impact of TiO_2 particles on intestinal function would not be representative for the situation encountered in humans. The accumulation of TiO_2 particle in the intestinal mucosa of humans takes place through uptake *via* M cells in the FAE across an otherwise undamaged epithelium [56, 144].

Instead of chemically-induced colitis models, mouse models that develop spontaneous inflammation in the small intestine, specifically the terminal ileum, could be used to investigate potential effects of TiO_2 on the initiation and progression of the inflammation. However, only few such models are available at the moment. For example, mice that do not express X-box-binding protein 1 in epithelial cells develop spontaneous enteritis and have increased susceptibility to DSS-induced colitis [410]. Another model is the senescence accelerated mouse P1/Yit strain. These mice develop spontaneous inflammation in the ileum and caecum after 10 weeks of age when kept under conventional or specific pathogen free conditions [411]. It has been shown that these mice also develop disease symptoms under germ-free conditions, which indicates that the inflammation occurs independently of bacteria [412]. The inflammation in the senescence accelerated mouse P1/Yit strain resembles CD with discontinuous, transmural lesions, increased numbers of T cells, neutrophils, and macrophages in the inflamed mucosa, and a Th1 cytokine profile [411, 413]. Therefore, it has been suggested that this mouse model is ideally suited for studies specifically investigating CD-like inflammation in the ileum [389].

6.3 Future perspectives

To sum up, the results presented in this dissertation showed that food-grade TiO_2 particles accumulated in GALT as a consequence of intake with the diet (Chapter 3). Furthermore, *in vitro* exposure to these exogenous dietary particles caused cell activation and led to the secretion of the pro-inflammatory cytokine IL-1β, which has important functions in the regulation of intestinal homeostasis (Chapter 2). Despite the fact that *Nod2*$^{m/m}$ mice did not

develop spontaneous intestinal inflammation as a consequence of dietary TiO_2 exposure (Chapter 4), cells from *Nod2*$^{m/m}$ mice were more susceptible to stimulation with TiO_2 particles and bacterial antigens (Chapter 2). Furthermore, gastrointestinal TiO_2 particle uptake also led to changes in the urine metabolome of WT and *Nod2*$^{m/m}$ mice (Chapter 5). These results highlight the need for further specific research about the effects of dietary TiO_2 particles on intestinal homeostasis.

For example, it would be important to further investigate the mechanism of TiO_2-induced IL-1β release to assess the role of NOD2 and inflammasomes in this context. Furthermore, the expression of cytokines and chemokines in the intestinal tract could be investigated *in vivo* after feeding dietary TiO_2, e.g. by quantifying the mRNA expression of the respective genes with real-time polymerase chain reaction. The *Nod2*$^{m/m}$ mouse model and/or other mouse models for CD, e.g. the senescence accelerated mouse P1/Yit strain, could be used to investigate these questions.

To assess potential influences of TiO_2 particles on intestinal homeostasis, several intestinal samples from mice fed a TiO_2-containing diet could be analysed with techniques from the fields of systems biology, i.e. genomics, proteomics, and metabolomics. With these techniques it would be possible to obtain detailed information about regulatory pathways and how these pathways would be affected in WT mice or mouse models for CD after dietary exposure to TiO_2 particles.

The results from the metabolomics study of urine samples presented in this dissertation already indicated that gastrointestinal TiO_2 particle uptake has influences on metabolic pathways, e.g. the tryptophan catabolism (Figures 5.8-5.11). Further studies could be carried out to investigate if the observed reduction of potential tryptophan metabolite levels in urine samples from WT and *Nod2*$^{m/m}$ mice on a TiO_2-containing diet are the consequence of aberrant gene and/or protein expression of enzymes from the tryptophan catabolism pathway. This question could be assessed in future *in vivo* experiments in which selected enzymes would be investigated by targeted genomics and/or proteomics approaches. For example, it has been shown that the gene expression of the enzyme indoleamine-2,3-dioxygenase, which catabolises tryptophan to kynurenine *via* formyl-kynurenine [353], was up-regulated in inflamed colon tissues obtained from CD patients [362]. Correspondingly, it has been shown that the serum levels of kynurenine were elevated in CD patients compared to healthy controls [361]. Moreover, the gene expression of indoleamine-2,3-dioxygenase was also increased in colon tissues of *Il10*$^{-/-}$ mice with colonic inflammation [414].

Furthermore, a targeted metabolomics analysis could be carried out to assess of the levels of tryptophan and its metabolites in plasma or serum from TiO_2-exposed WT and *Nod2*$^{m/m}$ mice or other CD mouse models. The data obtained from metabolomics could then be integrated with genomics and proteomics data for a systems biology approach to assess effects of oral TiO_2 exposure on intestinal homeostasis.

However, as there are inevitable drawbacks in using mouse models, *ex vivo* and *in vitro* experiments should also be carried out using cells derived from CD patients. Ideally, the *NOD2* genotype and other CD-associated genes would be assessed in these patients, so that the results obtained from such studies could be correlated to the respective genotypes. For example, it might be worthwhile to conduct another dietary intervention study with CD patients that have been genotyped for mutations in *NOD2* [233]. Such a study would be useful to assess the effects of dietary TiO_2 intake on disease progression and other clinically relevant measurements in CD patients with homozygous 1,007fs mutations in the *NOD2* gene.

Another possible dietary intervention study would be to examine the long-term effects of a diet that does not contain any dietary particles on children with CD. Such a study with paediatric CD patients could help to clarify the question whether dietary TiO_2 particles have a role in the establishment phase of CD. However, any future dietary intervention study with CD patients would require careful planning and potentially a large number of participants to yield scientifically valuable results.

6.4 Conclusion

In conclusion, more than 20 years have passed since the initial discovery that TiO_2 particles accumulate in PP immune cells. Nevertheless, only little research has been carried out to date to investigate the consequences of intestinal exposure to exogenous dietary particles. The present dissertation addresses this gap and adds to the work carried out during the last decade by Powell and colleagues. It lays the foundations for future investigations that will further explore this topic by using mouse models with disturbances in intestinal function.

Although no direct connection between exposure to TiO_2 particles with the diet and the development of intestinal inflammation in WT or *Nod2*$^{m/m}$ mice was observed, the results from this dissertation warrant further investigations. In the *in vitro* experiments with murine macrophages it has been shown that dietary TiO_2 particles can elicit pro-inflammatory responses by these phagocytes. Furthermore, bacterial antigens that act as ligands for NOD2

augmented those effects, especially in the presence of a mutation in *Nod2* that has been associated with increased susceptibility to CD in humans.

Furthermore, the *in vivo* studies presented in this dissertation showed for the first time that TiO_2 particles accumulated in PP immune cells as a result of ingestion of these particles with the diet. Since the initial discovery of exogenous particles in PPs it has been assumed that this was the most likely route of exposure, but it was and remains almost impossible to confirm such a direct connection between exogenous particle intake and accumulation of TiO_2 in PPs in humans. Therefore, animal models are an invaluable tool in the study of the effects of exogenous particles on intestinal function. However, more research with both animal models and human dietary intervention studies will be required before final conclusions about the role of exogenous particles in the development of intestinal inflammation and CD can be drawn.

Should such future studies confirm concerns that dietary TiO_2 particles are not just innocuous additives it will be important to reconsider its use as a whitening agent in processed foods and other products that are ingested by humans. It will also be important to raise awareness about potential risks associated with the consumption of TiO_2-containing products, so consumers will be able to make conscious decisions about their intake of exogenous dietary particles.

Moreover, the food, dental hygiene, and pharmaceutical industries will have to be notified about potential long-term adverse effects resulting from the intake of TiO_2 with processed foods, toothpastes, and pharmaceuticals. Consequently, should it turn out that ingested TiO_2 particles indeed negatively affect intestinal health and increase the risk to develop intestinal inflammation/CD, the respective industries that are using TiO_2 as a whitening agent must look for safer alternatives.

References

1. Hooper LV and Macpherson AJ (2010) Immune adaptations that maintain homeostasis with the intestinal microbiota. *Nature Reviews Immunology* **10**(3): 159-169.
2. Maynard CL, Elson CO, Hatton RD, and Weaver CT (2012) Reciprocal interactions of the intestinal microbiota and immune system. *Nature* **489**(7415): 231-241.
3. Peterson LW and Artis D (2014) Intestinal epithelial cells: regulators of barrier function and immune homeostasis. *Nature Reviews Immunology* **14**(3): 141-153.
4. Ross MH and Pawlina W (2006) *Histology: a text and atlas with correlated cell and molecular biology* (Lippincott Williams & Wilkins, Baltimore, Maryland) 5th edition, pp. 906.
5. Mowat AM (2003) Anatomical basis of tolerance and immunity to intestinal antigens. *Nature Reviews Immunology* **3**(4): 331-341.
6. Jung C, Hugot JP, and Barreau F (2010) Peyer's patches: the immune sensors of the intestine. *International Journal of Inflammation* **2010**: 823710.
7. Kunisawa J, Nochi T, and Kiyono H (2008) Immunological commonalities and distinctions between airway and digestive immunity. *Trends in Immunology* **29**(11): 505-513.
8. Lane PJL, McConnell FM, Withers D, Gaspal F, Saini M, and Anderson G (2009) Lymphoid tissue inducer cells: bridges between the ancient innate and the modern adaptive immune systems. *Mucosal Immunology* **2**(6): 472-477.
9. Kunisawa J, Kurashima Y, and Kiyono H (2012) Gut-associated lymphoid tissues for the development of oral vaccines. *Advanced Drug Delivery Reviews* **64**(6): 523-530.
10. Kunisawa J, Gohda M, Hashimoto E, Ishikawa I, Higuchi M, Suzuki Y, Goto Y, Panea C, Ivanov II, Sumiya R*, et al.* (2013) Microbe-dependent $CD11b^+$ IgA^+ plasma cells mediate robust early-phase intestinal IgA responses in mice. *Nature Communications* **4**: 1772.
11. Varol C, Zigmond E, and Jung S (2010) Securing the immune tightrope: mononuclear phagocytes in the intestinal lamina propria. *Nature Reviews Immunology* **10**(6): 415-426.
12. Coombes JL and Powrie F (2008) Dendritic cells in intestinal immune regulation. *Nature Reviews Immunology* **8**(6): 435-446.
13. Loftus EVJ (2004) Clinical epidemiology of inflammatory bowel disease: incidence, prevalence, and environmental influences. *Gastroenterology* **126**(6): 1504-1517.

14. Molodecky NA, Soon IS, Rabi DM, Ghali WA, Ferris M, Chernoff G, Benchimol EI, Panaccione R, Ghosh S, Barkema HW*, et al.* (2012) Increasing incidence and prevalence of the inflammatory bowel diseases with time, based on systematic review. *Gastroenterology* **142**(1): 46-54.
15. Gearry RB, Richardson A, Frampton CMA, Collett JA, Burt MJ, Chapman BA, and Barclay ML (2006) High incidence of Crohn's disease in Canterbury, New Zealand: results of an epidemiologic study. *Inflammatory Bowel Diseases* **12**(10): 936-943.
16. Podolsky DK (2002) Inflammatory bowel disease. *New England Journal of Medicine* **347**(6): 417-429.
17. Baumgart DC and Sandborn WJ (2012) Crohn's disease. *Lancet* **380**(9853): 1590-1605.
18. Bouma G and Strober W (2003) The immunological and genetic basis of inflammatory bowel disease. *Nature Reviews Immunology* **3**(7): 521-533.
19. Hart AL and Ng SC (2011) Crohn's disease. *Medicine* **39**(4): 229-236.
20. Mosmann TR, Cherwinski H, and Bond MW (1986) Two types of murine helper T cell clone: definition according to profiles of lymphokine activities and secreted proteins. *Journal of Immunology* **136**(7): 2348-2357.
21. Zhu J, Yamane H, and Paul WE (2010) Differentiation of effector CD4 T cell populations. *Annual Review of Immunology* **28**: 445-489.
22. Korn T, Bettelli E, Oukka M, and Kuchroo VK (2009) IL-17 and Th17 cells. *Annual Review of Immunology* **27**: 485-517.
23. Aggarwal S, Ghilardi N, Xie M-H, de Sauvage FJ, and Gurney AL (2003) Interleukin-23 promotes a distinct CD4 T cell activation state characterized by the production of interleukin-17. *Journal of Biological Chemistry* **278**(3): 1910-1914.
24. Kimura A, Naka T, and Kishimoto T (2007) IL-6-dependent and -independent pathways in the development of interleukin 17-producing T helper cells. *Proceedings of the National Academy of Sciences of the United States of America* **104**(29): 12099-12104.
25. Veldhoen M, Hocking RJ, Atkins CJ, Locksley RM, and Stockinger B (2007) TGFβ in the context of an inflammatory cytokine milieu supports de novo differentiation of IL-17-producing T cells. *Immunity* **24**(2): 179-189.
26. Weaver CT, Elson CO, Fouser LA, and Kolls JK (2013) The Th17 pathway and inflammatory diseases of the intestines, lungs, and skin. *Annual Review of Pathology: Mechanisms of Disease* **8**: 477-512.

27. Wilson NJ, Boniface K, Chan JR, McKenzie BS, Blumenschein WM, Mattson JD, Basham B, Smith K, Chen T, Morel F*, et al.* (2007) Development, cytokine profile and function of human interleukin 17-producing helper T cells. *Nature Immunology* **8**(9): 950-957.

28. Brand S (2009) Crohn's disease: Th1, Th17 or both? The change of a paradigm: new immunological and genetic insights implicate Th17 cells in the pathogenesis of Crohn's disease. *Gut* **58**(8): 1152-1167.

29. Monteleone G, Biancone L, Marasco R, Morrone G, Marasco O, Luzza F, and Pallone F (1997) Interleukin 12 is expressed and actively released by Crohn's disease intestinal lamina propria mononuclear cells. *Gastroenterology* **112**(4): 1169-1178.

30. Parronchi P, Romagnani P, Annunziato F, Sampognaro S, Becchio A, Giannarini L, Maggi E, Pupilli C, Tonelli F, and Romagnani S (1997) Type 1 T-helper cell predominance and interleukin-12 expression in the gut of patients with Crohn's disease. *American Journal of Pathology* **150**(3): 823-832.

31. Fuss IJ, Neurath M, Boirivant M, Klein JS, de la Motte C, Strong SA, Fiocchi C, and Strober W (1996) Disparate CD4+ lamina propria (LP) lymphokine secretion profiles in inflammatory bowel disease: Crohn's disease LP cells manifest increased secretion of IFN-γ, whereas ulcerative colitis LP cells manifest increased secretion of IL-5. *Journal of Immunology* **157**(3): 1261-1270.

32. Kastelein RA, Hunter CA, and Cua DJ (2007) Discovery and biology of IL-23 and IL-27: related but functionally distinct regulators of inflammation. *Annual Review of Immunology* **25**: 221-242.

33. Elson CO, Cong Y, Weaver CT, Schoeb TR, McClanahan TK, Fick RB, and Kastelein RA (2007) Monoclonal anti–interleukin 23 reverses active colitis in a T cell–mediated model in mice. *Gastroenterology* **132**(7): 2359-2370.

34. Hue S, Ahern P, Buonocore S, Kullberg MC, Cua DJ, McKenzie BS, Powrie F, and Maloy KJ (2006) Interleukin-23 drives innate and T cell-mediated intestinal inflammation. *Journal of Experimental Medicine* **203**(11): 2473-2483.

35. Leppkes M, Becker C, Ivanov II, Hirth S, Wirtz S, Neufert C, Pouly S, Murphy AJ, Valenzuela DM, Yancopoulos GD*, et al.* (2009) RORγ-expressing Th17 cells induce murine chronic intestinal inflammation via redundant effects of IL-17A and IL-17F. *Gastroenterology* **136**(1): 257-267.

36. Yen D, Cheung J, Scheerens H, Poulet F, McClanahan T, McKenzie B, Kleinschek MA, Owyang A, Mattson J, Blumenschein W*, et al.* (2006) IL-23 is essential for T cell–

mediated colitis and promotes inflammation via IL-17 and IL-6. *Journal of Clinical Investigation* **116**(5): 1310-1316.

37. Fuss IJ, Becker C, Yang Z, Groden C, Hornung RL, Heller F, Neurath MF, Strober W, and Mannon PJ (2006) Both IL-12p70 and IL-23 are synthesized during active Crohn's disease and are down-regulated by treatment with anti-IL-12 p40 monoclonal antibody. *Inflammatory Bowel Diseases* **12**(1): 9-15.
38. Pène J, Chevalier S, Preisser L, Vénéreau E, Guilleux M-H, Ghannam S, Molès J-P, Danger Y, Ravon E, Lesaux S*, et al.* (2008) Chronically inflamed human tissues are infiltrated by highly differentiated Th17 lymphocytes. *Journal of Immunology* **180**(11): 7423-7430.
39. Acosta-Rodriguez EV, Rivino L, Geginat J, Jarrossay D, Gattorno M, Lanzavecchia A, Sallusto F, and Napolitani G (2007) Surface phenotype and antigenic specificity of human interleukin 17-producing T helper memory cells. *Nature Immunology* **8**(6): 639-646.
40. Annunziato F, Cosmi L, Santarlasci V, Maggi L, Liotta F, Mazzinghi B, Parente E, Filì L, Ferri S, Frosali F*, et al.* (2007) Phenotypic and functional features of human Th17 cells. *Journal of Experimental Medicine* **204**(8): 1849-1861.
41. Kleinschek MA, Boniface K, Sadekova S, Grein J, Murphy EE, Turner SP, Raskin L, Desai B, Faubion WA, de Waal Malefyt R*, et al.* (2009) Circulating and gut-resident human Th17 cells express CD161 and promote intestinal inflammation. *Journal of Experimental Medicine* **206**(3): 525-534.
42. Kugathasan S, Saubermann LJ, Smith L, Kou D, Itoh J, Binion DG, Levine AD, Blumberg RS, and Fiocchi C (2007) Mucosal T-cell immunoregulation varies in early and late inflammatory bowel disease. *Gut* **56**(12): 1696-1705.
43. Strober W and Fuss IJ (2011) Proinflammatory cytokines in the pathogenesis of inflammatory bowel diseases. *Gastroenterology* **140**(6): 1756-1767.
44. Reimund JM, Wittersheim C, Dumont S, Muller CD, Kenney JS, Baumann R, Poindron P, and Duclos B (1996) Increased production of tumour necrosis factor-α, interleukin-1β, and interleukin-6 by morphologically normal intestinal biopsies from patients with Crohn's disease. *Gut* **39**(5): 684-689.
45. Reinecker HC, Steffen M, Witthoeft T, Pflueger I, Schreiber S, MacDermott RP, and Raedler A (1993) Enhanced secretion of tumour necrosis factor-alpha, IL-6, and IL-1β by isolated lamina propria mononuclear cells from patients with ulcerative colitis and Crohn's disease. *Clinical and Experimental Immunology* **94**(1): 174-181.

46. Maynard CL and Weaver CT (2009) Intestinal effector T cells in health and disease. *Immunity* **31**(3): 389-400.

47. Izcue A, Coombes JL, and Powrie F (2009) Regulatory lymphocytes and intestinal inflammation. *Annual Review of Immunology* **27**: 313-338.

48. Franke A, Balschun T, Karlsen TH, Sventoraityte J, Nikolaus S, Mayr G, Domingues FS, Albrecht M, Nothnagel M, Ellinghaus D*, et al.* (2008) Sequence variants in *IL10*, *ARPC2* and multiple other loci contribute to ulcerative colitis susceptibility. *Nature Genetics* **40**(11): 1319-1323.

49. Glocker EO, Kotlarz D, Boztug K, Gertz EM, Schäffer AA, Noyan F, Perro M, Diestelhorst J, Allroth A, Murugan D*, et al.* (2009) Inflammatory bowel disease and mutations affecting the interleukin-10 receptor. *New England Journal of Medicine* **361**(21): 2033-2045.

50. Kühn R, Löhler J, Rennick D, Rajewsky K, and Müller W (1993) Interleukin-10-deficient mice develop chronic enterocolitis. *Cell* **75**(2): 263-274.

51. Hugot JP, Zouali H, Lesage S, and Thomas G (1999) Etiology of the inflammatory bowel diseases. *International Journal of Colorectal Disease* **14**(1): 2-9.

52. Thompson NP, Driscoll R, Pounder RE, Wakefield AJ, and Bowel I (1996) Genetics versus environment in inflammatory bowel disease: results of a British twin study. *British Medical Journal* **312**(7023): 95-96.

53. Tysk C, Lindberg E, Jarnerot G, and Floderus-Myrhed B (1988) Ulcerative colitis and Crohn's disease in an unselected population of monozygotic and dizygotic twins: a study of heritability and the influence of smoking. *Gut* **29**(7): 990-996.

54. Hugot JP, Cézard JP, Colombel JF, Belaiche J, Almer S, Tysk C, Montague S, Gassull M, Christensen S, Finkel Y*, et al.* (2003) Clustering of Crohn's disease within affected sibships. *European Journal of Human Genetics* **11**(2): 179-184.

55. Powell JJ, Thoree V, and Pele LC (2007) Dietary microparticles and their impact on tolerance and immune responsiveness of the gastrointestinal tract. *British Journal of Nutrition* **98**(Suppl. 1): S59-S63.

56. Shepherd NA, Crocker PR, Smith AP, and Levison DA (1987) Exogenous pigment in Peyer's patches. *Human Pathology* **18**(1): 50-54.

57. Riordan AM, Ruxton CHS, and Hunter JO (1998) A review of associations between Crohn's disease and consumption of sugars. *European Journal of Clinical Nutrition* **52**(4): 229-238.

58. Hampe J, Cuthbert A, Croucher PJP, Mirza MM, Mascheretti S, Fisher S, Frenzel H, King K, Hasselmeyer A, MacPherson AJS*, et al.* (2001) Association between insertion mutation in *NOD2* gene and Crohn's disease in German and British populations. *Lancet* **357**(9272): 1925-1928.

59. Hugot JP, Chamaillard M, Zouali H, Lesage S, Cézard JP, Belaiche J, Almer S, Tysk C, O'Morain CA, Gassull M*, et al.* (2001) Association of NOD2 leucine-rich repeat variants with susceptibility to Crohn's disease. *Nature* **411**(6837): 599-603.

60. Ogura Y, Bonen DK, Inohara N, Nicolae DL, Chen FF, Ramos R, Britton H, Moran T, Karaliuskas R, Duerr RH*, et al.* (2001) A frameshift mutation in *NOD2* associated with susceptibility to Crohn's disease. *Nature* **411**(6837): 603-606.

61. Inohara N, Ogura Y, Fontalba A, Gutierrez O, Pons F, Crespo J, Fukase K, Inamura S, Kusumoto S, Hashimoto M*, et al.* (2003) Host recognition of bacterial muramyl dipeptide mediated through NOD2: implications for Crohn's disease. *Journal of Biological Chemistry* **278**(8): 5509-5512.

62. Philpott DJ, Sorbara MT, Robertson SJ, Croitoru K, and Girardin SE (2014) NOD proteins: regulators of inflammation in health and disease. *Nature Reviews Immunology* **14**(1): 9-23.

63. Shaw MH, Kamada N, Warner N, Kim YG, and Nuñez G (2011) The ever-expanding function of NOD2: autophagy, viral recognition, and T cell activation. *Trends in Immunology* **32**(2): 73-79.

64. Strober W, Murray PJ, Kitani A, and Watanabe T (2006) Signalling pathways and molecular interactions of NOD1 and NOD2. *Nature Reviews Immunology* **6**(1): 9-20.

65. Ting JPY, Duncan JA, and Lei Y (2010) How the noninflammasome NLRs function in the innate immune system. *Science* **327**(5963): 286-290.

66. Cho JH and Abraham C (2007) Inflammatory bowel disease genetics: Nod2. *Annual Review of Medicine* **58**: 401-416.

67. Strober W, Asano N, Fuss I, Kitani A, and Watanabe T (2014) Cellular and molecular mechanisms underlying NOD2 risk-associated polymorphisms in Crohn's disease. *Immunological Reviews* **260**(1): 249-260.

68. Franke A, McGovern DPB, Barrett JC, Wang K, Radford-Smith GL, Ahmad T, Lees CW, Balschun T, Lee J, Roberts R*, et al.* (2010) Genome-wide meta-analysis increases to 71 the number of confirmed Crohn's disease susceptibility loci. *Nature Genetics* **42**(12): 1118-1125.

69. Hugot JP, Laurent-Puig P, Gower-Rousseau C, Olson JM, Lee JC, Beaugerie L, Naom I, Dupas JL, van Gossum A, Orholm M*, et al.* (1996) Mapping of a susceptibility locus for Crohn's disease on chromosome 16. *Nature* **379**(6568): 821-823.

70. Ogura Y, Inohara N, Benito A, Chen FF, Yamaoka S, and Núñez G (2001) Nod2, a Nod1/Apaf-1 family member that is restricted to monocytes and activates NF-κB. *Journal of Biological Chemistry* **276**(7): 4812-4818.

71. Lesage S, Zouali H, Cezard JP, Colombel JF, Belaiche J, Almer S, Tysk C, O'Morain C, Gassull M, Binder V*, et al.* (2002) *CARD15/NOD2* mutational analysis and genotype-phenotype correlation in 612 patients with inflammatory bowel disease. *American Journal of Human Genetics* **70**(4): 845-857.

72. Burton PR, Clayton DG, Cardon LR, Craddock N, Deloukas P, Duncanson A, Kwiatkowski DP, McCarthy MI, Ouwehand WH, Samani NJ*, et al.* (2007) Genome-wide association study of 14,000 cases of seven common diseases and 3,000 shared controls. *Nature* **447**(7145): 661-678.

73. Hampe J, Franke A, Rosenstiel P, Till A, Teuber M, Huse K, Albrecht M, Mayr G, de la Vega FM, Briggs J*, et al.* (2007) A genome-wide association scan of nonsynonymous SNPs identifies a susceptibility variant for Crohn disease in *ATG16L1*. *Nature Genetics* **39**(2): 207-211.

74. Libioulle C, Louis E, Hansoul S, Sandor C, Farnir F, Franchimont D, Vermeire S, Dewit O, de Vos M, Dixon A*, et al.* (2007) Novel Crohn disease locus identified by genome-wide association maps to a gene desert on 5p13.1 and modulates expression of *PTGER4*. *Plos Genetics* **3**(4): e58.

75. Rioux JD, Xavier RJ, Taylor KD, Silverberg MS, Goyette P, Huett A, Green T, Kuballa P, Barmada MM, Datta LW*, et al.* (2007) Genome-wide association study identifies new susceptibility loci for Crohn disease and implicates autophagy in disease pathogenesis. *Nature Genetics* **39**(5): 596-604.

76. Gearry RB, Roberts RL, Burt MJ, Frampton CMA, Chapman BA, Collett JA, Shirley P, Allington MDE, Kennedy MA, and Barclay ML (2007) Effect of inflammatory bowel disease classification changes on *NOD2* genotype-phenotype associations in a population-based cohort. *Inflammatory Bowel Diseases* **13**(10): 1220-1227.

77. Hirano A, Yamazaki K, Umeno J, Ashikawa K, Aoki M, Matsumoto T, Nakamura S, Ninomiya T, Matsui T, Hirai F*, et al.* (2013) Association study of 71 European

Crohn's disease susceptibility loci in a Japanese population. *Inflammatory Bowel Diseases* **19**(3): 526-533.

78. Inoue N, Tamura K, Kinouchi Y, Fukuda Y, Takahashi S, Ogura Y, Inohara N, Núñez G, Kishi Y, Koike Y*, et al.* (2002) Lack of common NOD2 variants in Japanese patients with Crohn's disease. *Gastroenterology* **123**(1): 86-91.
79. Kugathasan S, Loizides A, Babusukumar U, McGuire E, Wang T, Hooper P, Nebel J, Kofman G, Noel R, Broeckel U*, et al.* (2005) Comparative phenotypic and CARD15 mutational analysis among African American, Hispanic, and white children with Crohn's disease. *Inflammatory Bowel Diseases* **11**(7): 631-638.
80. Barrett JC, Hansoul S, Nicolae DL, Cho JH, Duerr RH, Rioux JD, Brant SR, Silverberg MS, Taylor KD, Barmada MM*, et al.* (2008) Genome-wide association defines more than 30 distinct susceptibility loci for Crohn's disease. *Nature Genetics* **40**(8): 955-962.
81. Duerr RH, Taylor KD, Brant SR, Rioux JD, Silverberg MS, Daly MJ, Steinhart AH, Abraham C, Regueiro M, Griffiths A*, et al.* (2006) A genome-wide association study identifies *IL23R* as an inflammatory bowel disease gene. *Science* **314**(5804): 1461-1463.
82. Ferguson LR, Han DY, Fraser AG, Huebner C, Lam WJ, and Morgan AR (2010) *IL23R* and *IL12B* SNPs and haplotypes strongly associate with Crohn's disease risk in a New Zealand population. *Gastroenterology Research and Practice* **2010**: 539461.
83. Ferguson LR, Han DY, Fraser AG, Huebner C, Lam WJ, Morgan AR, Duan H, and Karunasinghe N (2010) Genetic factors in chronic inflammation: single nucleotide polymorphisms in the STAT-JAK pathway, susceptibility to DNA damage and Crohn's disease in a New Zealand population. *Mutation Research: Fundamental and Molecular Mechanisms of Mutagenesis* **690**(1-2): 108-115.
84. Roberts RL, Gearry RB, Hollis-Moffatt JE, Miller AL, Reid J, Abkevich V, Timms KM, Gutin A, Lanchbury JS, Merriman TR*, et al.* (2007) IL23R R381Q and ATG16L1 T300A are strongly associated with Crohn's disease in a study of New Zealand Caucasians with inflammatory bowel disease. *American Journal of Gastroenterology* **102**(12): 2754-2761.
85. Anderson CA, Boucher G, Lees CW, Franke A, D'Amato M, Taylor KD, Lee JC, Goyette P, Imielinski M, Latiano A*, et al.* (2011) Meta-analysis identifies 29 additional ulcerative colitis risk loci, increasing the number of confirmed associations to 47. *Nature Genetics* **43**(3): 246-252.

86. Jostins L, Ripke S, Weersma RK, Duerr RH, McGovern DP, Hui KY, Lee JC, Schumm LP, Sharma Y, Anderson CA*, et al.* (2012) Host-microbe interactions have shaped the genetic architecture of inflammatory bowel disease. *Nature* **491**(7422): 119-124.

87. Jung C, Colombel JF, Lemann M, Beaugerie L, Allez M, Cosnes J, Vernier-Massouille G, Gornet JM, Gendre JP, Cezard JP*, et al.* (2012) Genotype/phenotype analyses for 53 Crohn's disease associated genetic polymorphisms. *Plos One* **7**(12): e52223.

88. Inohara N, Koseki T, Del Peso L, Hu Y, Yee C, Chen S, Carrio R, Merino J, Liu D, Ni J*, et al.* (1999) Nod1, an Apaf-1-like activator of caspase-9 and nuclear factor-κB. *Journal of Biological Chemistry* **274**(21): 14560-14567.

89. Biswas A and Kobayashi KS (2013) Regulation of intestinal microbiota by the NLR protein family. *International Immunology* **25**(4): 207-214.

90. Chen G, Shaw MH, Kim YG, and Nuñez G (2009) NOD-like receptors: role in innate immunity and inflammatory disease. *Annual Review of Pathology: Mechanisms of Disease* **4**: 365-398.

91. Abreu MT, Fukata M, and Arditi M (2005) TLR signalling in the gut in health and disease. *Journal of Immunology* **147**(8): 4458-4460.

92. Werts C, Rubino S, Ling A, Girardin SE, and Philpott DJ (2011) Nod-like receptors in intestinal homeostasis, inflammation, and cancer. *Journal of Leukocyte Biology* **90**(3): 471-482.

93. Abreu MT (2010) Toll-like receptor signalling in the intestinal epithelium: how bacterial recognition shapes intestinal function. *Nature Reviews Immunology* **10**(2): 131-143.

94. Inohara N and Nuñez G (2003) NODs: intracellular proteins involved in inflammation and apoptosis. *Nature Reviews Immunology* **3**(5): 371-382.

95. Girardin SE, Boneca IG, Viala J, Chamaillard M, Labigne A, Thomas G, Philpott DJ, and Sansonetti PJ (2003) Nod2 is a general sensor of peptidoglycan through muramyl dipeptide (MDP) detection. *Journal of Biological Chemistry* **278**(11): 8869-8872.

96. Grimes CL, Ariyananda LDZ, Melnyk JE, and O'Shea EK (2012) The innate immune protein Nod2 binds directly to MDP, a bacterial cell wall fragment. *Journal of the American Chemical Society* **134**(33): 13535-13537.

97. Mo J, Boyle JP, Howard CB, Monie TP, Davis BK, and Duncan JA (2012) Pathogen sensing by nucleotide-binding oligomerization domain-containing protein 2 (NOD2)

is mediated by direct binding to muramyl dipeptide and ATP. *Journal of Biological Chemistry* **287**(27): 23057-23067.

98. Pauleau AL and Murray PJ (2003) Role of Nod2 in the response of macrophages to Toll-like receptor agonists. *Molecular and cellular biology* **23**(21): 7531-7539.

99. Barnich N, Aguirre JE, Reinecker HC, Xavier R, and Podolsky DK (2005) Membrane recruitment of NOD2 in intestinal epithelial cells is essential for nuclear factor-KB activation in muramyl dipeptide recognition. *Journal of Cell Biology* **170**(1): 21-26.

100. Ogura Y, Lala S, Xin W, Smith E, Dowds TA, Chen FF, Zimmermann E, Tretiakova M, Cho JH, Hart J*, et al.* (2003) Expression of NOD2 in Paneth cells: a possible link to Crohn's ileitis. *Gut* **52**(11): 1591-1597.

101. Cossart P and Sansonetti PJ (2004) Bacterial invasion: the paradigms of enteroinvasive pathogens. *Science* **304**(5668): 242-248.

102. Herskovits AA, Auerbuch V, and Portnoy DA (2007) Bacterial ligands generated in a phagosome are targets of the cytosolic innate immune system. *PLoS Pathogens* **3**(3): e51.

103. Viala J, Chaput C, Boneca IG, Cardona A, Girardin SE, Moran AP, Athman R, Mémet S, Huerre MR, Coyle AJ*, et al.* (2004) Nod1 responds to peptidoglycan delivered by the *Helicobacter pylori cag* pathogenicity island. *Nature Immunology* **5**(11): 1166-1174.

104. Bielig H, Rompikuntal PK, Dongre M, Zurek B, Lindmark B, Ramstedt M, Wai SN, and Kufer TA (2011) NOD-like receptor activation by outer membrane vesicles from *Vibrio cholerae* non-O1 non-O139 strains is modulated by the quorum-sensing regulator HapR. *Infection and Immunity* **79**(4): 1418-1427.

105. Kaparakis M, Turnbull L, Carneiro L, Firth S, Coleman HA, Parkington HC, Le Bourhis L, Karrar A, Viala J, Mak J*, et al.* (2010) Bacterial membrane vesicles deliver peptidoglycan to NOD1 in epithelial cells. *Cellular Microbiology* **12**(3): 372-385.

106. Ismair MG, Vavricka SR, Kullak-Ublick GA, Fried M, Mengin-Lecreulx D, and Girardin SE (2006) hPepT1 selectively transports muramyl dipeptide but not Nod1-activating muramyl peptides. *Canadian Journal of Physiology and Pharmacology* **84**(12): 1313-1319.

107. Vavricka SR, Musch MW, Chang JE, Nakagawa Y, Phanvijhitsiri K, Waypa TS, Merlin D, Schneewind O, and Chang EB (2004) hPepT1 transports muramyl dipeptide, activating NF-κB and stimulating IL-8 secretion in human colonic Caco2/bbe cells. *Gastroenterology* **127**(5): 1401-1409.

108. Lee J, Tattoli I, Wojtal KA, Vavricka SR, Philpott DJ, and Girardin SE (2009) pH-dependent Internalization of muramyl peptides from early endosomes enables Nod1 and Nod2 signaling. *Journal of Biological Chemistry* **284**(35): 23818-23829.

109. Marina-García N, Franchi L, Kim YG, Hu Y, Smith DE, Boons GJ, and Núñez G (2009) Clathrin- and dynamin-dependent endocytic pathway regulates muramyl dipeptide internalization and NOD2 activation. *Journal of Immunology* **182**(7): 4321-4327.

110. Lécine P, Esmiol S, Métais JY, Nicoletti C, Nourry C, McDonald C, Nunez G, Hugot JP, Borg JP, and Ollendorff V (2007) The NOD2-RICK complex signals from the plasma membrane. *Journal of Biological Chemistry* **282**(20): 15197-15207.

111. Park JH, Kim YG, McDonald C, Kanneganti TD, Hasegawa M, Body-Malapel M, Inohara N, and Nunez G (2007) RICK/RIP2 mediates innate immune responses induced through Nod1 and Nod2 but not TLRs. *Journal of Immunology* **178**(4): 2380-2386.

112. Abbott DW, Wilkins A, Asara JM, and Cantley LC (2004) The Crohn's disease protein, NOD2, requires RIP2 in order to induce ubiquitinylation of a novel site on NEMO. *Current Biology* **14**(24): 2217-2227.

113. Hasegawa M, Fujimoto Y, Lucas PC, Nakano H, Fukase K, Núñez G, and Inohara N (2008) A critical role of RICK/RIP2 polyubiquitination in Nod-induced NF-κB activation. *EMBO Journal* **27**(2): 373-383.

114. Windheim M, Lang C, Peggie M, Plater LA, and Cohen P (2007) Molecular mechanisms involved in the regulation of cytokine production by muramyl dipeptide. *Biochemical Journal* **404**(2): 179-190.

115. Yang Y, Yin C, Pandey A, Abbott D, Sassetti C, and Kelliher MA (2007) NOD2 pathway activation by MDP or *Mycobacterium tuberculosis* infection involves the stable polyubiquitination of Rip2. *Journal of Biological Chemistry* **282**(50): 36223-36229.

116. Vallabhapurapu S and Karin M (2009) Regulation and function of NF-κB transcription factors in the immune system. *Annual Review of Immunology* **27**: 693-733.

117. Wullaert A, Bonnet MC, and Pasparakis M (2011) NF-κB in the regulation of epithelial homeostasis and inflammation. *Cell Research* **21**(1): 146-158.

118. Coskun M, Olsen J, Seidelin JB, and Nielsen OH (2011) MAP kinases in inflammatory bowel disease. *Clinica Chimica Acta* **412**(7-8): 513-520.

119. Watanabe T, Kitani A, Murray PJ, and Strober W (2004) NOD2 is a negative regulator of Toll-like receptor 2-mediated T helper type 1 responses. *Nature Immunology* **5**(8): 800-808.

120. Watanabe T, Kitani A, Murray PJ, Wakatsuki Y, Fuss IJ, and Strober W (2006) Nucleotide binding oligomerization domain 2 deficiency leads to dysregulated TLR2 signaling and induction of antigen-specific colitis. *Immunity* **25**(3): 473-485.

121. Watanabe T, Asano N, Murray PJ, Ozato K, Tailor P, Fuss IJ, Kitani A, and Strober W (2008) Muramyl dipeptide activation of nucleotide-binding oligomerization domain 2 protects mice from experimental colitis. *Journal of Clinical Investigation* **118**(2): 545-559.

122. Kramer M, Netea MG, de Jong DJ, Kullberg BJ, and Adema GJ (2006) Impaired dendritic cell function in Crohn's disease patients with NOD2 3020insC mutation. *Journal of Leukocyte Biology* **79**(4): 860-866.

123. Netea MG, Kullberg BJ, de Jong DJ, Franke B, Sprong T, Naber THJ, Drenth JPH, and van der Meer JWM (2004) *NOD2* mediates anti-inflammatory signals induced by TLR2 ligands: implications for Crohn's disease. *European Journal of Immunology* **34**(7): 2052-2059.

124. Netea MG, Ferwerda G, de Jong DJ, Jansen T, Jacobs L, Kramer M, Naber THJ, Drenth JPH, Girardin SE, Kullberg BJ*, et al.* (2005) Nucleotide-binding oligomerization domain-2 modulates specific TLR pathways for the induction of cytokine release. *Journal of Immunology* **174**(10): 6518-6523.

125. Kobayashi KS, Chamaillard M, Ogura Y, Henegariu O, Inohara N, Nuñez G, and Flavell RA (2005) Nod2-dependent regulation of innate and adaptive immunity in the intestinal tract. *Science* **307**(5710): 731-734.

126. Wehkamp J, Harder J, Weichenthal M, Schwab M, Schäffeler E, Schlee M, Herrlinger KR, Stallmach A, Noack F, Fritz P*, et al.* (2004) NOD2 (CARD15) mutations in Crohn's disease are associated with diminished mucosal α-defensin expression. *Gut* **53**(11): 1658-1664.

127. Wehkamp J, Salzman NH, Porter E, Nuding S, Weichenthal M, Petras RE, Shen B, Schaeffeler E, Schwab M, Linzmeier R*, et al.* (2005) Reduced Paneth cell *α*-defensins in ileal Crohn's disease. *Proceedings of the National Academy of Sciences of the United States of America* **102**(50): 18129-18134.

128. Simms LA, Doecke JD, Walsh MD, Huang N, Fowler EV, and Radford-Smith GL (2008) Reduced α-defensin expression is associated with inflammation and not NOD2 mutation status in ileal Crohn's disease. *Gut* **57**(7): 903-910.

129. Shanahan MT, Carroll IM, Grossniklaus E, White A, von Furstenberg RJ, Barner R, Fodor AA, Henning SJ, Sartor RB, and Gulati AS (2014) Mouse Paneth cell antimicrobial function is independent of Nod2. *Gut* **63**(6): 903-910.

130. Kuballa P, Huett A, Rioux JD, Daly MJ, and Xavier RJ (2008) Impaired autophagy of an intracellular pathogen induced by a Crohn's disease associated ATG16L1 variant. *Plos One* **3**(10): e3391.

131. Maeda S, Hsu LC, Liu HJ, Bankston LA, Iimura M, Kagnoff MF, Eckmann L, and Karin M (2005) *Nod2* mutation in Crohn's disease potentiates NF-*x*B activity and IL-1β processing. *Science* **307**(5710): 734-738.

132. Dionne S, D'Agata ID, Hiscott J, Vanounou T, and Seidman EG (1998) Colonic explant production of IL-1 and its receptor antagonist is imbalanced in inflammatory bowel disease (IBD). *Clinical and Experimental Immunology* **112**(3): 435-442.

133. Li J, Moran T, Swanson E, Julian C, Harris J, Bonen DK, Hedl M, Nicolae DL, Abraham C, and Cho JH (2004) Regulation of IL-8 and IL-1 beta expression in Crohn's disease associated *NOD2/CARD15* mutations. *Human Molecular Genetics* **13**(16): 1715-1725.

134. Netea MG, Ferwerda G, de Jong DJ, Girardin SE, Kullberg BJ, and van der Meer JWM (2005) *NOD2* 3020insC mutation and the pathogenesis of Crohn's disease: impaired IL-Iβ production points to a loss-of-function phenotype. *Netherlands Journal of Medicine* **63**(8): 305-308.

135. Netea MG, Ferwerda G, de Jong DJ, Werts C, Boneca IG, Jéhanno M, van der Meer JWM, Mengin-Lecreulx D, Sansonetti PJ, Philpott DJ*, et al.* (2005) The frameshift mutation in *Nod2* results in unresponsiveness not only to Nod2- but also Nod1-activating peptidoglycan agonists. *Journal of Biological Chemistry* **280**(43): 35859-35867.

136. van Heel DA, Ghosh S, Butler M, Hunt KA, Lundberg AMC, Ahmad T, McGovern DPB, Onnie C, Negoro K, Goldthorpe S*, et al.* (2005) Muramyl dipeptide and toll-like receptor sensitivity in *NOD2*-associated Crohn's disease. *Lancet* **365**(9473): 1794-1796.

137. Hommes D, van den Blink B, Plasse T, Bartelsman J, Xu C, Macpherson B, Tytgat G, Peppelenbosch M, and van Deventer S (2002) Inhibition of stress-activated

MAP kinases induces clinical improvement in moderate to severe Crohn's disease. *Gastroenterology* **122**(1): 7-14.

138. Favus MJ (1985) Factors that influence absorption and secretion of calcium in the small intestine and colon. *American Journal of Physiology* **248**(2): G147-G157.
139. Powell JJ, Whitehead MW, Ainley CC, Kendall MD, Nicholson JK, and Thompson RPH (1999) Dietary minerals in the gastrointestinal tract: hydroxypolymerisation of aluminium is regulated by luminal mucins. *Journal of Inorganic Biochemistry* **75**(3): 167-180.
140. Gomez-Morilla I, Thoree V, Powell JJ, Kirkby KJ, and Grime GW (2006) Identification and quantitative analysis of calcium phosphate microparticles in intestinal tissue by nuclear microscopy. *Nuclear Instruments and Methods in Physics Research Section B: Beam Interactions with Materials and Atoms* **249**: 665-669.
141. Schedl HP, Osbaldiston GW, and Mills IH (1968) Absorption, secretion, and precipitation of calcium in the small intestine of the dog. *American Journal of Physiology* **214**(4): 814-819.
142. Thomas-McKay E (2010) *Endogenous dietary microparticles: form and function*. PhD thesis (University of Cambridge, Cambridge, United Kingdom).
143. Pele L and Powell JJ (2005) Microparticles: a link between modern life and inflammatory bowel disease? In *Inflammatory Bowel Disease: Translation from Basic Research to Clinical Practice,* Falk Symposium, eds Colombel JF, Gasche C, Scholmerich J, and Vucelic B (Springer, Dordrecht, Netherlands), vol. 140, pp. 123-137.
144. Urbanski SJ, Arsenault AL, Green FH, and Haber G (1989) Pigment resembling atmospheric dust in Peyer's patches. *Modern Pathology* **2**(3): 222-226.
145. Govers MJAP, Termont DSML, van Aken GA, and van der Meer RV (1994) Characterization of the adsorption of conjugated and unconjugated bile acids to insoluble, amorphous calcium phosphate. *Journal of Lipid Research* **35**(5): 741-748.
146. Lomer MCE, Thompson RPH, and Powell JJ (2002) Fine and ultrafine particles of the diet: influence on the mucosal immune response and association with Crohn's disease. *Proceedings of the Nutrition Society* **61**(1): 123-130.
147. Powell JJ, Ainley CC, Harvey RSJ, Mason IM, Kendall MD, Sankey EA, Dhillon AP, and Thompson RPH (1996) Characterisation of inorganic microparticles in pigment cells of human gut associated lymphoid tissue. *Gut* **38**(3): 390-395.
148. Codex Alimentarius (1995) Codex general standard for food additives. pp. 1-332.

149. European Parliament and Council (2011) Commission regulation (EU) No 1129/2011. *Official Journal of the European Union* **L 295**: 1-177.

150. Lomer MCE, Hutchinson C, Volkert S, Greenfield SM, Catterall A, Thompson RPH, and Powell JJ (2004) Dietary sources of inorganic microparticles and their intake in healthy subjects and patients with Crohn's disease. *British Journal of Nutrition* **92**(6): 947-955.

151. Australia New Zealand Food Standards Code (2013) Labelling of ingredients. *Standard 1.2.4*: 1-18.

152. Kosikowski FV and Brown DP (1969) Application of titanium dioxide to whiten mozzarella cheese. *Journal of Dairy Science* **52**(7): 968-970.

153. Phillips LG and Barbano DM (1997) The influence of fat substitutes based on protein and titanium dioxide on the sensory properties of lowfat milks. *Journal of Dairy Science* **80**(11): 2726-2731.

154. Lomer MCE, Thompson RPH, Commisso J, Keen CL, and Powell JJ (2000) Determination of titanium dioxide in foods using inductively coupled plasma optical emission spectrometry. *Analyst* **125**(12): 2339-2343.

155. Weir A, Westerhoff P, Fabricius L, Hristovski K, and von Goetz N (2012) Titanium dioxide nanoparticles in food and personal care products. *Environmental Science and Technology* **46**(4): 2242-2250.

156. European Parliament and Council (1994) European Parliament and Council directive 94/36/EC. *Official Journal of the European Communities* **L 237**: 13-29.

157. Anton R, Barlow S, Boskou D, Castle L, Crebelli R, Dekant W, Engel K-H, Forsythe S, Grunow W, Heinonen M*, et al.* (2004) Opinion of the Scientific Panel on Food Additives, Flavourings, Processing Aids and Materials in Contact with Food on a request from the Commission related to the safety in use of rutile titanium dioxide as an alternative to the presently permitted anatase form. *EFSA Journal* **163**: 1-12.

158. Ministry of Agriculture Fisheries and Food (1993) Dietary intake of food additives in the UK: initial surveillance. In *Food Surveillance Paper No. 37*, (H.M. Stationary Office, London, United Kingdom).

159. European Parliament and Council (2012) Commission regulation (EU) No 380/2012. *Official Journal of the European Union* **L 119**: 14-38.

160. Powell JJ, Ainley CC, Evans R, and Thompson RPH (1994) Intestinal perfusion of dietary levels of aluminium: association with the mucosa. *Gut* **35**(8): 1053-1057.

161. Powell JJ, Evans SM, Lomer MCE, and Thompson RPH (1999) What are intestinal pigment cells? *Inflammatory Bowel Disease Monitor* **1**(3): 71-74.

162. Thoree V, Skepper J, Deere H, Pele LC, Thompson RPH, and Powell JJ (2008) Phenotype of exogenous microparticle-containing pigment cells of the human Peyer's patch in inflamed and normal ileum. *Inflammation Research* **57**(8): 374-378.

163. Powell JJ, Faria N, Thomas-McKay E, and Pele LC (2010) Origin and fate of dietary nanoparticles and microparticles in the gastrointestinal tract. *Journal of Autoimmunity* **34**(3): J226-J233.

164. Kalgaonkar S and Lönnerdal B (2009) Receptor-mediated uptake of ferritin-bound iron by human intestinal Caco-2 cells. *Journal of Nutritional Biochemistry* **20**(4): 304-311.

165. Iannuccelli V, Montanari M, Bertelli D, Pellati F, and Coppi G (2011) Microparticulate polyelectrolyte complexes for gentamicin transport across intestinal epithelia. *Drug Delivery* **18**(1): 26-37.

166. Turner JR (2009) Intestinal mucosal barrier function in health and disease. *Nature Reviews Immunology* **9**(11): 799-809.

167. Ulluwishewa D, Anderson RC, McNabb WC, Moughan PJ, Wells JM, and Roy NC (2011) Regulation of tight junction permeability by intestinal bacteria and dietary components. *Journal of Nutrition* **141**(5): 769-776.

168. Awaad A, Nakamura M, and Ishimura K (2012) Imaging of size-dependent uptake and identification of novel pathways in mouse Peyer's patches using fluorescent organosilica particles. *Nanomedicine: Nanotechnology, Biology, and Medicine* **8**(5): 627-636.

169. Volkheimer G (1974) Passage of particles through the wall of the gastrointestinal tract. *Environmental Health Perspectives* **9**: 215-225.

170. Hillyer JF and Albrecht RM (2001) Gastrointestinal persorption and tissue distribution of differently sized colloidal gold nanoparticles. *Journal of Pharmaceutical Sciences* **90**(12): 1927-1936.

171. Ermak TH and Giannasca PJ (1998) Microparticle targeting to M cells. *Advanced Drug Delivery Reviews* **34**(2-3): 261-283.

172. Jani PU, McCarthy DE, and Florence AT (1994) Titanium dioxide (rutile) particle uptake from the rat GI tract and translocation to systemic organs after oral administration. *International Journal of Pharmaceutics* **105**(2): 157-168.

173. Ermak TH, Dougherty EP, Bhagat HR, Kabok Z, and Pappo J (1995) Uptake and transport of copolymer biodegradable microspheres by rabbit Peyer's patch M cells. *Cell and Tissue Research* **279**(2): 433-436.

174. Jani PU, McCarthy DE, and Florence AT (1992) Nanosphere and microsphere uptake via Peyer's patches: observation of the rate of uptake in the rat after a single oral dose. *International Journal of Pharmaceutics* **86**(2-3): 239-246.

175. Jepson MA, Simmons NL, Savidge TC, James PS, and Hirst BH (1993) Selective binding and transcytosis of latex microspheres by rabbit intestinal M cells. *Cell and Tissue Research* **271**(3): 399-405.

176. Pappo J and Ermak TH (1989) Uptake and translocation of fluorescent latex particles by rabbit Peyer's patch follicle epithelium: a quantitative model for M cell uptake. *Clinical and Experimental Immunology* **76**(1): 144-148.

177. Primard C, Rochereau N, Luciani E, Genin C, Delair T, Paul S, and Verrier B (2010) Traffic of poly(lactic acid) nanoparticulate vaccine vehicle from intestinal mucus to sub-epithelial immune competent cells. *Biomaterials* **31**(23): 6060-6068.

178. Sass W, Dreyer HP, and Seifert J (1990) Rapid insorption of small particles in the gut. *American Journal of Gastroenterology* **85**(3): 255-260.

179. Zigmond E and Jung S (2013) Intestinal macrophages: well educated exceptions from the rule. *Trends in Immunology* **34**(4): 162-168.

180. Rescigno M, Urbano M, Valzasina B, Francolini M, Rotta G, Bonasio R, Granucci F, Kraehenbuhl JP, and Ricciardi-Castagnoli P (2001) Dendritic cells express tight junction proteins and penetrate gut epithelial monolayers to sample bacteria. *Nature Immunology* **2**(4): 361-367.

181. Niess JH, Brand S, Gu X, Landsman L, Jung S, McCormick BA, Vyas JM, Boes M, Ploegh HL, Fox JG*, et al.* (2005) CX_3CR1-mediated dendritic cell access to the intestinal lumen and bacterial clearance. *Science* **307**(5707): 254-258.

182. Lelouard H, Henri S, de Bovis B, Mugnier B, Chollat-Namy A, Malissen B, Meresse S, and Gorvel JP (2010) Pathogenic bacteria and dead cells are internalized by a unique subset of Peyer's patch dendritic cells that express lysozyme. *Gastroenterology* **138**(1): 173-184.

183. Lelouard H, Fallet M, de Bovis B, Méresse S, and Gorvel J (2012) Peyer's patch dendritic cells sample antigens by extending dendrites through M cell-specific transcellular pores. *Gastroenterology* **142**(3): 592-601.

184. Vallon-Eberhard A, Landsman L, Yogev N, Verrier B, and Jung S (2006) Transepithelial pathogen uptake into the small intestinal lamina propria. *Journal of Immunology* **176**(4): 2465-2469.

185. Iavicoli I, Leso V, Fontana L, and Bergamaschi A (2011) Toxicological effects of titanium dioxide nanoparticles: a review of *in vitro* mammalian studies. *European Review for Medical and Pharmacological Sciences* **15**(5): 481-508.

186. de Berardis B, Civitelli G, Condello M, Lista P, Pozzi R, Arancia G, and Meschini S (2010) Exposure to ZnO nanoparticles induces oxidative stress and cytotoxicity in human colon carcinoma cells. *Toxicology and Applied Pharmacology* **246**(3): 116-127.

187. Gerloff K, Albrecht C, Boots AW, Forster I, and Schins RPF (2009) Cytotoxicity and oxidative DNA damage by nanoparticles in human intestinal Caco-2 cells. *Nanotoxicology* **3**(4): 355-364.

188. Gerloff K, Fenoglio I, Carella E, Kolling J, Albrecht C, Boots AW, Förster I, and Schins RPF (2012) Distinctive toxicity of TiO_2 rutile/anatase mixed phase nanoparticles on Caco-2 cells. *Chemical Research in Toxicology* **25**(3): 646-655.

189. Koeneman BA, Zhang Y, Westerhoff P, Chen Y, Crittenden JC, and Capco DG (2010) Toxicity and cellular responses of intestinal cells exposed to titanium dioxide. *Cell Biology and Toxicology* **26**(3): 225-238.

190. Zhang AP and Sun YP (2004) Photocatalytic killing effect of TiO_2 nanoparticles on Ls-174-t human colon carcinoma cells. *World Journal of Gastroenterology* **10**(21): 3191-3193.

191. Morishige T, Yoshioka Y, Tanabe A, Yao X, Tsunoda Si, Tsutsumi Y, Mukai Y, Okada N, and Nakagawa S (2010) Titanium dioxide induces different levels of IL-1β production dependent on its particle characteristics through caspase-1 activation mediated by reactive oxygen species and cathepsin B. *Biochemical and Biophysical Research Communications* **392**(2): 160-165.

192. Xia T, Hamilton Jr RF, Bonner JC, Crandall ED, Elder A, Fazlollahi F, Girtsman TA, Kim K, Mitra S, Ntim SA*, et al.* (2013) Interlaboratory evaluation of *in vitro* cytotoxicity and inflammatory responses to engineered nanomaterials: the NIEHS Nano GO Consortium. *Environmental Health Perspectives* **121**(6): 683-690.

193. Lucarelli M, Gatti AM, Savarino G, Quattroni P, Martinelli L, Monari E, and Boraschi D (2004) Innate defence functions of macrophages can be biased by nano-sized ceramic and metallic particles. *European Cytokine Network* **15**(4): 339-346.

194. Zhang J, Song W, Guo J, Sun Z, Li L, Ding F, and Gao M (2012) Cytotoxicity of different sized TiO_2 nanoparticles in mouse macrophages. *Toxicology and Industrial Health* **29**(6): 523-533.

195. Möller W, Hofer T, Ziesenis A, Karg E, and Heyder J (2002) Ultrafine particles cause cytoskeletal dysfunctions in macrophages. *Toxicology and Applied Pharmacology* **182**(3): 197-207.

196. Kim SB and Tao H (2011) Nanoscale titanium dioxide particles modulate signaling cascades for tumor necrosis factor-α release from macrophages. *Journal of Health Science* **57**(2): 177-183.

197. Palomäki J, Karisola P, Pylkkänen L, Savolainen K, and Alenius H (2010) Engineered nanomaterials cause cytotoxicity and activation on mouse antigen presenting cells. *Toxicology* **267**(1-3): 125-131.

198. Sohaebuddin SK, Thevenot PT, Baker D, Eaton JW, and Tang L (2010) Nanomaterial cytotoxicity is composition, size, and cell type dependent. *Particle and Fibre Toxicology* **7**: 22.

199. Wilhelmi V, Fischer U, van Berlo D, Schulze-Osthoff K, Schins RPF, and Albrecht C (2012) Evaluation of apoptosis induced by nanoparticles and fine particles in RAW 264.7 macrophages: facts and artefacts. *Toxicology in Vitro* **26**(2): 323-334.

200. Xia T, Kovochich M, Brant J, Hotze M, Sempf J, Oberley T, Sioutas C, Yeh JI, Wiesner MR, and Nel AE (2006) Comparison of the abilities of ambient and manufactured nanoparticles to induce cellular toxicity according to an oxidative stress paradigm. *Nano Letters* **6**(8): 1794-1807.

201. Xiong S, George S, Yu H, Damoiseaux R, France B, Ng KW, and Loo JSC (2013) Size influences the cytotoxicity of poly (lactic-co-glycolic acid) (PLGA) and titanium dioxide (TiO_2) nanoparticles. *Archives of Toxicology* **87**(6): 1075-1086.

202. National Cancer Institute (1979) Bioassay of titanium dioxide for possible carcinogenicity. In *Carcinogenesis: Technical Report Series No. 97* (U.S. Department of Health, Eduction, and Welfare, Bethesda, Maryland), pp. 1-130.

203. Trouiller B, Reliene R, Westbrook A, Solaimani P, and Schiestl RH (2009) Titanium dioxide nanoparticles induce DNA damage and genetic instability *in vivo* in mice. *Cancer Research* **69**(22): 8784-8789.

204. Zhang R, Niu Y, Li Y, Zhao C, Song B, and Zhou Y (2010) Acute toxicity study of the interaction between titanium dioxide nanoparticles and lead acetate in mice. *Environmental Toxicology and Pharmacology* **30**(1): 52-60.

205. Wang J, Zhou G, Chen C, Yu H, Wang T, Ma Y, Jia G, Gao Y, Li B, Sun J*, et al.* (2007) Acute toxicity and biodistribution of different sized titanium dioxide particles in mice after oral administration. *Toxicology Letters* **168**(2): 176-185.

206. Warheit DB, Webb TR, Reed KL, Frerichs S, and Sayes CM (2007) Pulmonary toxicity study in rats with three forms of ultrafine-TiO_2 particles: differential responses related to surface properties. *Toxicology* **230**(1): 90-104.

207. Tassinari R, Cubadda F, Moracci G, Aureli F, D'Amato M, Valeri M, de Berardis B, Raggi A, Mantovani A, Passeri D*, et al.* (2014) Oral, short-term exposure to titanium dioxide nanoparticles in Sprague-Dawley rat: focus on reproductive and endocrine systems and spleen. *Nanotoxicology* **8**(6): 654-662.

208. Nogueira CM, de Azevedo WM, Zaidan Dagli ML, Toma SH, Leite AZA, Lordello ML, Nishitokukado I, Ortiz-Agostinho CL, Seixas Duarte MI, Ferreira MA*, et al.* (2012) Titanium dioxide induced inflammation in the small intestine. *World Journal of Gastroenterology* **18**(34): 4729-4735.

209. Bu Q, Yan G, Deng P, Peng F, Lin H, Xu Y, Cao Z, Zhou T, Xue A, Wang Y*, et al.* (2010) NMR-based metabonomic study of the sub-acute toxicity of titanium dioxide nanoparticles in rats after oral administration. *Nanotechnology* **21**(12): 125105.

210. Wang J, Li N, Zheng L, Wang S, Wang Y, Zhao X, Duan Y, Cui Y, Zhou M, Cai J*, et al.* (2010) P38-Nrf-2 signaling pathway of oxidative stress in mice caused by nanoparticulate TiO_2. *Biological Trace Element Research* **140**(2): 186-197.

211. Duan Y, Liu J, Ma L, Li N, Liu H, Wang J, Zheng L, Liu C, Wang X, Zhao X*, et al.* (2010) Toxicological characteristics of nanoparticulate anatase titanium dioxide in mice. *Biomaterials* **31**(5): 894-899.

212. Warheit DB, Hoke RA, Finlay C, Donner EM, Reed KL, and Sayes CM (2007) Development of a base set of toxicity tests using ultrafine TiO_2 particles as a component of nanoparticle risk management. *Toxicology Letters* **171**(3): 99-110.

213. Fröhlich E and Roblegg E (2012) Models for oral uptake of nanoparticles in consumer products. *Toxicology* **291**(1-3): 10-17.

214. Berglund F and Carlmark B (2011) Titanium, sinusitis, and the yellow nail syndrome. *Biological Trace Element Research* **143**(1): 1-7.

215. Ashwood P, Thompson RPH, and Powell JJ (2007) Fine particles that adsorb lipopolysaccharide *via* bridging calcium cations may mimic bacterial pathogenicity towards cells. *Experimental Biology and Medicine* **232**(1): 107-117.

216. Powell JJ, Harvey RSJ, Ashwood P, Wolstencroft R, Gershwin ME, and Thompson RPH (2000) Immune potentiation of ultrafine dietary particles in normal subjects and patients with inflammatory bowel disease. *Journal of Autoimmunity* **14**(1): 99-105.

217. Evans SM, Ashwood P, Warley A, Berisha F, Thompson RPH, and Powell JJ (2002) The role of dietary microparticles and calcium in apoptosis and interleukin-1β release of intestinal macrophages. *Gastroenterology* **123**(5): 1543-1553.

218. Butler M, Boyle JJ, Powell JJ, Playford RJ, and Ghosh S (2007) Dietary microparticles implicated in Crohn's disease can impair macrophage phagocytic activity and act as adjuvants in the presence of bacterial stimuli. *Inflammation Research* **56**(9): 353-361.

219. Evans SM, Powell JJ, Ashwood P, Thompson RPH, and Harvey RSJ (1999) Ultrafine particles in the aetiology of Crohn's disease. *Inflammatory Bowel Disease Monitor* **1**(2): 39-45.

220. Latz E, Xiao TS, and Stutz A (2013) Activation and regulation of the inflammasomes. *Nature Reviews Immunology* **13**(6): 397-411.

221. Dinarello CA (2009) Immunological and inflammatory functions of the interleukin-1 family. *Annual Review of Immunology* **27**: 519-550.

222. Becker HM, Bertschinger MM, and Rogler G (2012) Microparticles and their impact on intestinal immunity. *Digestive Diseases* **30**(Suppl. 3): 47-54.

223. Schroder K and Tschopp J (2010) The inflammasomes. *Cell* **140**(6): 821-832.

224. Shi H, Magaye R, Castranova V, and Zhao J (2013) Titanium dioxide nanoparticles: a review of current toxicological data. *Particle and Fibre Toxicology* **10**: 15.

225. Baan R, Straif K, Grosse Y, Secretan B, El Ghissassi F, and Cogliano V (2006) Carcinogenicity of carbon black, titanium dioxide, and talc. *Lancet Oncology* **7**(4): 295-296.

226. Baan RA (2007) Carcinogenic hazards from inhaled carbon black, titanium dioxide, and talc not containing asbestos or asbestiform fibers: recent evaluations by an IARC Monographs Working Group. *Inhalation Toxicology* **19**(SUPPL. 1): 213-228.

227. Heinrich U, Fuhst R, Rittinghausen S, Creutzenberg O, Bellmann B, Koch W, and Levsen K (1995) Chronic inhalation exposure of Wistar rats and two different strains of mice to Diesel engine exhaust, carbon black, and titanium dioxide. *Inhalation Toxicology* **7**(4): 533-556.

228. Koizumi A, Tsukada M, Hirano S, Kamiyama S, Masuda H, and Suzuki KT (1993) Energy restriction that inhibits cellular proliferation by torpor can decrease susceptibility to spontaneous and asbestos-induced lung tumors in A/J mice. *Laboratory Investigation* **68**(6): 728-739.

229. Pott F and Roller M (2005) Carcinogenicity study with nineteen granular dusts in rats. *European Journal of Oncology* **10**(4): 249-281.

230. Boffetta P, Soutar A, Cherrie JW, Granath F, Andersen A, Anttila A, Blettner M, Gaborieau V, Klug SJ, Langard S*, et al.* (2004) Mortality among workers employed in the titanium dioxide production industry in Europe. *Cancer Causes and Control* **15**(7): 697-706.

231. Böckmann J, Lahl H, Eckert T, and Unterhalt B (2000) Titan-Blutspiegel vor und nach Belastungsversuchen mit Titandioxid [Blood levels of titanium before and after oral administration of titanium dioxide]. *Pharmazie* **55**(2): 140-143.

232. Lomer MCE, Harvey RSJ, Evans SM, Thompson RPH, and Powell JJ (2001) Efficacy and tolerability of a low microparticle diet in a double blind, randomized, pilot study in Crohn's disease. *European Journal of Gastroenterology and Hepatology* **13**(2): 101-106.

233. Lomer MCE, Grainger SL, Ede R, Catterall AP, Greenfield SM, Cowan RE, Vicary FR, Jenkins AR, Fidler H, Harvey RS*, et al.* (2005) Lack of efficacy of a reduced microparticle diet in a multi-centred trial of patients with active Crohn's disease. *European Journal of Gastroenterology and Hepatology* **17**(3): 377-384.

234. Lee JCW, Halpern S, Lowe DG, Forbes A, and LennardJones JE (1996) Absence of skin sensitivity to oxides of aluminium, silicon, titanium or zirconium in patients with Crohn's disease. *Gut* **39**(2): 231-233.

235. Lapre JA, de Vries HT, Koeman JH, and van der Meer R (1993) The antiproliferative effect of dietary calcium on colonic epithelium is mediated by luminal surfactants and dependent on the type of dietary fat. *Cancer Research* **53**(4): 784-789.

236. van der Meer R, Welberg JWM, Kuipers F, Kleibeuker JH, Mulder NH, Termont DSML, Vonk RJ, de Vries HT, and de Vries EGE (1990) Effects of supplemental dietary calcium on the intestinal association of calcium, phosphate, and bile acids. *Gastroenterology* **99**(6): 1653-1659.

237. Penman ID, Liang QL, Bode J, Eastwood MA, and Arends MJ (2000) Dietary calcium supplementation increases apoptosis in the distal murine colonic epithelium. *Journal of Clinical Pathology* **53**(4): 302-307.

238. Liu K, Iyoda T, Saternus M, Kimura Y, Inaba K, and Steinman RM (2002) Immune tolerance after delivery of dying cells to dendritic cells in situ. *Journal of Experimental Medicine* **196**(8): 1091-1097.

239. Sauter B, Albert ML, Francisco L, Larsson M, Somersan S, and Bhardwaj N (2000) Consequences of cell death: exposure to necrotic tumor cells, but not primary tissue cells or apoptotic cells, induces the maturation of immunostimulatory dendritic cells. *Journal of Experimental Medicine* **191**(3): 423-433.

240. Smythies LE, Sellers M, Clements RH, Mosteller-Barnum M, Meng G, Benjamin WH, Orenstein JM, and Smith PD (2005) Human intestinal macrophages display profound inflammatory anergy despite avid phagocytic and bacteriocidal activity. *Journal of Clinical Investigation* **115**(1): 66-75.

241. Ellingsen JE (1991) A study on the mechanism of protein adsorption to TiO_2. *Biomaterials* **12**(6): 593-596.

242. Horie M, Nishio K, Fujita K, Endoh S, Miyauchi A, Saito Y, Iwahashi H, Yamamoto K, Murayama H, Nakano H*, et al.* (2009) Protein adsorption of ultrafine metal oxide and its influence on cytotoxicity toward cultured cells. *Chemical Research in Toxicology* **22**(3): 543-553.

243. Gullberg E and Söderholm JD (2006) Peyer's patches and M cells as potential sites of the inflammatory onset in Crohn's disease. *Annals of the New York Academy of Sciences* **1072**: 218-232.

244. Chess S, Olander G, Puestow CB, Benner W, and Chess D (1950) Regional enteritis: clinical and experimental observations. *Surgery Gynecology and Obstetrics* **91**(3): 343-350.

245. Reichert FL and Mathes ME (1936) Experimental lymphedema of the intestinal tract and its relation to regional cictrizing enteritis. *Annals of Surgery* **104**(4): 601-616.

246. Harvey R, Powell JJ, and Thompson RPH (1996) A review of the geochemical factors linked to podoconiosis. *Environmental Geochemistry and Health* **113**: 255-260.

247. Fiocchi C (1998) Inflammatory bowel disease: etiology and pathogenesis. *Gastroenterology* **115**(1): 182-205.

248. McAlindon ME, Hawkey CJ, and Mahida YR (1998) Expression of interleukin 1β and interleukin 1β converting enzyme by intestinal macrophages in health and inflammatory bowel disease. *Gut* **42**(2): 214-219.

249. Geddes K, Rubino SJ, Magalhaes JG, Streutker C, Le Bourhis L, Cho JH, Robertson SJ, Kim CJ, Kaul R, Philpott DJ*, et al.* (2011) Identification of an innate T helper type 17 response to intestinal bacterial pathogens. *Nature Medicine* **17**(7): 837-844.

250. van Beelen AJ, Zelinkova Z, Taanman-Kueter EW, Muller FJ, Hommes DW, Zaat SAJ, Kapsenberg ML, and de Jong EC (2007) Stimulation of the intracellular bacterial sensor NOD2 programs dendritic cells to promote interleukin-17 production in human memory T cells. *Immunity* **27**(4): 660-669.

251. Rovedatti L, Kudo T, Biancheri P, Sarra M, Knowles CH, Rampton DS, Corazza GR, Monteleone G, Di Sabatino A, and MacDonald TT (2009) Differential regulation of

interleukin 17 and interferon γ production in inflammatory bowel disease. *Gut* **58**(12): 1629-1636.

252. Miossec P, Korn T, and Kuchroo VK (2009) Interleukin-17 and type 17 helper T cells. *New England Journal of Medicine* **361**(9): 888-898.

253. Hsu LC, Ali SR, McGillivray S, Tseng PH, Mariathasan S, Humke EW, Eckmann L, Powell JJ, Nizet V, Dixit VM*, et al.* (2008) A NOD2-NALP1 complex mediates caspase-1-dependent IL-1β secretion in response to *Bacillus anthracis* infection and muramyl dipeptide. *Proceedings of the National Academy of Sciences of the United States of America* **105**(22): 7803-7808.

254. Pujalté I, Passagne I, Brouillaud B, Tréguer M, Durand E, Ohayon-Courtès C, and L'Azou B (2011) Cytotoxicity and oxidative stress induced by different metallic nanoparticles on human kidney cells. *Particle and Fibre Toxicology* **8**(10).

255. Filipe V, Hawe A, and Jiskoot W (2010) Critical evaluation of nanoparticle tracking analysis (NTA) by NanoSight for the measurement of nanoparticles and protein aggregates. *Pharmaceutical Research* **27**(5): 796-810.

256. Davies JQ and Gordon S (2005) Isolation and culture of murine macrophages. In *Basic Cell Culture Protocols,* Methods in Molecular Biology, eds Helgason CD and Miller CL (Humana Press, Totowa, New Jersey), 3rd edition, vol. 290, pp. 91-104.

257. Masters JR and Stacey GN (2007) Changing medium and passging cell lines. *Nature Protocols* **2**(9): 2276-2284.

258. Marim FM, Silveira TN, Lima DS, Jr., and Zamboni DS (2010) A method for generation of bone marrow-derived macrophages from cryopreserved mouse bone marrow cells. *Plos One* **5**(12): e15263.

259. Pan QL, Mathison J, Fearns C, Kravchenko VV, Correia JD, Hoffman HM, Kobayashi KS, Bertin J, Grant EP, Coyle AJ*, et al.* (2007) MDP-induced interleukin-1β processing requires Nod2 and CIAS1/NALP3. *Journal of Leukocyte Biology* **82**(1): 177-183.

260. Winter M, Beer HD, Hornung V, Kärmer U, Schins RPF, and Förster I (2011) Activation of the inflammasome by amorphous silica and TiO_2 nanoparticles in murine dendritic cells. *Nanotoxicology* **5**(3): 326-340.

261. Hong HA, Khaneja R, Tam NMK, Cazzato A, Tan S, Urdaci M, Brisson A, Gasbarrini A, Barnes I, and Cutting SM (2009) *Bacillus subtilis* isolated from the human gastrointestinal tract. *Research in Microbiology* **160**(2): 134-143.

262. Hewitt RE, Pele LC, Tremelling M, Metz A, Parkes M, and Powell JJ (2012) Immuno-inhibitory PD-L1 can be induced by a peptidoglycan/NOD2 mediated pathway in primary monocytic cells and is deficient in Crohn's patients with homozygous NOD2 mutations. *Clinical Immunology* **143**(2): 162-169.

263. Pan QL, Kravchenko V, Katz A, Huang S, Ii M, Mathison JC, Kobayashi K, Flavell RA, Schreiber RD, Goeddel D*, et al.* (2006) NF-*κ*B-inducing kinase regulates selected gene expression in the Nod2 signaling pathway. *Infection and Immunity* **74**(4): 2121-2127.

264. Suzuki H, Toyooka T, and Ibuki Y (2007) Simple and easy method to evaluate uptake potential of nanoparticles in mammalian cells using a flow cytometric light scatter analysis. *Environmental Science and Technology* **41**(8): 3018-3024.

265. Austyn JM and Gordon S (1981) F4/80, a monoclonal antibody directed specifically against the mouse macrophage. *European Journal of Immunology* **11**(10): 805-815.

266. Zucker RM, Massaro EJ, Sanders KM, Degn LL, and Boyes WK (2010) Detection of TiO_2 nanoparticles in cells by flow cytometry. *Cytometry Part A* **77**(7): 677-685.

267. Azuma M, Ito D, Yagita H, Okumura K, Phillips JH, Lanier LL, and Somoza C (1993) B70 antigen is a second ligand for CTLA-4 and CD28. *Nature* **366**(6450): 76-79.

268. Freeman G, Gribben J, Boussiotis V, Ng J, Restivo V, Lombard L, Gray G, and Nadler L (1993) Cloning of B7-2: a CTLA-4 counter-receptor that costimulates human T cell proliferation. *Science* **262**(5135): 909-911.

269. Linsley PS, Brady W, Grosmaire L, Aruffo A, Damle NK, and Ledbetter JA (1991) Binding of the B cell activation antigen B7 to CD28 costimulates T cell proliferation and interleukin 2 mRNA accumulation. *Journal of Experimental Medicine* **173**(3): 721-730.

270. Carreno BM and Collins M (2002) The B7 family of ligands and its receptors: new pathways for costimulation and inhibition of immune responses. *Annual Review of Immunology* **20**: 29-53.

271. R Development Core Team (2010) *R: a language and environment for statistical computing* (R Foundation for Statistical Computing, Vienna, Austria).

272. Dalgaard P (2008) *Introductory statistics with R* (Springer Science+Business Media, New York, New York) 2nd edition, pp. 363.

273. Kabacoff RI (2011) *R in action: data analysis and graphics with R* (Manning Publications, Shelter Island, New York) pp. 450.

274. Prasad RY, Wallace K, Daniel KM, Tennant AH, Zucker RM, Strickland J, Dreher K, Kligerman AD, Blackman CF, and Demarini DM (2013) Effect of treatment media on the agglomeration of titanium dioxide nanoparticles: impact on genotoxicity, cellular interaction, and cell cycle. *ACS Nano* **7**(3): 1929-1942.

275. Geissmann F, Gordon S, Hume DA, Mowat AM, and Randolph GJ (2010) Unravelling mononuclear phagocyte heterogeneity. *Nature Reviews Immunology* **10**(6): 453-460.

276. Weigmann B, Tubbe I, Seidel D, Nicolaev A, Becker C, and Neurath MF (2007) Isolation and subsequent analysis of murine lamina propria mononuclear cells from colonic tissue. *Nature Protocols* **2**(10): 2307-2311.

277. Stringer B, Imrich A, and Kobzik L (1995) Flow cytometric assay of lung macrophage uptake of environmental particulates. *Cytometry* **20**(1): 23-32.

278. Shukla RK, Kumar A, Gurbani D, Pandey AK, Singh S, and Dhawan A (2013) TiO_2 nanoparticles induce oxidative DNA damage and apoptosis in human liver cells. *Nanotoxicology* **7**(1): 48-60.

279. Wolfkamp SCS, Verseyden C, Vogels EWM, Meisner S, Boonstra K, Peters CP, Stokkers PCF, and te Velde AA (2014) *ATG16L1* and *NOD2* polymorphisms enhance phagocytosis in monocytes of Crohn's disease patients. *World Journal of Gastroenterology* **20**(10): 2664-2672.

280. Fleischer J, Soeth E, Reiling N, Grage-Griebenow E, Flad HD, and Ernst M (1996) Differential expression and function of CD80 (B7-1) and CD86 (B7-2) on human peripheral blood monocytes. *Immunology* **89**(4): 592-598.

281. Tsay T-B, Chang C-J, Chen P-H, Hsu C-M, and Chen L-W (2009) Nod2 mutation enhances NF-kappaB activity and bacterial killing activity of macrophages. *Inflammation* **32**(6): 372-378.

282. Takeda K, Kaisho T, and Akira S (2003) Toll-like receptors. *Annual Review of Immunology* **21**: 335-376.

283. Maino VC and Picker LJ (1998) Identification of functional subsets by flow cytometry: intracellular detection of cytokine expression. *Cytometry* **34**(5): 207-215.

284. Bennett WE and Cohn ZA (1966) The isolation and selected properties of blood monocytes. *Journal of Experimental Medicine* **123**(1): 145-160.

285. Lovelock JE and Bishop MWH (1959) Prevention of freezing damage to living cells by dimethyl sulphoxide. *Nature* **183**(4672): 1394-1395.

286. Xing L and Remick DG (2005) Mechanisms of dimethyl sulfoxide augmentation of IL-1β production. *Journal of Immunology* **174**(10): 6195-6202.

287. Ahn H, Kim J, Jeung EB, and Lee GS (2014) Dimethyl sulfoxide inhibits NLRP3 inflammasome activation. *Immunobiology* **219**(4): 315-322.

288. Pele L, Haas CT, Hewitt R, Faria N, Brown A, and Powell J (2014) Artefactual nanoparticle activation of the inflammasome platform: *in vitro* evidence with a nano-formed calcium phosphate. *Nanomedicine* **Electronic publication ahead of print**: 1-12.

289. Hazuda DJ, Lee JC, and Young PR (1988) The kinetics of interleukin 1 secretion from activated monocytes: differences between interleukin 1α and interleukin 1β. *Journal of Biological Chemistry* **263**(17): 8473-8479.

290. Lonnemann G, Endres S, Meer JWMVD, Cannon JG, Koch KM, and Dinarello CA (1989) Differences in the synthesis and kinetics of release of interleukin 1α, interleukin 1β and tumor necrosis factor from human mononuclear cells. *European Journal of Immunology* **19**(9): 1531-1536.

291. Cho WS, Kang BC, Lee JK, Jeong J, Che JH, and Seok SH (2013) Comparative absorption, distribution, and excretion of titanium dioxide and zinc oxide nanoparticles after repeated oral administration. *Particle and Fibre Toxicology* **10**: 9.

292. Hummel TZ, Kindermann A, Stokkers PCF, Benninga MA, and ten Kate FJW (2014) Exogenous pigment in Peyer's patches of children suspected for inflammatory bowel disease. *Journal of Pediatric Gastroenterology and Nutrition* **58**(4): 477-480.

293. The Jackson Laboratory. *Mouse Phenome Database*. Available from: http://phenome.jax.org (accessed June 2014).

294. American Institute of Nutrition (1977) Report of the American Institute of Nutrition *ad hoc* Committee on standards for nutritional studies. *Journal of Nutrition* **107**(7): 1340-1348.

295. American Institute of Nutrition (1980) Second report of the *ad hoc* Committee on standards for nutritional studies. *Journal of Nutrition* **110**(8): 1726.

296. Keller E and Goldman RD (2006) Light microscopy. In *Basic methods in microscopy: protocols and concepts from "Cells: a laboratory manual"*, eds Spector DL and Goldman RD (Cold Spring Harbor Laboratory Press, Cold Spring Harbor, New York), pp. 1-42.

297. Murphy DB and Davidson MW (2013) *Fundamentals of light microscopy and electronic imaging* (Wiley-Blackwell, Hoboken, New Jersey) 2nd edition, pp. 538.

298. Fischer AH, Jacobson KA, Rose J, and Zeller R (2006) Preparation of cells and tissues for fluorescence microscopy. In *Basic methods in microscopy: protocols and concepts from "Cells: a laboratory manual"*, eds Spector DL and Goldman RD (Cold Spring Harbor Laboratory Press, Cold Spring Harbor, New York), pp. 105-118.

299. Hibbs AR (2004) *Confocal microscopy for biologists* (Kluwer Academic/Plenum Publishers, New York, New York) pp. 467.

300. Monici M (2005) Cell and tissue autofluorescence and diagnostic applications. *Biotechnology Annual Review* **11**: 227-256.

301. Sadiq R, Bhalli JA, Yan J, Woodruff RS, Pearce MG, Li Y, Mustafa T, Watanabe F, Pack LM, Biris AS*, et al.* (2012) Genotoxicity of TiO_2 anatase nanoparticles in B6C3F1 male mice evaluated using *Pig-a* and flow cytometric micronucleus assays. *Mutation Research: Genetic Toxicology and Environmental Mutagenesis* **745**(1-2): 65-72.

302. Duriancik DA and Hoag KA (2009) The identification and enumeration of dendritic cell populations from individual mouse spleen and Peyer's patches using flow cytometric analysis. *Cytometry Part A* **75**(11): 951-959.

303. Johansson-Lindbom B and Agace WW (2007) Generation of gut-homing T cells and their localization to the small intestinal mucosa. *Immunological Reviews* **215**(1): 226-242.

304. Barreau F, Meinzer U, Chareyre F, Berrebi D, Niwa-Kawakita M, Dussaillant M, Foligne B, Ollendorff V, Heyman M, Bonacorsi S*, et al.* (2007) CARD15/NOD2 is required for Peyer's patches homeostasis in mice. *Plos One* **2**(6): e523.

305. Witmer MD and Steinman RM (1984) The anatomy of peripheral lymphoid organs with emphasis on accessory cells: light-microscopic immunocytochemical studies of mouse spleen, lymph node, and Peyer's patch. *American Journal of Anatomy* **170**(3): 465-481.

306. Kelsall BL and Strober W (1996) Distinct populations of dendritic cells are present in the subepithelial dome and T cell regions of the murine Peyer's patch. *Journal of Experimental Medicine* **183**(1): 237-247.

307. Iwasaki A and Kelsall BL (2000) Localization of distinct Peyer's patch dendritic cell subsets and their recruitment by chemokines macrophage inflammatory protein (MIP)-3α, MIP-3β, and secondary lymphoid organ chemokine. *Journal of Experimental Medicine* **191**(8): 1381-1394.

308. Iwasaki A and Kelsall BL (2001) Unique functions of $CD11b^+$, $CD8\alpha^+$, and double-negative Peyer's patch dendritic cells. *Journal of Immunology* **166**(8): 4884-4890.

309. Johansson C and Kelsall BL (2005) Phenotype and function of intestinal dendritic cells. *Seminars in Immunology* **17**(4): 284-294.

310. Awaad A, Nakamura M, and Ishimura K (2012) Histochemical and biochemical analysis of the size-dependent nanoimmunoresponse in mouse Peyer's patches using fluorescent organosilica particles. *International journal of nanomedicine* **7**: 1423-1439.

311. Ellacott KLJ, Morton GJ, Woods SC, Tso P, and Schwartz MW (2010) Assessment of feeding behavior in laboratory mice. *Cell Metabolism* **12**(1): 10-17.

312. Barreau F, Madre C, Meinzer U, Berrebi D, Dussaillant M, Merlin F, Eckmann L, Karin M, Sterkers G, Bonacorsi S*, et al.* (2010) *Nod2* regulates the host response towards microflora by modulating T cell function and epithelial permeability in mouse Peyer's patches. *Gut* **59**(2): 207-217.

313. Kobayashi A, Donaldson DS, Erridge C, Kanaya T, Williams IR, Ohno H, Mahajan A, and Mabbott NA (2013) The functional maturation of M cells is dramatically reduced in the Peyer's patches of aged mice. *Mucosal Immunology* **6**(5): 1027-1037.

314. Gebert A, Steinmetz L, Fassbender S, and Wendlandt KH (2004) Antigen transport into Peyer's patches: increased uptake by constant numbers of M cells. *American Journal of Pathology* **164**(1): 65-72.

315. Mondot S, Barreau F, Al Nabhani Z, Dussaillant M, Le Roux K, Doré J, Leclerc M, Hugot JP, and Lepage P (2012) Altered gut microbiota composition in immune-impaired *Nod2*$^{-/-}$ mice. *Gut* **61**(4): 634-635.

316. Petnicki-Ocwieja T, Hrncir T, Liu YJ, Biswas A, Hudcovic T, Tlaskalova-Hogenova H, and Kobayashi KS (2009) Nod2 is required for the regulation of commensal microbiota in the intestine. *Proceedings of the National Academy of Sciences of the United States of America* **106**(37): 15813-15818.

317. Rehman A, Sina C, Gavrilova O, Häsler R, Ott S, Baines JF, Schreiber S, and Rosenstiel P (2011) Nod2 is essential for temporal development of intestinal microbial communities. *Gut* **60**(10): 1354-1362.

318. Florence AT (1997) The oral absorption of micro- and nanoparticulates: neither exceptional nor unusual. *Pharmaceutical Research* **14**(3): 259-266.

319. Desai MP, Labhasetwar V, Amidon GL, and Levy RJ (1996) Gastrointestinal uptake of biodegradable microparticles: effect of particle size. *Pharmaceutical Research* **13**(12): 1838-1845.

320. de Preter V and Vebeke K (2013) Metabolomics as a diagnostic tool in gastroenterology. *World Journal of Gastrointestinal Pharmacology and Therapeutics* **4**(4): 97-107.

321. Mamas M, Dunn WB, Neyses L, and Goodacre R (2011) The role of metabolites and metabolomics in clinically applicable biomarkers of disease. *Archives of Toxicology* **85**(1): 5-17.

322. Holmes E, Wilson ID, and Nicholson JK (2008) Metabolic phenotyping in health and disease. *Cell* **134**(5): 714-717.

323. Fathi F, Kyani A, Nejad MR, Rezaye-Tavirani M, Naderi N, Zali MR, Tafazzoli M, and Oskouie AA (2012) A metabonomics study on Crohn's disease using nuclear magnetic resonance spectroscopy. *HealthMED* **6**(11): 3577-3583.

324. Jansson J, Willing B, Lucio M, Fekete A, Dicksved J, Halfvarson J, Tysk C, and Schmitt-Kopplin P (2009) Metabolomics reveals metabolic biomarkers of Crohn's disease. *Plos One* **4**(7): 1-10.

325. Marchesi JR, Holmes E, Khan F, Kochhar S, Scanlan P, Shanahan F, Wilson ID, and Wang Y (2007) Rapid and noninvasive metabonomic characterization of inflammatory bowel disease. *Journal of Proteome Research* **6**(2): 546-551.

326. Schicho R, Shaykhutdinov R, Ngo J, Nazyrova A, Schneider C, Panaccione R, Kaplan GG, Vogel HJ, and Storr M (2012) Quantitative metabolomic profiling of serum, plasma, and urine by 1H NMR spectroscopy discriminates between patients with inflammatory bowel disease and healthy individuals. *Journal of Proteome Research* **11**(6): 3344-3357.

327. Williams HRT, Cox IJ, Walker DG, North BV, Patel VM, Marshall SE, Jewell DP, Ghosh S, Thomas HJW, Teare JP*, et al.* (2009) Characterization of inflammatory bowel disease with urinary metabolic profiling. *American Journal of Gastroenterology* **104**(6): 1435-1444.

328. Winterkamp S, Weidenhiller M, Otte P, Stolper J, Schwab D, Hahn EG, and Raithel M (2002) Urinary excretion of N-methylhistamine as a marker of disease activity in inflammatory bowel disease. *American Journal of Gastroenterology* **97**(12): 3071-3077.

329. Tautenhahn R, Cho K, Uritboonthai W, Zhu Z, Patti GJ, and Siuzdak G (2012) An accelerated workflow for untargeted metabolomics using the METLIN database. *Nature Biotechnology* **30**(9): 826-828.

330. Chen C, Shah YM, Morimura K, Krausz KW, Miyazaki M, Richardson TA, Morgan ET, Ntambi JM, Idle JR, and Gonzalez FJ (2008) Metabolomics reveals that hepatic stearoyl-CoA desaturase 1 downregulation exacerbates inflammation and acute colitis. *Cell Metabolism* **7**(2): 135-147.

331. Strober W and Fuss IJB, R. S. (2002) The immunology of mucosal models of inflammation. *Annual Review of Immunology* **20**: 495-549.

332. Lin HM, Edmunds SJ, Helsby NA, Ferguson LR, and Rowan DD (2009) Nontargeted urinary metabolite profiling of a mouse model of Crohn's disease. *Journal of Proteome Research* **8**(4): 2045-2057.

333. Lin HM, Barnett MP, Roy NC, Joyce NI, Zhu S, Armstrong K, Helsby NA, Ferguson LR, and Rowan DD (2010) Metabolomic analysis identifies inflammatory and noninflammatory metabolic effects of genetic modification in a mouse model of Crohn's disease. *Journal of Proteome Research* **9**(4): 1965-1975.

334. Murdoch TB, Fu H, MacFarlane S, Sydora BC, Fedorak RN, and Slupsky CM (2008) Urinary metabolic profiles of inflammatory bowel disease in interleukin-10 gene-deficient mice. *Analytical Chemistry* **80**(14): 5524-5531.

335. Otter D, Cao MS, Lin HM, Fraser K, Edmunds S, Lane G, and Rowan D (2011) Identification of urinary biomarkers of colon inflammation in IL10$^{-/-}$ mice using short-column LCMS metabolomics. *Journal of Biomedicine and Biotechnology* **2011**: 974701.

336. Nicholson JK, Connelly J, Lindon JC, and Holmes E (2002) Metabonomics: a platform for studying drug toxicity and gene function. *Nature Reviews Drug Discovery* **1**(2): 153-161.

337. Büscher JM, Czernik D, Ewald JC, Sauer U, and Zamboni N (2009) Cross-platform comparison of methods for quantitative metabolomics of primary metabolism. *Analytical Chemistry* **81**(6): 2135-2143.

338. Chambers MC, Maclean B, Burke R, Amodei D, Ruderman DL, Neumann S, Gatto L, Fischer B, Pratt B, Egertson J*, et al.* (2012) A cross-platform toolkit for mass spectrometry and proteomics. *Nature Biotechnology* **30**(10): 918-920.

339. Kessner D, Chambers M, Burke R, Agus D, and Mallick P (2008) ProteoWizard: open source software for rapid proteomics tools development. *Bioinformatics* **24**(21): 2534-2536.

340. Smith CA, Want EJ, O'Maille G, Abagyan R, and Siuzdak G (2006) XCMS: processing mass spectrometry data for metabolite profiling using nonlinear peak alignment, matching and identification. *Analytical Chemistry* **78**(3): 779-787.

341. Veselkov KA, Vingara LK, Masson P, Robinette SL, Want E, Li JV, Barton RH, Boursier-Neyret C, Walther B, Ebbels TM*, et al.* (2011) Optimized preprocessing of ultra-performance liquid chromatography/mass spectrometry urinary metabolic profiles for improved information recovery. *Analytical Chemistry* **83**(15): 5864-5872.

342. Oksanen J, Blanchet FG, Kindt R, Legendre P, Minchin PR, O'Hara RB, Simpson GL, Solymos P, Stevens MHH, and Wagner H (2013) vegan: community ecology package (http://CRAN.R-project.org/package=vegan, R package version 2.0-10).

343. Xia J, Mandal R, Sinelnikov IV, Broadhurst D, and Wishart DS (2012) MetaboAnalyst 2.0: a comprehensive server for metabolomic data analysis. *Nucleic Acids Research* **40**(Web Server issue): W127-W133.

344. The Metabolomics Innovation Center. *MetaboAnalyst 2.0: A Comprehensive Tool Suite for Metabolomic Data Analysis*. Available from: http://www.metaboanalyst.ca (accessed June 2014).

345. Xia J, Psychogios N, Young N, and Wishart DS (2009) MetaboAnalyst: a web server for metabolomic data analysis and interpretation. *Nucleic Acids Research* **37**(Web Server issue): W652-W660.

346. Xia J and Wishart DS (2011) Metabolomic data processing, analysis, and interpretation using MetaboAnalyst. In *Current Protocols in Bioinformatics* (Wiley Online Library), pp. 14.10.11-14.10.48.

347. Scripps Center For Metabolomics. *METLIN: Metabolite and Tandem MS Database*. Available from: http://metlin.scripps.edu (accessed June 2014).

348. Smith CA, O'Maille G, Want EJ, Qin C, Trauger SA, Brandon TR, Custodio DE, Abagyan R, and Siuzdak G (2005) METLIN: a metabolite mass spectral database. *Therapeutic Drug Monitoring* **27**(6): 747-751.

349. The Metabolomics Innovation Center. *Human Metabolome Database (HMDB) version 3.6*. Available from: http://www.hmdb.ca (accessed June 2014).

350. Wishart DS, Tzur D, Knox C, Eisner R, Guo AC, Young N, Cheng D, Jewell K, Arndt D, Sawhney S*, et al.* (2007) HMDB: the human metabolome database. *Nucleic Acids Research* **35**(Suppl. 1): D521-D526.

351. Higa S and Markey SP (1985) Identification and quantification of 5-methoxyindole-3-acetic acid in human urine. *Analytical Biochemistry* **144**(1): 86-93.

352. Manna SK, Patterson AD, Yang Q, Krausz KW, Idle JR, Fornace AJ, and Gonzalez FJ (2011) UPLC–MS-based urine metabolomics reveals indole-3-lactic acid and phenyllactic acid as conserved biomarkers for alcohol-induced liver disease in the *Ppara*-null mouse model. *Journal of Proteome Research* **10**(9): 4120-4133.

353. Kanehisa Laboratories. *KEGG: Kyota Encyclopedia of Genes and Genomes*. Available from: http://www.kegg.jp (accessed June 2014).

354. Plumb R, Granger J, Stumpf C, Wilson ID, Evans JA, and Lenz EM (2003) Metabonomic analysis of mouse urine by liquid-chromatography-time of flight mass spectrometry (LC-TOFMS): detection of strain, diurnal and gender differences. *Analyst* **128**(7): 819-823.

355. Ryan D, Robards K, Prenzler PD, and Kendall M (2011) Recent and potential developments in the analysis of urine: a review. *Analytica Chimica Acta* **684**(1-2): 17-29.

356. Warrack BM, Hnatyshyn S, Ott K-H, Reily MD, Sanders M, Zhang H, and Drexler DM (2009) Normalization strategies for metabonomic analysis of urine samples. *Journal of Chromatography B* **877**(5-6): 547-552.

357. Mellor AL and Munn DH (2004) IDO expression by dendritic cells: tolerance and tryptophan catabolism. *Nature Reviews Immunology* **4**(10): 762-774.

358. Moffett JR and Namboodiri MAA (2003) Tryptophan and the immune response. *Immunology and Cell Biology* **81**(4): 247-265.

359. Fallarino F, Grohmann U, You S, McGrath BC, Cavener DR, Vacca C, Orabona C, Bianchi R, Belladonna ML, Volpi C*, et al.* (2006) The combined effects of tryptophan starvation and tryptophan catabolites down-regulate T cell receptor ζ-chain and induce a regulatory phenotype in naive T cells. *Journal of Immunology* **176**(11): 6752-6761.

360. Taher YA, Piavaux BJA, Gras R, van Esch BCAM, Hofman GA, Bloksma N, Henricks PAJ, and van Oosterhout AJM (2008) Indoleamine 2,3-dioxygenase–dependent tryptophan metabolites contribute to tolerance induction during allergen immunotherapy in a mouse model. *Journal of Allergy and Clinical Immunology* **121**(4): 983-991.

361. Forrest C, Youd P, Kennedy A, Gould S, Darlington LG, and Stone T (2002) Purine, kynurenine, neopterin and lipid peroxidation levels in inflammatory bowel disease. *Journal of Biomedical Science* **9**(5): 436-442.

362. Wolf AM, Wolf D, Rumpold H, Moschen AR, Kaser A, Obrist P, Fuchs D, Brandacher G, Winkler C, Geboes K*, et al.* (2004) Overexpression of indoleamine 2,3-dioxygenase in human inflammatory bowel disease. *Clinical Immunology* **113**(1): 47-55.

363. Turner JK, Xu JL, and Tapping RI (2009) Substrains of 129 mice are resistant to *Yersinia pestis* KIM5: implications for interleukin-10-deficient mice. *Infection and Immunity* **77**(1): 367-373.

364. Casini-Raggi V, Kam L, Chong YJT, Fiocchi C, Pizarro TT, and Cominelli F (1995) Mucosal imbalance of IL-1 and IL-1 receptor antagonist in inflammatory bowel disease: a novel mechanism of chronic intestinal inflammation: a novel mechanisms of chronic inflammation. *Journal of Immunology* **154**(5): 2434-2440.

365. Martinon F, Burns K, and Tschopp J (2002) The inflammasome: a molecular platform triggering activation of inflammatory caspases and processing of proIL-β. *Molecular Cell* **10**(2): 417-426.

366. Martinon F, Mayor A, and Tschopp J (2009) The inflammasomes: guardians of the body. *Annual Review of Immunology* **27**: 229-265.

367. de Alba E (2009) Structure and interdomain dynamics of apoptosis-associated speck-like protein containing a CARD (ASC). *Journal of Biological Chemistry* **284**(47): 32932-32941.

368. Villani AC, Lemire M, Fortin G, Louis E, Silverberg MS, Collette C, Baba N, Libioulle C, Belaiche J, Bitton A*, et al.* (2009) Common variants in the *NLRP3* region contribute to Crohn's disease susceptibility. *Nature Genetics* **41**(1): 71-76.

369. Monie TP (2013) NLR activation takes a direct route. *Trends in Biochemical Sciences* **38**(3): 131-139.

370. Martinon F, Petrilli V, Mayor A, Tardivel A, and Tschopp J (2006) Gout-associated uric acid crystals activate the NALP3 inflammasome. *Nature* **440**(7081): 237-241.

371. Dostert C, Pétrilli V, van Bruggen R, Steele C, Mossman BT, and Tschopp J (2008) Innate immune activation through Nalp3 inflammasome sensing of asbestos and silica. *Science* **320**(5876): 674-677.

372. Hornung V, Bauernfeind F, Halle A, Samstad EO, Kono H, Rock KL, Fitzgerald KA, and Latz E (2008) Silica crystals and aluminum salts activate the NALP3 inflammasome through phagosomal destabilization. *Nature Immunology* **9**(8): 847-856.

373. Yazdi AS, Guarda G, Riteau N, Drexler SK, Tardivel A, Couillin I, and Tschopp J (2010) Nanoparticles activate the NLR pyrin domain containing 3 (Nlrp3) inflammasome and cause pulmonary inflammation through release of IL-1α and IL-1β. *Proceedings of the National Academy of Sciences of the United States of America* **107**(45): 19449-19454.

374. Pazár B, Ea HK, Narayan S, Kolly L, Bagnoud N, Chobaz V, Roger T, Lioté F, So A, and Busso N (2011) Basic calcium phosphate crystals induce monocyte/macrophage IL-1β secretion through the NLRP3 inflammasome in vitro. *Journal of Immunology* **186**(4): 2495-2502.

375. Colomar A, Marty V, Médina C, Combe C, Parnet P, and Amédée T (2003) Maturation and release of interleukin-1β by lipopolysaccharide-primed mouse Schwann cells require the stimulation of $P2X_7$ receptors. *Journal of Biological Chemistry* **278**(33): 30732-30740.

376. Pétrilli V, Papin S, Dostert C, Mayor A, Martinon F, and Tschopp J (2007) Activation of the NALP3 inflammasome is triggered by low intracellular potassium concentration. *Cell Death and Differentiation* **14**(9): 1583-1589.

377. Martinon F, Agostini L, Meylan E, and Tschopp J (2004) Identification of bacterial muramyl dipeptide as activator of the NALP3/Cryopyrin inflammasome. *Current Biology* **14**(21): 1929-1934.

378. Marina-García N, Franchi L, Kim YG, Miller D, McDonald C, Boons GJ, and Núñez G (2008) Pannexin-1-mediated intracellular delivery of muramyl dipeptide induces caspase-1 activation via cryopyrin/NLRP3 independently of Nod2. *Journal of Immunology* **180**(6): 4050-4057.

379. Franchi L, Munoz-Planillo R, and Núñez G (2012) Sensing and reacting to microbes through the inflammasomes. *Nature Immunology* **13**(4): 325-332.

380. Faustin B, Lartigue L, Bruey JM, Luciano F, Sergienko E, Bailly-Maitre B, Volkmann N, Hanein D, Rouiller I, and Reed JC (2007) Reconstituted NALP1 inflammasome reveals two-step mechanism of caspase-1 activation. *Molecular Cell* **25**(5): 713-724.

381. Franchi L, Warner N, Viani K, and Nuñez G (2009) Function of Nod-like receptors in microbial recognition and host defense. *Immunological Reviews* **227**(1): 106-128.

382. Neurath MF (2014) Cytokines in inflammatory bowel disease. *Nature Reviews Immunology* **14**(5): 329-342.

383. Monteleone G, Monteleone I, Fina D, Vavassori P, Del Vecchio Blanco G, Caruso R, Tersigni R, Alessandroni L, Biancone L, Naccari GC*, et al.* (2005) Interleukin-21 enhances T-helper cell type I signaling and interferon-γ production in Crohn's disease. *Gastroenterology* **128**(3): 687-694.

384. Pickert G, Neufert C, Leppkes M, Zheng Y, Wittkopf N, Warntjen M, Lehr HA, Hirth S, Weigmann B, Wirtz S*, et al.* (2009) STAT3 links IL-22 signaling in intestinal epithelial cells to mucosal wound healing. *Journal of Experimental Medicine* **206**(7): 1465-1472.

385. Maynard CL, Harrington LE, Janowski KM, Oliver JR, Zindl CL, Rudensky AY, and Weaver CT (2007) Regulatory T cells expressing interleukin 10 develop from $Foxp3^+$ and $Foxp3^-$ precursor cells in the absence of interleukin 10. *Nature Immunology* **8**(9): 931-941.

386. Maul J, Loddenkemper C, Mundt P, Berg E, Giese T, Stallmach A, Zeitz M, and Duchmann R (2005) Peripheral and intestinal regulatory CD4+CD25high T cells in inflammatory bowel disease. *Gastroenterology* **128**(7): 1868-1878.

387. Griffith JW, Sokol CL, and Luster AD (2014) Chemokines and chemokine receptors: positioning cells for host defense and immunity. *Annual Review of Immunology* **32**: 659-702.

388. Mizoguchi A and Mizoguchi E (2008) Inflammatory bowel disease, past, present and future: lessons from animal models. *Journal of Gastroenterology* **43**(1): 1-17.

389. Wirtz S and Neurath MF (2007) Mouse models of inflammatory bowel disease. *Advanced Drug Delivery Reviews* **59**(11): 1073-1083.

390. Kararli TT (1995) Comparison of the gastrointestinal anatomy, physiology, and biochemistry of humans and commonly used laboratory animals. *Biopharmaceutics and Drug Disposition* **16**(5): 351-380.

391. Zhang Q, Widmer G, and Tzipori S (2013) A pig model of the human gastrointestinal tract. *Gut Microbes* **4**(3): 193-200.

392. Mizoguchi A and Mizoguchi E (2010) Animal models of IBD: linkage to human disease. *Current Opinion in Pharmacology* **10**(5): 578-587.

393. Ferguson LR (2012) Potential value of nutrigenomics in Crohn's disease. *Nature Reviews Gastroenterology and Hepatology* **9**(5): 260-270.

394. Maeda S (2011) Corrections and clarifications: *Nod2* mutation in Crohn's disease potentiates NF-κB activity and IL-1β processing [Maeda S *et al.* (2005) *Science* **307**(5710): 734-738]. *Science* **333**(6040): 288.

395. Ali SR, Timmer AM, Bilgrami S, Park EJ, Eckmann L, Nizet V, and Karin M (2011) Anthrax toxin induces macrophage death by p38 MAPK inhibition but leads to inflammasome activation via ATP leakage. *Immunity* **35**(1): 34-44.

396. Biswas A, Liu YJ, Hao L, Mizoguchi A, Salzman NH, Bevins CL, and Kobayashi KS (2010) Induction and rescue of Nod2-dependent Th1-driven granulomatous inflammation of the ileum. *Proceedings of the National Academy of Sciences of the United States of America* **107**(33): 14739-14744.

397. Mähler M, Bristol IJ, Leiter EH, Workman AE, Birkenmeier EH, Elson CO, and Sundberg JP (1998) Differential susceptibility of inbred mouse strains to dextran sulfate sodium-induced colitis. *American Journal of Physiology: Gastrointestinal and Liver Physiology* **274**(3): G544-G551.

398. Berg DJ, Davidson N, Kühn R, Müller W, Menon S, Holland G, Thompson-Snipes L, Leach MW, and Rennick D (1996) Enterocolitis and colon cancer in interleukin-10-deficient mice are associated with aberrant cytokine production and $CD4^+$ Th1-like responses. *Journal of Clinical Investigation* **98**(4): 1010-1020.

399. Roy N, Barnett M, Knoch B, Dommels Y, and McNabb W (2007) Nutrigenomics applied to an animal model of inflammatory bowel diseases: transcriptomic analysis of the effects of eicosapentaenoic acid- and arachidonic acid-enriched diets. *Mutation Research: Fundamental and Molecular Mechanisms of Mutagenesis* **622**(1-2): 103-116.

400. Sellon RK, Tonkonogy S, Schultz M, Dieleman LA, Grenther W, Balish E, Rennick DM, and Sartor RB (1998) Resident enteric bacteria are necessary for development of spontaneous colitis and immune system activation in interleukin-10-deficient mice. *Infection and Immunity* **66**(11): 5224-5231.

401. Balish E and Warner T (2002) *Enterococcus faecalis* induces inflammatory bowel disease in interleukin-10 knockout mice. *American Journal of Pathology* **160**(6): 2253-2257.

402. Colombel JF, Rutgeerts P, Malchow H, Jacyna M, Nielsen OH, Rask-Madsen J, van Deventer S, Ferguson A, Desreumaux P, Forbes A*, et al.* (2001) Interleukin 10 (Tenovil) in the prevention of postoperative recurrence of Crohn's disease. *Gut* **49**(1): 42-46.

403. Tilg H, Ulmer H, Kaser A, and Weiss G (2002) Role of IL-10 for induction of anemia during inflammation. *Journal of Immunology* **169**(4): 2204-2209.

404. Wirtz S, Neufert C, Weigmann B, and Neurath MF (2007) Chemically induced mouse models of intestinal inflammation. *Nature Protocols* **2**(3): 541-546.

405. Dieleman LA, Ridwan BU, Tennyson GS, Beagley KW, Bucy RP, and Elson CO (1994) Dextran sulfate sodium-induced colitis occurs in severe combined immunodeficient mice. *Gastroenterology* **107**(6): 1643-1652.

406. Okayasu I, Hatakeyama S, Yamada M, Ohkusa T, Inagaki Y, and Nakaya R (1990) A novel method in the induction of reliable experimental acute and chronic ulcerative colitis in mice. *Gastroenterology* **98**(3): 694-702.

407. Morris GP, Beck PL, Herridge MS, Depew WT, Szewczuk MR, and Wallace JL (1989) Hapten-induced model of chronic inflammation and ulceration in the rat colon. *Gastroenterology* **96**(3): 795-803.

408. Neurath MF, Fuss I, Kelsall BL, Stüber E, and Strober W (1995) Antibodies to interleukin 12 abrogate established experimental colitis in mice. *Journal of Experimental Medicine* **182**(5): 1281-1290.

409. Kitajima S, Takuma S, and Morimoto M (1999) Changes in colonic mucosal permeability in mouse colitis induced with dextran sulfate sodium. *Experimental Animals* **48**(3): 137-143.

410. Kaser A, Lee A-H, Franke A, Glickman JN, Zeissig S, Tilg H, Nieuwenhuis EES, Higgins DE, Schreiber S, Glimcher LH*, et al.* (2008) XBP1 links ER stress to intestinal inflammation and confers genetic risk for human inflammatory bowel disease. *Cell* **134**(5): 743-756.

411. Matsumoto S, Okabe Y, Setoyama H, Takayama K, Ohtsuka J, Funahashi H, Imaoka A, Okada Y, and Umesaki Y (1998) Inflammatory bowel disease-like enteritis and caecitis in a senescence accelerated mouse P1/Yit strain. *Gut* **43**(1): 71-78.

412. Bamias G, Okazawa A, Rivera-Nieves J, Arseneau KO, de la Rue SA, Pizarro TT, and Cominelli F (2007) Commensal bacteria exacerbate intestinal inflammation but are not essential for the development of murine ileitis. *Journal of Immunology* **178**(3): 1809-1818.

413. Kosiewicz MM, Nast CC, Krishnan A, Rivera-Nieves J, Moskaluk CA, Matsumoto S, Kozaiwa K, and Cominelli F (2001) Th1-type response mediate spontaneous ileitis in a novel murine model of Crohn's disease. *Journal of Clinical Investigation* **107**(6): 695-702.

414. Knoch B, Barnett MPG, Zhu S, Park ZA, Nones K, Dommels YEM, Knowles SO, McNabb WC, and Roy NC (2009) Genome-wide analysis of dietary eicosapentaenoic acid- and oleic acid-induced nodulation of colon inflammation in interleukin-10 gene-deficient mice. *Journal of Nutrigenetics and Nutrigenomics* **2**(1): 9-28.

Appendices

Appendix A Normality and variance equality analysis *Chapter 2*

Supplementary Table 1 Chapter 2 p-*value results of Shapiro-Wilk normality test and Bartlett's test for variance equality as well as tests used for group comparisons and post-hoc pairwise comparisons of means if applicable.*

Assay	***Time (h)***	***Co-stimulation***	***Shapiro-Wilk***	***Bartlett's***	***Group comparison***	**Post-hoc *test***
WST-1	3	-	0.10	0.22	Two-way ANOVA	n/a[2]
		MDP	0.20	< 0.05	Two-way ANOVA	n/a
		PGN	0.38	0.14	Two-way ANOVA	n/a
	3 + 21	-	0.25	0.89	Two-way ANOVA	n/a
		MDP	0.39	0.90	Two-way ANOVA	n/a
		PGN	0.06	0.43	Two-way ANOVA	n/a
FC	3	-	< 0.01	0.96	Two-way ANOVA	n/a
- viability		MDP	0.11	< 0.05	Two-way ANOVA	n/a
		PGN	< 0.01	0.67	Two-way ANOVA	n/a
	3 + 21	-	0.16	< 0.05	Two-way ANOVA	Tukey's HSD
		MDP	< 0.01	0.39	Two-way ANOVA	n/a
		PGN	< 0.01	0.49	Two-way ANOVA	n/a
- F4/80	3	-	< 0.05	0.12	Two-way ANOVA	n/a
		MDP	0.88	1.00	Two-way ANOVA	n/a
		PGN	< 0.05	0.08	Two-way ANOVA	n/a
	3 + 21	-	< 0.001	0.67	Two-way ANOVA	n/a
		MDP	< 0.001	< 0.05	Two-way ANOVA	n/a
		PGN	< 0.001	0.99	Two-way ANOVA	n/a

(continued on next page)

Supplementary Table 1 Chapter 2 p-*value results of Shapiro-Wilk normality test and Bartlett's test for variance equality as well as tests used for group comparisons and post-hoc pairwise comparisons of means if applicable (continued).*

Assay	*Time (h)*	*Co-stimulation*	*Shapiro-Wilk*	*Bartlett's*	*Group comparison*	**Post-hoc** *test*
FC	3	-	< 0.05	0.70	Two-way ANOVA	n/a
- *FSC*		MDP	0.09	0.79	Two-way ANOVA	n/a
		PGN	0.58	< 0.05	Two-way ANOVA	n/a
	3 + 21	-	< 0.05	< 0.05	Two-way ANOVA	n/a
		MDP	< 0.01	< 0.001	Two-way ANOVA	n/a
		PGN	0.15	0.19	Two-way ANOVA	n/a
- *SSC*	3	-	< 0.001	0.94	Two-way ANOVA	n/a
		MDP	< 0.01	0.83	Two-way ANOVA	n/a
		PGN	< 0.001	0.86	Two-way ANOVA	n/a
	3 + 21	-	< 0.01	0.94	Two-way ANOVA	n/a
		MDP	< 0.01	0.98	Two-way ANOVA	n/a
		PGN	< 0.001	0.95	Two-way ANOVA	n/a
- *SSC*	3	-	< 0.01	0.46	Two-way ANOVA	n/a
relative		MDP	< 0.01	0.59	Two-way ANOVA	n/a
		PGN	< 0.001	0.77	Two-way ANOVA	n/a
	3 + 21	-	< 0.01	0.94	Two-way ANOVA	n/a
		MDP	< 0.01	0.74	Two-way ANOVA	n/a
		PGN	< 0.01	0.93	Two-way ANOVA	n/a

(continued on next page)

Supplementary Table 1 Chapter 2 p-*value results of Shapiro-Wilk normality test and Bartlett's test for variance equality as well as tests used for group comparisons and post-hoc pairwise comparisons of means if applicable (continued).*

Assay	*Time (h)*	*Co-stimulation*	*Shapiro-Wilk*	*Bartlett's*	*Group comparison*	**Post-hoc** *test*
FC	3	-	0.06	0.69	Two-way ANOVA	n/a
- CD80		MDP	< 0.001	< 0.001	Two-way ANOVA	Tukey's HSD
		PGN	< 0.01	0.99	Two-way ANOVA	n/a
	3 + 21	-	0.10	0.11	Two-way ANOVA	n/a
		MDP	0.18	0.11	Two-way ANOVA	n/a
		PGN	0.77	0.46	Two-way ANOVA	n/a
- CD86	3	-	< 0.01	0.11	Two-way ANOVA	n/a
		MDP	< 0.001	< 0.001	Two-way ANOVA	Tukey's HSD
		PGN	< 0.001	< 0.001	Two-way ANOVA	n/a
	3 + 21	-	0.11	0.22	Two-way ANOVA	n/a
		MDP	< 0.01	0.59	Two-way ANOVA	n/a
		PGN	< 0.01	0.22	Two-way ANOVA	Tukey's HSD
ELISA	3	-	< 0.01	< 0.001	Two-way ANOVA	n/a
(mouse)		MDP	< 0.01	< 0.01	Two-way ANOVA	n/a
- TNF-a		PGN	0.87	< 0.05	Two-way ANOVA	n/a
	3 + 21	-	< 0.001	< 0.001	Two-way ANOVA	n/a
		MDP	0.25	0.28	Two-way ANOVA	n/a
		PGN	< 0.01	0.59	Two-way ANOVA	n/a
- IL-1β	3	-	< 0.001	0.68	Two-way ANOVA	n/a
		MDP	< 0.001	0.06	Two-way ANOVA	n/a
		PGN	< 0.001	< 0.01	Two-way ANOVA	Tukey's HSD
	3 + 21	-	< 0.001	0.78	Two-way ANOVA	n/a
		MDP	< 0.001	0.33	Two-way ANOVA	n/a
		PGN	0.07	0.35	Two-way ANOVA	Tukey's HSD

(continued on next page)

Supplementary Table 1 Chapter 2 p-*value results of Shapiro-Wilk normality test and Bartlett's test for variance equality as well as tests used for group comparisons and post-hoc pairwise comparisons of means if applicable (continued).*

Assay	***Time (h)***	***Co-stimulation***	***Shapiro-Wilk***	***Bartlett's***	***Group comparison***	**Post-hoc *test***
ELISA	3	-	< 0.05	0.99	Kruskal-Wallis test	n/a
(human)		MDP	0.15	0.79	One-way ANOVA	n/a
- IL-1β		PGN	0.10	0.47	One-way ANOVA	n/a
	3 + 21	-	0.09	0.74	One-way ANOVA	n/a
		MDP	< 0.05	0.96	Kruskal-Wallis test	n/a
		PGN	0.22	0.72	One-way ANOVA	n/a
- IL-1β	3	-	< 0.001	< 0.001	Kruskal-Wallis	n/a
relative		MDP	0.09	< 0.001	Kruskal-Wallis	n/a
		PGN	< 0.05	< 0.001	Kruskal-Wallis	n/a
	3 + 21	-	< 0.001	< 0.001	Kruskal-Wallis	n/a
		MDP	0.19	< 0.001	Kruskal-Wallis	n/a
		PGN	0.06	< 0.001	Kruskal-Wallis	Wilcoxon[1]
- IL-17	3 + 69	-	0.87	1.00	One-way ANOVA	n/a
		MDP	0.78	0.33	One-way ANOVA	Tukey's HSD
		PGN	0.94	0.99	One-way ANOVA	n/a
- IL-17	3 + 69	-	< 0.01	< 0.001	Kruskal-Wallis	n/a
relative		MDP	0.20	< 0.001	Kruskal-Wallis	Wilcoxon
		PGN	0.41	< 0.001	Kruskal-Wallis	Wilcoxon

[1]Wilcoxon rank sum test with Bonferroni correction for multiple comparisons. [2]Abbreviations specific for this table: n/a = not applicable.

Appendix B Average number of bone marrow cells per mouse

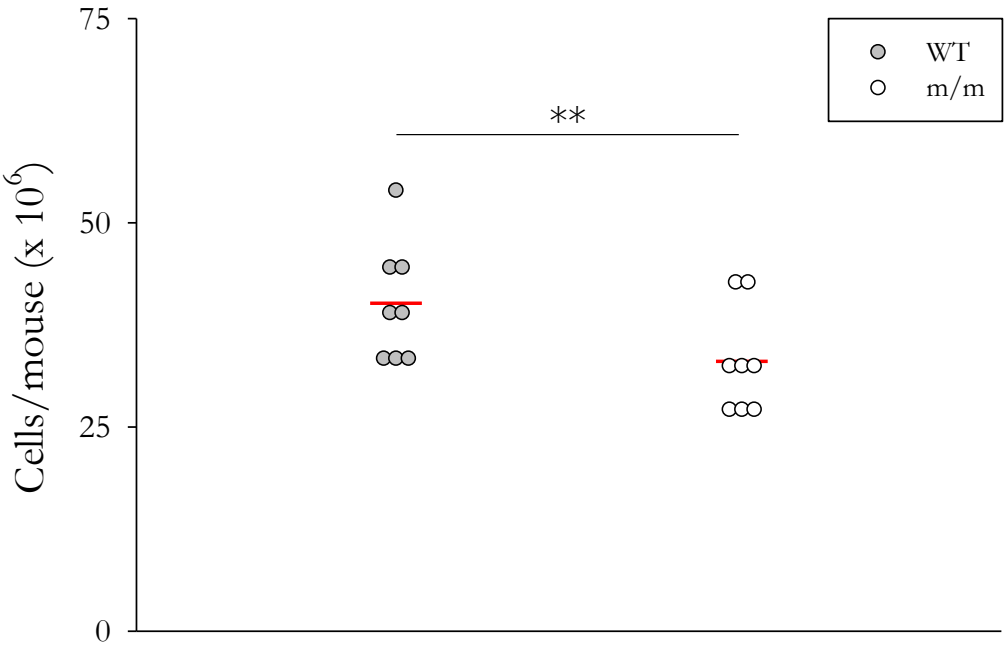

Supplementary Figure 1 *Bone marrow cells per mouse.*

Average number of bone marrow cells obtained per mouse from WT and *Nod2*$^{m/m}$ (m/m) mice (see Section 2.3.3). Each data point represents a separate tissue collection; $n = 8$. Results were compared with paired Student's *t*-test; $^{**}p < 0.01$.

Appendix C Normality and variance equality analysis *Chapter 3*

Supplementary Table 2 Chapter 3 p-*value results of Shapiro-Wilk normality test and Bartlett's test for variance equality as well as tests used for group comparisons and post-hoc pairwise comparisons of means if applicable.*

Parameter	***Weeks***	***Shapiro-Wilk***	***Bartlett's***	***Group comparison***	**Post-hoc *test***
Females	6	< 0.001	0.95	Kruskal-Wallis	n/a[1]
- Age	12	< 0.001	1.00	Kruskal-Wallis	n/a
	18	< 0.001	0.98	Kruskal-Wallis	n/a
- Initial	6	0.05	0.06	One-way ANOVA	n/a
body weight	12	0.17	< 0.05	Kruskal-Wallis	n/a
	18	0.38	0.98	One-way ANOVA	n/a
- Final	6	0.29	0.14	One-way ANOVA	n/a
body weight	12	0.42	0.19	One-way ANOVA	n/a
	18	0.29	0.23	One-way ANOVA	n/a
- Weight	6	0.81	0.30	One-way ANOVA	n/a
gain	12	0.96	0.69	One-way ANOVA	n/a
	18	0.09	0.54	One-way ANOVA	n/a
- Daily food	6	0.88	0.12	One-way ANOVA	n/a
intake	12	0.45	0.12	One-way ANOVA	n/a
	18	0.09	0.85	One-way ANOVA	n/a

(continued on next page)

Supplementary Table 2 Chapter 3 p-*value results of Shapiro-Wilk normality test and Bartlett's test for variance equality as well as tests used for group comparisons and post-hoc pairwise comparisons of means if applicable (continued).*

Parameter	***Weeks***	***Shapiro-Wilk***	***Bartlett's***	***Group comparison***	**Post-hoc *test***
Males	6	< 0.001	0.97	Kruskal-Wallis	n/a
- Age	12	< 0.001	0.96	Kruskal-Wallis	n/a
	18	< 0.001	0.99	Kruskal-Wallis	n/a
- Initial	6	< 0.01	0.17	Kruskal-Wallis	n/a
body weight	12	0.83	0.92	One-way ANOVA	n/a
	18	< 0.05	0.12	Kruskal-Wallis	n/a
- Final	6	0.17	0.73	One-way ANOVA	n/a
body weight	12	0.09	0.64	One-way ANOVA	n/a
	18	0.56	0.40	One-way ANOVA	Tukey's HSD
- Weight	6	< 0.001	< 0.05	Kruskal-Wallis	n/a
gain	12	0.51	0.49	One-way ANOVA	n/a
	18	0.75	0.78	One-way ANOVA	n/a
- Daily food	6	0.45	0.37	One-way ANOVA	n/a
intake	12	< 0.05	< 0.05	Kruskal-Wallis	n/a
	18	< 0.01	0.42	Kruskal-Wallis	n/a

(continued on next page)

Supplementary Table 2 Chapter 3 p-*value results of Shapiro-Wilk normality test and Bartlett's test for variance equality as well as tests used for group comparisons and post-hoc pairwise comparisons of means if applicable (continued).*

Parameter	***Diet***	***Shapiro-Wilk***	***Bartlett's***	***Group comparison***	**Post-hoc *test***
Females	6.25	0.24	0.70	One-way ANOVA	n/a
- Daily TiO_2	62.5	0.28	0.66	One-way ANOVA	n/a
intake	625	< 0.05	0.58	Kruskal-Wallis	n/a
- Daily TiO_2	6.25	< 0.05	0.10	Kruskal-Wallis	Tukey's HSD
dose	62.5	0.36	0.52	One-way ANOVA	Tukey's HSD
	625	0.80	0.67	One-way ANOVA	Tukey's HSD
Males	6.25	0.11	0.85	One-way ANOVA	n/a
- Daily TiO_2	62.5	< 0.05	< 0.05	Kruskal-Wallis	n/a
intake	625	< 0.05	0.75	Kruskal-Wallis	n/a
- Daily TiO_2	6.25	0.89	0.65	One-way ANOVA	n/a
dose	62.5	< 0.01	0.13	Kruskal-Wallis	n/a
	625	0.70	0.93	One-way ANOVA	Tukey's HSD

(continued on next page)

Supplementary Table 2 Chapter 3 p-*value results of Shapiro-Wilk normality test and Bartlett's test for variance equality as well as tests used for group comparisons and post-hoc pairwise comparisons of means if applicable (continued).*

Tissue	***Population***	***Shapiro-Wilk***	***Bartlett's***	***Group comparison***	**Post-hoc *test***
Lymphocytes	all	< 0.05	< 0.05	Two-way ANOVA	n/a
- PP	$CD4^+$ T cells	0.06	0.23	Two-way ANOVA	n/a
	$CD8^+$ T cells	0.73	0.42	Two-way ANOVA	n/a
	$CD45R^+$ B cells	0.35	0.10	Two-way ANOVA	n/a
- MLN	all	< 0.001	< 0.05	Two-way ANOVA	n/a
	$CD4^+$ T cells	0.49	0.06	Two-way ANOVA	n/a
	$CD8^+$ T cells	0.56	< 0.01	Two-way ANOVA	n/a
	$CD45R^+$ B cells	0.28	< 0.05	Two-way ANOVA	n/a
Monocytes	all	< 0.001	< 0.001	Two-way ANOVA	n/a
- PP	$CD11b^+$ $CD11c^{-/low}$ MΦ[1]	< 0.01	0.25	Two-way ANOVA	n/a
	$CD11c^{high}$ DCs	0.60	0.85	Two-way ANOVA	n/a
- MLN	all	< 0.001	< 0.001	Two-way ANOVA	n/a
	$CD11b^+$ $CD11c^{-/low}$ MΦ	0.20	0.19	Two-way ANOVA	n/a
	$CD11c^{high}$ DCs	0.13	0.25	Two-way ANOVA	n/a
DCs	$CD8^+$ $CD11b^-$ DCs	0.74	0.09	Two-way ANOVA	n/a
- PP	$CD8^-$ $CD11b^+$ DCs	0.78	< 0.05	Two-way ANOVA	n/a
	$CD8^-$ $CD11b^-$ DCs	< 0.001	< 0.01	Two-way ANOVA	n/a
- MLN	$CD8^+$ $CD11b^-$ DCs	0.10	0.55	Two-way ANOVA	n/a
	$CD8^-$ $CD11b^+$ DCs	0.33	0.67	Two-way ANOVA	n/a
	$CD8^-$ $CD11b^-$ DCs	0.12	< 0.05	Two-way ANOVA	n/a

(continued on next page)

Supplementary Table 2 Chapter 3 p-*value results of Shapiro-Wilk normality test and Bartlett's test for variance equality as well as tests used for group comparisons and post-hoc pairwise comparisons of means if applicable (continued).*

Parameter	***Shapiro-Wilk***	***Bartlett's***	***Group comparison***	**Post-hoc *test***
Reflection spots analysis threshold comparison	< 0.001	< 0.001	Kruskal-Wallis	Tukey's HSD
Reflection spots analysis group comparison	< 0.001	< 0.001	Two-way ANOVA	Tukey's HSD
SED areas comparison	< 0.001	0.70	Two-way ANOVA	n/a

[1]Abbreviations specific for this table: n/a = not applicable; MΦ = macrophages.

Appendix D Normality and variance equality analysis *Chapter 4*

Supplementary Table 3 Chapter 4 p-*value results of Shapiro-Wilk normality test and Bartlett's test or* F-*test for variance equality as well as tests used for group comparisons and post-hoc pairwise comparisons of means if applicable.*

Study	***Parameter***	***Shapiro-Wilk***	***Bartlett's/ F-test***[1]	***Group comparison***	**Post-hoc *test***
Bone marrow collection	*Age*	< 0.01	0.77	Wilcoxon	n/a[2]
	Body weight	0.80	0.19	Student	n/a
	Number of PPs	< 0.01	0.43	Wilcoxon	n/a
	Small intestine length	0.23	0.34	Student	n/a
	Colon length	0.88	0.18	Student	n/a
Dietary TiO_2 exposure	*Age*	< 0.05	0.76	Two-way ANOVA	n/a
	Initial body weight	0.74	0.67	Two-way ANOVA	n/a
	Final body weight	0.46	0.92	Two-way ANOVA	n/a
	Body weight gain	0.54	0.39	Two-way ANOVA	n/a
	Daily food intake	0.30	0.70	Two-way ANOVA	n/a
	Daily TiO_2 intake	0.52	0.76	Student	n/a
	Daily TiO_2 dose	0.98	0.65	Student	n/a
	Number of PPs	0.26	0.61	Two-way ANOVA	n/a
	Small intestine length	0.06	0.28	Two-way ANOVA	n/a
	Colon length	0.34	0.12	Two-way ANOVA	n/a
	Ileum histology score	< 0.05	0.06	Two-way ANOVA	n/a
	Colon histology score	< 0.001	0.10	Two-way ANOVA	n/a
	Ileum crypt length	0.17	0.12	Two-way ANOVA	n/a
	Ileum villi length	0.53	0.40	Two-way ANOVA	n/a
	Colon crypt length	< 0.001	< 0.01	Two-way ANOVA	n/a
	Reflection spots analysis group comparison	< 0.001	< 0.05	Two-way ANOVA	Tukey's HSD
	SED areas comparison	0.52	0.82	Two-way ANOVA	Tukey's HSD

(continued on next page)

Supplementary Table 3 Chapter 4 p-*value results of Shapiro-Wilk normality test and Bartlett's test or* F-*test for variance equality as well as tests used for group comparisons and post-hoc pairwise comparisons of means if applicable (continued).*

Study	***Parameter***	***Shapiro-Wilk***	***Bartlett's/* F-*test***	***Group comparison***	**Post-hoc *test***
Monocyte Populations in PPs	*Monocytes*	0.19	0.59	Student	n/a
	CD11b^{+} *CD11c*$^{-/low}$ *MΦ*[2]	0.24	< 0.05	Wilcoxon	n/a
	CD11c^{high} *DCs*	< 0.01	0.09	Wilcoxon	n/a
	CD8^{+} *DCs* *CD11b*$^{-}$	< 0.01	0.77	Wilcoxon	n/a
	CD8^{-} *DCs* *CD11b*$^{+}$	< 0.01	0.71	Wilcoxon	n/a
	CD8^{-} *DCs* *CD11b*$^{-}$	< 0.01	0.71	Wilcoxon	n/a

[1]The *F*-test was used to compare the variances between two groups; Bartlett's test was used to compare the variances between more than two groups. [2]Abbreviations specific for this table: n/a = not applicable; MΦ = macrophages.

Appendix E R code for metabolomics data analysis

```
library(xcms)

library(rgl)

library(gplots)

library(limma)

library(vegan)

library(mixOmics)

library(agricolae)

library(multtest)

setwd("Directory:/Path_to_folder_with_mzXML_files_AnalysisX")

filenames <- read.delim(file="SampleList_AnalysisX.txt", sep="\t",
stringsAsFactors=FALSE)

filenames$Filename <-
paste("Directory:/Path_to_folder_with_mzXML_files_AnalysisX",
filenames$Filename, sep="")

library(xcms)

xset <- group(xset)

xset2 <- retcor(xset, method="loess", plottype="deviation")

xset2 <- group(xset2, bw = 10)

xset3 <- fillPeaks(xset2)

PeakTable <- peakTable(xset3)

write.csv(PeakTable,"PeakIntensityTable_AnalysisX.csv")
```

Appendix F R code for statistical analysis of metabolomics data

```
values.raw <- groupval(xset3, value="into",method="medret")

values.raw.trt <- values.raw[,filenames$Sample !="ref"]

filenames.trt <- filenames[filenames$Sample !="ref",]

par(mar=c(6,6,3,4))

boxplot(values.raw.trt,las=2)

normalize.medFC <- function(mat) {
  # Perform median fold change normalisation
  #           X - data set [Variables & Samples]
  medSam <- apply(mat, 1, median)
  medSam[which(medSam==0)] <- 0.0001
  mat <- apply(mat, 2, function(mat, medSam){
    medFDiSmpl <- mat/medSam
    vec<-mat/median(medFDiSmpl)
    return(vec)
  }, medSam)
  return (mat) }
values.medFC <- normalize.medFC(values.raw.trt)

boxplot(values.medFC,las=2)

values.medFC.log <- log2(values.medFC+10)

boxplot(values.medFC.log,las=2, ylim=c(1,40))

library(vegan)
```

First *in vivo* study

```
adonis(t(values.medFC.log)~filenames.trt$Sex * filenames.trt$Group *
filenames.trt$Diet)
```

Second *in vivo* study

```
adonis(t(values.medFC.log)~filenames.trt$Genotype * filenames.trt$TimePoint *
filenames.trt$Diet)
```